PACIFIC GAS AND ELECTRIC COMPANY
GEOSCIENCES DEPARTMENT
QUALITY RELATED TECHNICAL REPORT

Report Number: GEO. DCPP.TR.13.01
Report Revision: 0
Report Date: May 17, 2013
Quality Related: Y

REPORT TITLE:

Stratigraphic Framework for Assessment of Fault Activity Offshore of the Central California Coast Between Point San Simeon and Point Sal

SIGNATORIES

PREPARED BY: [signature] DATE: May 17, 2013

Hans AbramsonWard — LCI

Printed Name — Organization

VERIFIED BY: [signature] DATE: 17 May 2013

KATHRYN L. HANSON — AMEC E&I

Printed Name — Organization

APPROVED BY: [signature] DATE: May 30, 2013

Richard Klimczak — PG&E Geosciences

Printed Name — Organization

RECORD OF REVISIONS

Rev. No.	Reason for Revision	Revision Date
0	Initial Report	5/17/2013

TABLE OF CONTENTS

LISTS OF TABLES, FIGURES, PLATES, APPENDICES, AND ATTACHMENTS

Tables

Figures

Plates

Appendices

Attachment

ABBREVIATIONS, ACRONYMS, AND SYMBOLS

$\delta^{18}O$	oxygen isotope ratio (*refer to glossary*)
2D	two-dimensional
3D	three-dimensional
AMEC	AMEC Environment & Infrastructure, Inc.
ASME	American Society of Mechanical Engineers
cm	centimeters
CRADA	Cooperative Research and Development Agreement
CSUMB	California State University Monterey Bay
CWA	Contract Work Authorization
DCPP	Diablo Canyon Power Plant
DEM	digital elevation model
ELP	early–late Pliocene unconformity
GPS	global positioning system
HFZ	Hosgri fault zone
Hz	hertz
IHO	International Hydrographic Office
ka	thousand years ago (*also* thousand years old)
kHz	kilohertz
km	kilometers
kyr	thousand years
LCI	Lettis Consultants International, Inc.
LGM	Last Glacial Maximum
LiDAR	light detection and ranging
LOFZ	Los Osos fault zone
LTSP	Long Term Seismic Program
m	meters
Ma	million years ago (*also* million years old)
MBES	multibeam echosounder
MIS	marine oxygen isotope stage
mm/yr	millimeters per year
ms	milliseconds
m/s	meters per second
NQA	Nuclear Quality Assurance

NRC	Nuclear Regulatory Commission
PG&E	Pacific Gas and Electric Company
PSHA	probabilistic seismic hazard analysis
QA	quality assurance
QC	quality control
s	seconds
SBL	Subbottom Logger
SMT	Seismic Micro-Technology
SSC	Seismic Source Characterization
SSHAC	Senior Seismic Hazard Advisory Committee
twtt	two-way travel time
USGS	U.S. Geological Survey
UTM	Universal Transverse Mercator
WGS	World Geodetic System

1.0 INTRODUCTION

This report summarizes the results of the mapping of Quaternary stratigraphy and faulting on the continental shelf offshore of the Diablo Canyon power plant (DCPP). This mapping is based primarily on interpretation of two-dimensional (2D) high-resolution seismic-reflection profiles collected from Point Piedras Blancas to Point Sal at the south end of San Luis Obispo Bay in 2008 and 2009 by the U.S. Geological Survey (USGS; Sliter et al., 2009), and three-dimensional (3D)/2D seismic-reflection profiles collected along the northward projection of the Shoreline fault in 2010 by Fugro Consultants, Inc. (2011a).

The interpretations presented herein were developed in accordance with the scope of work laid out in Contract Work Authorization (CWA) 3500940841 for 2012 between Pacific Gas and Electric Company (PG&E) and Lettis Consultants International, Inc. (LCI) and CWA 3500941895 between PG&E and AMEC Environment & Infrastructure, Inc. (AMEC). This mapping study was authorized pursuant to the DCPP Long Term Seismic Program (LTSP) hazard update and in furtherance of the Senior Seismic Hazard Advisory Committee (SSHAC) Level 3 process. The project is consistent with the federal mandate issued by the U.S. Nuclear Regulatory Commission (NRC) in a letter dated March 12, 2012 ("the 50.54(f) letter"), requiring existing nuclear power plants to update their probabilistic seismic hazard analysis (PSHA). This study was conducted in accordance with the PG&E Geosciences Quality Assurance (QA) Program, which meets the requirements of Appendix B of 10 CFR 50 and the reporting requirements of 10 CFR 21. Section 10.0 of this report addresses the limitations on the use of the results and conclusions presented herein. Section 11.0 addresses any impacts that the results and conclusions have on other PG&E Geosciences documents. The report verification summary is documented in Attachment 1. This work for both contractors was tracked under SAP notifications 50492333 and 50497747, respectively.

A Glossary of Terms is attached to the end of this report. Abbreviations, acronyms and symbols are listed before the introduction.

1.1 Purpose

The purpose of this project is to map Quaternary stratigraphic features imaged in existing seismic-reflection data offshore of the DCPP in order to use them to evaluate rates and style of Quaternary fault deformation. This project builds on the results of earlier assessments that were presented in the *Shoreline Fault Zone Report* (PG&E, 2011) and on the preliminary assessment of paleoshorelines and unconformities near the Hosgri fault zone performed by AMEC (AMEC; 2012a).

The Quaternary stratigraphy presented in this report was developed through analysis of the USGS high-resolution 2D seismic-reflection data and the Fugro Point Buchon 3D/2D data set as an aid to better assess the recency, style, and rate of slip on offshore faults. Key stratigraphic units are interpreted in a sequence-stratigraphic framework, and their ages are estimated through correlation to known late Quaternary sea-level highstands and lowstands. Prominent sequence-bounding horizons are erosional unconformities that are correlated regionally based on their seismic stratigraphic signature (primarily, amplitude and styles of underlying and overlying unconformities), and connectivity with shore-parallel tie lines. Where these sequence-bounding horizons intersect active faults, the amount and sense of vertical separation across the faults are measured, together with estimated uncertainties. These measurements are used to evaluate the recency, style, and rate of Quaternary fault deformation in the study area.

1.2 Geologic Setting

This section presents a brief summary of the regional stratigraphy and tectonic setting of the study area.

1.2.1 Regional Quaternary Stratigraphy

As shown on Figure 1-1, the study area is located on the continental shelf from Point Piedras Blancas in the north to Point Sal in the south. The continental shelf in the study area slopes gently westward. The shelf is 5 to 20 kilometers (km) wide and lies between the coastline and the shelf break, a prominent break in slope to the steeper continental slope at water depths of approximately 120 to 140 meters (m) (Figure 1-1). The study area includes two broad bays: Estero Bay to the northwest of the DCPP and San Luis Obispo Bay to the southeast of the DCPP. The largest streams and rivers onshore of the study area drain into San Luis Obispo Bay, including the Santa Maria River, Arroyo Grande Creek, and San Luis Obispo Creek. Smaller streams drain into the remainder of the study area to the north. Within the study area, the seafloor consists mostly of Quaternary sediment (PG&E, 2011, Watt et al., in preparation,). Drop cores taken during the Long Term Seismic Program (LTSP) indicate that these sediments consist of sand and silty sand with minor gravel deposits that become progressively fine-grained offshore (PG&E, 1988). Outcrops of bedrock locally protrude from the Quaternary sediment, with the highest concentrations occurring offshore of Point Piedras Blancas, Cambria, the stretch of coastline from Point Buchon to Point San Luis, and Point Sal (Figure 1-1).

Local evidence of Quaternary sea level changes is preserved onshore of the study area as a series of at least 12 uplifted marine terraces (Hanson et al., 1994). Near the DCPP, the lowest two terraces in this sequence are correlated to marine oxygen isotope stages (MIS) 5a and 5e based on uranium-series ages of coral and vertebrate bone samples, amino acid racemization analyses, and paleoclimatic analyses of invertebrate faunal assemblages. The ages of the lower terraces provide local calibration of the terrace sequence for correlation with paleosea-level curves developed from worldwide data (e.g., Lisiecki and Raymo, 2005; Waelbroeck et al., 2002). These correlations suggest that the oldest of these terraces are greater than 500 thousand years old (ka; Hanson et al., 1994). Additionally, a record of sea-level lowstands is preserved as extensive eolian deposits inland of the Estero and San Luis Obispo bays (Orme, 1992). These dune sequences are interpreted to have formed during periods of low sea level when shelf sediments were exposed to wind erosion and were transported inland (Orme, 1992).

Geologic mapping reported by PG&E (2011) shows that the seafloor offshore of the Irish Hills is underlain by Quaternary marine sediment. Where this sediment is absent, most of the seafloor is composed of gently to steeply dipping Tertiary strata exposed in stratigraphic sequences from south to north, including the Obispo Formation, the Monterey Formation, and the Miguelito Member of the Pismo Formation. Basement rock of the Franciscan Complex and Cretaceous sandstone locally underlie the seafloor offshore of Point San Luis. The similarity in seafloor texture offshore of Cambria to that offshore of Point San Luis suggests that much of the shelf offshore of Cambria is underlain by basement rock. Seafloor textures also suggest that the rocky part of the shelf offshore of Point San Simeon and Point Piedras Blancas is underlain by a mixture of basement rock and Tertiary marine sedimentary rock (Johnson and Watt, 2012, Watt et al., in preparation).

1.2.2 Tectonic Setting

The Central Coast of California is characterized by transpressional deformation between the San Andreas Fault Zone to the east and the San Gregorio–San Simeon–Hosgri fault system of near-coastal faults to the west (Figure 1-2). Transpressional deformation in the region is likely driven by three distinct but interacting processes (Lettis et al., 2004):

1. Northward left transfer of slip from the San Andreas fault zone to the Rinconada and West Huasna faults to the Hosgri–San Simeon fault zone.
2. Clockwise rotation of the western Transverse Ranges domain (transrotational deformation of Luyendyk [1991] and Dickinson [2004a, 2004b]), which imparts north-directed strain into the region.
3. An unknown amount of possible plate-normal convergence across the region.

This transform regime initiated approximately 30 million years ago (Ma) when the transform process between the Pacific and North American plates introduced an episode of strike-slip tectonics that prevails today (Atwater, 1970).

Although the dominant sense of deformation across strike-slip faults is lateral, persistent patterns of relative uplift or subsidence across strike slip faults commonly occur at “restraining” and “releasing” bends (Mitra and Paul, 2011; Mann, 2007). In right-lateral strike-slip fault systems, such as the San Gregorio-San Simeon-Hosgri fault system, left-stepping faults or restraining bends are associated with zones of compression (*transpression*) and uplift between parallel faults; right-stepping faults and releasing bends are associated with zones of tension (*transtension*) and subsidence between parallel faults (Rodgers, 1980). Continued transtension may then form pull-apart (graben-like) basins, half grabens, or depressions (Burchfiel and Stewart, 1966; Crowell, 1974). The expression of these are observed in the Central Coast topography and bathymetry as en-echelon linear to lens-shaped ridges and rhomboid basins, as proposed by Howell et al. (1980); characteristic patterns of drag folds and secondary faults typical of strike-slip fault zones also are observed.

Transpressional deformation along the southern part of the San Gregorio–San Simeon–Hosgri fault system has produced several distinct but interacting crustal domains and tectonic structures (Figure 1-2; PG&E, 1988). The study area lies within the western margin of the Los Osos domain, a triangular-shaped region consisting of northwest-striking reverse, oblique, and strike-slip faults that border uplifted blocks and subsiding basins within the domain (Lettis et al., 2004). Locally, these include the Santa Maria Valley, San Luis/Pismo, and Los Osos structural blocks. Two parts of the San Gregorio–San Simeon–Hosgri fault system (Figure 1-2 inset map) are included within the study area: the San Simeon fault zone, at the northern end of the Los Osos domain, and the Hosgri fault zone (HFZ), which defines the western boundary of the Los Osos domain from Estero Bay southward to Point Arguello. As previously mapped, the HFZ was interpreted to bend slightly westward offshore of Estero Bay and end before reaching the Piedras Blancas anticlinorium, as shown on Figure 1-2 (Hanson et al., 2004; Willingham et al., 2013;

PG&E, 1988). In this interpretation the offshore HFZ transfers slip to the onshore San Simeon fault zone across a right step-over associated with a rhomboidal basin of Quaternary age (DiSilvestro et al., 1990; Lettis et al., 1990; Hanson et al., 2004).

Recent studies of high-resolution seismic-reflection and multibeam echosounder (MBES) bathymetric data reveal the presence of a continuous, throughgoing fault that directly connects the HFZ to the onshore San Simeon fault (Johnson and Watt, 2012). Based on this direct connection, Johnson and Watt (2012) suggest that the entire fault zone retain the name of "Hosgri," also implying that the name "San Simeon" should be abandoned. But abandoning this name would contradict the well-established literature associated with the San Simeon fault onshore (Hanson et al., 2004; Hanson and Lettis, 1994; Hall et al., 1979; Hall, 1976). For the purposes of this report, therefore, the name of the San Simeon fault zone is retained, and the boundary between the HFZ and the San Simeon fault zone is selected offshore of Cambria at the gap in evidence for continuous faulting (Plate 1). This location coincides with the northern limit of continuous traces that bound the west side of the rhomboidal basin described by DiSilvestro et al. (1990), Lettis et al. (1990), and Hanson et al. (2004), and is located northeast of the northern limit of the western branch of the Hosgri fault (Section 7.2.2).

1.3 Intended Use of the Results

The interpretations and analyses presented in this report are intended to provide information for use in characterizing faults as seismic sources under the DCPP SSHAC Level 3 Seismic Source Characterization (SSC) Project. This report provides context for a series of more specific ongoing investigations of the Hosgri and other offshore faults imaged in seismic-reflection data offshore of southern San Luis Obispo County. This project builds on earlier analyses that were presented in the *Shoreline Fault Zone Report* (PG&E, 2011), the report on the Point Buchon 3D/2D seismic-reflection investigation (PG&E, 2012), and the preliminary assessment of paleoshorelines and unconformities near the HFZ (AMEC, 2012a). The analyses completed for this project are expected to provide guidance as to where future detailed studies may be pursued.

2.0 GEOPHYSICAL AND GEOLOGICAL DATA

The following data sources served as a basis for either mapping Quaternary geologic features or facilitating comparisons to previous interpretations.

2.1 USGS High-Resolution 2D Seismic-Reflection Survey

The primary data source used for mapping Quaternary geologic features was high-resolution single-channel seismic-reflection data acquired by the USGS in 2008 and 2009 (Figure 2-1). These data were collected between Piedras Blancas and Pismo Beach along shore-perpendicular transects spaced 800 m apart extending from close to shore to beyond the 3-mile limit of California State waters. The data set also includes several widely spaced cross lines that were collected to help correlate stratigraphy between inlines. This survey was completed as part of the PG&E–USGS Cooperative Research and Development Agreement (CRADA), the California State Waters Mapping Program, the USGS Coastal and Marine Geology Program, and the USGS Earth Surface Processes Program. The data have been published as USGS Open-File Report 2009-1100 (Sliter et al., 2009).

The acquisition of the profile data was not performed under a nuclear QA (NQA) program, but it was performed in accordance with industry standards and specifications. The data were collected using a SIG 2Mille mini-sparker and EdgeTech SB-0512i chirp system (Sliter et al., 2009). The SIG mini-sparker system used a 500-J high-voltage electrical discharge, and the resulting source was received by a towed hydrophone streamer that was 15 m long. The mini-sparker source was fired at a rate of two times per second (s), which generally gave a data trace every 1 m and record lengths of 0.5 s. The EdgeTech 512 chirp subbottom-profiling system consisted of a source transducer and receiving hydrophones housed in a 500-pound “fish” towed several meters below the sea surface. The chirp source signal was 500–7,200 hertz (Hz) with a 30-millisecond (ms) sweep length, and record lengths were 0.35 s. These data were recorded in standard SEG-Y 32-bit floating-point format with Triton SB-Logger PC-based software that merged seismic-reflection data with differential global positioning system (GPS) navigation data, with digital sampling of 16 kilohertz (kHz) for the mini-sparker data and 12.5 kHz for the chirp data..

2.2 Point Buchon 3D/2D Survey

The Point Buchon 3D/2D data set was collected offshore of Point Buchon in 2010 and 2011 by Fugro Consultants (2011a) (Figure 2-2). These data were acquired to support PG&E’s analysis of faults offshore of the DCPP, including the Shoreline fault zone. The 3D data were collected at a 12.5 m line spacing; the 2D seismic-reflection data were collected at a 100 m line spacing. A total of 2,019.47 (km) of 3D/2D data were collected.

The Point Buchon 3D/2D data set was acquired and processed at specified standards as stated in the two survey data reports (Fugro Consultants, 2011a, 2011b) and the seismic data processing report (Fugro Seismic Imaging, 2011). All three reports state that the acquisition and processing of the data were done under quality control (QC) protocols as outlined in Lekkerkerk et al. (2006) and the NCS SubSea *Navigation Final Report* (NCS SubSea, 2011). These data were validated under the PG&E Geosciences QA program as specified in document GEO.DCPP.TR.12.01 R0, *DCPP 3D/2D Seismic-Reflection Investigation of Structures Associated with the Northern Shoreline Seismicity Lineament of the Point Buchon Region*, and Appendix A to that document, “Qualification of Point Buchon 3D & 2D Seismic Reflection Profiling Survey Data (October 2010 to February 2011)” (PG&E, 2012).

2.3 MBES Data

MBES bathymetry data were acquired from Estero Bay to San Luis Obispo Bay during 2007, 2009, and 2010 by the Seafloor Mapping Lab at California State University Monterey Bay. The 2007 survey covered a region near Point Buchon, the 2009 survey covered the region from Point Buchon to San Luis Obispo Bay, and the 2010 survey covered local nearshore areas at selected locations to better tie the onshore stratigraphy and structures to the offshore interpretations. The data sets were not collected under an NQA program, but they were collected in accordance with industry standards and specifications.

The data sets range from 1 m horizontal resolution for data from the 0–50 m depth range, to 2 m horizontal resolution for data from greater depths. The vertical precision of the data is ±10 centimeters (cm) (Appendix F of PG&E, 2011). Position and altitude data during data collection were obtained through an Applanix POS MV 320 v4 system with TrueHeave processing, which accounted for vessel motion such as heave, pitch, and roll (position accuracy ± 2 m; pitch, roll, and heading accuracy ± 0.02 degrees; heave accuracy ± 5% or 5 cm), with input from a C-Nav-enabled NavCom 2050 GPS. Additionally, kinematic GPS altitude data were used to account for tide-cycle fluctuations, and sound-velocity profiles were collected with an Applied Microsystems SV Plus sound velocimeter. Hillshade images that were developed from the digital elevation model (DEM) compiled for PG&E, and which contained both onshore (LiDAR) and offshore MBES bathymetry elevation models, were used for interpretation in this project. The data were maintained at International Hydrographic Survey (IHO) S-44 Special Order specifications, and across the entire MBES swath, an average of 95.8% of cross-line soundings fall within IHO Special Order tolerances, with 99.7% within IHO Order 1 (P. Iampietro, written communication to S. Nishenko, 2010).

2.4 Legacy 2D Seismic-Reflection Data

Numerous seismic-reflection surveys were collected in the vicinity of the DCPP in the 1970s and 1980s for various purposes. These surveys vary widely in line length, resolution, and depth of penetration, and were performed with a wide variety of energy sources and receiver arrays (Willingham et al., 2013; Rietman, 2011). Data from many of these surveys were transferred by PG&E into digital format to support previous assessments of seismic hazard at the DCPP (PG&E, 1988 1991). Much of the data were subsequently compiled in a database using IHS Kingdom software (referred to herein as “Kingdom”) by Fugro Consultants (2011b). The database (known as the “legacy database”) also includes the more recent USGS high-resolution 2D survey (described in Section 2.1) and the Point Buchon 3D/2D survey (described in Section 2.2), in addition to the early surveys.

The legacy data from the 1970s and 1980s were not collected under an NQA program. However, according to the PG&E Supervisor of Nuclear Quality Services, based on the pedigree of the 1988 Long Term Seismic Program (LTSP) and its acceptance by the NRC, the data generated during the 1988 LTSP is acceptable for use in the current quality related work (written correspondence from Jeff Hodges, April 10, 2013). These data sets are primarily used as follows:

- To compare the unconformities mapped as part of the current project to previously mapped unconformities, particularly those presented in Willingham et al. (2013).
- To observe stratigraphy and structure at greater depths than imaged by the USGS 2D survey.
- To observe stratigraphy and structure west of the Hosgri fault, specifically in areas beyond the western extent of the USGS 2D survey.

Legacy 2D seismic-reflection profiles that were studied for this project are listed below.

Data	QA Status	Notes
W-5-75-076A (B-B′)	Qualified per written correspondence from J. Hodges, April 10, 2013	Used to compare depths of Quaternary unconformities to regional unconformities mapped by Willingham et al. (2013)
FLEC 3 (H-H′)	Qualified as specified in written correspondence from J. Hodges, April 10, 2013	Used to compare depths of Quaternary unconformities to regional unconformities mapped by Willingham et al. (2013)

CM86-1 CM86-2 CM86-3	Qualified as specified in written correspondence from J. Hodges, April 10, 2013	Used to extend mapping of top of pre-Quaternary rock into northeastern San Luis Obispo Bay.

2.5 Geologic Data

Background geologic data including reports, maps, profiles, and digital fault and horizon files were examined to facilitate comparison of our current interpretations to previous interpretations, and to evaluate the geological/geographical context of the study area. Of these data, only the digital files containing the faults that were interpreted by PG&E from the Point Buchon 3D/2D data set (PG&E, 2012) were adopted for this study and integrated into the results presented in this report. The remainder of the geologic data (listed below) were only used for comparison to the mapping presented in this report.

Data	QA Status	Notes
Offshore geologic map from the *Shoreline Fault Zone Report* (PG&E 2011)	Not qualified	Not used as the basis of Quaternary mapping. However, locations of the Shoreline and San Luis Bay faults from this map are included on Plate 3 of this report for comparison to the new mapping described herein. .
Map of submerged strandlines from Appendix I of the *Shoreline Fault Zone Report* (PG&E 2011)	Not qualified	Not used as the basis of Quaternary mapping. However, locations of submerged strandlines from this map are included on Plate A-1 of Appendix A of this report for comparison to the new mapping described herein.
Structural trend map, annotated seismic-reflection profiles from the LTSP Final Report (PG&E, 1988, 1991)	Qualified as specified in written correspondence from J. Hodges, April 10, 2013	Not used as the basis of Quaternary mapping.
Structural trend map, annotated seismic-reflection profiles from Willingham et al. (2013)	Peer reviewed USGS publication	Not used as the basis of Quaternary mapping.
Preliminary assessment of paleoshorelines and unconformities near the HFZ (AMEC, 2012a)	Not qualified	Planning document only. Not used as the basis of Quaternary mapping. However, initial interpretations of seafloor horizons were incorporated into the final seafloor horizon.
Offshore geology and geomorphology maps from Piedras Blancas to Pismo Beach, San Luis Obispo and Santa Barbara counties, California (Watt et al., *in preparation*; draft dated February 15, 2012).	USGS publication in final preparation;.	Not used as the basis of Quaternary mapping. However, distribution of bedrock outcrops and sedimentary cover from this map were used to provide general background information for this study (Figure 1-1).

3.0 METHODOLOGY

This section describes the methodology used to map Quaternary geologic features in the USGS 2D data. The methodology for data interpretation is consistent with the geological and geophysical interpretation of seismic-reflection data outlined by Sheriff (1982), Yilmaz (2001), and Brown (2004). Quaternary geologic mapping was conducted according to the procedures described in the Project Instructions (GEO DCPP PI 12 03_LTSP) and the Project Planning Document (GEO DCPP PPD 12 02 R0_LTSP). These procedures are described in the following sections.

3.1 Flattening of USGS Seismic-Reflection Profiles

The USGS 2D data contain artifacts that were likely caused by heave and pitching of the survey vessel and hydrophones during data collection. Because of these artifacts, the seafloor and shallow reflectors appear wavy in the profiles, even in areas where the MBES data indicate the seafloor is relatively smooth. In order to improve the interpretability of shallow stratigraphy, and to facilitate mapping of Quaternary features, these data were flattened to the seafloor in areas where the MBES data indicated the seafloor is relatively smooth. These areas correspond with regions where the seafloor consists of Quaternary marine sediments.

The USGS 2D seismic-reflection profiles were flattened in Kingdom by mapping the seafloor reflector as a horizon. The seafloor reflector was mapped by digitizing the first peak reflection using the autopick-fill and 2D hunt modes set to pick the peak of the reflection within an interval of 0.0011 s, which was determined to be the most useful range for the thickness of the reflection and amplitude of the artifact waves for the USGS 2D data (AMEC, 2012a). Once mapped, the profiles were flattened to the seafloor horizon. This function set the selected horizon as an arbitrary zero value, and adjusted the remainder of the seismic-reflection profile to be displayed in relative two-way travel time (twtt; in seconds) above and below the selected horizon. An example of a profile flattened to the digitized seafloor horizon is shown on Figure 3-1. As shown on this figure, flattening the profile enhances interpretability of shallow features and improves accuracy when mapping shallow reflectors. However, the natural slope of the seafloor is lost, and the dips of reflectors are modified with this method. Analyses that required the true positions of reflectors (e.g., measuring Quaternary fault displacement) were performed on unflattened profiles.

3.2 Seismic Stratigraphic Correlation Procedures

This section describes the criteria used to develop consistent seismic stratigraphic mapping and regional unconformity correlations within the USGS 2D and Fugro 3D/2D data.

3.2.1 Mapping Procedures and Confidence Assessment

Quaternary unconformities were mapped where evident in the USGS 2D data and the Point Buchon 3D/2D data. Most of the unconformity mapping was focused on the USGS 2D data because this data set images shallow stratigraphy at a higher resolution than the Point Buchon

3D/2D data. Unconformities were interpreted as Quaternary in age if they meet the following criteria:

- They occur within sequences of relatively coherent seismic reflectors that dip gently or parallel the seafloor.
- They do not underlie a rough, presumably rocky seafloor or highly reflective rough buried surface that likely represents the top of pre-Quaternary rock.

Quaternary unconformities were mapped in Kingdom by digitizing horizons along seismic reflectors that meet specified criteria, as follows:

- Reflectors are truncated against the unconformity in onlapping, downlapping, or toplapping relationships against upper- or lower-bounding surfaces, commonly indicating a hiatus and/or variation in systems tract deposition.
- Presumed younger strata overlying an angular-eroded surface of tilted/folded older strata indicate an angular unconformity.
- Distinct coherent stratigraphic sequences are separated from surrounding stratigraphy by unconformities, such as sequences of foreset beds within shelf-edge deltas.

A stratigraphic type section was established in the western part of line PBS-50, where a series of alternating stratigraphic sequences suggests the presence of alternating sea-level lowstand and highstand deposits (Figure 3-2). These relationships represent an opportunity to estimate ages of stratigraphic horizons because the section includes at least three distinct sequences of clinoforms (seaward dipping strata) that appear to represent lowstand shelf-edge deltaic deposits. The conceptual framework for interpreting the depositional environment of these deposits is described in Section 3.2.2. Unconformities were extended regionally from this type section by digitizing horizons along the corresponding seismic reflectors as far as they could be followed in the seismic-reflection profiles. Unconformities were correlated between parallel seismic-reflection profiles by tracing reflectors along intersecting seismic-reflection profiles (“tie lines”). If unconformities could not be traced directly along “tie lines,” correlations of unconformities were interpreted based on similarities in seismic stratigraphic sequences.

The degree of confidence in the mapping and correlation of unconformities varies regionally and depends on a number of factors, including data quality and continuity, continuity of Quaternary basins, relationship to adjacent surrounding stratigraphy, and strength of reflection. In order to track uncertainties in mapping and correlation of key regional unconformities, each unconformity was divided into regions with assigned grades that ranged from A (high) to C (low) based on qualitative assessments of their lateral continuity to the type section, strength of reflection, and uniqueness. These regions were defined by digitizing “grade” polygons for each key unconformity in Kingdom. The criteria for assigning these grades are presented in Table 3-1 and in Work Instruction SSP.WI.12.03. In regions designated as having lower confidence in mapping and correlation of unconformities (i.e., grades B and C), unconformity interpretations are not unique. Within these lower confidence regions, the unconformity mapping presented in this report represents our preferred stratigraphic interpretation, but other interpretations may be allowed.

3.2.2 Identification of Systems Tracts

The concept of sequence stratigraphy was developed as a tool to define genetically related deposits of similar age. even though the lithofacies change as the depositional setting changes with distance from continental, to marginal marine, basin margin, and downslope environments (e.g., Vail et al., 1977; Posamentier and Allen, 1999). Sequence stratigraphic interpretive analysis involves identifying discrete sediment body geometries of genetically related strata (sequences) that are bounded by unconformities at their upper and lower surfaces (Vail et al., 1977). Sequences are composed of a succession of genetically linked deposition systems (systems tracts) that are diagnostic of specific parts of the sea-level cycle (e.g., highstand, lowstand, and intermediate depositional systems; Posamentier et al., 1988). Individual systems tracts contain deposits from a single sea-level highstand, lowstand, transgression, or regression. These are typically bounded by unconformities created by changes in sea level and may be both erosional and depositional in nature (Figure 3-3). In a modern environment, such as the study area, the ages of these surfaces may be estimated because the timing of late Quaternary sea-level changes are relatively well known (Figure 3-4). These sequence-bounding unconformities are the primary target of this study, as they define regionally correlative horizons of a definable age. As Figure 3-3 illustrates, the sequence stratigraphic record on the continental shelf and upper slope is composed of three primary systems tracts:

1. Highstand systems tracts. These are characterized by prograding sequences of fine-grained deposits (with respect to lowstand systems tracts) that become finer with distance offshore from the sediment source (the coastline). Because Quaternary sea-level changes have been cyclic within the past 500 thousand years (kyr; Figure 3-4), highstand systems tracts typically overlie transgressive systems tracts:
2. Lowstand systems tracts. These commonly consist of prograding deltaic deposits (clinoform sequences) developed at the shelf edge and on the continental slope. Because they are deposited during lowstands, they are not present in the central and inner parts of the shelf.
3. Transgressive systems tracts. These commonly are characterized by deposits onlapping onto the erosional transgressive surface.

The seismic signatures of system tracts were used to interpret the timing and depositional environment of the Quaternary unconformities mapped for this project.

3.2.3 Identification of Paleochannels

Buried channels, or paleochannels, are generally identified in seismic lines by their shape, disruption of reflectors, and inconsistency of infilled deposits with neighboring reflectors. Possible paleochannels incised into the continental shelf and continental slope are observed locally, and occasionally are incised into key Quaternary unconformities that were mapped for this project (Figure 3-5). When observed and correlated on either side of a fault, offset paleochannels may provide constraints on fault slip rates. However, because the USGS 2D tracklines are spaced 800 m apart, potentially offset channels cannot be positively correlated at this time.

3.2.4 Identification of Paleoshorelines

Submerged remnants of erosional paleoshorelines are identified where relatively gently seaward-sloping wave-cut platforms at their landward edges intersect relatively steeper paleosea cliffs. The point of intersection observed in cross section (e.g., in a seismic profile) is referred to as the shoreline angle (Figure 3-6). Such features were mapped when observed on the continental shelf in the seismic-reflection data. The relatively flat wave-cut platforms were digitized manually as horizons in Kingdom. The depths of shoreline angles were measured in seconds below seafloor, twtt. These depths were converted to meters using an assumed seismic velocity of 1,600 m/s, and added to the depth of the seafloor DEM (indicated by MBES data) at the corresponding location to estimate the true position of shoreline angles below modern sea level. These newly mapped paleoshorelines supplement the detailed paleoshorelines mapped between Estero Bay and Pismo Beach for the *Shoreline Fault Zone Report* (PG&E, 2011, Appendix I). Maps showing the locations of the newly mapped paleoshorelines and a brief description of the identification, documentation, and analysis of paleoshoreline features and explanatory figures are presented in Appendix A.

3.3 Fault Mapping Criteria

Numerous faults have been identified in the USGS 2D and Point Buchon 3D/2D data sets. For the purposes of this report, a fault is meant to describe a discrete, near-planar discontinuity that has accommodated relative displacement. In some parts of this report, the term *fault strand* is used to designate an individual fault in a set of closely spaced parallel or subparallel faults. Groups of structurally related, closely spaced faults are described as fault zones. Examples of fault zones within the study area include the Hosgri, Los Osos, Point Buchon, Shoreline, San Luis Bay, and San Simeon fault zones. Multiple named fault zones that are structurally related may be part of a fault system. The Hosgri and San Simeon fault zones are part of the Hosgri–San Gregorio fault system.

The seismic signature of faults imaged in the study area varies considerably, and depends on a number of factors, as follows:

- Data quality.
- The amount of vertical separation of strata or surfaces across the fault.
- The seismic signature of strata offset by the fault.

Faults that intersected Quaternary stratigraphy were identified and mapped based on the following criteria. An illustration of the fault mapping criteria used for this project is provided on Figure 3-7.

- Abrupt lateral truncation of reflectors.
- Displaced, offset, or broken reflectors.
- Correlations of offset reflectors across a fault plane.
- Acoustical anomalies (e.g., presence of diffractions, especially at a reflector termination or fault tip, or presence of laterally short and bright reflectors adjacent to a plane that appear as “flags” or contrasting acoustic signals separated by a plane).
- Visible drag and rollover of reflectors.

- Loss or substantial decrease in acoustic coherence beneath a fault plane, or distorted dips observed through a fault plane.

Continuous Quaternary faults were correlated between seismic lines based on amount, sense, and relative age of displacement, as well as consideration of strike. Many faults could not be correlated confidently between seismic lines. These faults generally exhibit less displacement and are interpreted to be less significant than the correlated faults. These faults were mapped on individual profiles but were not assigned fault names. Additionally, unassigned faults are mapped on profiles where the seismic signature may include several of the criteria listed above, but the seismic expression of the fault is weak. The tops of unassigned faults appear as "+" symbols on Plate 1.

The strike of correlated faults was measured in map view using Kingdom software by placing a protractor against the computer monitor and recording the azimuth of the fault trace. At locations where the fault strike changes across the seismic line, both measurements were recorded and were considered to represent the range of uncertainty in fault strike.

Correlated faults were named according to their associated fault zone and numbered sequentially as they were interpreted, starting with 1000. The fault zones observed and example fault names are listed below:

Fault or Fault Zone	Assigned Fault Number
Hosgri fault zone	HF####
Los Osos fault zone	LO####
Casmalia fault	CF####
Southwest Boundary Zone faults	SWBF####
San Simeon fault zone	SS####

In locations where interpreted faults deform one or more key Quaternary unconformities and coincide with faults assigned unique fault numbers in the Point Buchon Report (PG&E, 2012), those previously assigned names (fault numbers) were adopted (e.g., 11006, 51203).

Uncertainty in the location of faults that are named and correlated between seismic lines was assessed at each line intersection. Faults whose location could be constrained within an uncertainty of less than ±50 m are shown on maps in this report as solid lines. Faults with greater location uncertainty are shown as dashed lines. Faults that could not be directly interpreted on a particular profile, but whose position is inferred based on correlation to adjacent lines, are shown as dotted lines. Faults whose existence is uncertain are shown as queried lines.

It should be noted that the HFZ is a dominantly strike-slip fault zone, and vertical separation may only be present near fault bends and step-overs. The ability to recognize individual faults in the shallow marine stratigraphy is predicated on the presence of some component of near-fault vertical deformation (i.e., discrete fault offset or folding) or juxtaposition of stratigraphy due to translation. Faults without a vertical, or an apparent vertical, component of separation may not be recognized as faults, especially where the Quaternary section is thin and young (e.g., in locations with only thin sedimentary cover over bedrock) and where deformation rates are low.

3.4 Assessment of Timing and Amount of Quaternary Fault Displacement

Where regional Quaternary unconformities can be correlated across offshore fault strands, key fault parameters were recorded to assess the timing, amount, and rate of Quaternary fault deformation. These include the presence or absence of vertical separation of unconformities across the fault, the amount of vertical separation and uncertainty, the width of fault deformation, the age of the youngest deformed unconformity, and if present, the oldest unconformity that crosses the fault strand without deformation. These measurements are presented in Appendix B.

On most profiles, fault-related deformation is not limited to discrete faulting, but also includes near-fault folding. In some locations, near-fault folding *increases* the amount of on-fault deformation relative to far-field deformation (such as in a section of collapse between two transtensional fault strands), whereas in other locations, near-fault folding (e.g., drag folding) *decreases* the amount of on-fault deformation relative to far-field deformation. We interpret near-fault folding to be largely a localized phenomenon, and less representative of fault deformation at depth than far-field deformation. Therefore, vertical separation measurements used to assess fault deformation are taken from the projection of unconformities from outside the zone of observed fault deformation. The types of measurements documented that relate to the assessment of fault deformation are defined in the table below. Example vertical separation measurements are provided on Figure 3-8 to illustrate how these fault parameters were measured.

Measurements of vertical separation and uncertainty were made in seconds twtt and converted into meters using an assumed seismic velocity of 1,600 meters per second (m/s). The degree of confidence in the vertical separation measurements is variable and depends on several factors, including data quality and continuity, strength of reflection, the horizontal extent of unconformity mapping, the presence of secondary faults, folds, and the degree of deformation proximal to the fault. In order to track qualitative assessments of these factors, each vertical separation measurement was assigned a grade from A (high confidence) to C (low confidence). Additional information recorded at each Quaternary fault intersection includes apparent fault dip, dip direction, angle of intersection of the fault with the seismic profile, true fault dip, description of the structural setting, and other relevant notes (Appendix B). It should be noted that the HFZ is a dominantly strike-slip fault zone. As a result, vertical separation measurements presented in Appendix B do not represent the total fault separation.

Type of Measurement	Definition
Vertical separation	The vertical separation across a fault strand and associated secondary faults and folds. Net separation measurements were completed by projecting a given unconformity from outside the zone of fault-related deformation to the fault from each side of the fault, and measuring the vertical separation at the location of the fault strand. These are the measurements reported on Plates 2a through 2c.
Discrete vertical separation	The amount of vertical separation of a reflector measured at a fault strand. Excludes secondary folding. Discrete vertical separation was recorded only in cases where an unconformity is observed to intersect a fault on both sides.
Net vertical separation across zone	The combined vertical separation across all strands within the

	HFZ. Because there are very few profiles with offset equivalent unconformities preserved on both sides of each strand within the HFZ, these measurements also include locations where vertical separation has been measured from correlative surfaces that are not equivalent (e.g., locations where a transgressive unconformity developed in sediment on one side of a fault is correlated to the eroded top of rock on the opposite side of the fault). These cumulative measurements of net vertical separation are shown west of the HFZ on Plates 2a through 2c, and presented in Table 8-1.
Width of deformation	The horizontal distance in meters from the fault to the edge of fault-related deformation. Separate measurements were completed on each side of the fault.
Multi-fault measurement	Where zones of fault-related deformation from two or more closely spaced faults overlap and deformation could not be assigned to individual strands, vertical separation was measured across all the closely spaced faults and identified as a multi-fault measurement. For example, on the left side of the profiles on Figure 3-8, vertical separation of unconformity H30 is measured by projecting across HF1004b, HF1006, and an unassigned fault. In locations where vertical separation measurements incorporate two correlated faults, measurements of the unconformity projections were made at each fault individually, and then averaged. This average value is shown on Plates 2a through 2c and in Appendix B.
Youngest deformed unconformity	The youngest deformed unconformity correlated across the fault. For example, on Figure 3-8, fault HF1018b terminates in and deforms unconformity H30, while H10 is undeformed.
Uncertainty	Uncertainty in the vertical separation measurement reflects the maximum and minimum offsets allowed by the data.
Downthrown Direction	Sense of displacement of the unconformity across the fault, recorded as either down to the west or down to the east.

4.0 ASSUMPTIONS

In the interpretation and comparison of the USGS 2D data with other data sets, no attempt has been made to review or critique the data sets regarding their acquisition and processing. Several specific assumptions regarding these data sets were made, as follows:

1. All seismic-reflection data studied for this project are displayed in seconds twtt. Actual depths of features and dips of surfaces interpreted from the seismic-reflection data are estimated using an assumed seismic velocity of 1,600 m/s. This assumption provides a reasonable approximation of true depth of features buried within the uppermost several meters of unconsolidated sediment. However, because the velocity of seawater is generally less than 1,600 m/s, this assumption tends to overestimate the actual depth of the seafloor. Likewise, because seismic velocity probably increases with depth, and in higher-velocity materials such as basement rock, using an assumed velocity of 1,600 m/s

tends to underestimate the actual depth of deeper features observed in seismic-reflection profiles.

2. The previous studies by PG&E (2011) of the Shoreline fault zone, and the observations and data provided in these reports, are acceptable for use in this study. For example, the geologic and structural interpretation of the MBES bathymetry presented in the *Shoreline Fault Zone Report* (PG&E, 2011) is assumed to provide a good foundation for this study. This assumption is supported where georeferenced data sets overlap, showing the same structures within the limits of each survey data set.
3. The seismic-reflection data used in the Long Term Seismic Program (LTSP) report (PG&E, 1988) were collected to industry standards at the time of acquisition, and the results based on these data were carefully checked through a rigorous peer-review process, and subsequently accepted by the NRC. Based on this pedigree, these data and interpretations are considered qualified for use in this study (written correspondence from J. Hodges, April 10, 2013). .

5.0 SOFTWARE

Two primary software programs (IHS Kingdom Suite and ArcGIS) were used to interpret seismic-reflection data and to develop maps presented in this report. Kingdom is a PC-based industry, government, and academia-accepted program and was the primary seismic-reflection interpretive software used in this project. Kingdom's capabilities include viewing mapping on vertical profiles and horizontal time slices and viewing seismic lines and interpretations in 3D space. Interpretations were completed using a QA-controlled version of the IHS 2d/3dPak version 8.6 software Hot Fix 4 on a QA-verified operating system.

ESRI's ArcGIS Version 10.1 is a mapping and analysis program that is also considered acceptable software by industry, government, and academia. ArcGIS is used to georeference and map spatial data and was specifically used in this project to present interpretations made in Kingdom through maps (plates and figures). Previously interpreted geologic and structure maps (Johnson and Watt, 2012; PG&E, 2011; Willingham et al., 2013) were compared with the mapping presented in this report using both Kingdom and ArcGIS.

6.0 SEISMIC STRATIGRAPHY

The offshore late Quaternary geologic record varies significantly with changes in depth below modern sea level and horizontal position on the continental shelf and upper continental slope. This results in a unique stratigraphic record that is closely related to fluctuations in sea level. These variations in location and nature of stratigraphy are interpreted in a sequence stratigraphic framework, as described in Section 3.2.2 of this report. The efficacy of this stratigraphic framework as a tool to develop vertical slip rate estimates is predicated on our ability to (1) identify and correlate unique seismic stratigraphic horizons present throughout the project area, and (2) use the sequence stratigraphic characteristics of those horizons to develop correlations to published sea level curves for the purpose of estimating ages of offset marker horizons. This approach has previously been used to document location and timing of active deformation on the California continental margin (e.g., Burger et al., 2002; Spinelli and Field, 2003; Grossman et al., 2006; Le Dantec et al., 2010; Hogarth et al., 2012).

The expression of sequence stratigraphic horizons and their associated systems tracts in the seismic record is, above all, a function of sea level, sediment supply, and tectonic deformation (Posamentier and Allen, 1999). The rise and fall of global eustatic sea level primarily results from variations in the amount of ice stored within polar ice caps and continental ice sheets during periods of cooler climate (Figure 3-4) and is the primary driver in determining at what depth and in what manner sediments are deposited on the continental shelf and upper slope. This study does not attempt to evaluate temporal variations in sediment supply during the mid- to late Quaternary; however, we do recognize that spatial variations in sediment supply exist within the study area. Sediment accumulations overlying correlated unconformities on the outer shelf are greater in San Luis Obispo Bay than anywhere else in the study area, suggesting that sediment supply is greatest in San Luis Obispo Bay. The increased sediment supply in San Luis Obispo Bay is probably due to deposition from the Santa Maria River and other large drainages that empty into the bay (Figure 1-1; Plate 1). North of San Luis Obispo Bay, sediment supply appears limited, as suggested by the relatively small catchments of streams that drain into Estero Bay and the trapping of sediment behind the spit in Morro Bay at least during high sea level stands, and as evidenced by the restricted extent of progradational sediment packages in that region (Figure 1-1; Plate 1). The influence of tectonic deformation pattern and style of shelf deposition appears to be much less important in the study area than that of sea-level fluctuations because rates of Quaternary eustatic sea-level rise (~10–26 mm/yr. post-glacial rise; Stanford et al., 2012) and fall (~1.1 mm/yr, mean rate of fall between the MIS 5e and the Last Glacial Maximum [LGM] lowstand; Figure 3-4) are orders of magnitude greater than tectonic uplift (~0.2 mm/yr for the Irish Hills; Hanson et al., 1994) and subsidence rates (maximum subsidence of 0.19 to 0.21 mm/yr for the offshore Santa Maria Basin west of San Luis Obispo Bay estimated by Hanson et al. [2004] based on depth of the early–late Pliocene unconformity of Willingham et al. [2013]). However, tectonic deformation does influence the distribution of sediment deposition because isolated pull-apart basins and other depocenters (e.g., areas west of the HFZ) in the study area are likely tectonic in origin.

Aside from the San Luis Obispo Bay depocenter, the majority of the continental shelf in the study area is mantled with relatively thin accumulations of Quaternary sediment. Based on this, we infer that highstand deposition rates in the study area are relatively low. In San Luis Obispo Bay, greater volumes of highstand sediment combined with probable tectonic subsidence effectively protect older sections of the sedimentary record from erosion during younger sea-level fluctuations. Outside San Luis Obispo Bay, highstand deposits are preserved only locally and are limited mostly to isolated basins/grabens related to local extensional deformation in the HFZ. With a relative lack of highstand deposits in most of the study area, mapping of sequence stratigraphic boundaries is focused near the shelf break, where the sequence stratigraphic record is more complete. Because of the general lack of highstand deposits, this study focuses on lowstand systems tracts and transgressive unconformities illustrated in Figure 3-3.

The following descriptions of sequence stratigraphic units (Sections 6.1 through 6.5) are presented in the context of a sequence-stratigraphic age model, in which the youngest transgressive surface was developed during the transgression from the LGM lowstand, which ended about 19,000 years ago (19 ka), to the Holocene sea-level highstand, which began about 7 ka (Figure 3-4). A pronounced unconformity that marks the base of a shelf-edge clinoform sequence, H20, is interpreted to represent the base of deposits from the LGM lowstand. Deeper regionally-correlated unconformities, H30, and H40, are interpreted to represent erosional surfaces that result from major Quaternary sea-level transgressions. Other transgressive unconformities are recognized on some profiles but are not easily correlated because they are usually too deep to be imaged in the shallow USGS data, and hence, are not discussed separately. This is our preferred age model. Following the descriptions of sequence-stratigraphic units and bounding unconformities, in Section 6.6, we present a discussion of alternative age models and constraints on possible ages of key unconformities. Finally, in Section 6.7, we describe the unconformity mapped at the top of pre-Quaternary rock, which is the deepest unconformity mapped for this project.

6.1 Late Quaternary Transgressive Sequence (Seafloor to Unconformity H10)

Unconformity H10 is recognized throughout the project area (Figure 6-2) as the uppermost regionally correlated unconformity. Within the USGS 2D data, the unconformity is defined along the ravinement surface bounding the upper margin of the youngest lowstand systems tract. It is commonly characterized as a subtle to conspicuous angular unconformity. Unconformity H10 is best defined near the shelf break and locations with notable vertical tectonic displacement and/or tilting. Above the inferred elevation of effective wave base during the LGM (close to 130 m below modern sea level), overlying reflectors commonly define a paraconformity or subtle onlap, consistent with the transgressive systems tract (Posamentier and Allen, 1999; Figure 6-1). Below the inferred LGM sea-level elevation, overlying stratigraphy commonly defines a paraconformity atop a high-amplitude reflector. Thickness of post-H10 sediment ranges from 0 to as much as 30 m in the southern part of San Luis Obispo Bay (PBS-325, Figure 3-6). On many of the seismic profiles, particularly on the inner continental shelf and near the HFZ, the presence of H10 is inferred to be located within a few meters of seafloor but was not mapped, as it is likely obscured by the bubble pulse[1] (e.g., Figure 3-2). Where rock outcrops at the seafloor on the continental shelf, unconformity H10 is interpreted to merge with the top of rock. Unconformity H10 was not mapped on the USGS 2D data in these areas because it is better represented by the MBES bathymetry.

A shore-parallel channel-like erosion feature was noted in the feasibility study report (AMEC, 2012a), and hypothesized to be related to lowstand sea-level conditions. Detailed mapping of unconformity H10 performed for this report shows that the erosion feature is partially eroded into H10, indicating that it postdates the latest transgression. Therefore, this feature is most likely related to submarine currents (e.g., contourite drifts of Faugeres et al., 1999) rather than high-energy coastal processes.

6.1.1 Confidence Assessment

The distribution of unconformity H10 as mapped from the USGS 2D data is represented on Figure 6-2 with polygons delineating spatial differences in the strength of the interpretation. We

[1] The pulse character of the seafloor within the USGS 2D data includes a series of high amplitude reflections that parallel the seafloor and overprint possible reflections of shallow strata. This series of reflections is described in this report as the bubble pulse. Within the USGS 2D data, the bubble pulse commonly ranges from approximately 2 to 5 m thick.

assessed relative levels of confidence in the mapping of unconformity H10, delineated areas marking differences in confidence assessment, and assigned grades using the criteria presented in Table 3-1. Along much of its mapped extent paralleling the Irish Hills coastline, unconformity H10 is imaged immediately below the bubble pulse offshore of the shelf break. Near the HFZ, H10 is obscured by the bubble pulse. As a result, the mapped distribution of unconformity H10 appears as a narrow band along the western margin of the study area. Additionally, isolated grade B polygons are mapped adjacent to the fault where post-H10 strata thicken and H10 is imaged below the bubble pulse. Unconformity H10 is well preserved in San Luis Obispo Bay, where it unconformably overlies remnants of the penultimate highstand systems tract. In the northeastern part of San Luis Obispo Bay, unconformity H10 interacts with fluvial/marginal marine sediments shed by relatively large drainages, San Luis Obispo and Arroyo Grande creeks. The mapping of H10 is truncated where this interaction occurs because of uncertainty related to distinguishing the transgressive systems tract from these fluvial/marginal marine deposits.

6.2 Last Glacial Maximum Lowstand Systems Tract (Unconformity H10 to H20)

Unconformity H20 is recognized beneath the shelf break, from near the northern extent of the study area southward to a location west of Point San Luis where the shelf break becomes less distinct. Unconformity H20 may continue farther to the south; however, the seismic signature of the unconformity becomes unrecognizable, and it cannot be distinguished from adjacent reflectors above and below it. The unconformity is not recognized in San Luis Obispo Bay.

Unconformity H20 defines the base of the uppermost clinoform sequence in the PBS-50 type section (Figures 3-2 and 6-3). Where it underlies the shelf break, unconformity H20 is typically overlain by downlapping reflectors of the clinoform sequence. Farther offshore, on the upper continental slope, unconformity H20 is expressed as a paraconformity imaged as a low-amplitude reflector. Unconformity H20 does not extend above the inferred depth of lowstand sea level during the LGM, about 120–130 m below modern sea level (Stanford et al., 2011; Murray-Wallace, 2007, Siddall et al., 2003). As shown on Figure 6-3, unconformity H20 is eroded slightly into underlying parallel reflectors directly beneath the shelf break. Elsewhere, unconformity H20 is associated with prominent angular unconformities, many of which indicate significant localized erosion. These unconformable relationships and the position of the clinoform sequence localized along the shelf break are both typical of lowstand systems tracts (Posamentier and Allen, 1999; Figure 3-3). The inclined strata were likely deposited near lowstand sea level as a prograding constructional shoreline, resulting in an outbuilt shelf-margin wedge, similar to those documented by Lobo et al. (2005). Because it is the uppermost, and therefore the youngest, lowstand systems tract, the clinoform sequence and associated deposits between unconformities H20 and H10 are interpreted to have been developed during the LGM, about 20 ka.

It is unclear as to why such a prominent unconformity that is clearly associated with the base of an extensive lowstand deposit is not better preserved/imaged in the southern section of the project area below the inferred LGM elevation. We note that where it is well imaged, it is localized along the shelf break, and that the shelf break is missing in the southern part of the study area. Johnson and Watt (2012) speculate that the absence of a distinct shelf break in San Luis Obispo Bay is due to the relatively high sediment supply available, which effectively buries the shelf break and extends the Santa Maria River delta farther offshore. It is possible that the presence of a highly active delta caused progradation of the lowstand shoreline farther westward, and therefore, unconformity H20 may be present in outer San Luis Obispo Bay west of the USGS 2D survey boundary.

6.2.1 Confidence Assessment

Figure 6-4 presents a map showing the extent of unconformity H20 mapped for this project with polygons delineating spatial differences in the strength of the interpretation. We assessed relative levels of confidence in the mapping of unconformity H20, delineated areas marking differences in confidence assessment, and assigned grades using the criteria presented in Table 3-1. As shown on Figure 6-4, the aerial distribution of unconformity H20 is limited to the outer shelf from approximately 12 km south of Estero Bay and to the north.

6.3 Unconformity H30—Late Quaternary Transgressive Surface

Unconformity H30 is generally the most prominent and widely correlated unconformity in the project area, extending from San Luis Obispo Bay to the some of the northernmost seismic lines near Point Piedras Blancas. Throughout the majority of its mapped extent, unconformity H30 is characterized by a prominent angular unconformity at its base and is often associated with removal and planation of multiple underlying unconformities. It is commonly overlain by paraconformable deposits, suggesting it was followed by transgressive or highstand deposition. H30 is mapped within both Estero and San Luis Obispo Bays above the inferred depth of the LGM (about 120–130 m below modern sea level; Stanford et al., 2011; Murray-Wallace, 2007; Siddall et al., 2003). Unconformity H30 defines the transgressive surface capping the clinoform sequence of the penultimate lowstand systems tract, which is localized beneath the shelf break (Figure 3-2). Although it is commonly overlain by paraconformable highstand deposits (both above and below the shelf break), near the shelf break offshore of the Irish Hills, it is overlain by downlapping deposits that fill accommodation space created by down-to-the-west vertical displacement along the HFZ (Figure 6-5). Seismic lines in San Luis Obispo Bay image unconformity H30 continuously from depths well below the inferred depth of the LGM up to depths of approximately 60 m or 70 m below modern sea level. Above these depths, unconformity H30 has been eroded by subsequent sea-level fluctuations. Several MIS 3 sea-level fluctuations passed through depths of 60–70 m and may have overprinted the surface (Figure 3-4).

6.3.1 Confidence Assessment

As described above, H30 is the most widely correlated unconformity in the study area due to the fact that it is both well preserved and, in most places, buried deep enough that it is not obscured by the bubble pulse (as the H10 transgressive surface commonly is). Figure 6-6 illustrates the distribution of unconformity H30, symbolized by grade A, B, and C confidence assessments, which were developed using the criteria presented in Table 3-1. Unconformity H30 is well correlated along the coast-parallel tie lines (PBS-T2 and T2a, Figure 2-1) from the northern margin of Estero Bay to the northern margin of San Luis Obispo Bay. Farther south, H30 is difficult to distinguish because of poor imaging of crosslines near the fault zone at the depths of H30. One result of this poor imaging is that although H30 is clearly expressed within San Luis

Obispo Bay east of the HFZ, this region is assigned a grade B because of uncertainty in correlating it to the type section on line PBS-50. Correlation of unconformity H30 from San Luis Obispo Bay to the type section on line PBS-50 is possible at few locations, such as line PBS-56 (Figure 6-7), where the stratigraphy within the HFZ is preserved well enough to allow direct correlation from the western tie lines (PBS-T2 and T2a) to the eastern tie line (PBS-T1), and southward into San Luis Obispo Bay.

6.4 Unconformity H40—Late Quaternary Transgressive Surface

Unconformity H40 is the deepest regionally correlated unconformity imaged on the USGS 2D data in the study area. For the most part, H40 appears genetically similar to H30 in that it defines an angular unconformity that locally is eroded into clinoforms localized along the shelf edge, and it is commonly overlain by paraconformable reflectors or downlapping stratigraphy (Figure 6-8; also imaged in Figure 3-7). West of the HFZ near Point Buchon, down-to-the-west displacement has resulted in the creation of accommodation space and development of a sediment wedge overlying the unconformity, similar to the relationships described for H30 (Figure 6-5). At the type section on line PBS-50, as with other seismic lines, H40 defines the transgressive surface overlying the antepenultimate lowstand systems tract clinoform sequence (Figure 3-2). Similar to unconformity H30, unconformity H40 is mapped above the inferred LGM sea-level depth in many locations (Figure 6-9).

6.4.1 Confidence Assessment

Unconformity H40 was assigned confidence grade B for much of its mapped extent along the shelf break and into San Luis Obispo Bay (Figure 6-9). Although the seismic signature of the unconformity is commonly strong, the confidence assessment is lowered mostly because it exhibits greater vertical separation across strands of the HFZ than younger unconformities, introducing uncertainty to across-fault correlation of horizons. These correlations are often complicated due to growth of subsided basins, or erosion or uplifted surfaces. Additionally, several parts of the unconformity east of the HFZ are assigned a lower grade of C where across-fault correlations are more uncertain, or unconformities are mapped within isolated basins, thereby precluding direct correlation to the type section on line PBS-50.

6.5 Other Unconformities

Additional unconformities are mapped at a few locations within the project area. Most of these unconformities are interpreted as surfaces of intermediate age between the four described above. Additionally, an unconformity younger than H10 is locally identified. This shallow unconformity may represent the top of transgressive lag deposits and transition to highstand deposition. Several additional unconformities locally preserved beneath unconformity H40 may be earlier transgressive surfaces eroded into older lowstand sequences than the one associated with unconformity H40. These deeper clinoform sequences and unconformities could not be correlated regionally because they are imaged only locally.

Apart from those overlying the H10 transgressive surface, nearly all of these unconformities occur at depths greater than the LGM global eustatic sea-level elevation, estimated to be approximately 120 m to 130 m below modern sea level (Stanford et al., 2011; Murray-Wallace, 2007; Siddall et al., 2003). As with the regionally correlated unconformities, these additional unconformities are identified based on angular unconformities, downlap surfaces, onlap surfaces, shore-parallel erosional features, and other depositional irregularities, and likely represent systems tract boundaries for high, low, and intermediate stages of sea level throughout the middle to late Quaternary. Several of these additional unconformities are shown on Figure 3-2. These intermediate unconformities are locally useful to assist in correlation and interpretation of stratigraphy; however, because they are not correlated as widely as the four key unconformities described above, they are less useful for evaluation of fault displacements.

6.6 Considerations for Alternative Age Models

As noted above, the ultimate purpose of mapping unconformities using a sequence stratigraphic approach is to develop age estimates of regionally correlated seismic horizons in order to understand vertical slip rates on faults of the HFZ. The sequence stratigraphic framework of unconformities recognized within the study area allows for direct correlation of mapped horizons to Quaternary sea-level fluctuations. Using this approach, three of the four regionally correlated unconformities, H10, H30, and H40, are interpreted to represent erosional surfaces that result from major Quaternary sea-level transgressions. The other surface, H20, marks the base of a shelf-edge clinoform sequence that is interpreted to bound the base of a sea-level lowstand deposit. This section describes the rationale for our preferred age model, and also discusses alternative age models that may be allowed by the data. The alternative age models and supporting data are summarized in Table 6-1.

The three most distinct unconformities in the study area are interpreted as transgressive surfaces because transgressive surfaces are typically the best preserved and most readily identified in continental shelf environments (Posamentier and Allen, 1999). The primary reason for this is that across the majority of the shelf, transgressive surfaces commonly overprint regressive surfaces, resulting in significantly erosive unconformities, especially in relatively sediment-starved regions typical of the majority of the study area. The erosion represented by a transgressive surface on the continental shelf commonly results from a combination of three phases (Posamentier and Allen, 1999):

1. Wave erosion during a sea-level regression.
2. A period of nondeposition, weathering, and erosion during a sea-level lowstand.
3. Wave erosion during the subsequent transgression.

Transgressive surfaces are typically buried rapidly by transgressive and highstand deposits, increasing their chances of preservation in the sediment record (Figure 3-3). However, these surfaces will be preserved only under the following circumstances:

- Where transgressive and highstand deposits are sufficiently thick or resistant to erosion that they are not completely removed by subsequent sea-level fluctuations.
- Where relative subsidence creates accommodation space to facilitate sediment accumulation and burial, thereby protecting the surface from erosion during subsequent sea-level fluctuations.

This conceptual framework accounts for both the relative lack of sediment/unconformity preservation on the shelf, other than those associated with transgressions, and the ample preservation of unconformities below depths of eustatic sea-level minima (Figure 3-4). It should also be noted that unconformity H20, which underlies a shelf-edge clinoform sequence interpreted to be a lowstand deposit, is also the only regional horizon that cannot be consistently mapped to depths above the LGM sea level.

Unconformity H10: As described in Section 6.1, we interpret the youngest transgressive surface, unconformity H10, to represent the transgression following the LGM, with an age range of about 20–7 ka (Figure 3-4). Because it is time-transgressive, the shallower parts of the surface are younger than the deeper parts of the surface. An alternative, but less likely, interpretation of this surface is that it closely postdates the most recent transgression and it marks the boundary between transgressive system tract and the highstand system tract. However, this alternative model is inconsistent with several key observations:

- Strata between unconformities H10 and H30 near the shelf break in San Luis Obispo Bay range up to approximately 30 m or more in thickness (Figure 3-8). This significant thickness is not typical for a transgressive systems tract, which on the outer shelf typically consists of a thin coarse-grained lag between lowstand and highstand systems tracts (Posamentier and Allen, 1999).
- Unconformity H10 commonly occurs as an erosive angular unconformity (e.g., Figures 3-8 and 6-1), an uncommon relationship for the boundary between transgressive and highstand systems tracts (Posamentier and Allen, 1999).
- Where they are both disrupted by the same fault strand, unconformity H30 is usually offset significantly more than unconformity H10 (e.g., Figure 3-8), suggesting that it is significantly older than unconformity H10 (refer to Section 8.3 for a discussion of relative offset and ages of unconformities).
- Within San Luis Obispo Bay, paraconformable reflectors are preserved between unconformities H30 and H10, suggesting highstand deposition between these two surfaces.

Unconformity H30: The second youngest transgressive surface, unconformity H30 erodes clinoform sequences developed at depths similar to those interpreted as the last lowstand deposit and is also the most widely mapped unconformity in the study area. Its most likely correlative transgression followed the penultimate sea-level lowstand during MIS 6 at 135 ka, terminating at MIS 5e approximately 125 ka (Figure 3-4). It is unlikely that the penultimate transgressive surface represents an intermediate-stage lowstand, such as MIS 3 or MIS 4 (Figure 3-4), because the shelf-edge clinoform sequences it erodes are observed at depths well below those that might be expected for either of the intermediate lowstands. In addition, within San Luis Obispo Bay, unconformity H30 is overlain by paraconformable reflectors at depths shallower than the LGM sea level, and these reflectors were subsequently truncated during the formation of unconformity H10. These reflectors are smooth and continuous, consistent with sedimentation in relatively deep water from a distal source (e.g., during a sea-level highstand). These reflectors do not exhibit clinoforms or chaotic reflections as would be expected for deltaic or high-energy nearshore deposits. The presence of these highstand reflectors above the LGM sea level suggests that a highstand occurred after the development of H30 and before the development of H10. The most likely age of this highstand is MIS 5 (~80–125 ka).

Unconformity H40: The age of unconformity H40 is less well constrained than shallower unconformities because it is not as well preserved as unconformity H30 and cannot be traced as far into San Luis Obispo Bay as either H10 or H30. However, an obvious choice for the age of this transgressive surface is the transgression from the MIS 8 lowstand to the MIS 7 highstand, which occurred approximately 250–240 ka. This choice is logical because MIS 8 is the glacial maximum that precedes MIS 6 (the preferred age for unconformity H30). One drawback to this interpretation, however, is that oxygen isotope records suggest that minimum sea level during MIS 8 may have been as much as 20–30 m higher than the MIS 6 sea level (Figure 3-4). Despite the drawback, this is our preferred interpretation.

Another viable alternative age for unconformity H40 is the transgression from MIS 10 to MIS 9, which occurred approximately 340–330 ka. This interpretation has the benefit of inferring that unconformity H40 followed a very deep lowstand (Figure 3-4). This would explain the pronounced angular unconformity commonly associated with H40. However, a drawback to this interpretation is that it implies that an additional major lowstand occurred between the development of H30 and H40. No additional clinoform sequences suggesting lowstand deposition have been identified in the study area between those associated with H30 and H40.

The limiting maximum possible age of unconformity H40 is difficult to constrain. However, broad estimates for the limiting maximum age of H40 are possible by comparison to broad patterns observed in Quaternary sea-level curves and by comparison to deeper unconformities for which age constraints are available (e.g., the Early-Late Pliocene unconformity [ELP] of Willingham et. al. [2013]). Stacked oxygen isotope ($\delta^{18}O$) records for Quaternary sea-level fluctuations published by Lisiecki and Raymo (2005) suggest that the magnitude of global eustatic sea-level fluctuations increased during the late Quaternary. According to the Lisiecki and Raymo (2005) curve, the oldest Pleistocene sea-level lowstand with $\delta^{18}O$ ratios as low as the LGM was MIS 16, which occurred approximately 625 ka. Prior to that, all lowstands in the 5.3 Ma record exhibit $\delta^{18}O$ ratios notably less extreme than that of the LGM, suggesting that global eustatic sea level during these earlier lowstands was not as low as it was during the LGM. Comparison of the depth of H40 to the depth of the ELP indicates that H40 is much shallower than the ELP (Figures 6-10a and 6-10b). Willingham et al. (2013) report that the ELP ranges in age from 3.5 Ma to 2.7 Ma. Assuming constant sedimentation rates since the middle Pliocene suggests that unconformity H40 is only a small fraction of the age of the ELP, which does not contradict an estimate of 625 ka as the limiting maximum age of unconformity H40.

6.7 Top of Pre-Quaternary Rock

The top of pre-Quaternary bedrock is recognized throughout nearly the entire project area east of the HFZ as a high-amplitude basal reflector underlying generally subhorizontal Quaternary sediments. West of the HFZ, the reflector inferred to be the top of pre-Quaternary bedrock is observed only between the northern end of Estero Bay and Point Piedras Blancas where the primary fault zone traverses the continental shelf. The amplitude of this reflector is highly variable reflecting differences in impedance contrasts between varying types of Quaternary sediments overlying the unconformity and underlying bedrock lithologies. Bedrock in this region is also variable, and includes Pliocene and Miocene marine basin sediments, volcanic rocks, and Mesozoic basement rocks of various lithologies (PG&E, 2011). Low-amplitude reflections marking the top of pre-Quaternary bedrock probably result from a moderately to steeply dipping contact or low impedance contrast, or both. In these instances, the horizon is recognized as the interface between well-imaged coherent bedding (inferred to be Quaternary sediments) and chaotic or semitransparent units (inferred to represent the underlying bedrock). No correlation confidence assessments were developed for the top of pre-Quaternary bedrock.

Mapping of the top of pre-Quaternary bedrock was completed to assist in the identification of structural features such as fault grabens, fault scarps, and structural highs, particularly in areas where the bedrock shelf is buried by several tens of meters of sediment, and structural trends cannot be resolved with bathymetry alone (Figure 6-11). In addition, recognition of the bedrock surface provides a means of qualitatively estimating vertical displacement of horizons that intersect faults as a buttress unconformity against bedrock. Significant observations regarding the top of pre-Quaternary surface are discussed in Section 7.

7.0 CONSTRAINTS ON OFFSHORE FAULT ACTIVITY

Plate 1 presents an overview of the fault mapping performed for this project. The faults are color-coded according to the age of the most recent deformation indicated on each intersecting seismic-reflection profile (i.e., deformation of H10, H20, H30, and H40). Deformation may be expressed as either discrete faulting or fault-related folding, or both. At locations where the stratigraphic record is well preserved, this categorization closely approximates the age of most recent deformation on the faults (e.g., fault HF1018b on the right side of Figure 3-8). However, where significant sections of the record are missing, such as in regions of eroded seafloor, the minimum age of faulting cannot be directly constrained (e.g., fault HF1049 on the right side of Figure 6-7). Therefore, this map generally represents the maximum allowable age of most recent fault activity at each line crossing. With the exception of those segments where there is clear evidence of no deformation of unconformities H30 and H40 (e.g., fault HF1033 on Figure 3-7), the map does not present constraints on the minimum age of faulting.

Plates 2a through 2c present the same fault mapping at a larger scale, together with measurements of vertical separation of key unconformities across the faults. Vertical separations were measured using the procedures described in Section 3.4, whereby offset equivalent unconformities could be correlated across fault strands. These measurements and their uncertainties are shown as triangles on Plates 2a through 2c, and they are color-coded based on the age of the unconformities. Locations where key unconformities cross fault strands without apparent deformation are designated by squares of the corresponding color. Because they were measured from the projections of undeformed parts of the unconformities, these vertical separations include discrete fault offset and also near-fault folding. The folding incorporated in these measurements is typically limited to within about 100–300 m of a fault strand. At some locations, progressive tilting of older unconformities and growth between unconformities suggest larger-scale folding during the Quaternary within a few kilometers of fault strands. This larger-scale folding was not included in the offset measurements presented in this report. Therefore, the vertical separation rates presented in this report may underrepresent the total vertical separation rate of the faults at depth.

The following sections describe general characteristics of faults mapped for this project and the constraints on their activity provided by the seismic stratigraphic mapping described in Section 6.

7.1 San Simeon Fault Zone

Directly south of Point San Simeon, the offshore continuation of the San Simeon fault is clearly evident in seismic-reflection data (Plates 1 and 2a). These faults may be traced continuously for about 7.5 km south of Point San Simeon. Together, the two offshore traces of the San Simeon fault strike approximately 328 degrees (Plate 1). The amount of vertical separation of shallow Quaternary sediments along this reach (probably highstand deposits) appears minimal (<10 ms). These faults strike slightly more northerly than the onshore traces of the San Simeon fault zone with a strike of approximately 322–326 degrees (Hanson and Lettis, 1994). Due to the shallow, localized, and discontinuous nature of late Quaternary sediment on the inner continental shelf, none of the unconformities mapped for this project can be traced across the two offshore traces for use as vertical strain markers.

7.2 Hosgri Fault Zone

As shown on Plate 1, the HFZ consists of a zone of faulting that ranges from about 1 km to 4 km wide. Although numerous short strands are mapped within the fault zone, the dominant strands that exhibit evidence for the most late Quaternary activity are readily correlated between seismic lines and range in length up to about 15 km. Together, these dominant strands make up a relatively linear, continuous fault zone that extends from its northern end offshore of Cambria to the southern end of the study area offshore of Point Sal. Additionally, a western branch of the HFZ is composed of a set of short, discontinuous traces (HF1024 and HF1023) that diverge from this linear fault zone and extend northwest to approximately 12 km south of Point San Simeon. A more detailed discussion of the western branch follows in Section 7.2.2.

Within the study area, we divide the HFZ into five "reaches," based on changes in fault trace complexity, amount and sense of vertical separation, relationships to adjacent crustal blocks, and relationships to intersecting faults (Figure 7-1). These reaches differ somewhat from the reaches defined by Hanson et al. (2004). The most notable difference is that we now recognize a continuous fault connecting the San Simeon fault (onshore, in the northern part of the project study area) to the Hosgri fault in Estero Bay. This continuous fault locally bounds the western side of an asymmetric basin, which was interpreted by Hanson et al. (2004) as a step-over basin separating the Hosgri fault from the San Simeon fault. We define this as the Cambria reach, which extends from offshore of Cambria southward to a complex intersection with the Los Osos fault zone (LOFZ) and the western branch of the Hosgri fault within the deepest part of Estero Bay (Plate 1). The other four reaches, the Western Branch, Irish Hills, San Luis Obispo Bay, and Point Sal reaches, are similar to those defined by Hanson et al. (2004). The reaches defined here are also similar to the "sections" defined by Johnson and Watt (2012), and many of the same features that separate those sections are also used to separate the reaches presented here, although the Irish Hills and San Luis Obispo Bay reaches both incorporate more than one section. The five reaches of the Hosgri fault defined by this study are described below.

7.2.1 Cambria Reach: Offshore of Cambria to Estero Bay

The Cambria reach of the HFZ traverses the continental shelf from the northern end of the fault offshore of Cambria to a complex intersection with the offshore LOFZ and the western branch of the Hosgri fault at the deepest part of the shelf break in Estero Bay (Figure 7-1). The northern end of fault HF1034 marks the northernmost extent of evidence for faulting along the northward projection of the Hosgri fault in seismic-reflection profiles. This point lies about 6.5 km south of the southern limit of clearly defined San Simeon fault traces. Although no faulting is directly observed between these two points, a continuous fault is inferred because the faults project toward each other with only a slight bend of approximately 4–6 degrees, and seismic imaging is poor within this region of youthful, probably unconsolidated sediments overlying basement rock. South of this point, the HFZ widens into an increasing number of subparallel fault strands until it reaches a zone of up to four subparallel traces about 1.5 km wide at the southern end of the reach in Estero Bay (Plate 1). The southern limit of this reach is defined as the location where offshore faults diverge southeastward from the HFZ along the trend of the LOFZ.

The two primary fault strands in this reach, HF1030 and HF1034, are approximately 100 m apart and parallel for over 7 km. These two strands change strike from approximately 333 degrees offshore of Cambria, to a more northerly 339 degrees in the center of the reach near lines PBS-229 and PBS 212, then back to 326–328 degrees at the southern end of the reach. These two strands separate an elongate, asymmetric structural basin on the east from a block of uplifted bedrock on the west (Figures 7-2 and 6-11). Growth of strata within this basin indicates progressive westward tilting toward fault HF1030 during the late Quaternary. Unconformities within the basin are separated from the top of rock west of the fault, commonly by several tens of meters (Figure 7-2; Plate 2a). Vertical separations of unconformities from the top or rock reach a maximum on line PBS-210, with H10 nearly 20 m lower than the top of rock, H30 approximately 50–55 m, and H40 approximately 100 m lower than the top or rock, respectively (Plate 2a). As shown on Plate 2a, estimates of vertical separation decrease to the north and south of line PBS-210, toward the margins of the basin. Some of the relief on unconformity H10 is likely due to original relief on the H10 ravinement surface between the rocky platform on the west and the sedimentary basin on the east instead of tectonic displacement on the fault. During the transgression that created unconformity H10, it is likely that a fault-line scarp developed along fault HF 1030 as the result of differences in resistance to erosion of materials on opposite sides of the fault. This interpretation is supported by the common erosional rounding of the top of the scarp, which suggests that the scarp was present during the post-LGM transgression and the development of unconformity H10. It is also supported by the relatively small amount of vertical separation measured across HF1030 (2.4 m ± 0.8 m down to the east) and the absence of deformation of H10 across HF1034 observed on line PBS 232, the only line within the entire Cambria reach where unconformity H10 is preserved across either of these strands (Plate 2a).

Vertical separation estimates from deeper unconformities (H30 and H40) to the eroded top of rock are more uncertain than estimates for unconformity H10. Vertical separation of unconformity H10 can be interpreted as a maximum estimate because H10 was developed during the most recent transgression, and as a result, the bedrock surface west of the fault has been protected from erosion since that time. However, unconformities H30 and H40 are interpreted to be significantly older, and the shelf has undergone full cycles of sea-level transgression and regression since their development, which suggests that the bedrock surface may have been lowered by erosion since the development of unconformities H30 and H40. However, despite this unconstrained uncertainty, estimates of vertical separation of these older unconformities are valuable for comparison to each other and to unconformity H10, and for evaluation of patterns of deformation along the HFZ.

In the deeper part of Estero Bay, faults within this reach offset Quaternary stratigraphy, facilitating the measurement of vertical separation of key unconformities (Plate 2a). Near the southern end of the Cambria reach, fault HF1030 and the adjacent parallel HF1014 consistently displace horizons down to the east. Combined, unconformity H20 is displaced from 4.8 to 14.4 m down to the east, whereas H30 is displaced from 3.2 to 14.4 m, and H40 is displaced from 18.4 m to 28 m across these two faults. Although unconformity H10 is not mapped in this section because it is likely masked by the bubble pulse directly below the seafloor, both HF1030 and HF1014 can be traced upwards to the base of the bubble pulse, which suggests that they may deform the H10 unconformity. Near the southern end of the reach and east of HF1034, a series of three short faults are mapped subparallel to and approximately 700–800 m east of HF1034 and HF1030. These faults offset Quaternary sediments down to the east within the asymmetric graben. Vertical separation of H10 ranges from 0.8 m to 4 m, H30 ranges from 0.8 m to 4.4 m, and H40 ranges from 2.4 m to 19.2 m on these three faults. In summary, the primary strands of the Cambria reach deform the H10 unconformity in a dominantly down-to-the-east sense.

7.2.2 Western Branch: Estero Bay to Piedras Blancas Fold Belt

Near the intersection with the LOFZ in Estero Bay, the HFZ divides into two branches, the Western reach and the Cambria reach (Plate 1; Figure 7-1). The western branch consists of two faults that extend approximately 15 km to the northwest of the intersection and underlie the shelf break west of the Cambria reach. Along this reach, the faults in the Western reach typically separate uplifted rock on the east from Quaternary sediments of the upper continental slope on the west. These faults are imaged discontinuously and may be confidently correlated only for distances up to about 5 km. Much of the gap of 5.6 km between these correlated faults may be due to poor imaging resulting from presumed shelf-edge landslide deposits obscuring the image of faults at depth. However, at least one profile, PBS-235, exhibits evidence for unfaulted reflectors of probable Tertiary age, which extend continuously between the projections of these two strands, indicating that the two faults do not connect in the shallow subsurface. The two fault strands commonly underlie a series of well-preserved clinoform sequences.

Unconformity H40 crosses fault HF1023 fault without apparent deformation, and unconformity H30 crosses fault HF1024 without apparent deformation, indicating that no vertical displacement has occurred on the fault since those unconformities were developed (Figure 7-3; Plate 1). These strands approximately overlie the faults that make up the northern reach of the HFZ described by Hanson et al. (2004) and Willingham et al. (2013).

The western branch of the HFZ has been interpreted to transfer slip northward from the primary HFZ to the Piedras Blancas fold belt, a system of shallow northwest-trending folds that deform Tertiary strata south and west of Point Piedras Blancas (Hanson et al.,2004; Johnson and Watt, 2012; Willingham et al., 2013). A number of discontinuous fault strands and unassigned faults were mapped on the continental shelf to the north and northwest of the western branch of the HFZ. These faults may be related to this inferred connection. Sediment is very thin or absent on most of this part of the shelf, and no Quaternary unconformities older than unconformity H10 overlie these discontinuous strands to assess Quaternary activity. Similarly, because no Quaternary unconformities interact with the Piedras Blancas fold belt, these folds were not mapped as part of this project.

7.2.3 Irish Hills Reach

The Irish Hills reach is defined as the reach of the HFZ that bounds the western margin of the Irish Hills uplifted block. The fault marks the shelf break in the northern part of this reach (Figure 7-1). Along the southern and central parts of this reach, the HFZ traverses the outer continental shelf. Although most of this reach is characterized by a relatively simple, straight, narrow zone of faulting, the northern and southern boundaries are marked by wider, significantly more complex zones of faulting. The northern end of this reach is marked by a series of faults that diverge from the HFZ to the southeast, interpreted as the intersection with the offshore LOFZ. The southern end of this reach is marked by a complex zone of faulting up to about 2 km wide that is associated with an isolated zone of uplifted bedrock about 3 km long that extends through the entire fault zone (Figure 6-11). This zone of uplifted rock appears to disrupt most of the primary fault strands and to deflect the fault zone slightly to the west. It separates a relatively simple linear fault zone to the north from a much broader distributed fault zone to the south.

In the northern part of this reach, the HFZ is characterized by the convergence of the LOFZ from the southeast and the western branch from the northwest. The primary strand of the HFZ in this area of convergence, HF1014, is over 11 km long, and trends 323–331 degrees along its length. East of this strand, a series of faults diverge toward the southeast. The most recently active and most continuous of these are primary strands of the offshore LOFZ zone: LO1000, LO1001, and LO1002 (Plate 1). These faults are described in more detail in Section 7.3. Between these two primary fault zones of the HFZ and the LOFZ, several short faults deform the shallow rock surface beneath Estero Bay, and locally bound small, enclosed structural basins and tectonic ridges (Figure 6-11). These short faults locally deform horizons as young as H10, but are typically associated with little to no measurable vertical offset (less than 5 m for unconformity H30 and unconformity H40; Plate 2b). Several additional faults were identified within this region on individual seismic-reflection profiles, some of which deform mapped Quaternary unconformities; however, these faults could not be correlated because of variability in sense and/or youth of displacement between profiles (Plate 1).

South of HF1014, fault 10001 is the primary strand of the HFZ for its entire mapped length of approximately 16 km. The northern part of this strand strikes approximately of 333–334 degrees, whereas the southern part of the strand strikes approximately 337 degrees. A narrow pressure ridge on the east side of this strand (at line PBS-21) is marked by an elongate rock outcrop approximately 100 m wide and 500 m long that protrudes from the sediment-covered seafloor approximately at the location of this bend. The association of this pressure ridge with a bend in the fault was first suggested by Johnson and Watt (2012). Along the northern end of this strand, fault 11006 converges with fault 10001 from the southeast. These two strands bound a rock ridge approximately 4 km long and up to 500 m wide that separates a semi-enclosed Quaternary basin to the east from a thick sequence of Quaternary outer-shelf strata to the west. The eastern margin of this semi-enclosed basin strikes parallel to fault HF1013 (Figure 6-11). At the northern end of this ridge, where the two faults converge, the net deformation across the two faults is down to the east, with vertical separation of H30 of 12.4 m, and of H40, 15.2 m.

Near the southern end of 11006, the ridge between these two faults gives way to a subtle graben, and the sense of vertical separation on these two faults reverses. On line PBS-34, fault 11006 separates uplifted bedrock and Quaternary sediment to the east from the graben-filling sediments to the west. Here, the fault offsets H10 approximately 2.8 m down to the west. The west side of this small graben is marked by fault 10001, which offsets H30 approximately 1.6 m down to the east; however, together with the adjacent unassigned faults, the total vertical separation of H30 between the strata to the west and the base of the graben is approximately 14.9 m. This is the same graben that was identified at the northern end of the Point Buchon 2D/3D seismic-reflection study area (PG&E, 2012).

Between lines PBS-20 and PBS-30, fault 10001 defines the boundary between a region of shallow uplifted rock to the east (the Islay Shelf region of the Irish Hills block [PG&E, 2011]) and a thick sequence of Quaternary sediment to the west (the offshore Santa Maria Basin [Hanson et al., 2004; Willingham et al., 2013]). Because this fault separates a rocky platform from a Quaternary basin, there are no offset equivalent unconformities or surfaces that can be used to measure vertical separation (Plate 2b). However, some constraints on vertical separation may be inferred based on the presumed correlation of transgressive surfaces of erosion to the planated top of rock. Figure 7-4 is an excerpt of line PBS-23 illustrating the relationship between shallow, planated rock to the east and transgressive erosional surfaces to the west. On the right side of Figure 7-4, H10 is clearly expressed as an angular unconformity truncating underlying reflectors directly beneath the bubble pulse on the west side of fault 10001. This unconformity aligns with the erosional top of rock east of fault 10001 with approximately 0.8 m ± 0.8 m of vertical separation down to the west. Although these are not offset equivalents, because the transgressive surface is eroded into sediment west of the fault and rock east of the fault, they likely resulted from the same transgression and probably were a continuous surface when developed.

A similar correlation of H10 to the planated top of rock on line PBS-22 suggests approximately 2.4 m ± 0.8 m of vertical separation down to the west across fault 10001. Given that H30 is also a transgressive surface, it is likely that it was once approximately continuous with the planated top of rock east of the fault. Subsequent downfaulting across fault 10001 could have created accommodation space to allow for deposition of the downlapping sediments that bury H30, and for preservation of those deposits during the subsequent transgression that created H10. As shown on Figure 7-4, H30 is currently approximately 13.6 m lower on the west side of fault 10001 than the top of rock on the east side of the fault. This value should be considered approximate, however, because it is likely that the planated top of rock was lowered during the pre-LGM regression and post-LGM transgression. Furthermore, it may have been eroded slightly lower than the top of rock when it was initially developed, similar to unconformity H10 (as discussed above). Within this reach, H30 is consistently observed to be on the order of 10–20 m lower on the west side of fault 10001 than the top of rock on the east side of fault 10001, reaching a maximum of 26.7 m on line PBS-21 and a minimum of 7.2 m on line PBS 28. Net vertical separation across all strands of the HFZ is presented on Plate 2b.

West of fault 10001 and north of Point Buchon, a system of short north-trending faults was mapped on the Point Buchon 3D/2D data (PG&E, 2012). Most of these faults are deeply buried and do not extend above the seafloor multiple at a depth of approximately 200–220 m. Folding above the tips of three of these faults (51105, 51111, and 51203) deforms unconformities H30 and H40 down to the east. Because we have developed additional information to characterize these faults, they are shown on Plates 1 and 2b. The remainder of these north-trending faults do not deform any of the unconformities mapped for this project, and therefore they are not included on Plate 1 or Plate 2b.

At the southern end of this reach, the fault zone abruptly widens to about 2 km and strain appears distributed among five or more strands (Plate 1). These strands have a variable strike (315–340 degrees), and where they intersect Quaternary unconformities, they exhibit variable amounts of vertical separation (0.8–7.2 m of H30 and 0.4–10 m of H40; Plate 2b). This increased complexity is associated with a zone of uplifted bedrock about 3 km long that crosses the entire fault zone from line PBS-27 south to line PBS-52 (Figure 6-11; Plate 2b). Within this zone of shallow bedrock, faults are identified from juxtaposition of distinct rock types, or subtle ridges or steps on the seafloor, but no Quaternary stratigraphic markers are available to constrain the rate or youth of faulting. If these markers had been present at one time, they have subsequently been stripped by erosion. Likewise, if transgressive or highstand deposits are present in this region, they are too thin be distinguished beneath the bubble pulse. The top of bedrock surface and unconformities H40 and H30 become progressively deeper to the north and south of this bedrock zone, which suggests that this uplift has been active during the late Quaternary period.

7.2.4 San Luis Obispo Bay Reach

The San Luis Obispo Bay reach of the HFZ is characterized by a relatively broad zone of faulting up to about 3 km wide that extends from the zone of bedrock uplift west of Point San Luis southeast to the northern limit of shallow bedrock northwest of Point Sal (Figure 7-1). The eastern margin of the HFZ bounds the western extent of bedrock at the seafloor southwest of the Irish Hills, and also beneath the sediments of San Luis Obispo Bay farther to the south (Figure 6-11). Within the fault zone and to the west, the top of bedrock is not observed in the USGS 2D data. Here, the fault separates San Luis Obispo Bay from the offshore Santa Maria basin (Willingham et al., 2013). Within this reach, no distinct shelf break is observed (Figure 7-1). Instead, shallow sediment, most likely sourced from the onshore Santa Maria River, underlies a smooth, gradually sloping shelf.

The northern part of the San Luis Obispo Bay reach is characterized by a 2 km wide distributed zone of deformation that includes several assigned Hosgri fault strands with variable strikes (~320–340 degrees) and many unassigned faults. At the northernmost extent of this reach, south of the region of uplifted bedrock described above, near lines PBS 25 and PBS-18A, shallow strata are tilted and eroded within and adjacent to the fault zone, and correlated Quaternary unconformities commonly are not available to assess recent fault deformation. Where measurable, vertical separation across these faults is also variable, with measurements on the western strands for H30 ranging 1.6–12 m, and for H40 ranging 7.2–44 m, with dominantly down-to-the-east deformation (Plate 2c). The eastern strands juxtapose bedrock to the east against Quaternary sediment to the west in an apparent buttress unconformity; therefore, no correlative markers exist to constrain vertical separation on the eastern strands. Although offset of the most recent transgressive surface could not be directly measured, a maximum offset of 3.6 m down to the west across the easternmost fault strand (HF1005) in this set may be estimated by correlating the planated bedrock surface to the east with unconformity H10 to the west (Line PBS-48).

Downfaulting between the bounding strands of the fault zone has created a small Quaternary basin within the northern part of the San Luis Obispo Bay reach of the HFZ, the boundaries of which are well illustrated by structure contours on the top of pre-Quaternary rock (Figure 6-11). The deepest part of this basin occurs near line PBS-56, where Quaternary sediments in the basin have been deformed, both through discrete faulting and folding (Plate 1). The presence of a basin here may result from right transfer of slip to the eastern strands of the HFZ (HF 1049 and HF1005) from the western strands of the HFZ (HF1004b and HF1003) or from transtension due to prominent right bend in HF1004b, or a combination of the two. However, a set of west-northwest-trending folds within the basin adjacent and approximately parallel to HF1049 (Plate 1) attest to a dominance of northwest-directed dextral shear. HF1003, the western-bounding fault strand in this zone, exhibits the most vertical separation in the area (up to 11.2 m and 23.2 m of down-to-the-east separation of H30 and H40, respectively [Plate 2c]). Line PBS-13a (Plate 1) marks the southern end of this Quaternary basin. Immediately south of PBS-13a, the graben east of HF1004b is narrow and lacks large-scale folds and a sharp eastern boundary (Figure 6-11).

Farther south, the HFZ offsets sediments of San Luis Obispo Bay, and the broad spatial distribution of three prominent unconformities, H10, H30, and H40 allows for a more complete assessment of vertical separation across this reach of the HFZ than reaches to the north. HF1004b is the primary strand of the HFZ for over 18 km in the southern part of the San Luis Obispo Bay reach. Along its length, HF1004b maintains a strike between approximately 330 and 345 degrees, with several minor bends. The fault strand deforms shallow Quaternary strata along most of its length with down-to–the-east separation ranging from 0.8 to 5.6 m, 1.6 to 17.6 m, and 2.4 to 44 m, for unconformities H10, H30, and H40, respectively. However, within the central part of San Luis Obispo Bay, high-amplitude shallow reflectors obscure deeper stratigraphy. As a result, vertical separation of H30 and H40 cannot be measured along much of the length of HF1004b. Whereas HF1004b maintains a relatively consistent trend across the majority of San Luis Obispo Bay, the eastern strands, located approximately 2.5–5.5 km east of HF1004b, bend dramatically along their 14 km length. In southern San Luis Obispo Bay, between lines PBS 282 and PBS-288, these strands exhibit significantly more vertical separation of Quaternary unconformities than the central and northern parts.

Vertical separations across the southern part of the eastern strands range from 0 m to 3.2 m of H10, 3.2 m to 15.6 m of H30, and 11.2 m to 19.2 m of H40 down to the west. The decrease in vertical separation coincides with the occurrence of a north-trending fault (HF1017) that connects the eastern and western strands, and a marked 12 degrees bend in the eastern strands. Within this zone (PBS-279A), the eastern strands exhibit evidence for vertical separation of 0.8 m of H10, 4.0–4.8 m of H30, and 13.6 m of H40 down to the west. Farther to the north, a separate west bend of 24 degrees accompanies another decrease in down-to-the-west vertical separation to 0.4–1.2 m of H10, 0.8–2.4 m of H30, and 1.6–5.6 m of H40, down to the west (Plate 2c). Combined with HF1004b, these vertical separations suggest the presence of a subtle graben between the eastern and western strands of the HFZ. As shown on Figure 7-5, these eastern strands are significantly less active than HF1004b.

The southern end of this reach includes the intersection of a system of shallow folds that extend to the southeast, parallel with the Casmalia fault (Hanson et al., 2004; Willingham et al., 2013).

This intersection approximately coincides with the southern termination of HF 1019 (Plates 1 and 2c).

7.2.5 Point Sal Reach

The Point Sal reach of the HFZ extends from the southern end of fault HF1018 northwest of Point Sal southward to the southern end of the study area (Figure 7-1). Within this reach, the fault zone separates relatively shallow rock of the Point Sal block from the thick section of sediments of the offshore Santa Maria Basin (Figure 6-11; Hanson et al., 2004; Willingham et al., 2013). The northern boundary of the Point Sal reach accompanies a distinct change in the style of Quaternary separation. North of line PBS-318, the HFZ is expressed as two separate, widely spaced strands bounding a subtle transtensional graben, with net vertical separation down to the east. South of this line, the HFZ is much narrower and generally separates shallow rock to the east from a deep sedimentary basin to the west. As with the San Luis Obispo Bay reach, the fault zone traverses a smooth, gradually sloping shelf, and no distinct shelf break is evident.

Within the Point Sal reach the HFZ is a narrow zone of up to three parallel strands that strike approximately 330–340 degrees and range up to approximately 1 km apart. In the northern end of this zone, the two eastern strands bound a sediment-filled basin. However, the most recent displacement on the easternmost strand separates the H30 down to the east. The western strand in this zone, HF1020, is the most continuous and exhibits evidence for the most recent deformation of the three. This strand marks the western margin of an approximately 700 m wide anticline and the eastern margin of a deep sedimentary basin. This strand vertically offsets H10 by 0.4–3.2 m, H30 by 2.4–6.4 m, and H40 by 6.8 m down to the west. Line spacing south of PBS-318 is variable and as much as four times greater than the typical 800 m spacing of the survey to the north. As a result, the fault mapping is less well constrained here than to the north.

At the northern boundary of the Point Sal reach, on line PBS-317, a buried rock ridge occurs directly west of the HFZ, northward of the Point Sal block (informally defined here as the northern limit of shallow bedrock east of the fault). The highest point of the ridge is approximately 32 m beneath the seafloor (144 m below sea level) and is buried by unconformity H30. Other unconformities are evident within the sediment that buries this ridge, but they are not correlated. West of fault HF1020 the ridge ranges from about 160 to 280 m wide where imaged on line PBS-317. No comparable bedrock is imaged east of HF1020 or the adjacent HF1004b within the USGS 2D data, which provides clear imaging to a depth of about 112 m below the seafloor (225 m below sea level) at this location. This ridge may represent a sliver of the Point Sal block translated northward by right lateral slip on the western traces of the HFZ.

7.3 Los Osos Fault Zone

The offshore LOFZ consists of a broad zone of faults in Estero Bay that extends west-northwestward across the continental shelf from offshore of Morro Bay and curves northward to eventually merge with the HFZ at the boundary between the Cambria reach, the Irish Hills reach, and the western branch of the HFZ (Plate 1). Although numerous faults were identified on individual seismic profiles, many of which deform Quaternary strata, relatively few strands maintain similar sense, amount, and recency of displacement from line to line. Only those consistent strands are correlated between seismic lines. The correlated strands generally exhibit more vertical separation than the surrounding unassigned faults, and are interpreted to be the primary strands of the offshore Los Osos fault (Figure 7-6).

The primary strands of the LOFZ in the eastern part of Estero Bay, including LO1001 and the western third of LO1002, are associated with a marked step of about 10–20 m down to the north in the top of pre-Quaternary bedrock (Figure 6-11). This and younger unconformities are not constrained north of LO1002 and east of LO1005, but shallow stratigraphy suggests that the top of bedrock may descend even farther to the north and east, particularly at the northeastern end of line PBS-19 (Plate 1). This drop in the bedrock surface may be the western boundary of a structural basin previously identified to the east, beneath the southern part of Morro Bay (Lettis and Hall, 1994). Structure contours from Lettis and Hall (1994) on the top of Tertiary surface beneath Morro Bay indicate that the deepest part of the basin reaches a depth of 189 m below sea level immediately east of the eastern ends of lines PBS-19 and PBS-34. For the purposes of this report, no attempt has been made to resolve the depth or boundaries of this possible offshore extent of the Morro Bay basin due to uncertainties in the seismic signature of the (possible) Quaternary strata, and the absence of correlated Quaternary unconformities overlying this possible nearshore basin. However, further characterization of the Morro Bay basin (both onshore and offshore) should improve the understanding of the style and rate of deformation associated with the LOFZ.

Offshore strands of the LOFZ generally dip moderately to the southwest (Figure 7-6). On some profiles, the dip decreases near the surface as it intersects Quaternary stratigraphy. For example, on line PBS-264, the fault dips approximately 56 degrees to the south; however, as the fault approaches the seafloor, the dip decreases to a minimum of 26 degrees. Here, folded reflectors in the hanging wall indicate Quaternary activity, although the age of these reflectors is not known; the key unconformities mapped for this study could not be extended into this part of Estero Bay because of gaps in data or patches of chaotic shallow reflectors.

Farther offshore, where the LOFZ intersects mapped Quaternary unconformities, the primary strands exhibit a consistent sense of vertical separation down to the northeast that generally increases to the north (Plate 2b). Vertical separations of unconformity H10 across the primary Los Osos fault strands range from 0.8 ± 0.4 m to 5.6 +0.8/–1.2 m down to the east; vertical separations of unconformity H30 range from 2.8 ± 0.8 m to 6.4 +1.2/–1.6 m down to the east; and vertical separations of unconformity H40 range from 2.4 ± 0.8 m to 7.2 ± 0.8 m down to the east (Figure 7-6). These patterns of fault dip and sense of vertical separation are consistent with the offshore LOFZ accommodating reverse-oblique faulting.

At its northern end, the LOFZ merges with the HFZ (Plate 1). A bedrock ridge that is about 200–400 m wide marks the boundary between the LOFZ and the HFZ. The eastern side of the ridge is bounded by strand LO1000, and the western side of the ridge is bounded by HF1051 (Figure 6-11). The convergence of the LOFZ with the HFZ marks the southern end of a long asymmetric basin along the east side of the HFZ (Figure 6-11).

7.4 Shoreline Fault

The surface traces of the Shoreline fault are mapped primarily in the rocky part of the inner continental shelf, directly offshore of the Irish Hills (PG&E, 2011). This part of the fault does not intersect any of the Quaternary unconformities mapped for this project, and therefore, is not directly addressed in this report.

At its southern end, the Shoreline fault zone is inferred to extend southward from the rocky part of the continental shelf into the sediment-filled San Luis Obispo Bay (PG&E, 2011). South of this inferred extension, shallow strata are imaged on the USGS 2D seismic-reflection data that can be used to evaluate potential evidence for or against late Quaternary deformation. We examined the shallow strata south of the mapped extent of the Shoreline Fault zone in detail and observed no evidence for a fault that disrupts Quaternary stratigraphy in San Luis Obispo Bay (Figure 7-7). As shown on Figure 7-7, shallow strata that overlie the top of pre-Quaternary rock on line PBS-42 are not disrupted along the southward projection of the Shoreline fault zone. This relationship indicates one of two possibilities:

1. The Shoreline fault zone terminates to the north and does not cross line PBS-42.
2. The Shoreline fault zone crosses line PBS-42, and the slip rate on the fault is too low to be detected in the shallow strata in this part of San Luis Obispo Bay.

An approximate age of the strata that cross the southern projection of the Shoreline fault zone may be inferred from sea-level curves that document the timing and rate of sea-level rise during the post-LGM transgression. Line PBS-42 shows unfaulted reflectors that unconformably overlie and lap onto an erosional unconformity at the top of an acoustically chaotic sequence that we interpret as pre-Quaternary bedrock (Figure 7-7). This surface occurs at a depth of approximately 65–75 m below modern sea level. This erosional surface was likely developed by wave erosion during the post-LGM transgression, and the reflectors overlying it likely represent post-LGM transgressive and highstand systems tracts. Late Quaternary sea-level curves indicate that sea level passed these depths between 13 ka and 12 ka (Stanford et al., 2011), suggesting that the deeper part of this sequence of reflectors is approximately 12–13 ka. Given this probable age, if the Shoreline fault zone extends southward and crosses line PBS-42 (alternative 2, above), the unfaulted shallow reflectors indicate an absence of vertical separation within the resolution of the data, which we estimate to range from approximately 0.2 ms to 0.5 ms (~0.2–0.4 m) for this part of line PBS-42. These relationships and uncertainties imply a limiting maximum vertical separation rate of 0.01 millimeters per year (mm/yr) to 0.03 mm/yr on any potential fault inferred to intersect these strata.

Within this region, we also examined the structure contour map of the surface of pre-Quaternary bedrock. Although it is not a precise constraint because the spacing of the USGS 2D lines is fairly wide (800 m), it is interesting to note that no sharp step is evident in the top of pre-Quaternary surface along the southward projection of the Shoreline fault (Figure 7-8). The absence of a step in this sloping surface suggests that very little vertical or lateral displacement has occurred on the south projection of the Shoreline fault during the Quaternary period. This finding is consistent with a relatively low preferred slip rate (0.2-0.3 mm/yr) interpreted by PG&E (2011) for the Shoreline fault to the north.

7.5 Pecho Fault

The Pecho fault was originally identified during studies by PG&E for the Long Term Seismic Program (LTSP; PG&E, 1988). According to the LTSP Final Report, the Pecho fault was inferred from offshore geophysical data in San Luis Obispo Bay and an alignment of bathymetric scarps offshore of the Irish Hills.

As described on page 2-137 of the LTSP Final Report (PG&E, 1988):

> "The Pecho fault is expressed geomorphically by a trend of discontinuous seafloor scarps that extends about 5 kilometers from near the Hosgri fault zone at the latitude of Pecho Creek southeast toward San Luis Obispo Bay. The trend is featured by irregular, southwest-facing scarps in Franciscan or middle Tertiary bedrock.…
>
> Evidence of Quaternary activity along the Pecho fault is observed along the southeastern end of its northern trace in San Luis Obispo Bay (Figure 2-53). Sedimentary rocks believed to be of Wheelerian (early Pleistocene) age are separated about 17 meters by what is interpreted on high-resolution seismic reflection profiles to be a vertical fault)…
>
> Near the junction of the northern and southern traces of the Pecho fault, geophysical records show that the late Wisconsin unconformity is elevated up to 6 meters across the northern trace. The uplift may be due to faulting which suggests that slip occurred on this part of the northern trace of the Pecho fault within the past 18,000 years."

Our examination of USGS 2D seismic-reflection profiles and MBES bathymetry at the locations where the Pecho fault was originally identified (PG&E, 1988) revealed no evidence for faulting except for a few minor faults that disrupt deep Quaternary stratigraphy in eastern San Luis Obispo Bay (Plate 1). Unfaulted reflectors along the projections of these faults indicate that they extend no farther than 2.4 km along strike. Furthermore, they do not parallel the previously mapped Pecho fault, and they are buried by unfaulted reflectors much deeper than the late Quaternary unconformities mapped for this project.

Figure 7-7 shows unfaulted strata crossing previously mapped traces of the Pecho fault. This profile crosses near the junction of the northern and southern traces of the Pecho fault, where a step in the late Wisconsin unconformity (described in this report as the post-LGM transgressive surface) was inferred to represent late Quaternary activity on the fault. As described in Section 7.4, the observation of continuous reflectors crossing the previously mapped trace of the Pecho fault indicates no deformation within the past 12–13 kyr. Given the uncertainties in data resolution, the maximum allowable vertical rate on an inferred Pecho fault at this location is 0.01–0.03 mm/yr.

Figure 7-8 shows the location of the Pecho fault as mapped by PG&E (1988) overlain on structure contours of the top of pre-Quaternary bedrock mapped for this project. As shown in this figure, no significant step in this surface coincides with either the northern or southern traces of the Pecho fault, with the exception of a minor deflection at the southeastern limit of the northern trace (e.g., the eastern end of line PBS 282; see Plate 1 for location of line). The age of these strata is uncertain because none of the Quaternary reflectors mapped for this project could be extended confidently to this part of San Luis Obispo Bay. However, the significant depth (~145–165 m) of the top of pre-Quaternary surface and overlying reflectors suggests that they are substantially older than the Quaternary unconformities mapped for this project.

As described above, the northern part of the Pecho fault was originally interpreted to offset the rocky part of the continental shelf offshore of the Irish Hills (PG&E, 1988). High-resolution MBES bathymetric data from this part of the shelf show a series of parallel continuous ridges crossing the alignment of scarps that was originally used to infer the location of the Pecho fault (Figure 7-8). These bathymetric ridges have been interpreted as the result of differential erosion between bedding planes within Tertiary sedimentary rock (PG&E, 2011). The continuity of Tertiary strata across the alignment of scarps indicates that the scarps do not result from any single, continuous fault, and that they must have been formed by other processes.

At the locations that where evidence for the Pecho fault was originally observed, examination of higher resolution bathymetric and seismic-reflection data reveals that no northwest-trending, southwest-vergent, Quaternary-active reverse fault is present. Therefore, we recommend that PG&E remove the Pecho fault from future maps of Quaternary active faults.

7.6 Wilmar Avenue Fault

A region of uplifted, folded, and faulted strata is located offshore of the City of Pismo Beach along the trend and south of the Wilmar Avenue fault in water depths of about 10–20 m (Figure 7-9; Plate 1). These structures are mapped parallel to and up to about 1 km south of the offshore Wilmar Avenue fault as mapped by PG&E (2011), which is marked by a prominent rocky ridge that protrudes from the sediment-covered seafloor (Plate 3). The close proximity and parallel strike of these structures with the main trace of the Wilmar Avenue fault suggest that these may be secondary strands of the Wilmar Avenue fault zone, perhaps footwall breakout faults. The uplifted fold shown on Figure 7-9 aligns with a subtle ridge evident in the shaded-relief topographic image south of Highway 101, onshore, to the east (Plate 1), suggesting that these structures may continue onshore. Lines PBS 314 and PBS-10 show synclinal folding in reflectors between these structures and the Wilmar Avenue fault (Plate 1; Figure 7-9). The amount and timing of deformation could not be directly assessed because none of the key Quaternary unconformities mapped for this study could be confidently correlated across these folds or faults. However, the top of pre-Quaternary bedrock is partially mapped across the offshore structure and it indicates that much of the folding in the uppermost section is Quaternary.

7.7 Casmalia Fault

Evidence for a fault that discretely ruptures shallow Quaternary stratigraphy along the offshore trend of the Casmalia fault was observed on only one line in the USGS 2D seismic-reflection data set (Figure 7-10, Plate 1). However, this fault displaces unconformity H10, suggesting it has ruptured since the postglacial transgression. The Casmalia fault is associated with a significant step in the top of pre-Quaternary surface. Structure contours on this surface indicate that the intersection of the Casmalia fault with the HFZ marks the lowest point in this surface within the study area. Further evidence for latest Quaternary activity is a broad fold that extends to the northwest from Point Sal and is observed on several seismic-reflection profiles (Plate 1). Vertical separation across this fold and fault has continued during the late Quaternary, decreasing from about 13 m of vertical separation of H40 to about 4 m separation of H30 and 1.2 m separation of H10. Based on age estimates from our preferred age model, these measurements of vertical separation imply rates of 0.05, 0.03 and ~0.07 mm/yr respectively (Plate 2c; Appendix B).

8.0 INTERPRETATION OF OFFSHORE FAULT ACTIVITY

Plate 3 is a compilation map of Quaternary active faults in the study area. This map includes our interpretation of the location and activity of faults based on the constraints presented in Sections 3.3 and 7, respectively, of this report. The map also includes faults interpreted to be Quaternary active that were previously mapped and characterized by others. Faults are color-coded according to their recency of activity, as follows:

- Latest Quaternary (latest Pleistocene to Holocene)(blue)—Deforms H10. Fault strands are observed to deform unconformity H10 at one or more locations. Deformation may be expressed as either discrete faulting or fault-related folding.
- Likely latest Quaternary (latest Pleistocene to Holocene) (orange)—Fault strands are not directly observed to deform unconformity H10, but other evidence suggests latest Pleistocene to Holocene activity. Examples that fit into this category include fault strands that are aligned with other strands that do deform unconformity H10 and they significantly deform older unconformities, but younger unconformities are missing due to erosion or masking by the bubble pulse.
- Late Quaternary (green)—Deforms H30 or H40. Fault strands are observed to deform unconformity H30 or H40 and are overlain by an undeformed H10 unconformity.
- Quaternary (purple)—Does not deform H30 or H40. Fault strands displace older Quaternary deposits, but are overlain by unconformity H30 or H40 without deformation.
- Unknown (black)— Fault strands without information about the age of most recent deformation are classified as indeterminate. Examples that fit into this category include fault strands that deform bedrock but are either buried by unfaulted sediment of unknown age or are not buried by sediment.
- Unclassified (gray)—Faults compiled from other studies without age designations.

8.1 Faults Mapped for This Project

As shown on Plate 3, most strands of the HFZ are demonstrated to be latest Pleistocene to Holocene. There are two significant exceptions to this. The first is an 8 km section of the fault that extends from the latitude of the DCPP to the south. Unconformity H10 and much of the rest of the shallow stratigraphic section is missing from this region due to active uplift and erosion within the fault zone. Evidence for this uplift is described in Sections 7.2.3 and 7.2.4. Within this region, strands of the HFZ are classified as likely latest Pleistocene to Holocene based on their alignment and apparent continuity with strands that deform unconformity H10 both to the north and south. The other significant exception is the western branch of the HFZ. Both primary strands of the western branch of the HFZ (HF1023 and HF1024) are classified as late Quaternary because they are both clearly overlain by unconformities H30 or H40, neither of which exhibits any evidence for younger deformation.

The Quaternary activity of two other offshore faults is constrained by the seismic stratigraphic mapping performed for this study. Three primary strands of the LOFZ are classified as latest Pleistocene to Holocene because they deform unconformity H10 in at least one location. Additionally, although it is observed to rupture Quaternary stratigraphy on only one seismic-reflection profile, the Casmalia fault is classified as latest Pleistocene to Holocene because it deforms unconformity H10. As described in Section 7.7, the Casmalia fault is primarily expressed in the shallow subsurface as a system of northwest-trending folds that deform unconformity H10 and older surfaces. The folds may be fault propagation folds.

8.2 Faults Compiled from Other Studies

Four additional offshore faults, the Shoreline, Point Buchon, San Luis Bay, and Wilmar Avenue fault zones, are included on Plate 3 based on evidence for their activity presented in previous studies; however, no additional evidence was developed for this project to characterize their activity. A discussion of these faults is presented below.

8.2.1 Shoreline Fault Zone

The Shoreline fault zone is included on Plate 3 because, although no geologic evidence for Quaternary deformation has been identified for this study at the south end or at any other location along the Shoreline fault zone by PG&E (2011), it is associated with a trend of historical microseismicity (Hardebeck, 2010; PG&E, 2011). The mapped extent of the Shoreline fault zone is adopted from PG&E (2011).

8.2.2 Point Buchon Fault Zone

The Point Buchon fault zone as mapped by PG&E (2012) is included on Plate 3 primarily because of its intermediate position between the Shoreline fault zone to the south and the HFZ to the north. At its northern end, the Point Buchon fault zone aligns with HF10006, which locally exhibits evidence for deformation of unconformity H10. To the south, the Point Buchon fault zone projects toward the Shoreline fault zone and likely is the northern extension of the Shoreline fault zone. Based on these inferred correlations, the Point Buchon fault zone may be Quaternary active even though it does not clearly deform the top of pre-Quaternary rock (post-LGM transgressive surface) along most of its length (PG&E, 2012). Based on the inferred connection with the Shoreline fault zone, and the evidence for little to no vertical separation of top of pre-Quaternary rock (post-LGM transgression) the slip rate is interpreted to be very low. The mapped traces of the Point Buchon fault zone are adopted from PG&E (2012).

8.2.3 San Luis Bay Fault Zone

Although surface traces are very limited in extent, the San Luis Bay fault zone is included on Plate 3 because it deforms marine terraces onshore between Olson Hill and Rattlesnake Creek ranging in age from MIS 5a to MIS 5e (~80–125 ka; Hanson et al., 1994; PG&E, 2011). A planated bedrock surface offshore of Olson Hill and Rattlesnake Creek that has been interpreted as the offshore extension of the MIS 5a marine terrace is also deformed down to the south, suggesting that the San Luis Bay fault extends offshore to the west (PG&E, 2011). Correlation of submerged offshore marine terrace strandlines suggests that down-to-the-south deformation continues farther offshore to the HFZ approximately at the northern limit of bedrock exposure on the shelf southwest of the DCPP (PG&E, 2011). The fault zone extends eastward at least to San Luis Obispo Creek near Avila Bay, where a strand of the San Luis Bay fault displaces fluvial terrace deposits radiocarbon dated to 21 ka. The mapped traces of the San Luis Bay fault east of the Shoreline Fault zone are adopted from AMEC (2012b). The inferred western extension of the

San Luis Bay fault zone is adopted from the seismic source model presented in PG&E (2011) but its location is uncertain.

8.2.4 Wilmar Avenue Fault

The Wilmar Avenue fault is included on Plate 3 because it deforms marine terraces onshore within the city of Pismo Beach (Lettis et al., 1994) and because it has an apparent relationship to faults mapped for this project immediately south of its offshore extension. Deformation of MIS 5a and MIS 5e terraces onshore (~80 ka and 125 ka, respectively) indicates late Quaternary activity. Additional offshore fault strands to the south of the primary trace, perhaps related to footwall breakout, are observed to deform reflectors of unknown Quaternary age (Section 7.6) and therefore do not provide additional constraints on the age of fault activity. The mapped traces of the Wilmar Avenue fault zone are adopted from AMEC (2012b).

8.3 Analysis of Vertical Separation and Implications for Age Model

In order to test alternative age models, we examined the amount of vertical separation exhibited by sets of two or more unconformities offset by the same fault strands. The rationale for this is that older unconformities should be offset more than younger unconformities, and if the rate of vertical separation across the fault strand is relatively constant, the relative amounts of separation should correlate approximately with the relative ages of the unconformities.

Within the study area there are 37 locations where vertical separations are measured for both unconformities H10 and H30. At each location, the ratio of the vertical separation of H10 to the vertical separation of H30 was calculated. These ratios range from 1 to 14, and include one outlier value of 44. The mean of these ratios (excluding the outlier) is 4.2. However, this should be considered a minimum because ratios are calculated only on strands where both unconformities were preserved and displaced; locations where one of the unconformities is not offset were not incorporated. When the analysis is expanded to include locations with an observed vertical separation of 0, the number of locations rises to 61. This expanded analysis is based on the interpretation that the faults have continued to deform but the amount of deformation is below the limit of our ability to detect the deformation. Therefore, at locations where we observe no deformation in the USGS 2D data, an assumed vertical separation of 0.2 m is used to calculate ratios between H10 and H30. The mean of the ratios in the expanded analysis is 9.7 (again, excluding the outlier).

There are 80 locations where both H40 and H30 unconformities are preserved across fault strands and are available to constrain fault activity. The mean of the ratios between measured vertical separation across H40 and H30 is 2.2. When this analysis is expanded to include observations of no deformation, the mean of the ratios between H40 and H30 is 3.3. A similar analysis comparing H10 to H40 indicates that the mean of ratios between the two unconformities is 8.7, excluding observations of no deformation (based on 23 observations), and 22.6 when observations of no deformation are included (based on 39 observations). The results of this analysis are summarized below.

Unconformities Compared	Mean Ratio of Vertical Separation Measurements, Excluding Observations of No Deformation[1]	Mean Ratio of Vertical Separation Measurements, Including Observations of No Deformation[1,2]
H30/H10	4.2 (n = 37)	9.7 (n = 61)
H40/H30	2.2 (n = 80)	3.3 (n = 93)
H40/H10	8.7 (n = 23)	22.6 (n = 39)

[1] n equals number of measurements.

[2] Observations of no deformation (zero values) are given values of 0.2 m because this is judged to approximate the lower limit of resolution of the USGS 2D data.

Assuming a constant vertical slip rate, these ratios support an age model in which unconformity H30 is at least 4 times older than unconformity H10, and perhaps as much as 10 times as old. They also suggest that unconformity H40 is between 2 and 3 times as old as unconformity H30, and that unconformity H40 is between about 10 and 25 times as old as H10. These ratios are consistent with the preferred age model presented in Section 6.6. They are inconsistent with the alternative minimum age model presented in Section 6.6, in which unconformity H30 was assumed to have developed during the post-LGM transgression, and therefore is only slightly older than unconformity H10. The ratio of H40 to H10 suggests that if H10 was developed during the post-LGM transgression (~19–7 ka), then H40 is likely not more than 500,000 years old (i.e., ~20 ka multiplied by 25, the approximate ratio of offset of H40 to offset of H10).

8.4 Fault Interactions

The patterns of Quaternary active offshore fault strands presented here are similar to those mapped by Johnson and Watt (2012) and Hanson et al. (2004). We recognize the HFZ as a nearly continuous, approximately linear fault, similar to what is shown on previous maps, that extends at least 84 km from approximately offshore of Cambria to the southern limit of the study area offshore of Point Sal (Plate 1). The HFZ is also inferred to connect directly to the San Simeon fault to the north (Plate 1). The interaction between the HFZ and the San Simeon fault is discussed in Section 8.4.1, below.

Three Quaternary faults merge with the HFZ in the study area: the LOFZ, the Point Buchon fault, and the Casmalia fault (Plate 3). Each of these faults strikes northwest. The two northern faults, the LOFZ and the Point Buchon fault zone, both change strike as they approach the HFZ, bending northward to become nearly parallel to the HFZ (Plate 3). At the locations were these faults merge with the HFZ, structural basins filled with Quaternary sediment occur between their northern ends and the primary traces of the HFZ (Figure 6-11). The basin at the northern end of the LOFZ is significantly larger, measuring up to approximately 2 km wide by 14 km long. As described in the following section, this basin may not be related to the convergence of the LOFZ with the HFZ, and may instead result from a releasing step-over between the Hosgri and San Simeon faults. The basin at the northern end of the Point Buchon fault is substantially smaller, reaching maximum dimensions of approximately 1 km by 5 km. Active growth of this basin may result from a right step in slip between active traces of the HFZ at the location where the Point Buchon fault converges with the HFZ. Although it is not observed to merge with the HFZ, the

San Luis Bay fault is also inferred to merge with the HFZ. This possible interaction is discussed in Section 8.4.2, below.

8.4.1 Hosgri–San Simeon

The existence of a basin between the HFZ in Estero Bay and the San Simeon fault onshore to the north has long been recognized (DiSilvestro et al., 1990; Lettis et al., 1990; Hanson et al., 2004; Johnson and Watt, 2012). This basin has been consistently interpreted as the result of slip transfer across a right step between the right-lateral HFZ and the right-lateral San Simeon fault. The primary difference in interpretation between earlier studies (DiSilvestro et al., 1990; Lettis et al., 1990; Hanson et al., 2004) and more recent studies performed with the benefit of high-resolution bathymetric and seismic-reflection data (Johnson and Watt, 2012) is the width of the step-over and the existence of a potential connecting fault. Whereas the earlier interpreters described this basin as occupying a right step-over approximately 5 km wide, based on a postulated extension of the San Simeon fault along the linear Cambria coastline, Johnson and Watt (2012) note that the basin reaches a maximum width of 2,400 m. They, interpret the basin as the result of paired fault bends rather than a step-over between separate faults. They describe these paired bends and the basin as a lazy-Z pull-apart basin, following the terminology of Mann (2007). Our mapping supports the interpretation presented by Johnson and Watt (2012). We note that the eastern margin of the basin (shown on Figure 6-11 as the location where structure contours indicate a steepening of the top of bedrock) approximately aligns with the southward projection of the onshore part of the San Simeon fault. Therefore, we interpret the width of the basin (which we measure to be approximately 2 km) to scale approximately with a large-scale releasing bend between the HFZ in Estero Bay and the San Simeon fault onshore.

As indicated in Section 7.2.1, deformation of unconformities within the elongate structural basin along the Cambria reach is dominantly down to the east along primary strands bounding the western margin of the basin. This sense of displacement contrasts with the 0.1 mm/yr uplift of onshore marine terraces observed east of this location along the Cambria coastline north of Estero Bay (Muhs et al., 1992). The most likely explanation for this discrepancy is that fault deformation is localized within the basin and does not control regional patterns of uplift and subsidence. This interpretation is preferred over the postulated presence of an intervening fault between the basin and coastline, because the high-resolution MBES data do not indicate the existence of a significant throughgoing fault east of the structural basin.

The current configuration of the linkage between the Hosgri and San Simeon faults may be relatively youthful. The asymmetric basin described above is interpreted to result from right transfer of slip between the HFZ and the San Simeon fault zone. Vertical separation estimates from this basin are higher than from anywhere else in the study area (Table 8-1), suggesting a fairly rapid vertical separation rate in this basin (on the order of 0.5 mm/yr to 1 mm/yr). As noted above, these large vertical separation estimates may be enhanced by differential erosion across fault HF1030. If these rates were representative of the last few million years, this basin would be on the order of 1.5–3 km deep. Instead, the basin is relatively shallow and small. As shown on line PBS-209, (Figure 7-2), westward tilting of reflectors within the basin increases with depth, and deformation of H40 appears to represent nearly half the total depth of the graben. As a rough estimate, assuming a constant deformation rate, the basin itself is only about twice the age of

H40, about 500 ka to 700 ka with a maximum of 1.2 Ma (assuming a limiting maximum age of 625 ka for H40).

8.4.2 Hosgri–Shoreline/Hosgri–San Luis Bay Fault

Southwest of the DCPP, in the vicinity of line PBS-25, the HFZ increases in complexity and appears to be deflected slightly to the west. As described in Sections 7.2.3 and 7.2.4, bedrock within the fault zone, as well as folding and growth of late Quaternary reflectors adjacent to the bedrock, indicates that this region has undergone late Quaternary uplift. One possible explanation for this, suggested by Johnson and Watt (2012), is that the deflection is the surface expression of a sidewall ripout (as defined by Swanson, 2005). In this scenario, the sidewall ripout is created by a region of stiff crust that impinges on the Hosgri fault due to right-lateral translation along the Shoreline fault, which is located to the northeast and trends more westerly than the Hosgri fault.

As an alternative explanation, we propose that this zone of fault complexity and apparent left step could by caused by the intersection of the Hosgri fault with the west-trending, south-vergent San Luis Bay fault. The left step in the Hosgri fault is located at the intersection with a magnetic lineament that was proposed by PG&E (2011) as a possible offshore extension of the San Luis Bay fault. Although there is no surface expression of an offshore fault along this magnetic lineament, it represents one of two possible locations for the offshore extension of the boundary between the Irish Hills, which are constrained by Quaternary marine terraces to be rising at a rate of 0.2 mm/year, and San Luis Hill, which is constrained to be rising at a rate of 0.06 mm/yr (PG&E, 2011). In this scenario, uplift on the north side of a blind, north-dipping, west-trending San Luis Bay fault could impinge on the shallow part of the Hosgri fault, leading to a left step in the Hosgri surface trace.

No data were developed by this project that could resolve which of these explanations is correct.

8.5 Implications for Style and Rate of Deformation of the Hosgri Fault

The fault mapping and offset measurements presented here support the characterization of Quaternary activity on the HFZ as predominantly right-lateral strike-slip deformation, consistent with previous interpretations presented by Johnson and Watt (2012), Hanson et al. (2004), and PG&E (1988). Specific evidence for right-lateral strike-slip deformation is as follows:

- The HFZ is a long, generally linear fault.
- Fault strands within the HFZ are generally steeply dipping to vertical within the shallow subsurface imaged in the USGS 2D high-resolution seismic-reflection data (approximately the uppermost 50–250 m).
- Sense of vertical separation across the HFZ changes along strike.
- Contractional deformation and uplift are observed at locations where primary strands of the HFZ step to the left; extensional deformation and subsidence are observed where primary strands of the HFZ step to the right.
- The HFZ is interpreted to connect directly with the San Simeon fault onshore, where evidence is documented for Holocene and late Pleistocene right-lateral deformation (Hanson and Lettis, 1994; Hall et al, 1994).

Although a dominantly right-lateral sense of displacement for the HFZ may be inferred based on the observations listed above, no additional features, such as dated piercing points, were identified with which to constrain lateral slip rate. Although several channels were identified in the seismic lines, the orientation of tracklines perpendicular to the fault, and the wide spacing of tie lines limited the potential for identifying such piercing points.

8.5.1 Sense and Rate of Vertical Separation

In the study area the full amount and rate of net vertical separation across the HFZ are well constrained at only a few locations for the following reasons:

- Localized poor imaging in seismic-reflection data.
- Apparent fault-related folding within or near the fault zone that is not included in the vertical separation measurements.
- Absence of offset equivalent unconformities on both sides of each strand of the fault zone on a particular seismic line.

Consequently, the sum of vertical separation measurements across the HFZ rarely captures the total vertical separation across the zone. Despite this limitation, the measurements of vertical separation at the locations discussed below provide valuable information about the patterns, style, and rate of deformation on various strands of the HFZ.

Estimates of amounts and rates of vertical separation across the HFZ are presented in Table 8-1, including rates of vertical separation previously interpreted by other authors (Hanson et al., 2004; Johnson and Watt, 2012). Vertical separation rates presented by Hanson et al. (2004) were calculated from separation of the early-late Pliocene unconformity (ELP) mapped by Willingham et al. (2013) using an assumed age of approximately 2.8 Ma. Vertical separation rates reported by Johnson and Watt (2012) were calculated from analysis of the same data we use (the USGS 2D data); however, many of the vertical separation rates given by Johnson and Watt (2012) are described as a range for a fault section and are not tied to a specific measurement or line number.

The vertical separation rates reported by Hanson et al. (2004) differ in scale from the rates presented here. As shown on Figure 8-1 (Figure 16 of Hanson et al., 2004), these rates were based on vertical separation of the ELP unconformity[2] measured up to several kilometers from the fault strands. Because of this, these vertical separations incorporate faulting and folding, as well as depositional relief on the ELP unconformity. As shown on the schematic profile taken from San Luis Obispo Bay and presented in Figure 8-1, although far-field net vertical separation is reported down to the west, the actual offset relationships across the fault plane are down to the east. While this technique may be appropriate for relatively old surfaces, such as the ELP, we do not consider it appropriate for the Quaternary unconformities studied for this report, because the unconformities studied herein are not planar surfaces. Instead, they curve and slope as they traverse the continental slope, to the outer shelf and inner shelf. This original relief on the unconformities is much larger than the magnitude of vertical fault separation accumulated since

[2] Hanson et al. (2004) report that these vertical separation rates may be minima due to possible erosion of the unconformity east of the HFZ. Hanson et al. (2004) also report maximum vertical separation rates by adding maximum coastal uplift rates east of the fault zone to vertical separation rates calculated from the seismic reflection data.

the unconformities were developed. This difference in scale may explain why vertical separation across the San Luis Obispo Bay reach of the HFZ is reported by Hanson et al. (2004) to be down to the west, but is interpreted from the higher resolution data analyzed for this project to be down to the east (Table 8-1; Section 8.5.1.4).

8.5.1.1 Cambria Reach

In the Cambria reach the net Quaternary vertical separation is dominantly down to the east, accommodating growth of the asymmetric structural basin that occurs directly east of the main strands of the HFZ along most of this reach. Measurements of vertical separation are uncertain because the primary strands of the HFZ juxtapose bedrock against Quaternary sediment; therefore, vertical separation is estimated from correlative, but not equivalent, surfaces (refer to the discussion in Section 7.2.1). Despite this uncertainty, estimates of vertical separation rates across the HFZ are greater for the Cambria reach than anywhere else within the study area (Table 8-1). Estimates of vertical separation rates reach a maximum near the northern end of the basin between lines PBS-230 and PBS-209 (Table 8-1; Plate 2a). These lines coincide with a double bend in HF1030, the primary strand of the HFZ (Plate 1), which was described by Johnson and Watt (2012) as the cause of the asymmetric structural basin. Here, maximum vertical separation rates of 0.87–1.29 mm/yr down to the east are provided by separation of unconformity H10.

Alternative rates between 0.29 mm/yr and 0.42 mm/yr down to the east are provided by vertical separation of unconformities H30 and H40. Notably, the vertical separation rates implied by the two older unconformities are relatively stable, despite the fact that H40 is significantly older and the shelf was subject to wave erosion during at least one cycle of regression and transgression between the periods during which the two unconformities were developed. This stability in vertical separation rates suggests that the rate of tectonic vertical separation across the fault has been relatively constant, and that erosional lowering of the bedrock surface has a relatively small effect on the rate estimates. Therefore, although bounding minimum and maximum estimates of vertical separation rates are not well constrained for these older unconformities, the approximate vertical separation rates of 0.29–0.42 mm/yr provided by H30 and H40 are interpreted to better represent the true tectonic rate of vertical separation across this part of the HFZ than the maximum rates implied by separation of unconformity H10.

Our estimates of vertical separation rates across the HFZ decrease along the Cambria reach to the north and south from the center of this basin. Our estimates of vertical separation rates within the lazy-Z basin compare favorably with the rate of less than 1.0 mm/yr interpreted by Johnson and Watt (2012). However, as shown in Table 8-1, our estimates of vertical separation rates across the HFZ for other parts of this reach are significantly lower than those of Johnson and Watt (2012).

8.5.1.2 Western Branch

Net vertical separation across strands of the western branch of the HFZ is interpreted to be very low. As described in Section 7.2.2, the dominant strands are constrained to be older than unconformity H30 (~135–125 ka). These strands and other strands mapped on the continental shelf to the northeast strike more westerly than the dominant strike of the HFZ (Plate 1). If the main HFZ marks the direction of principal shear in the study area, then late Quaternary activity on these strands would probably be expressed as transpression, and would cause localized uplift across the strands. Evidence for uplift associated with these strands, such as fault scarps or actively deforming folds localized over the fault tip, is not observed. If active deformation has occurred during the late Quaternary on this branch of the HFZ, it must have occurred as long-wavelength folding (i.e., kilometer-scale) that did not rupture the shallow parts of the faults that are imaged on the USGS 2D data, and therefore would not have been recognized on the USGS 2D data.

8.5.1.3 Irish Hills Reach

Within the central part of the Irish Hills reach of the HFZ, strand 10001 represents the primary active trace. Because recent activity is concentrated on one trace, net vertical separation across the fault zone may be estimated with relatively few complications. Here, the fault zone separates relatively shallow, young sediments that overlie the planated surface of bedrock to the east from a deep sequence of Quaternary strata to the west. Although no offset equivalent unconformities are present in this part of the reach, estimates of offset of unconformity H30 may be inferred (as described in Section 7.3.3 and illustrated on Figure 7-4). Where H10 is not obscured or missing within this reach, it occurs approximately 0.8–3.2 m lower on the west than the (likely correlative) planated top of rock on the east (Table 8-1; Plate 2b). Similarly, H30 is consistently observed to be offset down to the west across fault 10001 (Section 7.3.3; Table 8-1). If the preferred age model for Quaternary unconformities is correct, these constraints provided by separation of unconformities suggest vertical separation rates of approximately 0.1–0.21 mm/yr across the HFZ in the central part of this reach (in the vicinity of lines PBS 22-33). This rate is in general agreement with the rate of approximately 0.1 to 0.14 calculated by Hanson et al. (2004) from separation of the ELP unconformity, which is estimated to be much older, approximately 2.8 Ma (Willingham et al., 2013). If correct, this suggests that vertical separation rates across this part of the HFZ have been relatively constant since middle Pliocene time.

Near the southern end of this reach, between lines PBS-31 and PBS-28, vertical separation of unconformities H30 and H40 suggests lower rates on the order of 0.03–0.1 mm/yr. These rates are somewhat lower than the longer-term rate published by Hanson et al. (2004), which may result from a number of factors, including differing methodology used to measure vertical separation, a change in rate of vertical separation across the HFZ, or the possibility that the measurements performed for this study do not span the entire HFZ.

West of the fault, unconformity H30 is relatively flat and occurs at a depth near 120 m below modern sea level. Below this depth, H30 steepens to the west and truncates a set of inclined reflectors below H30 that also thickens to the west and overlies H40 in a downlapping relationship. This shelf-edge wedge suggests upper slope outgrowth and deposition near sea level during a long-lived lowstand (Figure 3-3). The break in slope of H30 at approximately 120 m below sea level occurs near the depth of the MIS 6 glacial eustatic sea-level lowstand indicated by Quaternary sea-level curves (Figure 3-4). If this shelf-edge wedge was deposited near sea-level during the MIS 6 sea-level lowstand, and the break in slope of the transgressive surface (unconformity H30) marks the position of lowstand sea level, then its current position suggests that there has been very little uplift or subsidence west of strand 10001 since that time. If this is true, then the vertical separation rate across this strand should be expressed mostly as uplift east of the HFZ. The vertical separation rates presented in Table 8-1 are similar to the range of uplift rates for the Irish Hills inferred by onshore marine terraces, which range from 0.2 mm/yr near Point Buchon to 0.06 mm/yr at Point San Luis (Hanson et al., 1994). Together, these observations suggest that the boundary to uplift of the Irish Hills is the HFZ, and not another intervening fault, such as the Shoreline or Point Buchon faults, and not a separate fault to the west of the HFZ. These observations are consistent with the block uplift model for the Los Osos domain proposed by Lettis et al. (1994).

The vertical separation rates developed for this study area are also significantly lower than those published by Johnson and Watt (2012). We interpret this discrepancy to result from differences in age interpretations for key unconformities along the Irish Hills reach. Unconformity H30 is described by Johnson and Watt (2012) as the base of the Holocene section in data examples and offset measurements offshore of the Irish Hills.

8.5.1.4 San Luis Obispo Bay Reach

The San Luis Obispo Bay reach is one of the few locations where offset equivalents may be correlated across the HFZ, because in the southern part of this reach, the HFZ disrupts a thick sequence of Quaternary stratigraphy that includes correlated key unconformities. Within this reach, measurements of net vertical separation across the entire HFZ indicate dominant sense of deformation down to the east (Plate 2c; Table 8-1). Significant fault complexity in the northern part of this reach introduces additional uncertainty to estimates of total vertical separation across the HFZ because vertical separation is observed in opposite directions across parallel strands, and the absence of Quaternary unconformities east of the fault requires correlation of the bedrock surface to buried unconformities across the fault. Furthermore, folding of Quaternary reflectors within the fault zone complicates estimates of vertical separation.

Within the northern part of the reach (from lines PBS-17 to PBS-14), estimates of net vertical separation rates across the HFZ are very low, ranging from about 0.1 mm/yr down to the west, to zero, to 0.1 mm/yr down to the east (Table 8-1). In the central part of the San Luis Obispo Bay reach, between lines PBS-47A and PBS-285, the fault consists of relatively simple, parallel eastern and western strands, and estimates of net vertical separation rates across the HFZ are somewhat more consistent, with most lines ranging from approximately 0.15 mm/yr to 0.2 mm/yr down to the east. Because of the relative simplicity of the fault zone and the absence of significant folding here, these rates are selected as the most representative of the San Luis Obispo Bay reach. In the southern part of the reach, from lines PBS-288 to PBS-291, estimates of vertical separation rates are lower, ranging from approximately 0.03 mm/yr to 0.1 mm/yr down to the east.

Vertical separation rates across the San Luis Obispo reach of the HFZ estimated for this study differ significantly from previously published rates for the same part of the fault zone. Hanson et al. (2004) report post-ELP vertical separation rates that range from 0.13 mm/yr to 0.21 mm/yr, as similar rate but down to the west. The vertical separation rates reported here are also significantly lower than those reported by Johnson and Watt (2012), likely due to differences in age estimates for unconformities used to assess the rates of fault deformation.

8.5.1.5 Point Sal Reach

As noted in Section 7.2.5, seismic data for the Point Sal reach are lacking compared to data for other reaches (line spacing is up to four times greater than the consistent 0.8 km spacing to the north). However these data still provide estimates of sense and rate of vertical separation. Excluding the northern 3 km, the Point Sal reach is defined by net down-to-the-west displacement, recorded by offset of the late Quaternary reflectors, and in the longer term, by the presence of a planated bedrock high with a deep Neogene basin along its western faulted margin. Net down-to-the-west offset of H30 reaches a maximum of 5.6 m on line PBS-328 (Plate 2c), with a net vertical separation rate of 0.04 mm/yr (Table 8-1). Sense of displacement on the northern three seismic lines in the Point Sal reach (PBS-318, PBS-317, and PBS-316) is variable, with a maximum net vertical separation rate of 0.05 mm/yr down to the west (Table 8-1). In total, representative net down-to-the-west vertical separation rates range from 0.04 mm/yr to 0.16 mm/yr.

Our estimates of vertical separation rates across the HFZ in the Point Sal reach are somewhat lower than those of Hanson et al. (2004), who report post-ELP rates of 0.17–0.2 mm/yr, and Johnson and Watt (2012), who report Holocene rates of 0.1–0.4 mm/yr for this reach.

8.5.2 Discussion of Vertical Separation Rates

Our interpretations of vertical separation rates differ significantly from those of Johnson and Watt (2012) because of differences in the ages assigned to the unconformities. Johnson and Watt describe vertical separation of the post-LGM unconformity at many locations along the HFZ. Based on review of the same seismic-reflection data we believe that the surface measured by Johnson and Watt is actually unconformity H30, which we interpret to be on the order of 135–125 ka. Therefore, although we measure many of the same features to evaluate vertical separation, the rate of vertical separation that we infer from these measurements is approximately one order of magnitude lower than the rate of deformation interpreted by Johnson and Watt (2012). In their defense, the purpose of the Johnson and Watt analysis was meant to provide an overview geologic and fault map, and an analysis of fault kinematics; Quaternary stratigraphy was not the primary focus of that investigation.

8.5.3 Dip

Strands of the HFZ observed in the shallow stratigraphy mapped for this project are generally steeply dipping to vertical. However, only the uppermost parts (~50–250 m below the seafloor) of the fault strands are observed in this study. Therefore, this study does not provide direct information on fault dip at seismogenic depths of approximately 2–12 km.

9.0 CONCLUSIONS

9.1 Offshore Stratigraphy

Our analysis of the USGS 2D seismic-reflection data released by Sliter et al. (2009) has led to a significant improvement in the mapping and understanding of Quaternary stratigraphy in the study area. Several late Quaternary unconformities are identified on the profiles and correlated widely throughout the study area. The depositional setting of the most pronounced and widely correlated unconformities is interpreted based on relationships to surrounding reflectors using a sequence stratigraphic framework. We recognize sea-level lowstand deposits in Estero Bay as a distinctive wedge-shaped set of clinoforms localized directly beneath the modern shelf break. Similar distinctive clinoform sets buried beneath the outer shelf are interpreted as deposits from older sea-level lowstands. These lowstand deposits underlie and are eroded by pronounced unconformities that are recognized and correlated widely within the study area. With the exception of one unconformity (H20) these unconformities are interpreted as surfaces of erosion caused by past sea-level transgressions. Ages of these key unconformities are estimated based on correlation to Quaternary global eustatic sea-level cycles. The preferred ages for the unconformities in the study area are as follows:

- Unconformity H10 is interpreted as the post-LGM transgressive surface. Its age is estimated to range from approximately 19 ka to 7 ka, generally decreasing in age with decreasing depth below modern sea level.
- Unconformity H20 is interpreted as the base of the most recent lowstand systems tract and is limited to depths at or near the LGM elevation, distributed west of and up to the shelf break. Its age is estimated to range from approximately 27 ka to 19 ka.
- Unconformity H30 is interpreted as the transgressive surface developed between the MIS 6 lowstand and the MIS 5e highstand. Its age is estimated to range from approximately 135 ka to 125 ka. It is distributed well above the shelf break in San Luis Obispo and Estero Bays.
- Unconformity H40 is interpreted as the transgressive surface developed between the MIS 8 lowstand and the MIS 7 highstand, approximately 250–240 ka.

A shore-parallel channel-like erosion feature was noted in the feasibility study report (AMEC, 2012a), and hypothesized to be related to lowstand sea-level conditions. Detailed mapping of unconformity H10 performed for this study shows that the erosion feature is shallower than, and partially eroded into H10, indicating that it postdates the latest transgression. Therefore, this feature is most likely related to submarine currents (e.g., contourite drift/moat features of Faugeres et al., 1999) rather than high-energy coastal processes. Other similar erosion features were also identified seaward of the continental shelf break in Estero Bay.

Several small basins that are actively subsiding and accumulating sediment were identified in the USGS 2D dataset. These basins may provide targets for more detailed future investigations to better understand the timing and rate of individual faulting events in the Holocene.

9.2 Quaternary Fault Activity

Offshore fault strands are mapped within the USGS 2D data set, and the relationships of unconformities to faults are used to assess recency of activity, and the amounts and rates of vertical separation during the middle to late Quaternary. A fault activity map is presented on Plate 3 documenting the location and relative recency of Quaternary faults in the study area. Vertical separation measurements of unconformities offset by faults are presented on Plates 2a-2c.

Where seismic surveys overlap, mapping performed for this project aligns well with the mapping of the Point Buchon 3D/2D data (PG&E, 2012). The fault patterns presented here are also similar to those mapped by Johnson and Watt (2012) and Hanson et al. (2004).

9.2.1 Hosgri fault zone

We recognize the HFZ as a nearly continuous, approximately linear fault that extends at least 84 km from approximately offshore of Cambria to the southern limit of the study area offshore of Point Sal. Three Quaternary faults merge with the HFZ in the study area: the Los Osos fault zone (LOFZ), the Point Buchon fault, and the Casmalia fault. Each of these faults strikes northwest. The two northern faults, the LOFZ and the Point Buchon fault zone, both change strike as they approach the HFZ, bending northward to become nearly parallel to the HFZ. At the locations where these faults merge with the HFZ, structural basins filled with Quaternary sediment occur between their northern ends and the primary traces of the HFZ.

The sense, amount, and rate of vertical separation across the Hosgri fault zone (HFZ) vary considerably along strike. We divide the HFZ into five “reaches,” based on changes in fault trace complexity, amount and sense of vertical separation, relationships to adjacent crustal blocks, and relationships to intersecting faults. The reaches are the Cambria, Western Branch, Irish Hills, San Luis Obispo Bay, and Point Sal reaches. Our findings for each reach are summarized below:

- The Cambria reach of the HFZ is mapped 6–7 km south of and along strike with the San Simeon fault. It is dominated by an asymmetric basin bound on the west by two primary strands of the HFZ. We interpret this basin, or half graben, as a pull apart basin related to a right transfer of slip from the HFZ to the San Simeon fault. The basin margin faults displace late Quaternary to Holocene unconformities down to the east. Net vertical separation rates within this reach depend on position within this pull apart basin, and reach a maximum between lines PBS-209 and PBS-230, where the fault exhibits a double-bend to the right (first identified by Johnson and Watt, 2012). Maximum vertical separation rates are given by separation of unconformity H10, with a range of 0.87–1.23 mm/yr, although these rates may be exaggerated by differential erosion across the fault. Preferred vertical separation rates within this double bend are given by offset of unconformities H30 and H40, with a range of 0.29–0.41 mm/yr. The southern limit of the Cambria reach is coincident with the convergence of the LOFZ with the HFZ.
- The western branch of the HFZ diverges from the primary HFZ near the convergence with the LOFZ. Faults imaged at depth do not deform unconformities H30 or younger, which indicates that the western branch is not the current locus of deformation.
- The Irish Hills reach of the HFZ extends from Estero Bay to an area southwest of DCPP. This reach includes convergence zones of both the LOFZ and the Point Buchon fault zone. Here, the HFZ bounds the uplifting Irish Hills block to the east, and the relative sense of vertical separation across the majority of this reach is up on the east. Representative net vertical separation rates for this reach range from 0.1 mm/yr to 0.2 mm/yr offshore of Point Buchon, and from 0.03 mm/yr to 0.1 mm/yr at its southern end.
- The San Luis Obispo Bay reach of the HFZ is broadly defined by eastern and western fault strands with intermittent intervening faults and folds. The overall sense of vertical displacement is dominantly down to the east. Representative vertical separation rates taken from sites with relatively simple fault geometry and little folding range from 0.15 mm/yr to 0.20 mm/yr down to the east.
- The Point Sal reach of the HFZ extends from the intersection of the bedrock high along the eastern margin of the HFZ to the southern end of the study area and is characterized by dominantly down-to-the-west displacement. Net vertical separation rate measurements

are sparse and variable, with rates that range from 0.04 mm/yr to 0.16 mm/yr down to the west.

The stark contrast in rate of vertical separation and recency of activity between the Cambria reach of the HFZ and the western branch of the HFZ indicates that the current locus of deformation on the HFZ is on the Cambria reach, and suggests that the HFZ is directly connected to the San Simeon fault zone.

Net vertical separation rates for the Irish Hills reach (0.03 mm/yr in the south to 0.2 mm/yr offshore of Point Buchon; Table 8-1) are generally consistent with those defined by Hanson et al (2004; Table 8-1) suggesting that rates of vertical separation across the HFZ adjacent to the Irish Hills have remained relatively consistent since the late Pliocene. These vertical separation rates are also consistent with uplift rates for the Irish Hills constrained by onshore marine terraces, which range from 0.20 mm/yr at Point Buchon and decrease to 0.06 mm/yr at Point San Luis (Hanson et al., 1994). The similarity of these rates suggest that the boundary to uplift of the Irish Hills is the HFZ, and not another intervening fault, such as the Shoreline or Point Buchon faults, or a separate fault to the west of the HFZ. These observations are consistent with the block uplift model proposed by Lettis et al. (1994).

Net vertical separation rates for the San Luis Obispo Bay reach are generally similar in magnitude but define a sense of displacement (down to the east instead of down to the west) that is opposite of the more far field measurement by Hanson et al. (2004).

We identified several buried channels in Estero and San Luis Obispo bays in the vicinity of the HFZ. However, the geometry of these channels are not well defined because of the wide spacing of the seismic lines and the limited number of tie lines that are perpendicular to the channels on both sides of the fault. Therefore, no attempt was made to use the channels as piercing points to assess the lateral slip on the Hosgri fault zone.

9.2.2 Los Osos Fault

The offshore LOFZ consists of a broad zone of discontinuous faults in Estero Bay that extends west-northwestward across the continental shelf from offshore of Morro Bay and curves northward to eventually merge with the HFZ at the boundary between the Cambria reach, the Irish Hills reach, and the western branch of the HFZ. Numerous small, fault bounded basins occur within this zone. Offshore strands of the LOFZ generally dip moderately to the southwest. Where the LOFZ intersects mapped Quaternary unconformities, the primary strands offset the unconformities down to the northeast, suggesting the offshore LOFZ accommodates reverse-oblique faulting. At its northern end, the LOFZ merges with the HFZ at the southern end of a long asymmetric basin along the east side of the HFZ.

9.2.3 Pecho fault

Previous maps of Quaternary faults offshore of the DCPP (e.g., PG&E, 1988) include the Pecho fault, which splays southeastward from the HFZ across a rocky part of the continental shelf, and extends to the southeastern part of San Luis Obispo Bay. This fault was interpreted as a Quaternary-active, southwest-vergent reverse fault that represents a key part of the southwestern boundary zone of faults, which together accommodate uplift of the San Luis Range. Our examination of higher resolution bathymetric and seismic-reflection data reveals that at the locations that where evidence for the Pecho fault was originally observed by PG&E (1988), no northwest-trending, southwest-vergent, late-Quaternary-active reverse fault is present. Therefore, we recommend that PG&E remove the Pecho fault from future maps of Quaternary active faults.

9.2.4 Point Buchon fault

The Point Buchon fault was not a significant focus of this study because it is not well-imaged on the USGS 2D data. It is located entirely within the middle to inner continental shelf, where it is buried by sediments that post-date the LGM. No additional information was developed for this study to constrain the age or rate of faulting on the Point Buchon fault.

9.2.5 Shoreline fault

Our analysis of the seismic lines south of and across the projection of the Shoreline fault show no vertical deformation within the limits of resolution of the data, supporting the similar findings by PG&E (2011).

10.0 LIMITATIONS

Vertical separations reported herein do not represent total fault slip. These measurements are intended to be used as a guide to evaluate timing of recent movement, amount, and style of fault deformation among various strands of the fault zones. Because the study is based on examination of 2D seismic-reflection data, only vertical separations may be observed. However, the Hosgri fault is interpreted as a strike-slip fault (Johnson and Watt, 2012; Hanson et al., 2004). Therefore, it is likely that the vertical separations presented herein significantly underrepresent the total fault slip that has occurred on a particular fault strand during a particular time frame.

Limitations of depth of penetration, data gaps, and regions of poor interpretability impacted our ability to map and correlate unconformities in some parts of the study area, such that a complete characterization of vertical displacement throughout the late Quaternary is not possible in all locations. On some seismic lines, all correlated unconformities defined in this report are present and cross all observed mapped traces of the HFZ, allowing for a relatively complete characterization of late Quaternary vertical displacement. On a greater majority of seismic lines, some or all unconformities are absent, in which case net displacement cannot be characterized, or they do not cross fault traces, requiring proxy measurements (i.e., planated bedrock to a transgressive unconformity). Furthermore, many of the faults mapped for this project offset portions of unconformities assigned a low correlation confidence (i.e., grades B or C), suggesting that alternative viable age interpretations exist for the surfaces used to measure vertical separation. Therefore, inferred vertical separation rates include additional uncertainty in these regions of low correlation confidence.

11.0 IMPACT EVALUATION

The results and conclusions presented in this report do not impact other PG&E Geosciences documents. They do provide information on the Hosgri and Los Osos faults that may be used for the seismic source characterization models for the DCPP that is currently being conducted by PG&E using a SSHAC Level 3 process.

12.0 REFERENCES

AMEC Environment & Infrastructure, Inc. (AMEC), 2012a. *Preliminary Assessment of Paleoshorelines and Unconformities near the Hosgri Fault Zone, Point Buchon Area, San Luis Obispo County, California*, Preliminary consulting report submitted to PG&E Geosciences, 16 pp., 10 figures, January 19.

AMEC Environment & Infrastructure, Inc. (AMEC), 2012b. *Compilation of Geologic Maps and GIS Databases for the Irish Hills and Surrounding Areas, Diablo Canyon Power Plant, LTSP Update San Luis Obispo, California*, draft letter report submitted to PG&E, January.

Atwater, T.M., 1970. Implications of plate tectonics for the Cenozoic tectonic evolution of western North America, *Geological Society of America Bulletin* **81**: 3513–3536.

Brown, A.R., 2004. *Interpretation of Three-Dimensional Seismic Data*, Memoir 42, 6th Edition, American Association of Petroleum Geologists, Tulsa, Okla., 541 pp.

Burchfiel, B.C., and Stewart, J.H., 1966. 'Pull-apart' origin of the central segment of Death Valley, California, *Bulletin Geological Society of America* **77**: 439–442.

Burger, R.L., Fulthorpe, C.S., Austin, J.A., Gulick, S.P.S., 2002. Lower Pleistocene to present structural deformation and sequence stratigraphy of the continental shelf, offshore Eel River Basin, northern California. *Marine Geology* **185** (3–4): 249–281.

Carlson, A.E., 2008. Why there was not a Younger Dryas-like event during the Penultimate Deglaciation, *Quaternary Science Reviews* **27**: 882-887.

Crowell, J.C., 1974. Origin of late Cenozoic basins in southern California: in Dickinson, W.R. (editor), *Tectonics and Sedimentation*, SEPM Special Publication 22, Society for Sedimentary Geology, Tulsa, Okla., pp. 190–204.

Dickinson, W.R., 2004a. Evolution of the North American Cordillera, *Annual Reviews of Earth and Planetary Sciences* **32**: 13–45.

Dickinson, W.R., 2004b. *Kinematics of Transrotational Tectonism in the California Transverse Ranges and Its Contribution to Cumulative Slip Along the San Andreas Transform Fault System*, Geological Society of America Special Paper 305, pp. 1–46.

Di Silvestro, L.A., Hanson, K.L., Lettis, W.R., and Shiller, G.I., 1990. The San Simeon/Hosgri pull-apart basin, south-central coastal California (abs.), *EOS, Transactions of the American Geophysical Union* **71** (43): 1632.

Faugeres, J-C., Stow, D. A.V., Imbert, P., and Viana, A., 1999. Seismic features diagnostic of contourite drifts, *Marine Geology* **162**: 1–38.

Fugro Consultants, Inc., 2011a. *Field Operations Report 2010-2011 High-Resolution Marine Survey Offshore Diablo Canyon Power Plant, Central California*, prepared for PG&E, Fugro Project No. 04.B0992017, 875 pp., June.

Fugro Consultants, Inc., 2011b. *2D Seismic Data Processing Report 2010-2011 High-Resolution Marine Survey Offshore Diablo Canyon Power Plant, Central California*, prepared for PG&E, Fugro Project No. 04.B0992017, 13 pp., June.

Fugro Seismic Imaging, 2011. *Seismic Data Processing Report, 3D High-Resolution Marine Survey, California Offshore 2011, Diablo Canyon*, prepared for PG&E, Report No. 2010-4410_Draft01, 36 pp., May.

Grossman, E.E., Eittreim, S.L., Field, M.E., Wong, F.L., 2006. Shallow stratigraphy and sedimentation history during high-frequency sea-level changes on the central California shelf. *Continental Shelf Research* **26**: 1217–1239.

Hall, C.A., 1976. Geologic map of the San Simeon–Piedras Blancas region, San Luis Obispo County, California, Miscellaneous Field Studies Map MF-784, scale 1:24,000, U.S. Geological Survey.

Hall, C.A., Ernest, W.G., Prior, S.W., and Wiese, J.W., 1979. Geologic map of the San Luis Obispo–San Simeon region, California, U.S. Geological Survey Miscellaneous Investigations Series Map I-097, scale 1:48,000.

Hanson, K.L., Lettis, W.R., McLaren, M.K., Savage, W.U., and Hall, N.T., 2004. Style and rate of Quaternary deformation of the Hosgri fault zone, offshore south-central California: in Keller, M.A. (editor), *Evolution of Sedimentary Basins/Onshore Oil and Gas Investigations—Santa Maria Province*, U.S. Geological Survey Bulletin 1995, Chapter BB, 37 pp.

Hanson, K.L., and Lettis, W.R., 1994. Estimated Pleistocene slip rate for the San Simeon fault zone, south-central coastal California: in Alterman, I.B., McMullen, R.B., Cluff, L.S., and Slemmons, D.B. (editors), *Seismotectonics of the Central California Coast Range*, Geological Society of America Special Paper 292, pp. 133–150.

Hanson, K.L., Wesling, J.R., Lettis, W.R., Kelson, K.I., and Mezger, L., 1994. Correlation, ages, and uplift rates of Quaternary marine terraces, south-central California: in Alterman, I.B., McMullen, R.B., Cluff, L.S., and Slemmons, D.B. (editors), *Seismotectonics of the Central California Coast Range*, Geological Society of America Special Paper 292, pp. 45–72.

Hall, T., Hunt, T.D., and Vaughan, P.R., 1994. Holocene behavior of the San Simeon fault zone, south-central coastal California: in Alterman, I.B., McMullen, R.B., Cluff, L.S., and Slemmons, D.B. (editors), *Seismotectonics of the Central California Coast Range*, Geological Society of America Special Paper 292, pp. 167–189.

Hardebeck, J.L., 2010. Seismotectonics and fault structure of the California Central Coast, *Bulletin of the Seismological Society of America* **100**: 1031–1050.

Harland, W.B., 1971. Tectonic transpression in Caledonia Spitzbergen, *Geological Magazine*, **108**: 27–42.

Hogarth, L.J., Driscoll, N.W., Babcock, J.M., Orange, D.L., 2012. Transgressive deposits along the actively deforming Eel River margin, Northern California, *Marine Geology*, **303-306**: 99-114

Howell, D.G., Crouch, J.K., Greene, H.G., McCulloch, D.S., and Vedder, J.G., 1980. Basin development along the late Mesozoic and Cenozoic California margin; a plate tectonic margin of subduction, oblique subduction and transform tectonics: in Balance, P.F., and Reading, H.G. (editors), *Sediment in Oblique-Slip Mobile Zones*, Special Publication 4, International Association of Sedimentologists, pp. 43–62.

Johnson, S.Y., and Watt, J.T., 2012. Influence of fault trend, bends, and convergence on shallow structure and geomorphology of the Hosgri strike-slip fault, offshore central California, *Geosphere* **8** (6): 1632–1656.

Le Dantec, N., Hogarth, L.J., Driscoll, N.W., Babcock, J.M., Barnhardt, W.A., Schwab, W.C., 2010. Tectonic controls on nearshore sediment accumulation and submarine canyon morphology offshore La Jolla, southern California. *Marine Geology* **268**: 115–128.

Lekkerkerk, H-J., van der Velden, R., Roders, J., Haycock, T., de Vries, R., Jansen, P., and Beemster, C., 2006. *Handbook of Offshore Surveying, Volume II*, Clarkson Research Services Ltd., St Magnus House, London, 194 pp.

Lettis, W.R., Di Silvestro, L., Hanson, K.L., and Shiller, G.I., 1990, The San Simeon/Hosgri pull-apart basin: Implications for late Quaternary activity on the Hosgri Fault Zone: in Lettis, W.R., Hanson, K.L., Kelson, K.I., and Wesling, J.R. (editors), *Neotectonics of South-Central Coastal California*, Friends of the Pleistocene, Pacific Cell, 1990 Fall Field Trip Guidebook, pp. 91–138.

Lettis, W.R., and Hall, N.T., 1994. Los Osos fault zone, San Luis Obispo County, California: in Alterman, I.B., McMullen, R.B., Cluff, L.S., and Slemmons, D.B. (editors), *Seismotectonics of the Central California Coast Ranges*, Geological Society of America Special Paper 292, pp. 73–102.

Lettis, W.R., Hanson, K.L., Unruh, J.R., McLaren, M., and Savage, W.U., 2004. Quaternary Tectonic Setting of South-Central Coastal California: in Keller, M.A. (editor), *Evolution of Sedimentary Basins/Offshore Oil and Gas Investigations—Santa Maria Province*, Bulletin 1995, Chapter AA, U.S. Geological Survey, 24 pp.

Lettis, W.R., Kelson, K.I., Wesling, J.R., Angell, M., Hanson, K.L., and Hall, N.T., 1994. Quaternary deformation of the San Luis Range, San Luis Obispo County, California: in Alterman, I.B., McMullen, R.B., Cluff, L.S., and Slemmons, D.B. (editors), *Seismotectonics of the Central California Coast Ranges*, Geological Society of America Special Paper 292, pp. 111–132.

Lisiecki, L.E., and Raymo, M.E., 2005, A Pliocene-Pleistocene stack of 57 globally distributed benthic $\delta^{18}O$ records, *Paleoceanography* **20**, PA1003, doi:10.1029/2004PA001071, 17 pp.

Lobo, F.J., Dias, J.M.A., Hernandez-Molina, F.J., Gonzalez, R., Fernandez-Salas, L.M., and Diaz Del Rio, V., 2005. Late Quaternary shelf-margin wedges and upper slope progradation in the Gulf of Cadiz margin (SW Iberian Peninsula): in Hodgson, D.M., and Flint, S.S. (editors), *Submarine Slope Systems: Processes and Products*, Special Publication 244, Geological Society, London, pp. 7–25.

Luyendyk, B.P., 1991. A model for Neogene crustal rotations, transtension, and transpression in Southern California, *Geological Society of America Bulletin* **103**: 1528–1536.

Mann, P., 2007. Global catalogue, classification and tectonic origins of restraining- and releasing bends on active strike-slip fault systems: in Cunningham, W.D., and Mann, P. (editors), *Tectonics of Strike-Slip Restraining and Releasing Bends,* Special Publication 290, Geological Society, London, pp. 13–142.

McCulloch, D.S., 1987. Regional geology and hydrocarbon potential of offshore central California: in Scholl, D.W., Grantz, A., and Vedder, J.G. (editors), *Geology and Resource Potential of the Continental Margin of Western North America and Adjacent Ocean Basins—Beaufort Sea to Baja California*, Earth Science Series No. 6, Circum-Pacific Council for Energy and Mineral Resources, Houston, pp. 353–401.

Mitra, S., and Paul, D. 2011. Structural geometry and evolution of releasing and restraining bends: Insights from laser-scanned experimental models, *American Association of Petroleum Geologists Bulletin* **95** (7): 1147–1180.

Muhs, D.R., Rockwell, T.K., and Kennedy, G.L., 1992. Late Quaternary uplift rates of marine terraces on the Pacific coast of North America, southern Oregon to Baja California Sur, *Quaternary International* **15-16**: 212-133

Murray-Wallace, C.V., 2007. Eustatic sea-level changes since the last glaciations: in Elias, S.A. (editor), *Encyclopedia of Quaternary Science,* vol. 4 of four-volume set, pp. 3034–3043, Elsevier.

NCS SubSea, Inc., 2011. *Navigation Final Report, Diablo Canyon Power Plant 3D Survey*, Job Number J00344-FR-001-001, DCPP 3D Geophysical Survey, 18 pp.

Orme, A.R., 1992. *Late Quaternary Deposits near Point Sal, South-Central California: A Time Frame for Coastal-Dune Emplacement*, SEPM Special Publication 48, pp. 309–315.

Pacific Gas and Electric Company (PG&E), 1988. *Final Report of the Diablo Canyon Long Term Seismic Program*, U.S. Nuclear Regulatory Commission Enclosure 1, PG&E letter DCL-05-002, Docket No. 50-275 and No. 50-323.

Pacific Gas and Electric Company (PG&E), 1991. *Addendum to the 1988 Final Report of the Diablo Canyon Long Term Seismic Program*, U.S. Nuclear Regulatory Commission Docket No. 50-275 and No. 50-323, February.

Pacific Gas and Electric Company (PG&E), 2011. *Shoreline Fault Zone Report: Report on the Analysis of the Shoreline Fault Zone, Central Coastal California*, Report to the U.S. Nuclear Regulatory Commission, January, 2011. Available at http://www.pge.com/myhome/edusafety/systemworks/dcpp/shorelinereport/.

Pacific Gas and Electric Company (PG&E), 2012. *DCPP 3D/2D Seismic-Reflection Investigation of Structures Associated with the Northern Shoreline Seismicity Sublineament of the Point Buchon Region*, PG&E Technical Report GEO.DCPP.TR.12.01.

Posamentier, H.W., and Allen, G.P., 1999. *Siliciclastic Sequence Stratigraphy: Concepts and Applications*, SEPM Concepts in Sedimentology and Paleontology No. 7, Society for Sedimentary Geology, 210 pp.

Posamentier, H.W., Jervey, M.T., and Vail, P.R., 1988. Eustatic controls on clastic deposition. I. Conceptual framework: in Wilgus, C.K., Hastings, B.S., Kendall, C.G. St. C., Posamentier, H.W., Ross, C.A., and Van Wagoner, J.C. (editors), *Sea Level Changes—An Integrated Approach*, SEPM Special Publication No. 42, Society for Sedimentary Geology, pp. 110–124.

Rietman, J.D., 2011. The Long Term Seismic Program CDP seismic reflection and associated data sets, Presentation at the PG&E DCPP SHHAC SSC Workshop 1, November 30, 2011. Available at http://www.pge.com/includes/docs/pdfs/shared/edusafety/systemworks/dcpp/SSHAC/workshops/source_characterization/SSC_0209_Rietman_CPD_Seismic_Data.pdf.

Rodgers, D.A., 1980. Analysis of pull-apart basin development produced by en echelon strike slip faults: in Balance, P.F., and Reading, H.G. (editors), *Sediment in Oblique-Slip Mobile Zones*, International Association of Sedimentologists Special Publication 4, pp. 27–41.

SEPM Strata, 2013. Terminology List, Society for Sedimentary Geology (SEPM) stratigraphy website, http://www.sepmstrata.org/TerminologyList.aspx. Accessed March 28, 2013.

Sheriff, R.E., 1982. *Structural Interpretation of Seismic Data*, American Association of Petroleum Geologists, Education Course Note Series No. 23, Tulsa, Okla., 73 pp.

Siddall, M., Rohling, E.J., Almogi-Labin, A., Hemleben, C., Meischner, D., Schmelzer, I., and Smeed, D.A., 2003. Sea-level fluctuations during the last glacial cycle, *Nature* **423**: 853–857, doi:10.1038/nature01690.

Sliter, R.W., Triezenberg, P.J., Hart, P.E., Watt, J.T., Johnson, S.Y., and Scheirer, D.S., 2009 (revised 2010). *High-Resolution Seismic Reflection and Marine Magnetic Data Along the Hosgri Fault Zone, Central California*, U.S. Geological Survey Open File Report 2009-1100, version 1.1.

Spinelli, G.A., and Field, M.E., 2003. Controls of tectonics and sediment source locations on along-strike variations in transgressive deposits on the northern California margin. *Marine Geology* **197** (1–4): 35–47.

Stanford, J.D., Hemingway, R., Rohling, E.J., Challenor, P.G., Medina-Elizalde, M., and Lester, A.J., 2011. Sea-level probability for the last deglaciation: A statistical analysis of far-field records, *Global and Planetary Change* **79** (3-4): 193–203.

Swanson, M.T., 2005. Geometry and kinematics of adhesive wear in brittle strike-slip zones, *Journal of Structural Geology* **27**: 871–887.

U.S. Geological Survey and California Geological Survey (USGS and CGS), 2010, Quaternary fault and fold database for the United States, accessed January 2013, USGS web site: http//earthquakes.usgs.gov/regional/qfaults./

U.S. Nuclear Regulatory Commission (NRC), 2012. "Request for Information Pursuant to Title 10 of the Code of Federal Regulations 50.54(f) Regarding Recommendations 2.1, 2.3, and 9.3, of the Near-Term Task for Review of Insights from the Fukushima Dai-Ichi Accident," letter submitted to PG&E dated March 12.

Vail, P.R., Todd, R.G., and Sangree, J.B., 1977. Seismic Stratigraphy and Global Changes of Sea Level: Part 5. Chronostratigraphic Significance of Seismic Reflections: Section 2, Application of Seismic Reflection Configuration to Stratigraphic Interpretation Memoir 26, pp. 99–116.

Waelbroeck, C., Labeyrie, L., Michel, E., Duplessy, J.C., McManus J.F., Lambeck, K., Balbon, E., and Labracherie, M., 2002. Sea-level and deep water temperature changes derived from benthic foraminifera isotopic records, *Quaternary Science Reviews* **21**: 295–305.

Watt, J.T., Johnson, S.Y., Hartwell, S.R., and Roberts, M., [in preparation]. Offshore geology and geomorphology maps from Piedras Blancas to Pismo Beach, San Luis Obispo and Santa Barbara counties, California: U.S. Geological Survey Scientific Investigations Map XXXX, pamphlet XX p., 6 sheets, 1:35,000 scale, and database. Draft dated February 15, 2012. Will be available at http://pubs.usgs.gov/sim/XXXX/.

Weber, G.E., 1979, *Geologic Investigation of the Marine Terraces of the San Simeon Region and Pleistocene Activity on the San Simeon Fault Zone, San Luis Obsipo County, California*, Final Technical Report submitted to the National Earthquake Hazards Reduction Program, Contract No. 14-08-0001-18230.

Willingham, C.R., Rietman, J.D., Heck, R.G., and W.R. Lettis, 2013. Characterization of the Hosgri Fault Zone and adjacent structures in the offshore Santa Maria Basin, south-central California, in Keller, M.A. (editor), *Evolution of Sedimentary Basins/Onshore Oil and Gas Investigations—Santa Maria Province*, U.S. Geological Survey Bulletin 1995, Chapter CC,

Work Instruction SSP.WI.12.03, 2012, Correlation Confidence assessment criteria, issued November 15, 2012, completed February 19, 2013, 3 pp.

Yilmaz, O., 2001. *Seismic Data Analysis, Processing, Inversion, and Interpretation of Seismic Data*, Investigations in Geophysics No. 10, 2nd Ed., Society of Exploration Geophysicists, Tulsa, Okla., 2 Vols., 2,027 pp.

GLOSSARY OF TERMS

$\delta^{18}O$	The difference in oxygen isotope ratio (the ratio of a heavier stable oxygen isotope, ^{18}O, to the most common stable oxygen isotope, ^{16}O) relative to the reference standard (Standard Mean Ocean Water, or SMOW).
Angular unconformity	An unconformable relationship in which younger sediments rest upon the eroded surface of inclined (tilted and/or folded) strata (modified from SEPM strata, 2013).
Bubble pulse	The pulse character of the seafloor characterized by a series of high-amplitude reflections that parallel the seafloor and overprint possible reflections of shallow strata.
Clinoform sequence	A discrete set of inclined reflectors, commonly characterized by toplap above and downlap below. This pattern of deposition is commonly observed at delta fronts.
Continental shelf	The gently westward-sloping sea floor that lies between the coastline and the break in slope to the steeper (1.0–2.0 degrees) continental slope at water depths of 120–140 m.
DCPP	Diablo Canyon Power Plant. The area includes the power block, where the reactors and generators are located, and the adjacent support facilities.
Depocenter	The area of greatest deposition: commonly occurs in the center of a subsiding or deforming basin, but may also be controlled by sediment supply, as in deltaic deposition.
Downlap	A relationship between strata and a lower-bounding surface defined by initially inclined strata that terminate downdip against an initially horizontal or inclined surface (modified from SEPM strata, 2013).
Eustatic sea level	The global sea level independent of local factors.
Highstand	A stillstand of sea level created when global ice volume reaches temporary equilibrium between accumulating snow/ice and melting snow/ice, causing rising sea level to stop before falling.
Lowstand	A stillstand of sea level created when global ice volume reaches temporary equilibrium between melting snow/ice and accumulating snow/ice, causing falling sea level to stop before rising.
Mean sea level	Sea level measured at the mean of all tides in the region. This is approximately coincident with NAVD 88. The reference datum for all topographic surveys and all maps for this project is NAVD 88.
Onlap	A relationship between strata and a lower-bounding surface defined by either (1) originally horizontal strata that terminate progressively against an initially inclined surface, or (2) initially inclined strata that

	terminate progressively updip against a more steeply dipping surface (modified from SEPM strata, 2013).
Paleo	A combining form denoting the attribute of great age or remoteness in regard to time (*Paleozoic*), or involving ancient conditions (*paleoclimate*), ancestral origin, or fossil forms (*paleoanthropic*). Sometimes given as pale- before vowels (*paleoceanography*).
Paraconformity	An unconformable relationship characterized by relatively parallel strata with little evidence of erosion; however, an unconformity may be recognized based on the gap in the sedimentary record (modified from SEPM strata, 2013).
Project DEM	A composite digital elevation model (DEM) developed from various sources of bathymetric and topographic data in which the most accurate and detailed data sets supersede less detailed or regional data sets. Figures and plates presented in this report are based on version 2013.01 of the composite DEM data, which was compiled in 2013. The projection system for the data set is Universal Transverse Mercator (UTM), zone 10 North, NAD 83 with NAVD 88 vertical datum.
Quaternary	A division of geologic time spanning the past 2.6 million years. The Quaternary Period is divided into the Holocene (11.7 ka to present) and Pleistocene (2.6 Ma–11.7 ka) Series. The Pleistocene is further subdivided into the Early (2.6 Ma–780 ka), Middle (780 ka–120 ka), and Late (120 ka–11.7 ka) Stages. In this report, the late Quaternary refers informally to the past 0.5–1.0 million years.
Regression	A period of sea level fall resulting in a seaward shift of the shoreline and depositional facies. This usage corresponds to a “forced regression” of Posamentier and Allen (1999).
Sequence	A relatively conformable succession of genetically related strata that are bounded by unconformities at their upper and lower surfaces (Vail et al., 1977). A sequence is composed of a succession of deposition systems (systems tracts) and is interpreted to be deposited during a full cycle of sea level change (i.e., highstand, regression, lowstand, and transgression). Sequences and the systems tracts they enclose are subdivided and/or bounded by a variety of “key” surfaces that bound or envelop these discrete geometric bodies of sediment. They mark changes in depositional regime “thresholds” across that boundary (modified from SEPM strata, 2013).
Shoreline	The location where sea surface meets the land; this can include an entire tidal range.
Systems tract	Genetically linked stratigraphic units deposited during a single sea-level highstand, lowstand, transgression, or regression. These are

	typically bounded by unconformities created by changes in sea level and may be both erosional and depositional in nature.
Toplap	Termination of strata against an overlying surface mainly as a result of nondeposition (sedimentary bypassing) with perhaps only minor erosion (modified from SEPM strata, 2013).
Transgression	A period of sea level rise resulting in a landward shift of the shoreline and littoral facies.
Unconformity	A surface of erosion or nondeposition that separates younger strata from older strata, indicating a significant hiatus in deposition (modified from SEPM strata, 2013).

Table 3-1. Unconformity Grading Criteria

Confidence Level	Grading Criteria
A	Unconformity can be readily traced along tie lines to its type section. Unconformity is readily distinguishable from line to line by its reflection amplitude, style of associated unconformity, position with respect to other mapped horizons, and depth with respect to the seafloor. Where no tie line exists, unconformity remains distinguishable using the above listed characteristics. Where disrupted by faulting, unconformity is positively identified with correlation polygons. Grade A unconformities are deemed most useful in assessments of vertical fault displacement.
B	Unconformity cannot be readily traced along tie lines to its type section due to fault intersections and or data gaps. Unconformity is distinguishable from line to line by its reflection amplitude, style of associated unconformity, position with respect to other mapped horizons, and depth with respect to the seafloor. Where disrupted by faulting, correlation polygons strongly suggest horizons are correlative but alternative correlations cannot be disproven. Confidence remains high that unconformity is the same as that mapped in the type section.
C	Unconformity cannot be traced along tie lines to its type section. Unconformity may be separated from its type section by gaps of hundreds of meters to kilometers, most notably in fault-controlled sub-basins. Unconformity may be inconsistently distinguishable from line to line by its reflection amplitude, style of associated unconformity, position with respect to other mapped horizons, and depth with respect to the seafloor. Correlations are deemed most tentative from line to line or region to region (greater uncertainty) but may still allow for useful assessment of vertical fault displacement.

Table 6-1: Comparison of Age Models for Key Unconformities

Surface	Preferred Interpretation	Alternative Min	Alternative Max
H10	Transgressive surface from MIS 2 to MIS 1 (~19 ka to ~7 ka)	Boundary between transgressive systems tract and highstand systems tract (~19 ka to ~7 ka)	none
H20	Base of MIS 2 lowstand systems tract (~27 ka to ~19 ka)	Base of prograding clinoform sequence deposited during MIS 1 highstand (<~15 ka)	none
H30	Transgressive surface from MIS 6 to MIS 5 (~135 ka to ~125 ka)	Transgressive surface from MIS 2 to MIS 1 (~19 ka to ~7 ka)	Middle to late Pleistocene transgressive surface
H40	Transgressive surface from MIS 8 to MIS 7 (~250 ka to ~240 ka)	Transgressive surface from MIS 6 to MIS 5 (~135 ka to ~125 ka)	Middle Pleistocene transgressive surface. Age of surface is uncertain. Estimated by comparison to Quaternary sea-level curves and depth of ELP (refer to discussion in Section 6.6) (~640 ka)
Notes	Vertical separation rates of faults that intersect all three unconformities suggest that H30 is on the order of 4 times the age of H10, and that H40 is on the order of twice the age of H30 (Section 8). This model implies that post-LGM transgressive and highstand deposits are generally quite thin in much of the study area.	If this model is correct, the clinoform sequence overlying H20 is a transgressive or highstand deposit. However, if this were correct, transgressive or highstand clinoforms also would be expected on other parts of the shelf. Instead, this and deeper clinoform sequences are only observed below the elevation of lowstand sea level (~120–130 m below modern sea level [Stanford et al., 2011; Murray-Wallace, 2007; Siddall et al., 2003]). This alternative model fails to honor several key observations (refer to discussion in Section 6.6) between H10 and H30 in San Luis Obispo Bay	This model is based on the possibility that transgressions represented by H10, and/or H30 may have eroded the geologic record of more than one sea-level cycle. Therefore, it ignores the simplest explanation that the shallowest surfaces and strata are the youngest permissible age.

Table 8-1. Vertical Separation Rates

USGS Seismic Line	Net Vertical Separation (m)[1,2]	Net Vertical Separation Rate (mm/yr)[1,2,3]	Correspond-ing LTSP Seismic Line[4]	Post-ELP Vertical Separation Rate (mm/yr)[4,5]	Johnson and Watt (2012) Vertical Separation Rate (mm/yr)[6]
Cambria					
PBS-233	–3.6*	–0.24*	–	–	≤1.0
PBS-232	–2.4	–0.16	–	–	≤1.0
PBS-230	–15.2*	–1.01*	–	–	≤1.0
	–46*	–0.35*			
PBS-212	–17.6*	–1.17*	–	–	≤1.0
PBS-210	–19.4*	–1.29*	–	–	≤1.0
	–53.3*	–0.41*			
	–95.6*	–0.39*			
PBS-209	–13.1*	–0.87*	–	–	≤1.0
	–37.9*	–0.29*			
	–101.7*	–0.42*			
PBS-207	–14.7*	–0.98*	–	–	≤1.0
	–33.8*	–0.26*			
	–67.1*	–0.27*			
PBS-206	–10.3*	–0.08*	–	–	≤1.0
	-39*	–0.16*			
PBS-204A	–12.4*	–0.83*	–	–	≤1.0
	–24*	–0.18*			
	–29.7*	–0.12*			
PBS-49	–6.4	–0.26	–	–	≤1.0
PBS-50	3.6	0.03	–	–	≤1.0
	1.2	0			
PBS-38A	4.8	0.04	–	–	0.4–0.8
Western Branch					
PBS-261	–	–	CM-51		
PBS-201	0[†]	0[†]	W-76a		
Irish Hills					
PBS-37A	–	–	J-113	0.1	0.75–1.0
Between PBS-03 and PBC-06 at the HFZ	–	–	PGE-1	0.09	0.75–1.3
PBS-03	–14.8	–0.11	–	–	0.4–0.8
	–20.4	–0.08			

USGS Seismic Line	Net Vertical Separation (m)[1,2]	Net Vertical Separation Rate (mm/yr)[1,2,3]	Corresponding LTSP Seismic Line[4]	Post-ELP Vertical Separation Rate (mm/yr)[4,5]	Johnson and Watt (2012) Vertical Separation Rate (mm/yr)[6]
PBS-34	2.8	0.19	–	–	0.75–1.0
	9	0.07			
	18.6	0.08			
PBS-33	13.4*	0.1*	W-14	0.12	≤0.75–1.0
	34.3*	0.14*			
PBS-21	26.7*	0.21*	–	–	≤0.75–1.0
	41.4*	0.17*			
PBS-32	1.8*	0.12*	GSI-85	0.10–0.14	≤0.75–1.0
	18.2*	0.14*			
	44.1*	0.18*			
PBS-22	2.6*	0.17*	–	–	≥0.4
	12.6*	0.1*			
	22.8*	0.09*			
PBS-31	0*	0*	–	–	0.4–0.75
	5.4*	0.04*			
	7.7*	0.03*			
PBS-23	1.6*	0.11*	–	–	0.4–0.75
	5.4*	0.04*			
	11.9*	0.05*			
PBS-30	0*	0*	–	–	0.4–0.75
	13.2*	0.1*			
	21.4*	0.09*			
PBS-29	0.8*	0.05*	GSI-86	0.14	0.4–0.75
	9.6*	0.07*			
	13.3*	0.05*			
PBS-28	0*	0*	–	–	0.4–0.75
	7.2*	0.06*			
	16.1*	0.07*			
PBS-26	–	–	GSI-87	0.2	≥0.4
San Luis Obispo Bay					
PBS-18a	–	–	CM-119	0.21	0.5
PBS-17	8.2*	0.06*	–	–	–
	23.1*	0.09*			
PBS-56	–9.6*	–0.07*	–	–	–
	–22.4*	–0.09*			

USGS Seismic Line	Net Vertical Separation (m)[1,2]	Net Vertical Separation Rate (mm/yr)[1,2,3]	Correspond-ing LTSP Seismic Line[4]	Post-ELP Vertical Separation Rate (mm/yr)[4,5]	Johnson and Watt (2012) Vertical Separation Rate (mm/yr)[6]
PBS-15	–3*	–0.02*	–	–	–
PBS-14	6.7*	0.05*	–	–	–
	19.7*	0.08*			
PBS-47A	–2.4	–0.16	J-126	0.2	0.5
	–23.4	–0.18			
	–43.2	–0.18			
PBS-13A	2.4	0.16	–	–	–
PBS-12	–7.2	–0.06	–	–	–
PBS-45	–0.8	–0.05	–	–	–
	–20.4	–0.16			
	–48	–0.2			
PBS-10	–0.4	–0.03	GSI-97	0.21	–
	–12.8	–0.1			
PBS-09	–1.2	–0.08	–	–	–
PBS-281	–4.3	–0.29	–	–	–
PBS-282	–2.4	–0.16	–	–	–
PBS-283	–	–	GSI-100	0.19	
PBS-284A	0.4	0.02	–	–	–
PBS-285	3.2	0.21	–	–	–
PBS-288	–1.6	–0.1	PGE-3	0.18	–
	–12.8	–0.1			
PBS-289	–0.4	–0.03	–	–	–
	–4.4	–0.04			
PBS-290	–0.8	–0.05	GSI-101	0.13	–
	–11.2	–0.09			
	–18.4	–0.08			
PBS-291	0	0	–	–	–
	–9.6	–0.07			
	–22.4	–0.09			
PBS-316	–1.2	–0.08	–	–	–
	–3.2	–0.02			
	–4.8	–0.02			
Point Sal					
PBS-317	1.6	0.01	–	–	–
PBS-318	–4	–0.03	–	–	0.1

USGS Seismic Line	Net Vertical Separation (m)[1,2]	Net Vertical Separation Rate (mm/yr)[1,2,3]	Correspond-ing LTSP Seismic Line[4]	Post-ELP Vertical Separation Rate (mm/yr)[4,5]	Johnson and Watt (2012) Vertical Separation Rate (mm/yr)[6]
Between PBS-318 and PBS-328 at the HFZ	–	–	N-204	0.2	–
PBS-328	0.8	0.05	–	–	–
	5.6	0.04			
PBS-327A	0	0	–	–	–
Between PBS-327A and PBS-325 at the HFZ	–	–	GSI-106	0.17	–
PBS-325	2.4	0.16	–	–	–
	5.2	0.04			
PBS-324	0.4	0.027	–	–	0.3–0.4
	13*	0.1*			
PBS-322	0.4	0	–	–	–

1 Total vertical separation and separation rate are positive when separation is down to the west, negative when down to the east; color indicates age of unconformity measured.

2 Vertical separation measurements are reported to a level of precision commensurate with our interpretation of the resolution of the data. In most cases this is 0.5 milliseconds, but in some locations it is interpreted to be greater than that. Vertical separation measurements are converted to meters using an assumed seismic velocity of 1,600 m/s.

3 Net vertical separation rates calculated with the following age assumptions: H10 is 15 ka, H20 is 25 ka, H30 is 130 ka, and H40 is 245 ka.

4 ELP; early–late Pliocene unconformity (see Willingham et al. [2013] for a discussion of unconformity age estimates). Hanson et al. (2004) used an age of 2.8 Ma for the ELP in the calculation of vertical rates.

5 Corresponding LTSP-era seismic lines and post-ELP separation rates are presented in Hanson et al. (2004). As shown on Figure 8-1, vertical separation of the ELP was measured from equivalent surfaces up to several kilometers from the fault strands. Therefore, the rates from Hanson et al. (2004) incorporate faulting and folding, as well as depositional relief on the ELP.

6 Many vertical separation rates given by Johnson and Watt (2012) are described as a range for a fault section and are not tied to a specific measurement or line number.

* Indicates net separation estimated from correlative but not equivalent surfaces (e.g., transgressive surface to wave-cut platform).

† Post-ELP separation rate was reported by Hanson et al. (2004) based on total separation between the eroded seafloor near the coast and the ELP in the offshore Santa Maria basin west of the HFZ. Therefore, these rates represent the net separation across both the Cambria reach and the western branch of the HFZ. No vertical deformation of unconformities mapped for this project was observed on the western branch of the HFZ.

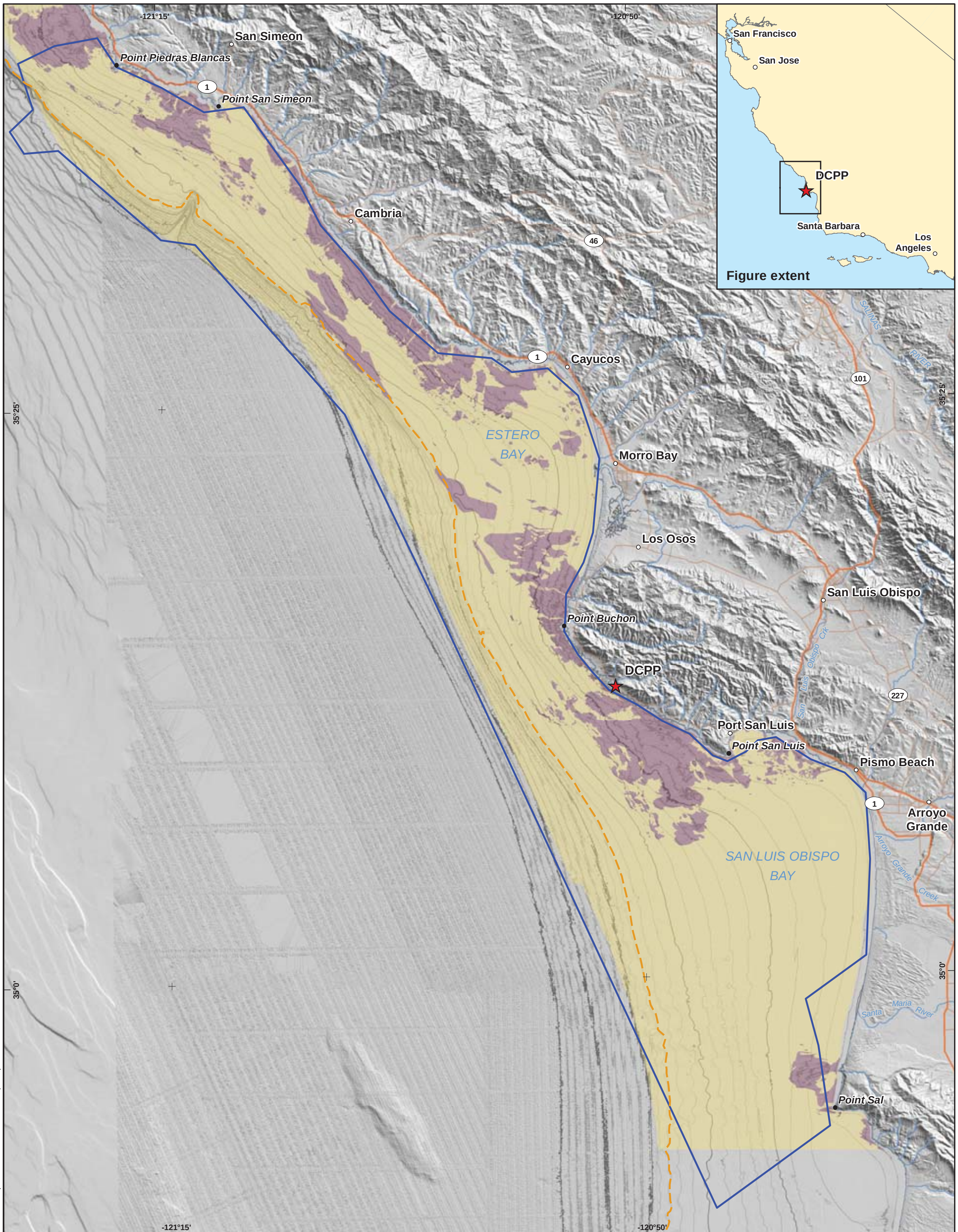

EXPLANATION

- Shelf break
- Highway
- Major road
- Stream or river
- Project Study Area
- Quaternary sediment
- Pre-Quaternary bedrock

0 2 4 6 8 mi.
0 4 8 12 16 km

Map projection and scale: WGS 84 / UTM Zone 10N,1:300,000

Sources:
- Project DEM compilation v2013.01. Bathymetric contour interval is 10 m. Heavy contours are 50 m isobaths.
- Offshore geology from Watt et al. (in prep.).

Map of Bedrock Outcrops and Sedimentary Cover in Study Area

DCPP OFFSHORE SEISMIC STRATIGRAPHY

Pacific Gas and Electric Company | Figure **1-1**

File path: S:\1005\026\GIS\Figures\Figure_1_1.mxd; Date: 05/14/2013; User: Jereme Chandler, LCI; Rev.1

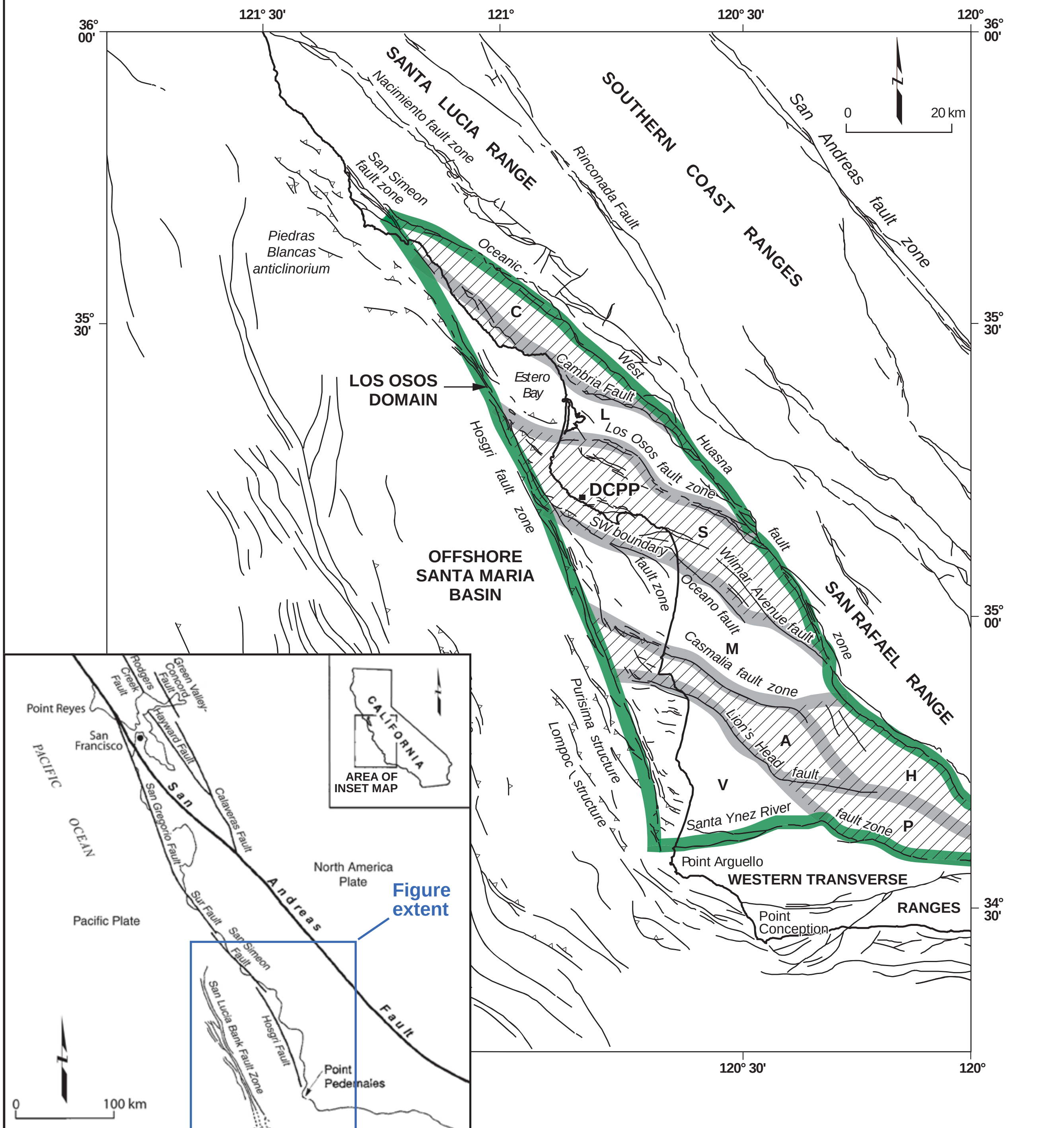

EXPLANATION

Uplifted structural blocks within the Los Osos domain, outlined by thick gray line

Boundary outlining Los Osos domain

Structural blocks within the Los Osos domain

A = Casmalia
C = Cambria
H = Solomon Hills
L = Los Osos
M = Santa Maria Valley
P = Purisima
S = San Luis/Pismo
V = Vandenberg/Lompoc

Sources:
PG&E (1988, 2011)
Regional Tectonic Sketch Map from (Hanson et al., 2004)

Tectonic Setting

DCPP SEISMIC STRATIGRAPHY PROJECT

Pacific Gas and Electric Company | Figure **1-2**

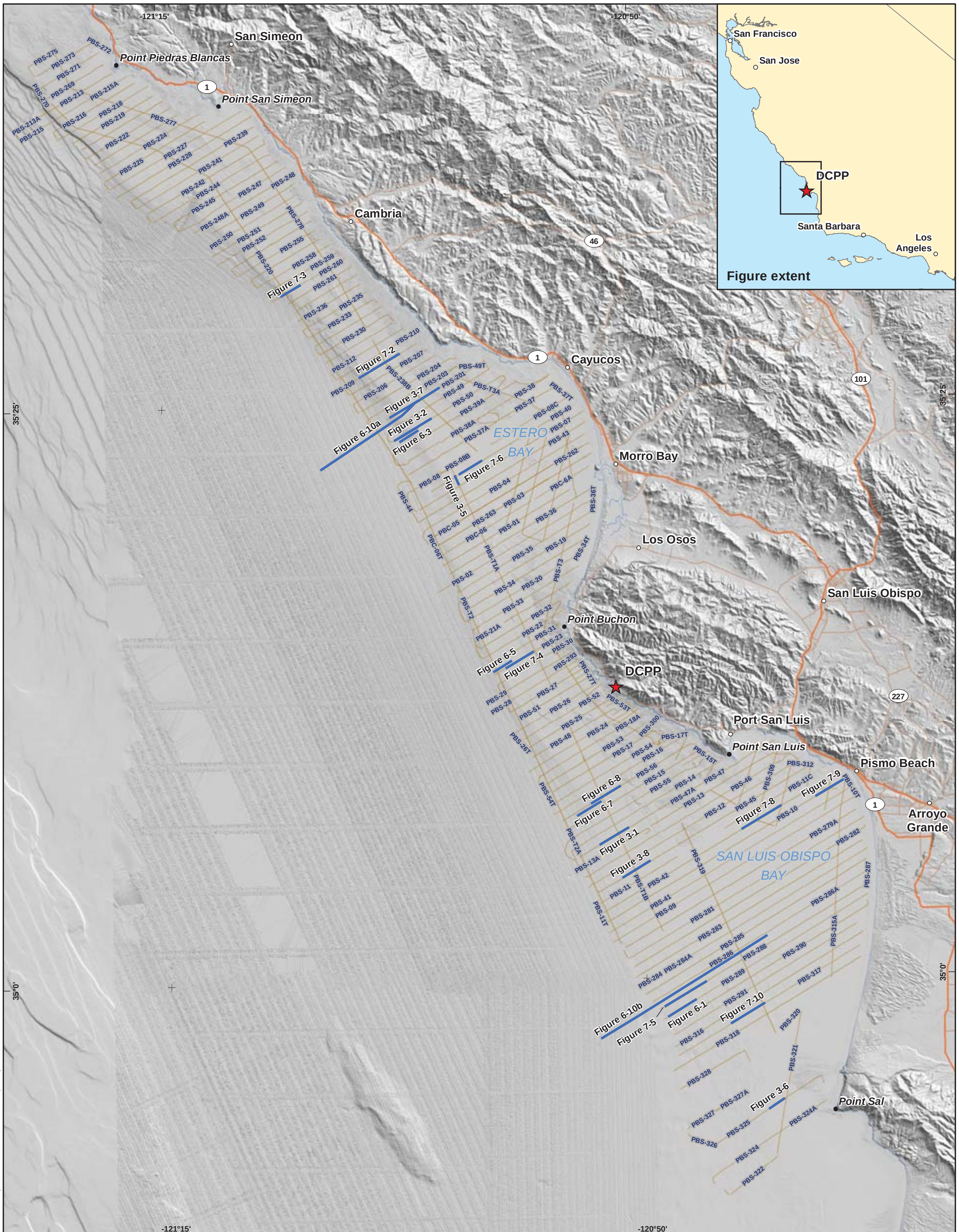

EXPLANATION

- PBS-07 — USGS survey trackline, number indicated
- Highway
- Major road
- Figure extent

Sources:
- USGS seismic-reflection data (Sliter et al., 2009).
- Project DEM compilation v2013.01.

N S E W

0 2 4 6 8 mi.

0 4 8 12 16 km

Map projection and scale: WGS 84 / UTM Zone 10N,1:300,000

Trackline Map of USGS High-Resolution 2D Survey

DCPP OFFSHORE SEISMIC STRATIGRAPHY

Pacific Gas and Electric Company | Figure **2-1**

File path: S:\1005\026\GIS\Figures\Figure_2_1.mxd; Date: 05/14/2013; User: Jereme Chandler, LCI; Rev.1

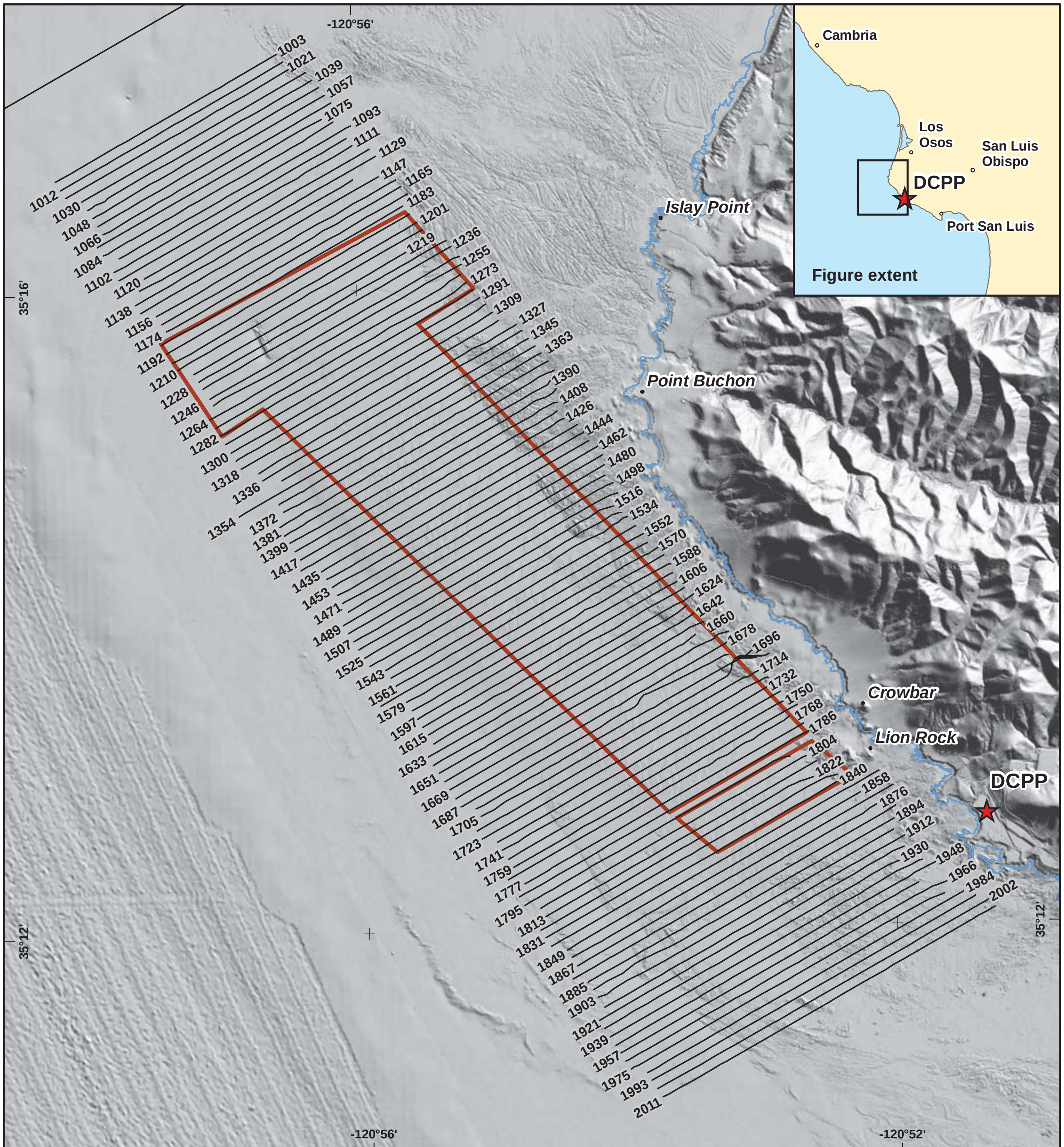

EXPLANATION

Point Buchon 2D survey trackline, approximately 100 m spacing

Data boundary for Point Buchon 3D seismic reflection surveys, approximately 12.5 m trackline spacing

Coastline

Sources:
- Project DEM compilation v2013.01.
- PG&E (2012).

N W E S

0 1 2 mi.

0 2 4 km

Map projection and scale: WGS 84 / UTM Zone 10N,1:68,300

Tracklines and 3D Block Boundaries from Point Buchon 3D/2D Survey

DCPP OFFSHORE SEISMIC STRATIGRAPHY

Pacific Gas and Electric Company | Figure **2-2**

File path: S:\1005\026\GIS\Figures\Figure_2_2.mxd; Date: 05/14/2013; User: Jereme Chandler, LCI; Rev.1

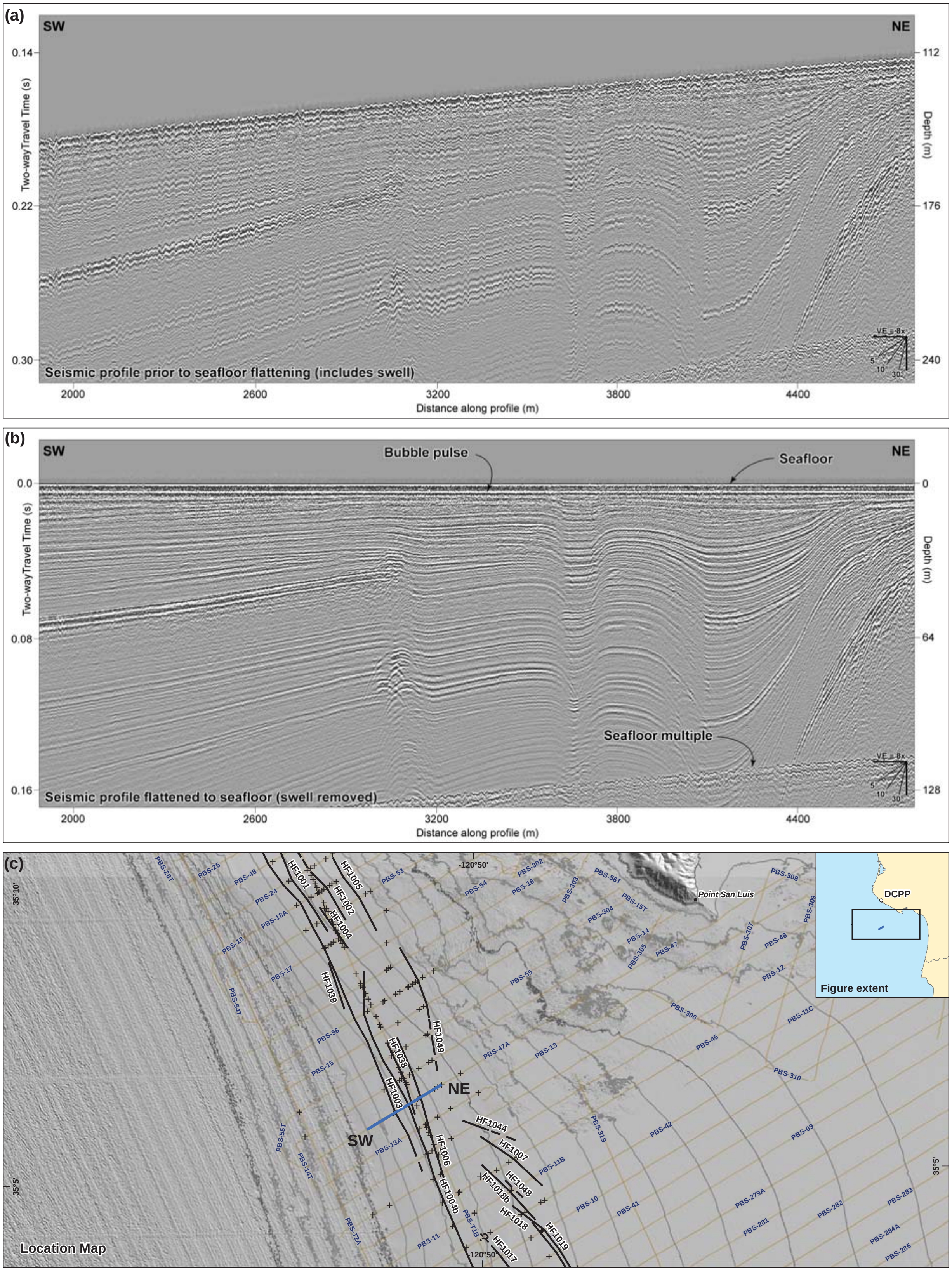

EXPLANATION

Fault interpreted from USGS seismic profiles, solid where well located, dashed where approximately located, dotted where inferred, queried where existence uncertain.

Location of seismic profile

PBS-07 USGS survey trackline, number indicated

+ Unassigned fault

Note:
1. Depth values on seismic profile assume a velocity of 1,600 m/s.

Sources:
- USGS seismic-reflection data (Sliter et al., 2009).
- Project DEM compilation v2013.01. Bathymetric contour interval is 10 m. Heavy contours are 50 m isobaths.

0 2 4 mi.
0 4 8 km

Map projection and scale: WGS 84 / UTM Zone 10N,1:120,000

Excerpt of Profile PBS-47A Showing Comparison of Flattened and Unflattened USGS 2D Profiles

DCPP OFFSHORE SEISMIC STRATIGRAPHY

Pacific Gas and Electric Company | Figure **3-1**

File path: S:\1005\026\GIS\Figures\Figure_3_1.mxd; Date: 05/15/2013; User: Jereme Chandler, LCI; Rev.1

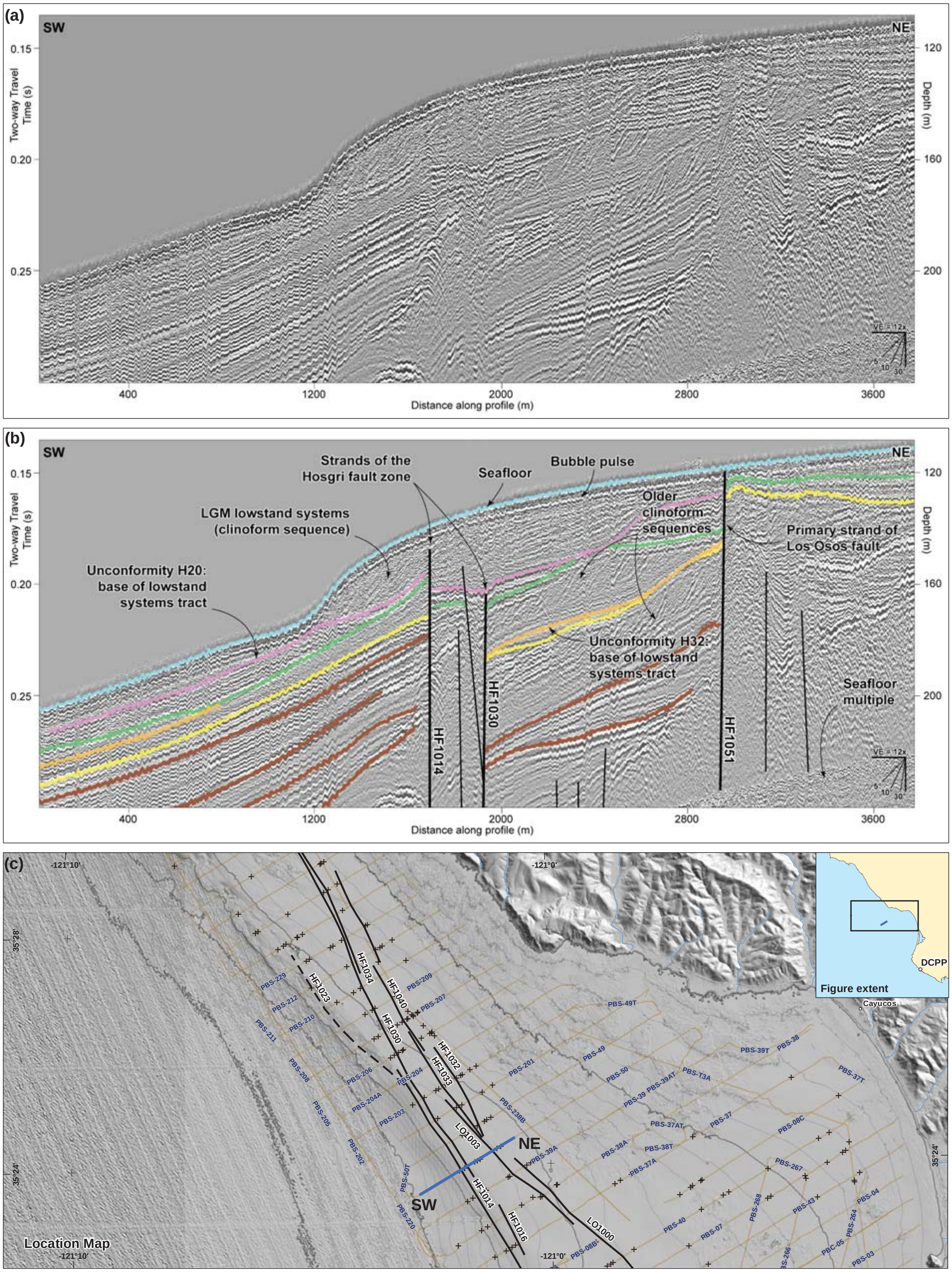

EXPLANATION

Fault interpreted from USGS seismic profiles, solid where well located, dashed where approximately located, dotted where inferred, queried where existence uncertain.

Location of seismic profile

PBS-07 USGS survey trackline, number indicated

+ Unassigned fault

Seafloor

Unconformity H20

Unconformity H30

Unconformity H32

Unconformity H40

Unconformities older than H40

0 2 4 mi.

0 4 8 km

Map projection and scale: WGS 84 / UTM Zone 10N, 1:120,000

Sources:
- USGS seismic-reflection data (Sliter et al., 2009).
- Project DEM compilation v2013.01. Bathymetric contour interval is 10 m. Heavy contours are 50 m isobaths.

Notes:
1. Depth values on seismic profile assume a velocity of 1,600 m/s.
2. Unconformity H10 is obscured by the bubble-pulse on this excerpt of profile PBS-50. Refer to Figure 6-1 for typical unconformable relationships associated with unconformity H10.
3. In profiles, thin black lines are unassigned faults, heavy black lines are named faults.

Excerpt of Profile PBS-50 Showing Type Section for Sequence Stratigraphy

DCPP OFFSHORE SEISMIC STRATIGRAPHY

Pacific Gas and Electric Company | Figure **3-2**

File path: S:\1005\026\GIS\Figures\Figure_3_2.mxd; Date: 05/15/2013; User: Jereme Chandler, LCI; Rev.1

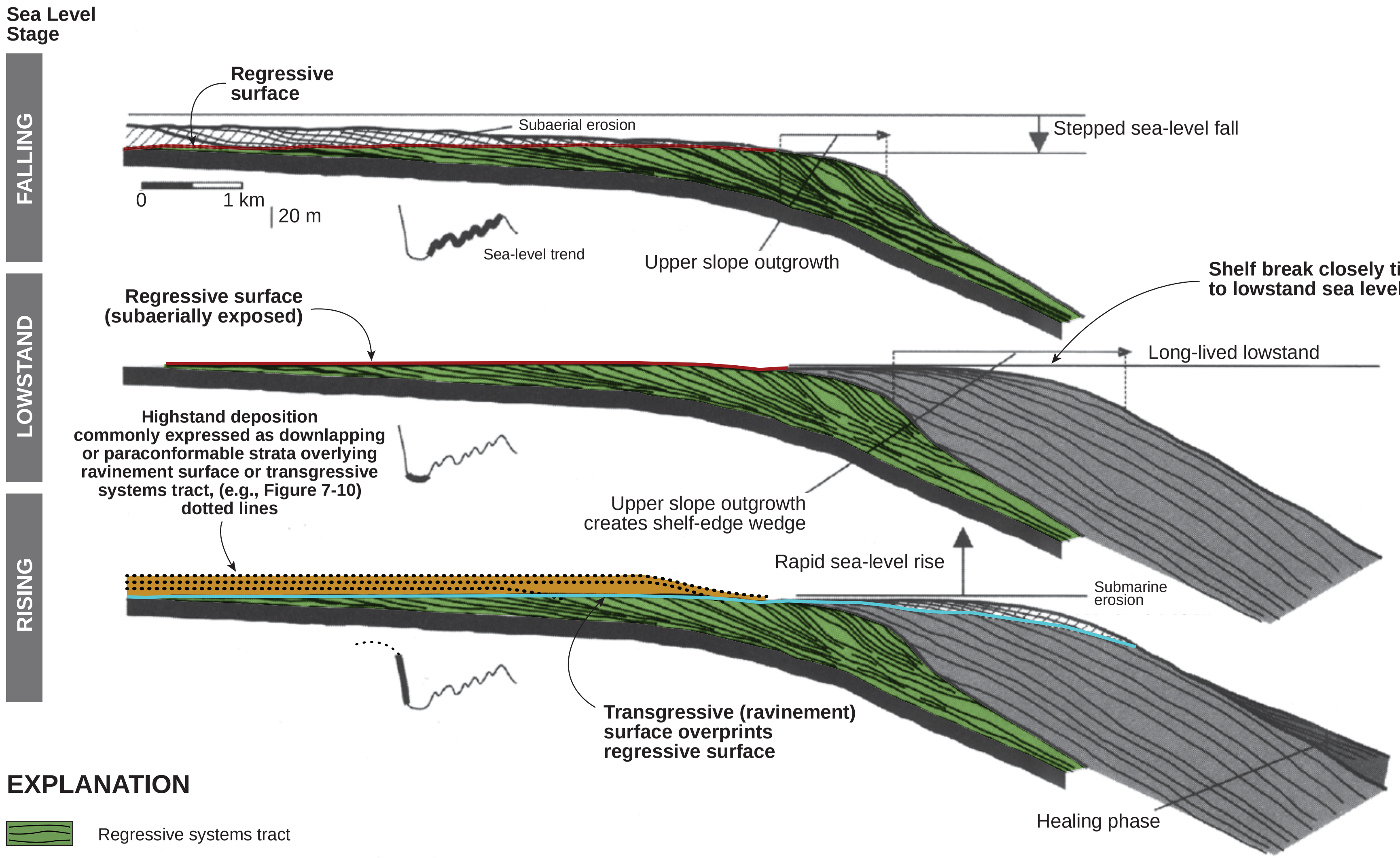

EXPLANATION

Regressive systems tract

Lowstand systems tract

Highstand systems tract

Notes:
1. Shelf-edge wedge consists of clinoforms constructed during falling and lowstand sea level.
2. No distinction between falling and lowstand systems tracts could be identified within the study area.
3. Paraconformable reflectors separating clinoform sequences (e.g., Figure 3-2) are interpreted as transgressive/highstand systems tracts.
4. Transgressive (ravinement) surface results from wave erosion during rapid sea-level rise.

Source:
Modified from Lobo et al. (2005), Figure 12B.

Characteristics of Continental Shelf Sequence Stratigraphy Related to Fall and Rise in Sea Level

DCPP SEISMIC STRATIGRAPHY PROJECT

Pacific Gas and Electric Company | Figure **3-3**

File path: S:\1005\026\GIS\Figures\Figure_3_3.ai; Date: 05/15/2013; User: Jereme Chandler, LCI; Rev.1

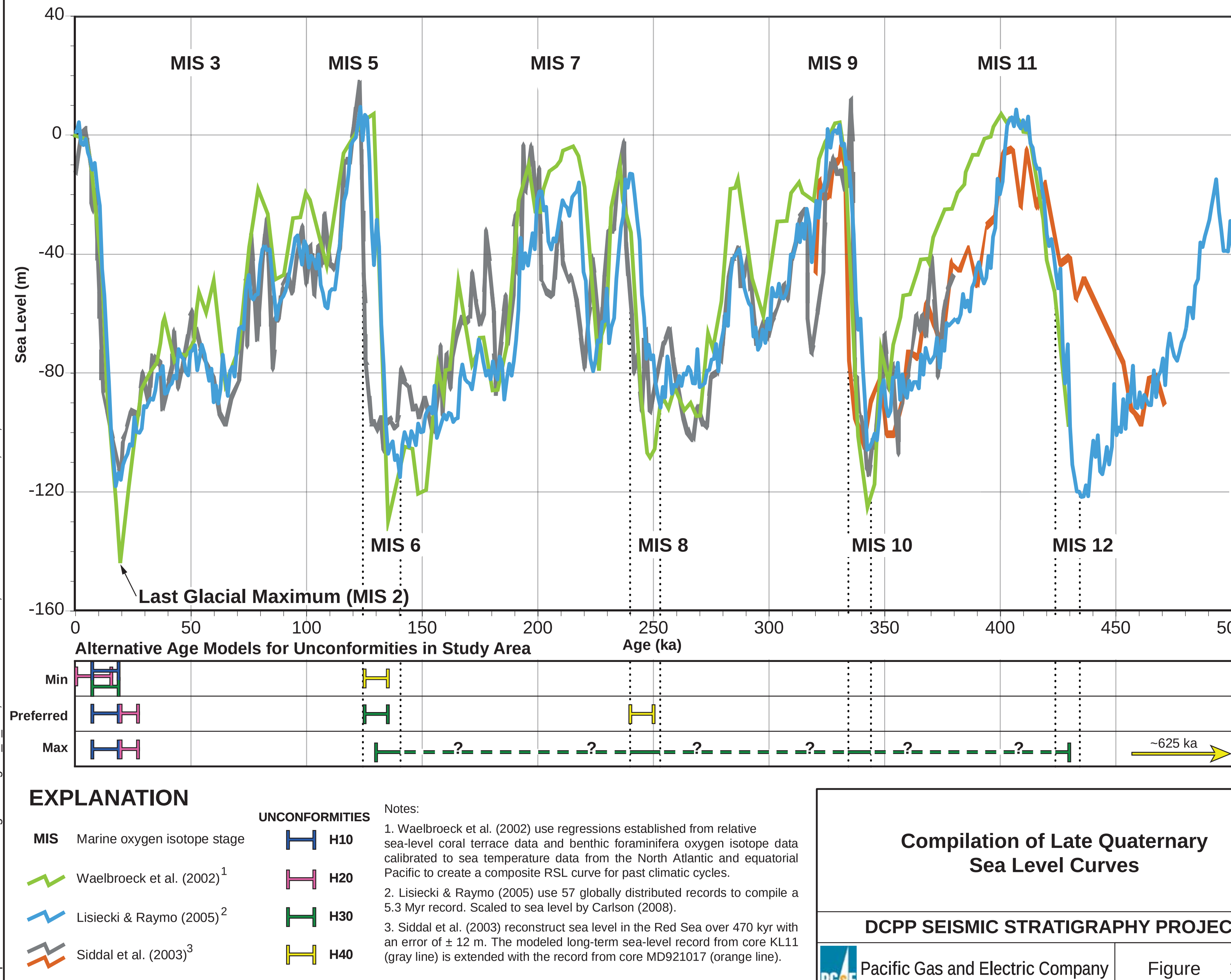

Notes:

1. Waelbroeck et al. (2002) use regressions established from relative sea-level coral terrace data and benthic foraminifera oxygen isotope data calibrated to sea temperature data from the North Atlantic and equatorial Pacific to create a composite RSL curve for past climatic cycles.

2. Lisiecki & Raymo (2005) use 57 globally distributed records to compile a 5.3 Myr record. Scaled to sea level by Carlson (2008).

3. Siddal et al. (2003) reconstruct sea level in the Red Sea over 470 kyr with an error of ± 12 m. The modeled long-term sea-level record from core KL11 (gray line) is extended with the record from core MD921017 (orange line).

Compilation of Late Quaternary Sea Level Curves

DCPP SEISMIC STRATIGRAPHY PROJECT

Pacific Gas and Electric Company

Figure **3-4**

File path: S:\1005\026\GIS\Figures\Figure_3_3.ai; Date: 04/04/2013; User: Jereme Chandler, LCI; Rev.1

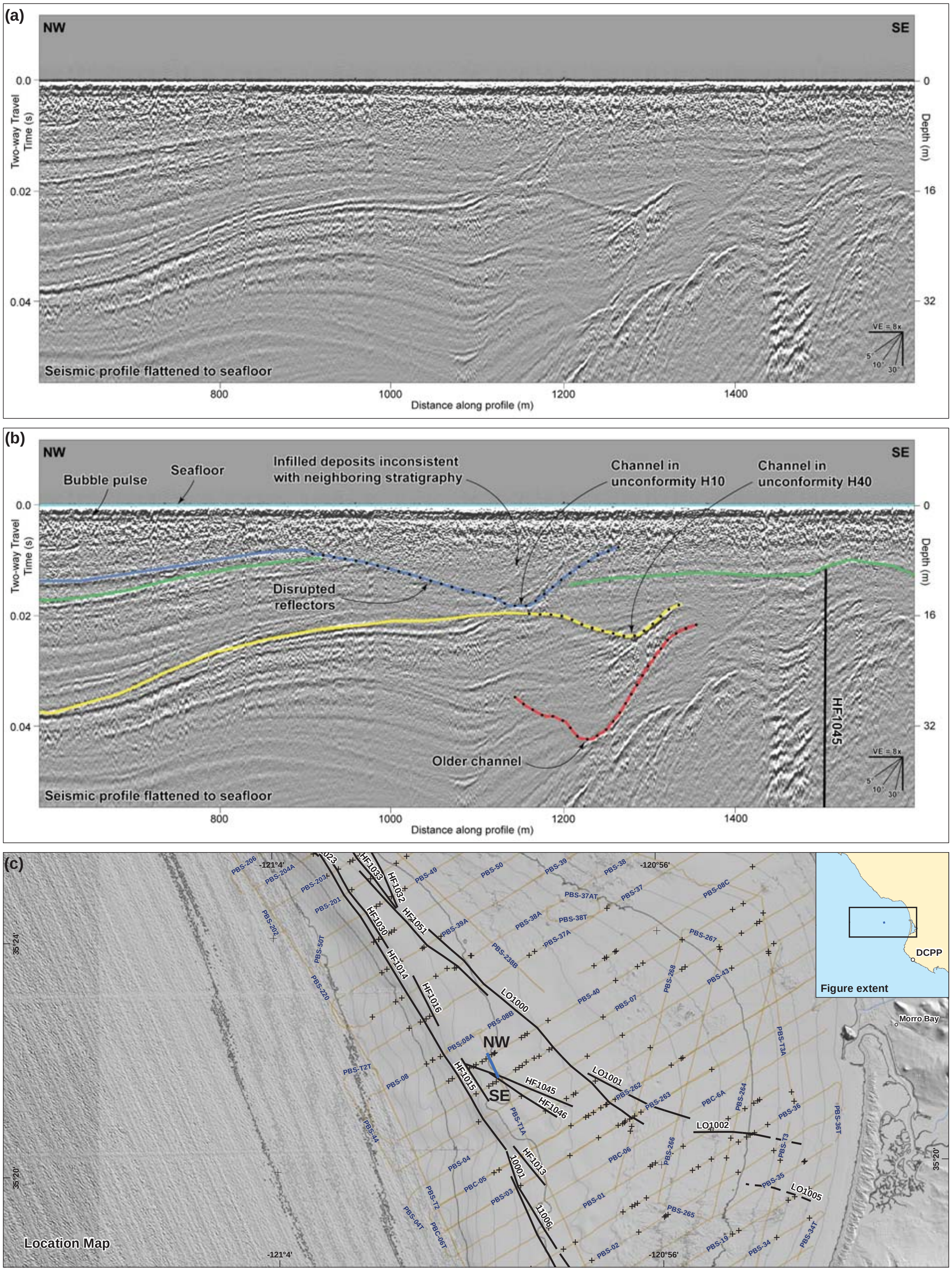

EXPLANATION

- Fault interpreted from USGS seismic profiles, solid where well located, dashed where approximately located, dotted where inferred, queried where existence uncertain.
- Location of seismic profile
- PBS-07 — USGS survey trackline, number indicated
- \+ Unassigned fault
- Seafloor horizon
- Unconformity H10
- Unconformity H30
- Unconformity H40
- Extent of channel

Note:
1. Depth values on seismic profile assume a velocity of 1,600 m/s.

Sources:
- USGS seismic-reflection data (Sliter et al., 2009).
- Project DEM compilation v2013.01. Bathymetric contour interval is 10 m. Heavy contours are 50 m isobaths.

0 2 4 mi.
0 4 8 km

Map projection and scale: WGS 84 / UTM Zone 10N, 1:120,000

Excerpt of Profile PBS-T1A Showing Example of Buried Paleochannels

DCPP OFFSHORE SEISMIC STRATIGRAPHY

Pacific Gas and Electric Company | Figure **3-5**

File path: S:\1005\026\GIS\Figures\Figure_3_5.mxd; Date: 05/15/2013; User: Jereme Chandler, LCI; Rev.1

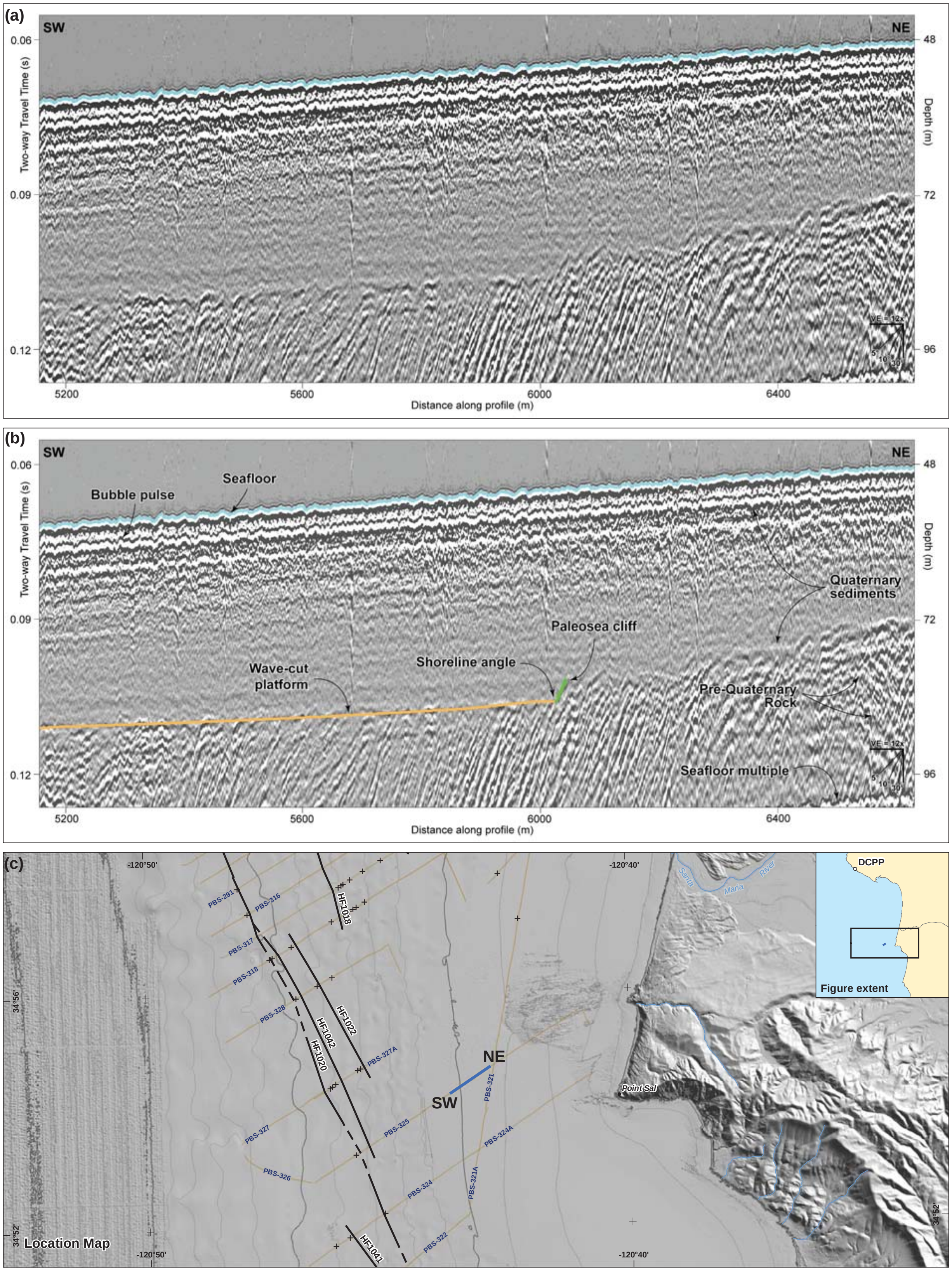

EXPLANATION

- Fault interpreted from USGS seismic profiles, solid where well located, dashed where approximately located, dotted where inferred, queried where existence uncertain.
- Location of seismic profile
- PBS-07 USGS survey trackline, number indicated
- + Unassigned fault
- Seafloor horizon
- Wave-cut platform
- Paleosea cliff

0 2 4 mi.
0 4 8 km

Map projection and scale: WGS 84 / UTM Zone 10N,1:120,000

Sources:
- USGS seismic-reflection data (Sliter et al., 2009).
- Project DEM compilation v2013.01. Bathymetric contour interval is 10 m. Heavy contours are 50 m isobaths.

Notes:
1. Depth values on seismic profile assume a velocity of 1,600 m/s.
2. Paleosea cliff is approximately 3.2 m high and 20 m wide, suggesting it is heavily eroded.
3. The wave-cut platform shown here is interpreted to be part of unconformity H10.

Excerpt of Profile PBS-325 Showing Example of Buried Paleoshoreline Features

DCPP OFFSHORE SEISMIC STRATIGRAPHY

Pacific Gas and Electric Company | Figure **3-6**

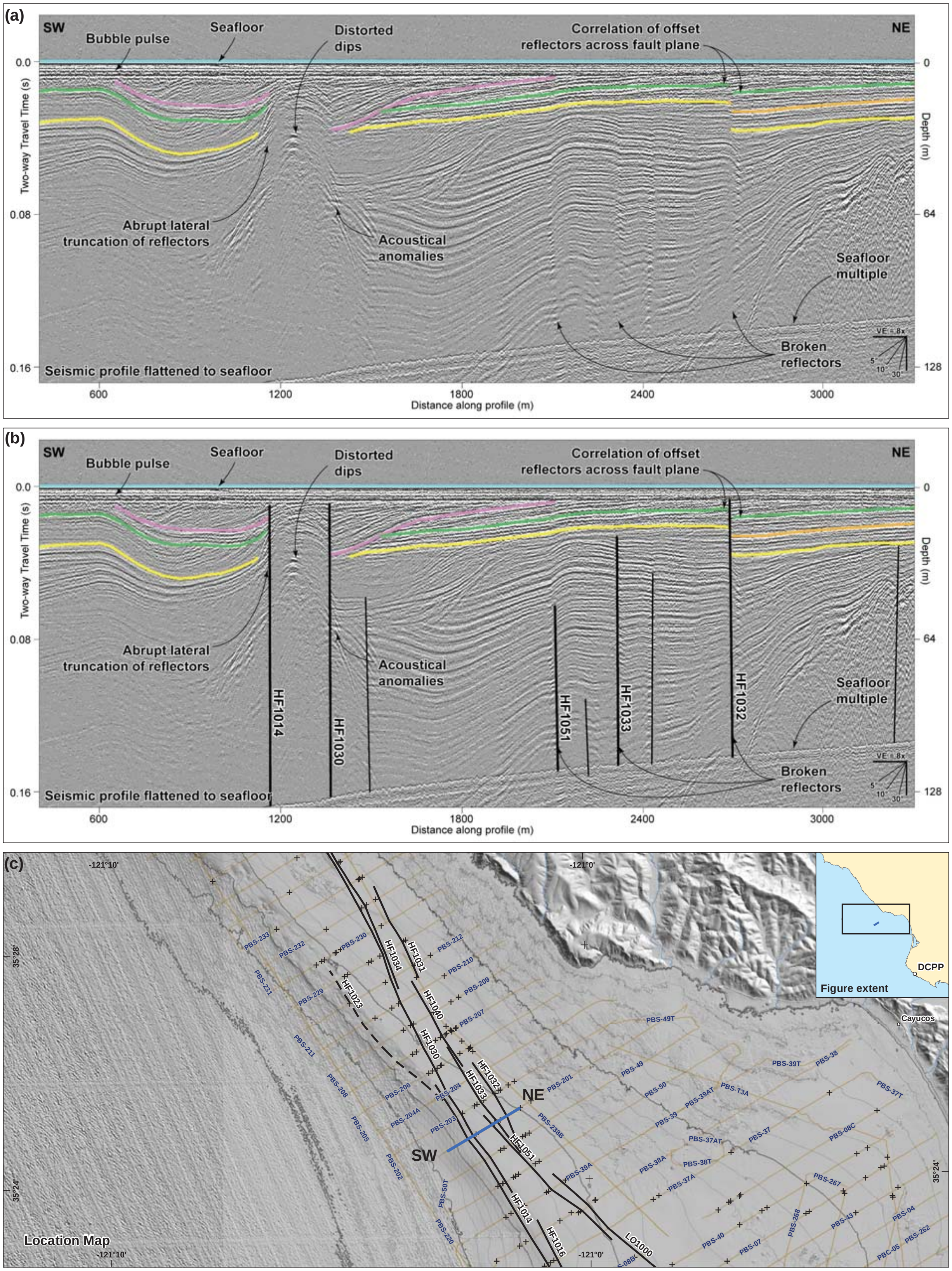

EXPLANATION

- Fault interpreted from USGS seismic profiles, solid where well located, dashed where approximately located, dotted where inferred, queried where existence uncertain.
- Location of seismic profile
- USGS survey trackline, number indicated (PBS-07)
- \+ Unassigned fault
- Seafloor
- Unconformity H20
- Unconformity H30
- Unconformity H32
- Unconformity H40

Map projection and scale: WGS 84 / UTM Zone 10N, 1:120,000

Notes:
1. Depth values on seismic profile assume a velocity of 1,600 m/s.
2. In profiles, thin black lines are unassigned faults, heavy black lines are named faults.

Sources:
- USGS seismic-reflection data (Sliter et al., 2009).
- Project DEM compilation v2013.01. Bathymetric contour interval is 10 m. Heavy contours are 50 m isobaths.

Excerpt of Profile PBS-201 Showing Criteria for Mapping Faults

DCPP OFFSHORE SEISMIC STRATIGRAPHY

Pacific Gas and Electric Company | Figure **3-7**

File path: S:\1005\026\GIS\Figures\Figure_3_7.mxd; Date: 05/15/2013; User: Jereme Chandler, LCI; Rev.1

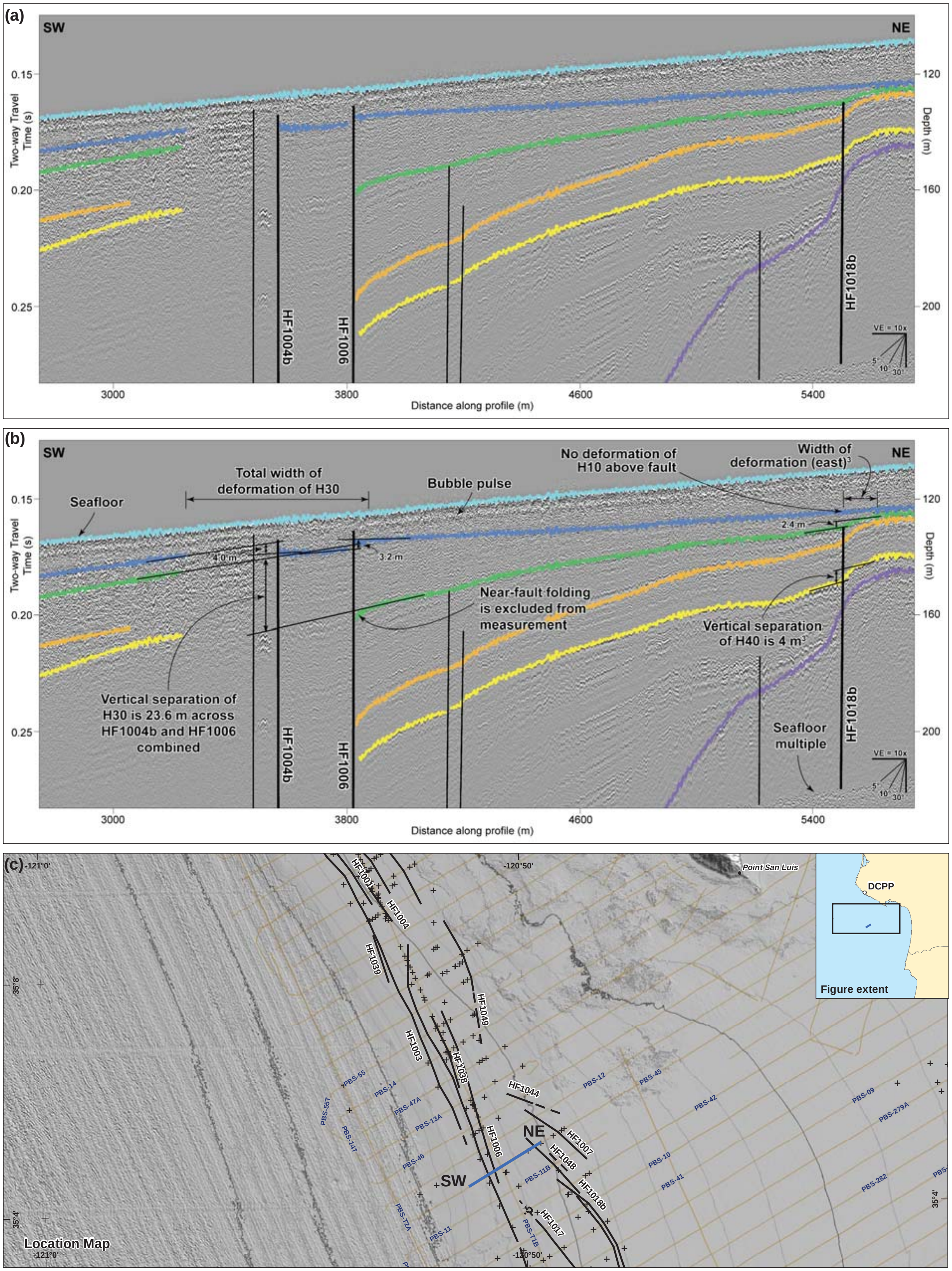

EXPLANATION

Fault interpreted from USGS seismic profiles, solid where well located, dashed where approximately located, dotted where inferred, queried where existence uncertain.

Location of seismic profile

PBS-07 USGS survey trackline, number indicated

+ Unassigned fault

Seafloor

Unconformity H10

Unconformity H30

Unconformity H32

Unconformity H40

Top of Pre-Quaternary

0 2 4 mi.

0 4 8 km

Map projection and scale: WGS 84 / UTM Zone 10N,1:120,000

Note:
1. Depth values on seismic profile assume a velocity of 1,600 m/s.
2. In profiles, thin black lines are unassigned faults, heavy black lines are named faults.
3. Vertical separation on this fault includes deformation (folding) east of the fault. The horizontal extent of this folding defines the width of deformation east of the fault.
4. Vertical separation measurements are taken from the projection of unconformities from outside the zone of fault-related deformation. They ignore the relative contribution of folding vs. discrete faulting. Downthrown direction is indicated.

Sources:
- USGS seismic-reflection data (Sliter et al., 2009).
- Project DEM compilation v2013.01. Bathymetric contour interval is 10 m. Heavy contours are 50 m isobaths.

Excerpt of Profile PBS-45 Showing Example of Vertical Separation Measurements

DCPP OFFSHORE SEISMIC STRATIGRAPHY

Pacific Gas and Electric Company

Figure **3-8**

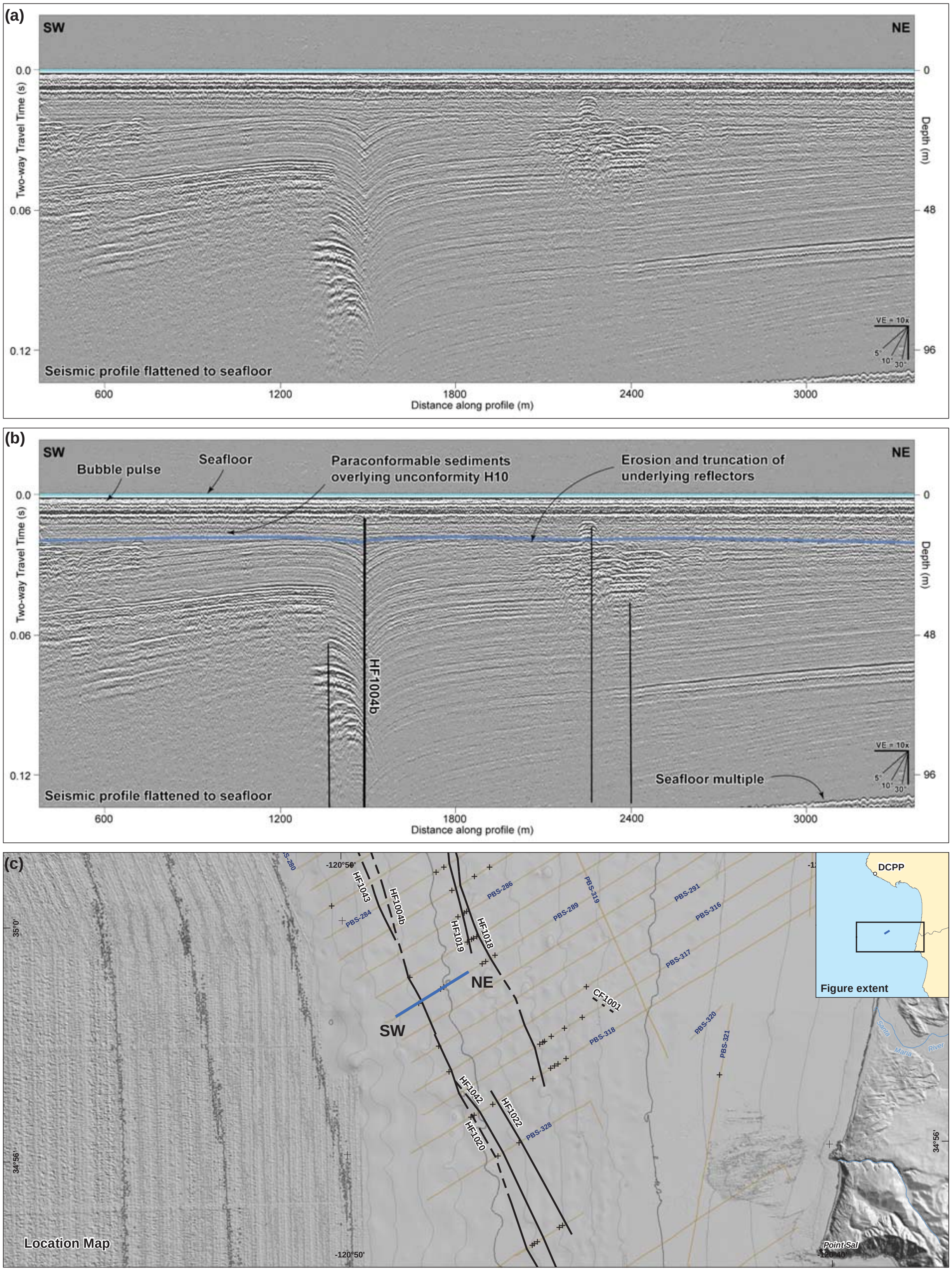

EXPLANATION

- Fault interpreted from USGS seismic profiles, solid where well located, dashed where approximately located, dotted where inferred, queried where existence uncertain.
- Location of seismic profile
- PBS-07 USGS survey trackline, number indicated
- + Unassigned fault
- Seafloor
- Unconformity H10

Notes:
1. Depth values on seismic profile assume a seismic velocity of 1,600 m/s.
2. In profiles, thin black lines are unassigned faults, heavy black lines are named faults.

Sources:
- USGS seismic-reflection data (Sliter et al., 2009).
- Project DEM compilation v2013.01. Bathymetric contour interval is 10 m. Heavy contours are 50 m isobaths.

0 2 4 mi.
0 4 8 km

Map projection and scale: WGS 84 / UTM Zone 10N, 1:120,000

Excerpt of Profile PBS-289 Showing Typical Unconformable Relationships Associated with Unconformity H10

DCPP OFFSHORE SEISMIC STRATIGRAPHY

Pacific Gas and Electric Company

Figure **6-1**

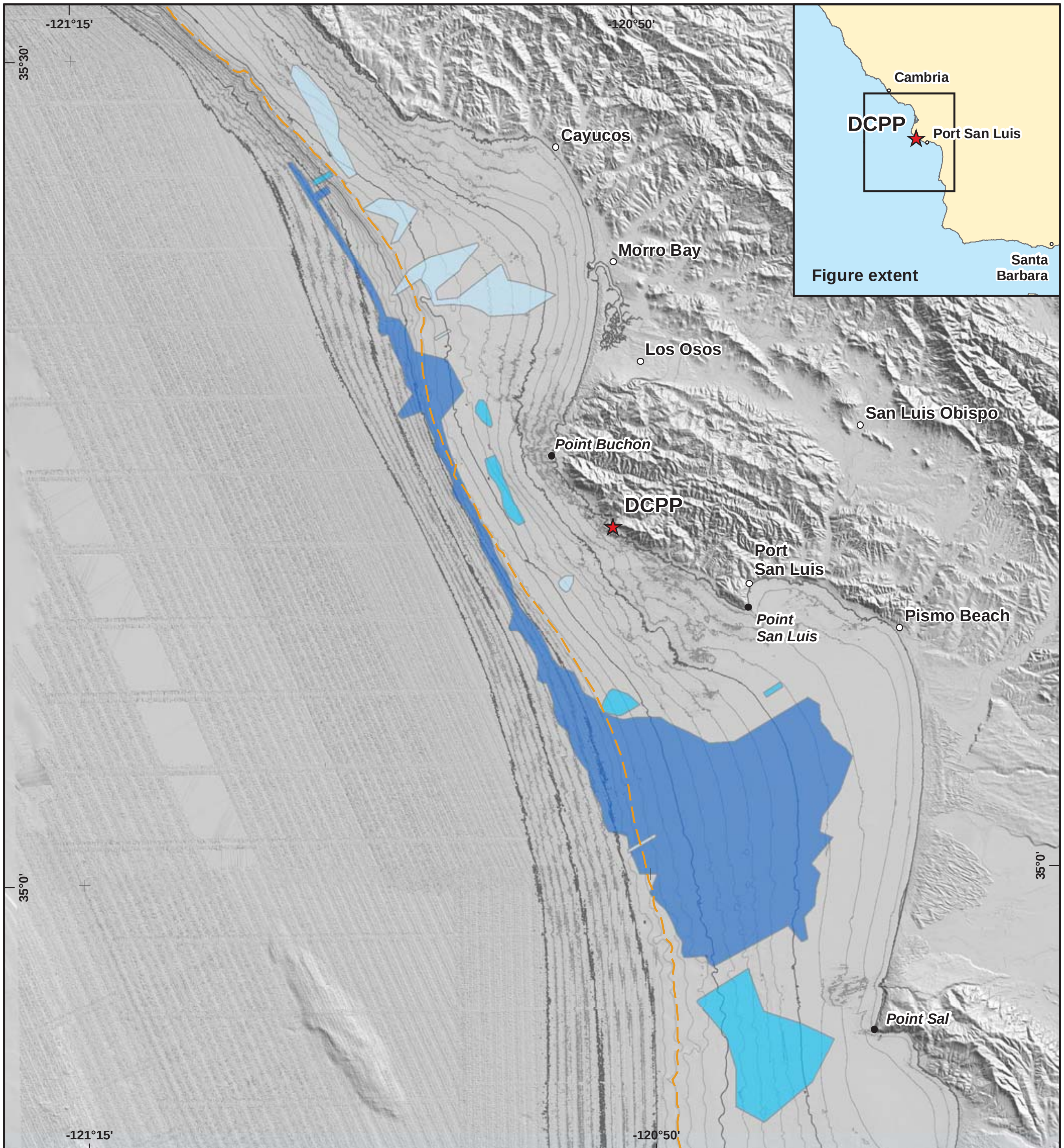

EXPLANATION

- Confidence Grade A
- Confidence Grade B
- Confidence Grade C
- Shelf break

Note:
1. Map only includes regions where H10 is imaged on USGS 2D data. H10 is inferred to extend farther eastward and between mapped areas but is either obscured by the bubble pulse or coincident with the top of pre-Quaternary rock.

Source:
- Project DEM compilation v2013.01. Bathymetric contour interval is 10 m. Heavy contours are 50 m isobaths.

0 2 4 6 8 mi.
0 4 8 12 16 km

Map projection and scale: WGS 84 / UTM Zone 10N,1:400,000

Correlation Confidence Assessment: Unconformity H10

DCPP OFFSHORE SEISMIC STRATIGRAPHY

Pacific Gas and Electric Company | Figure **6-2**

File path: S:\1005\026\GIS\Figures\Figure_6_2.mxd; Date: 05/17/2013; User: Jereme Chandler, LCI; Rev.1

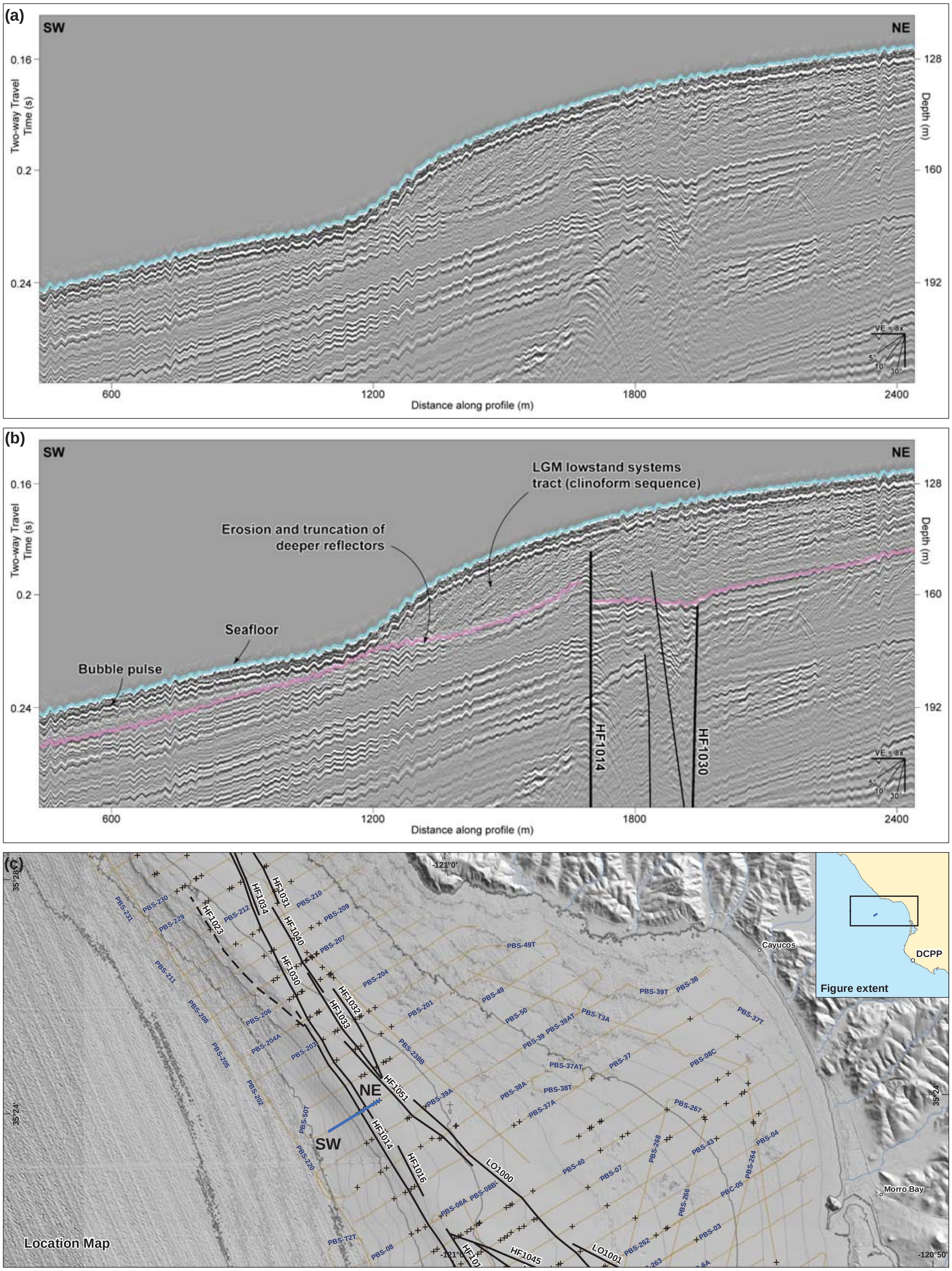

EXPLANATION

Fault interpreted from USGS seismic profiles, solid where well located, dashed where approximately located, dotted where inferred, queried where existence uncertain.

Location of seismic profile

PBS-07 USGS survey trackline, number indicated

\+ Unassigned fault

Seafloor

Unconformity H20

Notes:
1. Depth values on seismic profile assume a velocity of 1,600 m/s.
2. In profiles, thin black lines are unassigned faults, heavy black lines are named faults.

Sources:
- USGS seismic-reflection data (Sliter et al., 2009).
- Project DEM compilation v2013.01. Bathymetric contour interval is 10 m. Heavy contours are 50 m isobaths.

0 2 4 mi.
0 4 8 km

Map projection and scale: WGS 84 / UTM Zone 10N, 1:120,000

Excerpt of Profile PBS-50 Showing Typical Unconformable Relationships Associated with Unconformity H20

DCPP OFFSHORE SEISMIC STRATIGRAPHY

Pacific Gas and Electric Company

Figure **6-3**

File path: S:\1005\026\GIS\Figures\Figure_6_3.mxd; Date: 05/15/2013; User: Jeremy Chandler, LCI; Rev.1

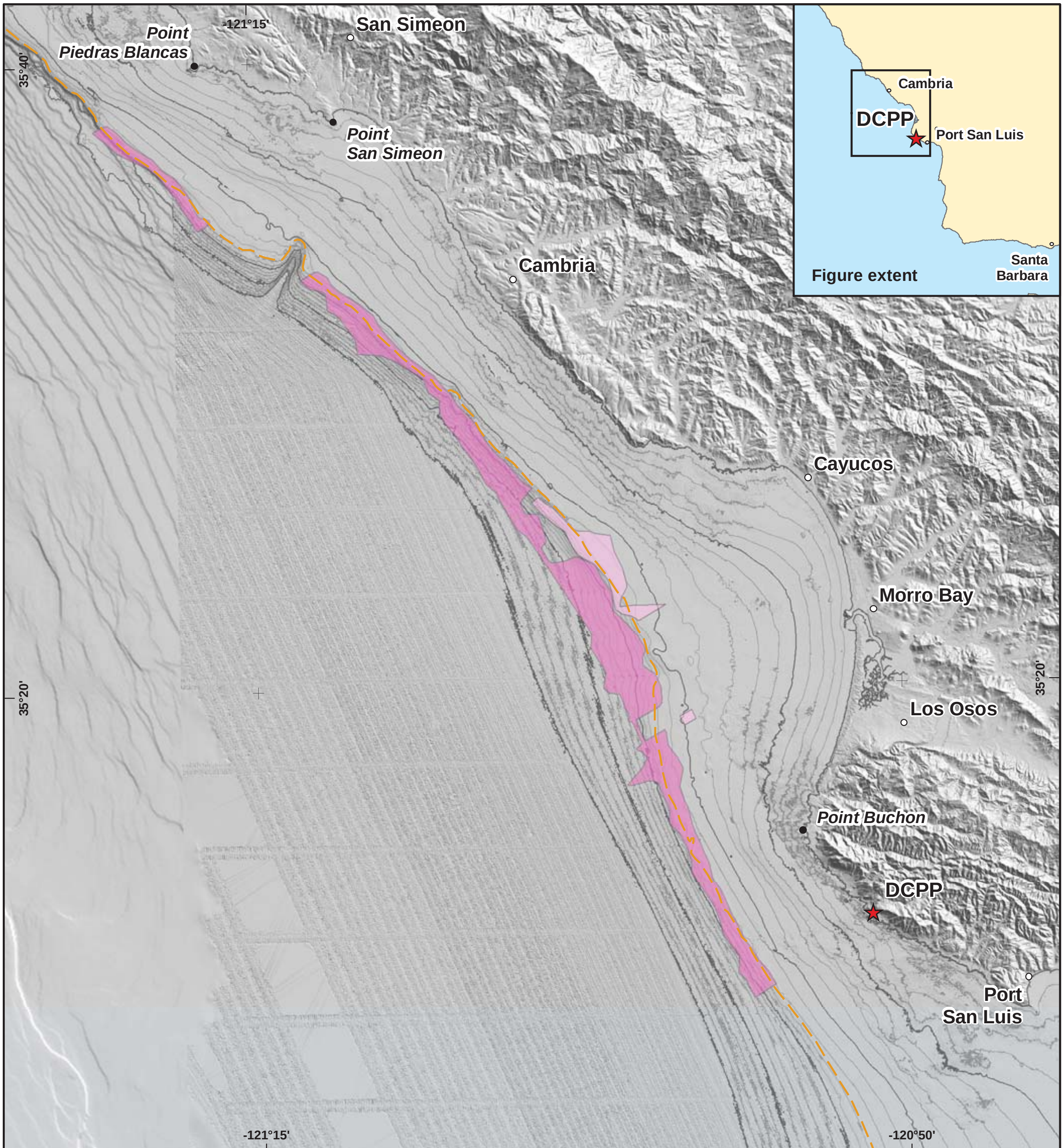

File path: S:\1005\026\GIS\Figures\Figure_6_4.mxd; Date: 05/15/2013; User: Jereme Chandler, LCI; Rev.1

EXPLANATION

- Confidence Grade B
- Confidence Grade C
- Shelf break

Note:
1. Unconformity H20 occurs mostly along the shelf break.

Source:
- Project DEM compilation v2013.01. Bathymetric contour interval is 10 m. Heavy contours are 50 m isobaths.

0 2 4 6 8 mi.
0 4 8 12 16 km

Map projection and scale: WGS 84 / UTM Zone 10N,1:350,000

Correlation Confidence Assessment: Unconformity H20

DCPP OFFSHORE SEISMIC STRATIGRAPHY

Pacific Gas and Electric Company | Figure **6-4**

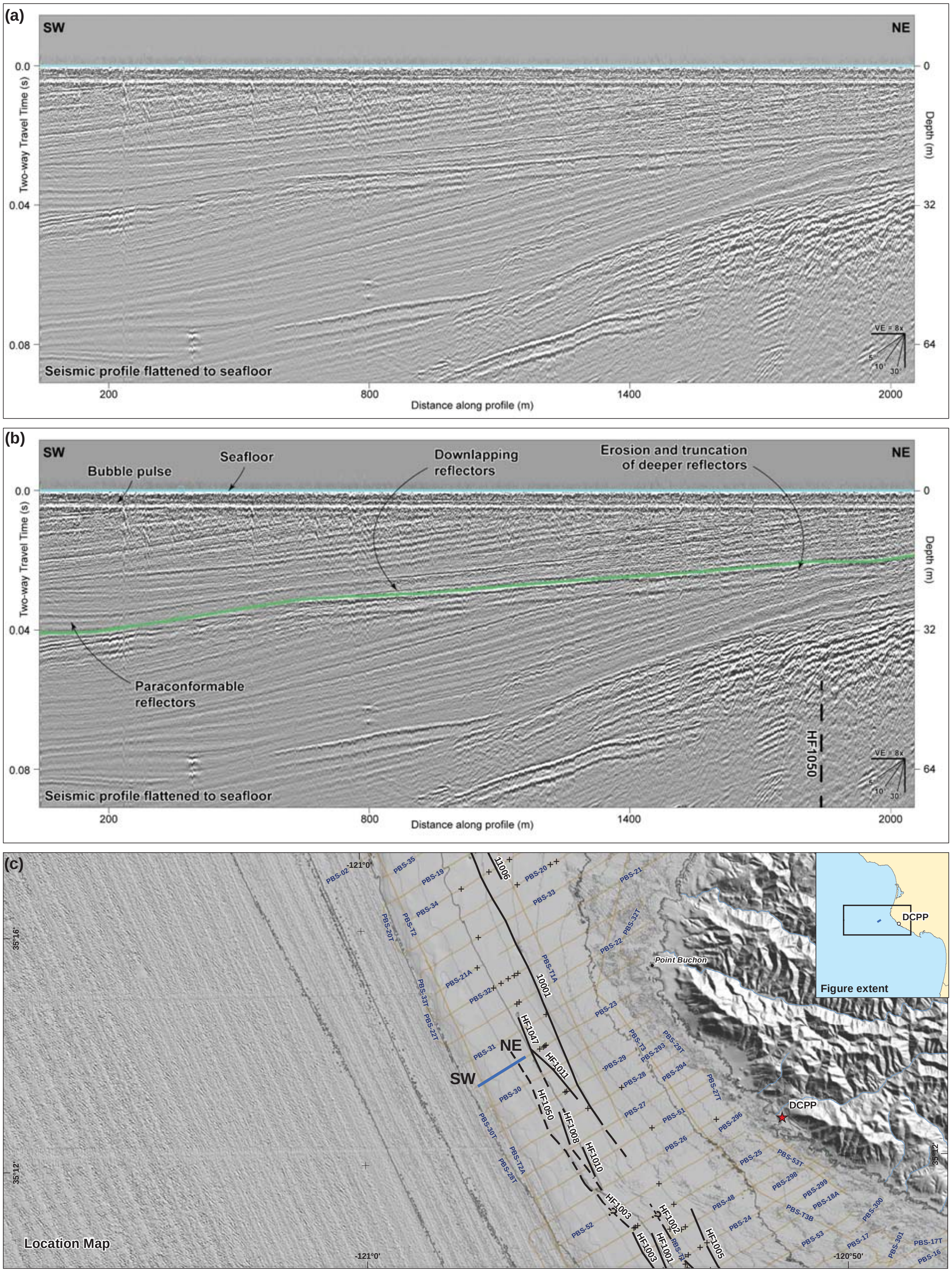

EXPLANATION

- Fault interpreted from USGS seismic profiles, solid where well located, dashed where approximately located, dotted where inferred, queried where existence uncertain.
- Location of seismic profile
- PBS-07 USGS survey trackline, number indicated
- \+ Unassigned fault
- Seafloor
- Unconformity H30

Sources:
- USGS seismic-reflection data (Sliter et al., 2009).
- Project DEM compilation v2013.01. Bathymetric contour interval is 10 m. Heavy contours are 50 m isobaths.

0 2 4 mi.
0 4 8 km

Map projection and scale: WGS 84 / UTM Zone 10N,1:120,000

Note:
1. Depth values on seismic profile assume a velocity of 1,600 m/s.

Excerpt of Profile PBS-23 Showing Typical Unconformable Relationships Associated with Unconformity H30

DCPP OFFSHORE SEISMIC STRATIGRAPHY

Pacific Gas and Electric Company | Figure **6-5**

File path: S:\1005\026\GIS\Figures\Figure_6_5.mxd; Date: 05/15/2013; User: Jereme Chandler, LCI; Rev.1

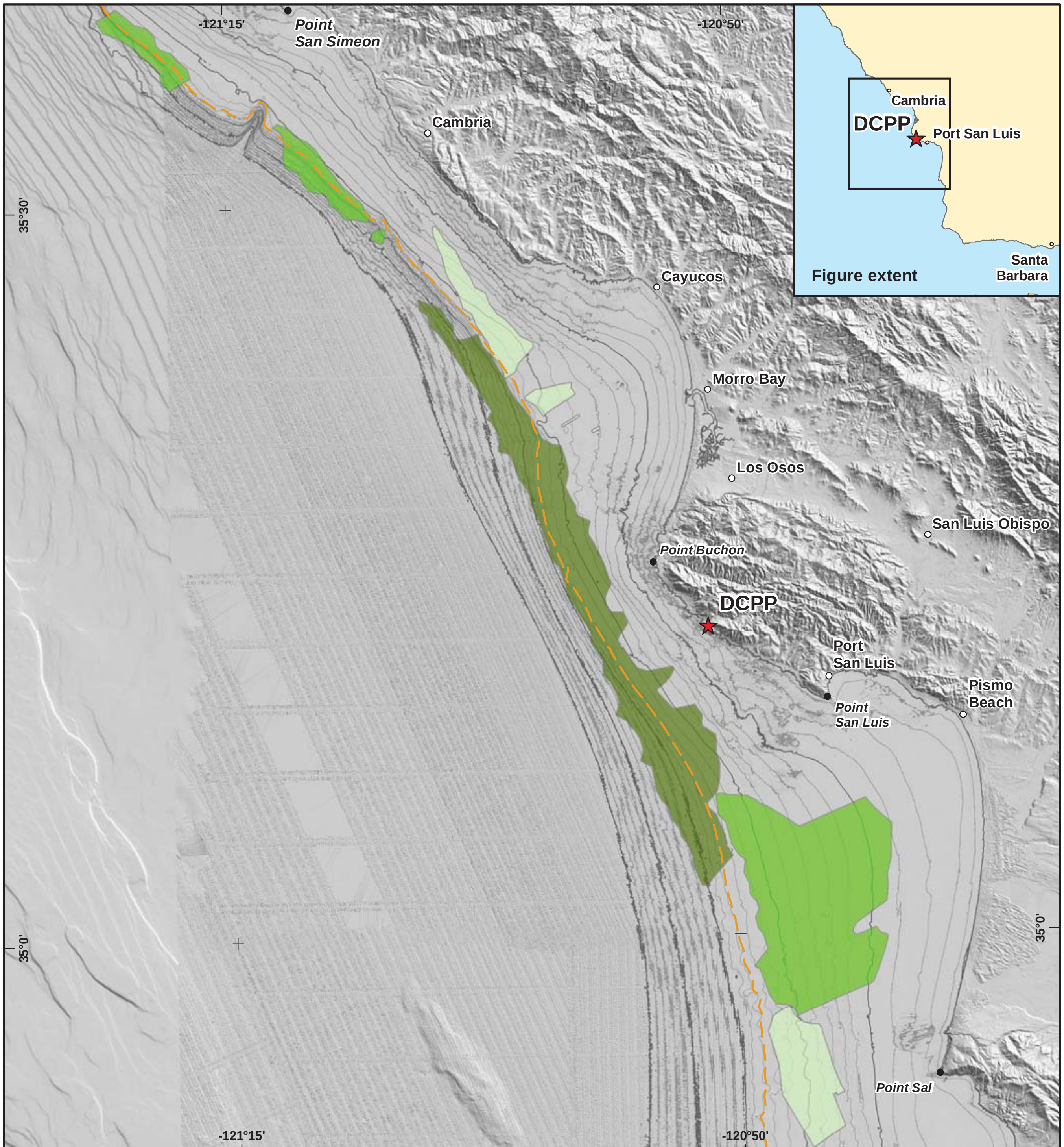

EXPLANATION

- Confidence Grade A
- Confidence Grade B
- Confidence Grade C
- Shelf break

0 2 4 6 8 mi.
0 4 8 12 16 km

Map projection and scale: WGS 84 / UTM Zone 10N,1:450,000

Source:
- Project DEM compilation v2013.01. Bathymetric contour interval is 10 m. Heavy contours are 50 m isobaths.

Correlation Confidence Assessment: Unconformity H30

DCPP OFFSHORE SEISMIC STRATIGRAPHY

Pacific Gas and Electric Company | Figure **6-6**

File path: S:\1005\026\GIS\Figures\Figure_6_6.mxd; Date: 05/15/2013; User: Jereme Chandler, LCI; Rev.1

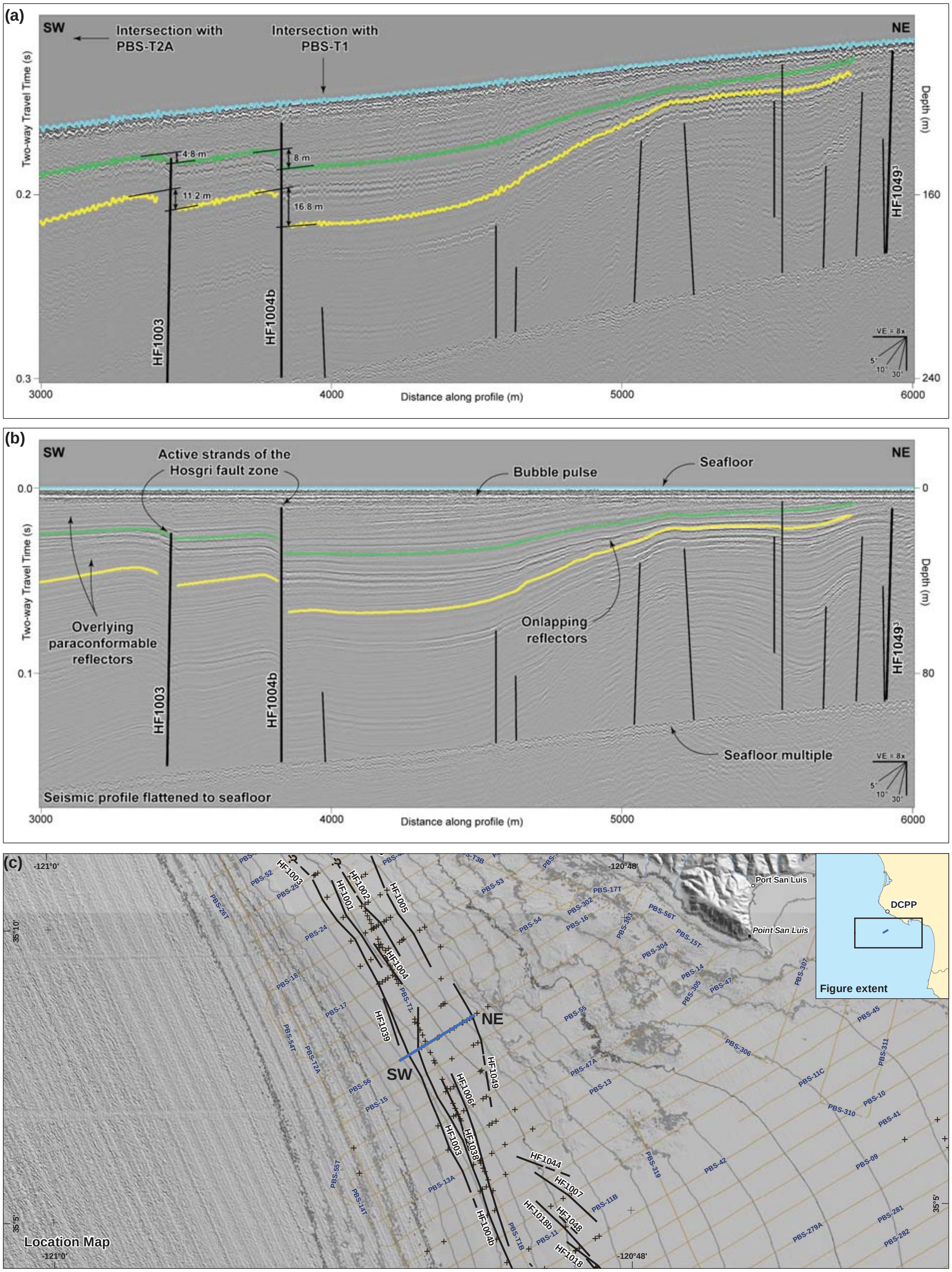

EXPLANATION

- Fault interpreted from USGS seismic profiles, solid where well located, dashed where approximately located, dotted where inferred, queried where existence uncertain.
- Location of seismic profile
- PBS-07 USGS survey trackline, number indicated
- \+ Unassigned fault
- Seafloor
- Unconformity H30
- Unconformity H40

Sources:
- USGS seismic-reflection data (Sliter et al., 2009).
- Project DEM compilation v2013.01. Bathymetric contour interval is 10 m. Heavy contours are 50 m isobaths.

0 2 4 mi.
0 4 8 km

Map projection and scale: WGS 84 / UTM Zone 10N, 1:120,000

Notes:
1. Depth values on seismic profile assume a velocity of 1,600 m/s.
2. In profiles, thin black lines are unassigned faults, heavy black lines are named faults.
3. HF1049 is shown on Plate 1 as yellow because it exhibits clear evidence for deformation of unconformity H40, and unconformity H30 is missing above HF1049. West of fault HF1049 an unassigned fault displaces unconformity H30 and older reflectors. Although the unassigned fault exhibits evidence for more recent activity than fault HF1049, it cannot be correlated on adjacent seismic profiles.

Excerpt of Profile PBS-56 Showing Unconformities H30 and H40 Between Strands of the Hosgri Fault Zone, Allowing Correlation of Stratigraphy Between Western (PBS-T2A) and Eastern (PBS-T1) Tie Lines

DCPP OFFSHORE SEISMIC STRATIGRAPHY

Pacific Gas and Electric Company | Figure **6-7**

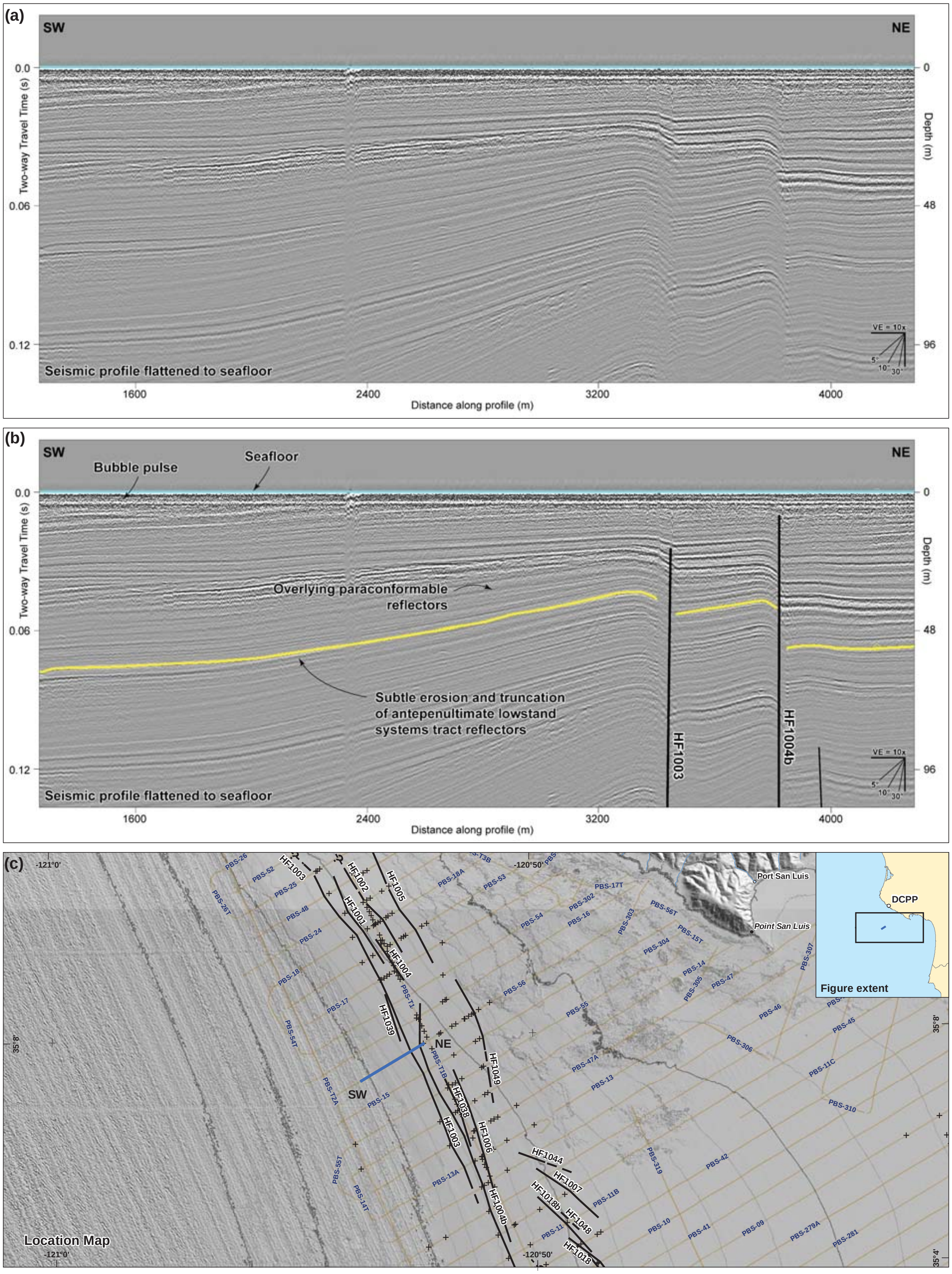

EXPLANATION

▬ ▬ ?···	Fault interpreted from USGS seismic profiles, solid where well located, dashed where approximately located, dotted where inferred, queried where existence uncertain.
▬ (blue)	Location of seismic profile
PBS-07	USGS survey trackline, number indicated
+	Unassigned fault
▬ (light blue)	Seafloor
▬ (yellow)	Unconformity H40

Sources:
- USGS seismic-reflection data (Sliter et al., 2009).
- Project DEM compilation v2013.01. Bathymetric contour interval is 10 m. Heavy contours are 50 m isobaths.

Notes:
1. Depth values on seismic profile assume a velocity of 1,600 m/s.
2. In profiles, thin black lines are unassigned faults, heavy black lines are named faults.

0 2 4 mi.
0 4 8 km

Map projection and scale: WGS 84 / UTM Zone 10N, 1:120,000

Excerpt of Profile PBS-56 Showing Typical Unconformable Relationships Associated with Unconformity H40

DCPP OFFSHORE SEISMIC STRATIGRAPHY

Pacific Gas and Electric Company | Figure **6-8**

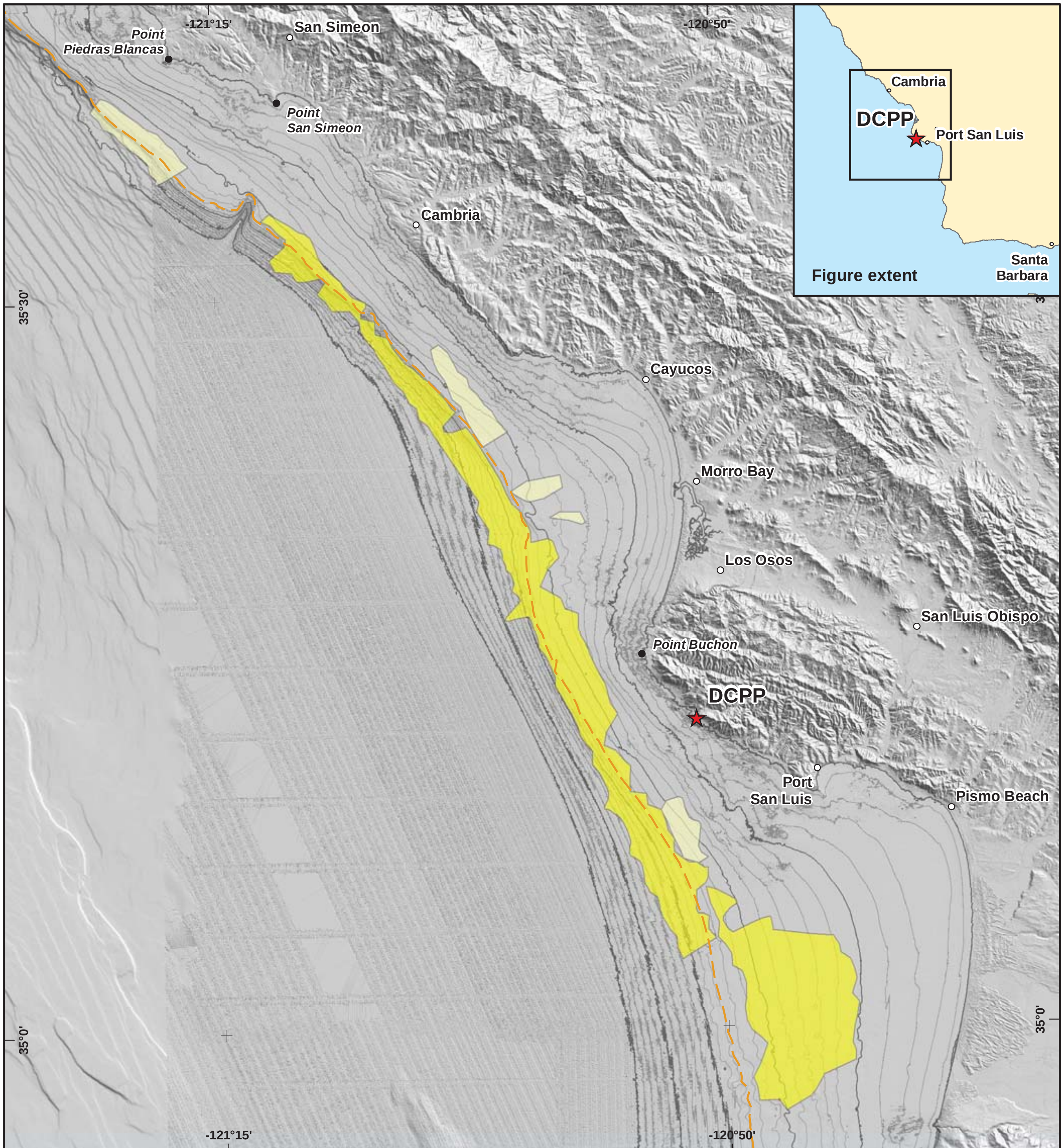

EXPLANATION

- Confidence Grade B
- Confidence Grade C
- Shelf break

Source:
- Project DEM compilation v2013.01. Bathymetric contour interval is 10 m. Heavy contours are 50 m isobaths.

0 2 4 6 8 mi.
0 4 8 12 16 km

Map projection and scale: WGS 84 / UTM Zone 10N,1:450,000

Correlation Confidence Assessment: Unconformity H40

DCPP OFFSHORE SEISMIC STRATIGRAPHY

Pacific Gas and Electric Company | Figure **6-9**

File path: S:\1005\026\GIS\Figures\Figure_6_9.mxd; Date: 05/15/2013; User: Jereme Chandler, LCI; Rev.1

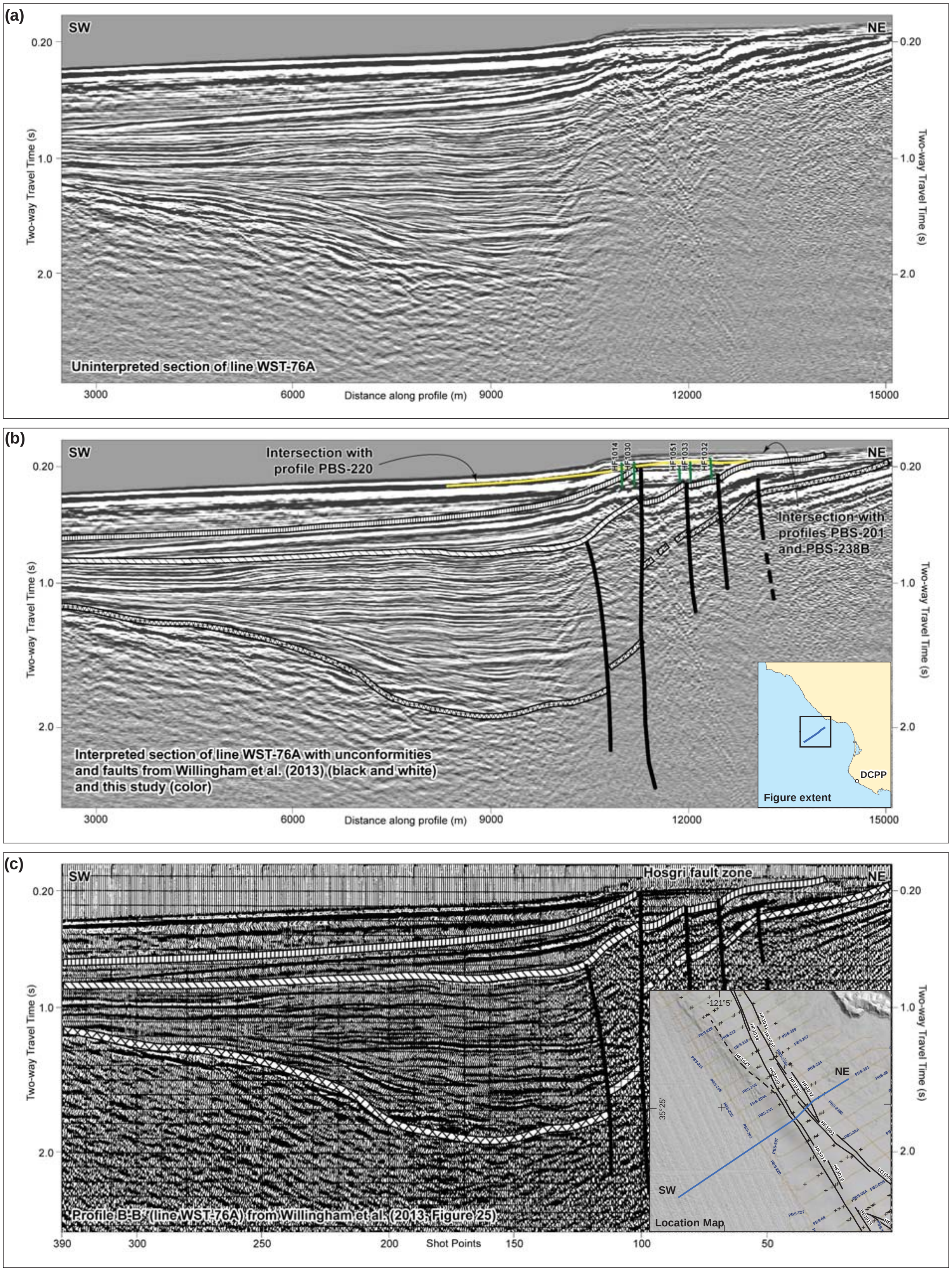

EXPLANATION

Interpretation from Willingham et al. (2013)

- Fault, dashed where continuity is inferred
- Early-late Pliocene unconformity, 3.5-2.7 Ma
- Top of Miocene unconformity, 5.5-5.1 Ma
- Top of pre-Miocene basement unconformity, 23-17.1 Ma

Interpretation from This Study, Projected from Adjacent USGS 2D Profile Numbers PBS-201 and PBS-49

- Fault
- Unconformity H40

- Location of seismic profile

Sources:
- USGS seismic-reflection data (Sliter et al., 2009).
- Interpreted seismic profile in Panel c from Willingham et al. (2013)
- Project DEM compilation v2013.01.

Notes:
1. Panel b shows a comparison of interpretations from two studies overlain on the same seismic profile. Unconformities and faults interpreted for this study are projected from adjacent USGS 2D seismic profiles. Downdip extent of faults is the approximate limit of interpretability of data at this site. Unconformities and faults from Willingham et al. (2013) are copied from their figure (Panel c) by digitizing them on the uninterpreted data in Kingdom software.
2. Refer to Plate 1 for explanation of profile inset map.

0 2 4 mi.

0 4 8 km

Map projection and scale: WGS 84 / UTM Zone 10N,1:213,000

Comparison of Unconformity H40 Mapped for This Study to Tertiary Unconformities on Line WST-76A, Offshore Santa Maria Basin

DCPP OFFSHORE SEISMIC STRATIGRAPHY

Pacific Gas and Electric Company | Figure **6-10a**

File path: S:\1005\026\GIS\Figures\Figure_6_10a.mxd; Date: 05/15/2013; User: Jereme Chandler, LCI; Rev.1

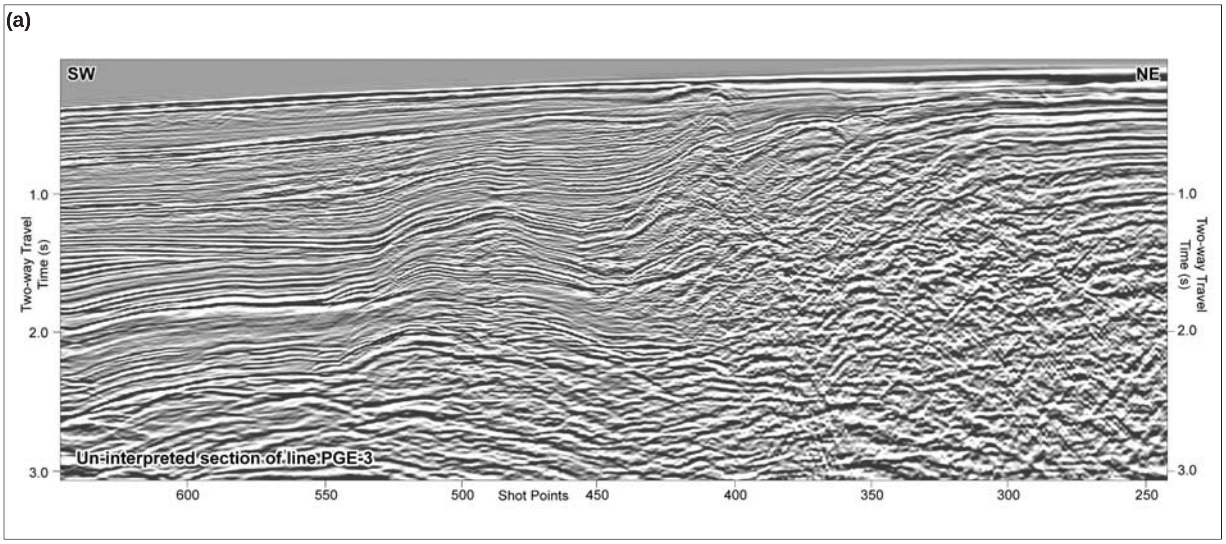

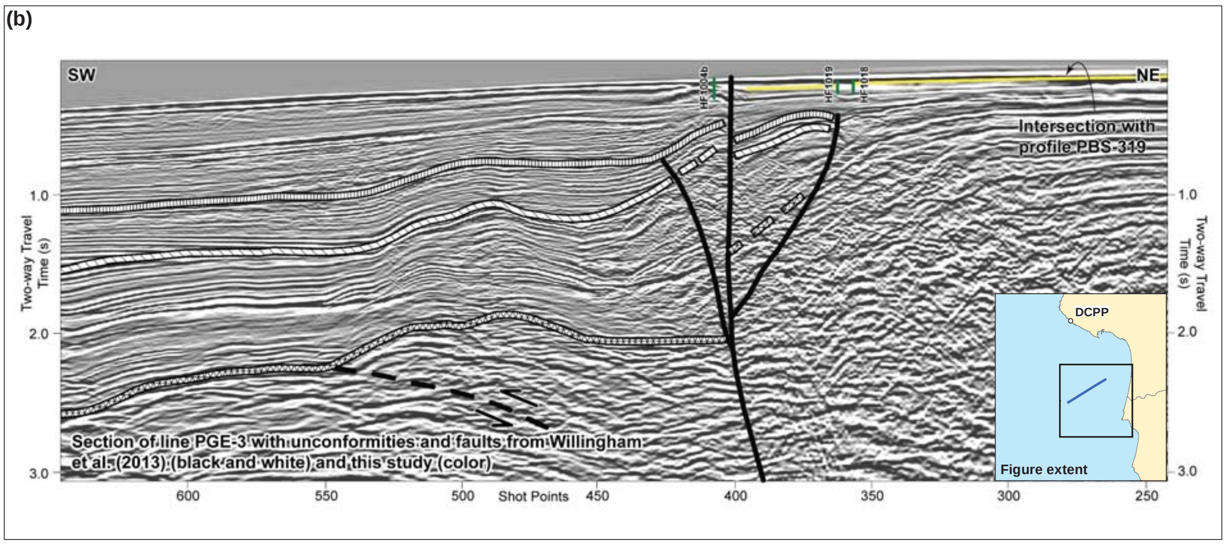

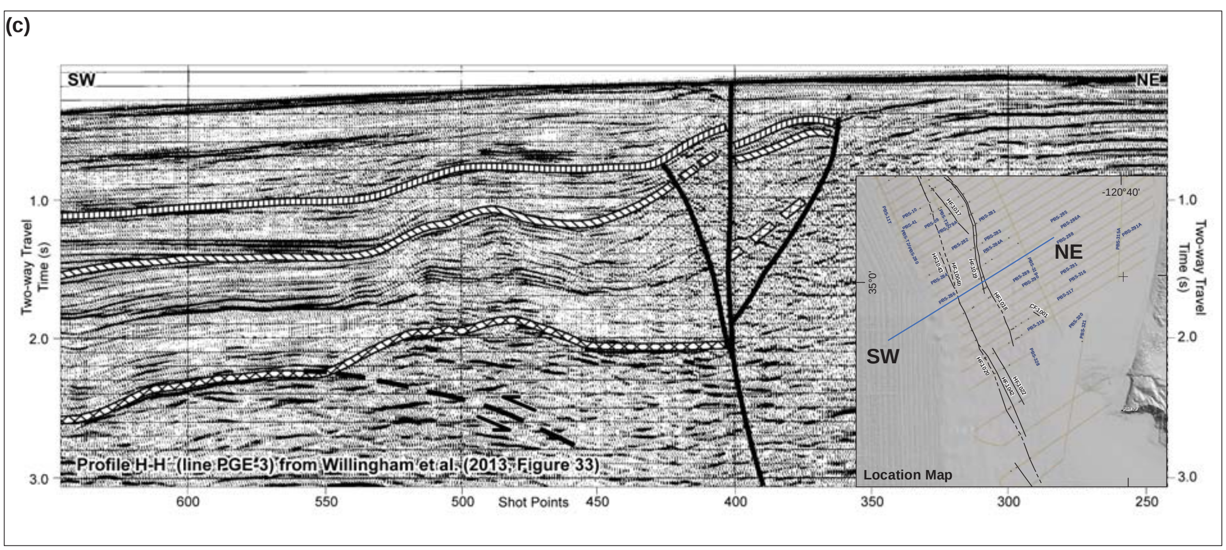

EXPLANATION

Interpretation from Willingham et al. (2013)

Fault, dashed where continuity is inferred; arrows show direction of relative displacement on low-angle detachments

Early-late Pliocene unconformity, 3.5-2.7 Ma

Top of Miocene unconformity, 5.5-5.1 Ma

Top of pre-Miocene basement unconformity, 23-17.1 Ma

Interpretation from This Study, Projected from Adjacent USGS 2D Profile Numbers PBS-286 and PBS-288

Fault

Unconformity H40

Location of seismic profile

Sources:
- USGS seismic-reflection data (Sliter et al., 2009).
- Interpreted seismic profile in Panel c from Willingham et al. (2013)
- Project DEM compilation v2013.01.

Notes:
1. Panel b shows a comparison of interpretations from two studies overlain on the same seismic profile. Unconformities and faults interpreted for this study are projected from adjacent USGS 2D seismic profiles. Downdip extent of faults is the approximate limit of interpretability of data at this site. Unconformities and faults from Willingham et al. (2013) are copied from their figure (Panel c) by digitizing them on the uninterpreted data in Kingdom software.
2. Refer to Plate 1 for explanation of profile inset map.

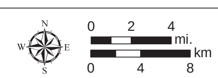

Map projection and scale: WGS 84 / UTM Zone 10N, 1:392,000

Comparison of Unconformity H40 Mapped for This Study to Tertiary Unconformities on Line PGE-3, Offshore Santa Maria Basin

DCPP OFFSHORE SEISMIC STRATIGRAPHY

Pacific Gas and Electric Company | Figure **6-10b**

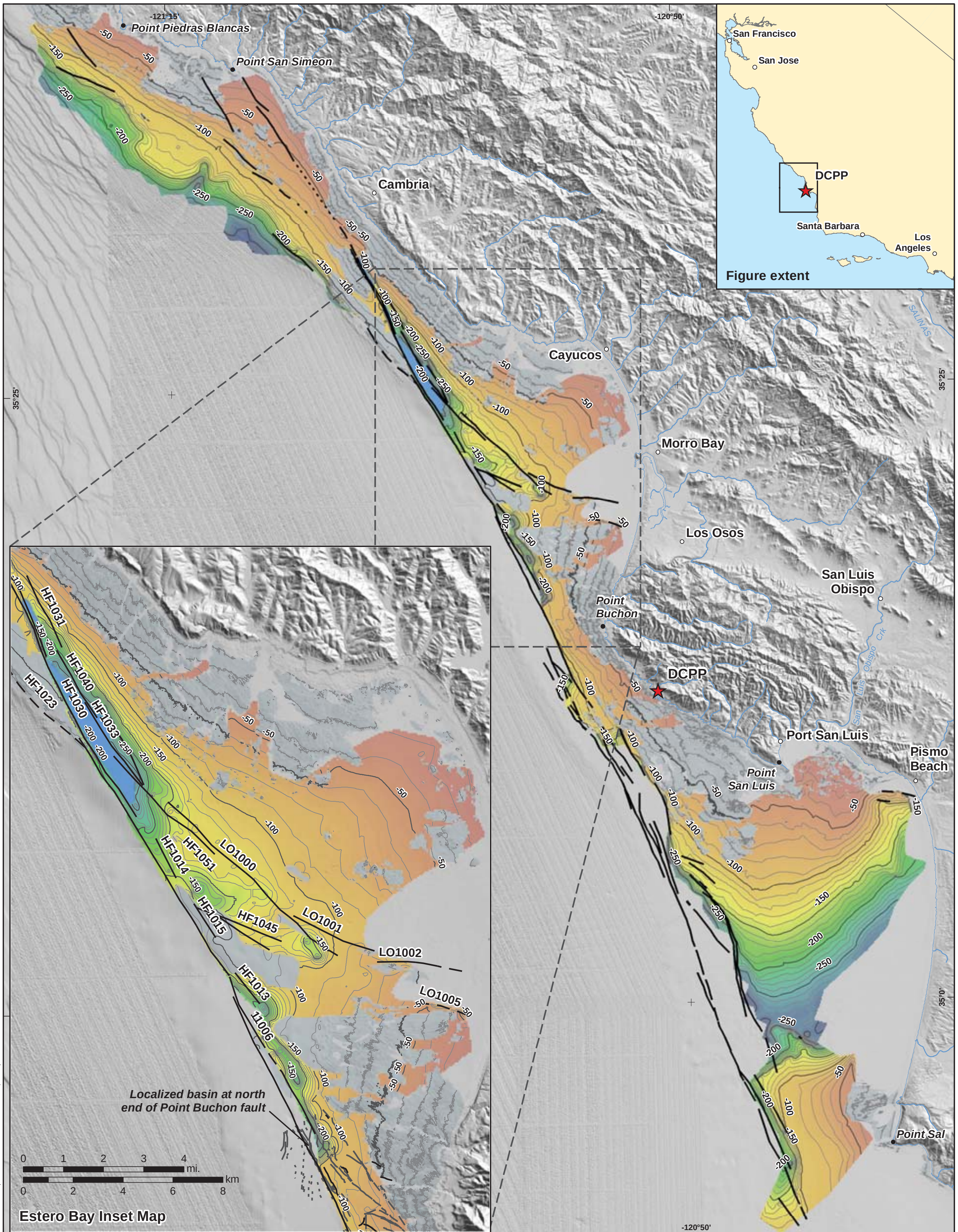

File path: S:\1005\026\GIS\Figures\Figure_6_11.mxd; Date: 05/16/2013; User: Jereme Chandler, LCI; Rev.1

EXPLANATION

Fault interpreted from USGS seismic profiles, solid where well located, dashed where approximately located, dotted where inferred, queried where existence uncertain.

Top of pre-Quaternary rock below limit of interpretability on USGS seismic profiles

Exposed bedrock

Top of Pre-Quaternary Rock Depth Below Sea Level

High : - 15 m

Low : -350 m

10 m structure contour interval, heavy contour are 50 m. Bathymetric contours are used in regions where bedrock is exposed at the seafloor.

Note: Where they meet, bathymetric contours do not align with interpreted contours on the top of pre-Quaternary because the USGS seismic profiles are not depth-migrated, and depths of structure contours interpreted from the seismic-reflection data were estimated using an assumed seismic velocity of 1,600 m/s. Therefore, the general shape of the structure contours is accurate, but the actual depths are an approximation.

Sources:
-Project DEM compilation v2013.01.
-Traces of Pt. Buchon fault from PG&E (2012).

0 2 4 6 8 mi.
0 4 8 12 16 km

Map projection and scale: WGS 84 / UTM Zone 10N,1:280,000

Structure Contour Map of the Top of Pre-Quaternary Rock

DCPP OFFSHORE SEISMIC STRATIGRAPHY

Pacific Gas and Electric Company | Figure **6-11**

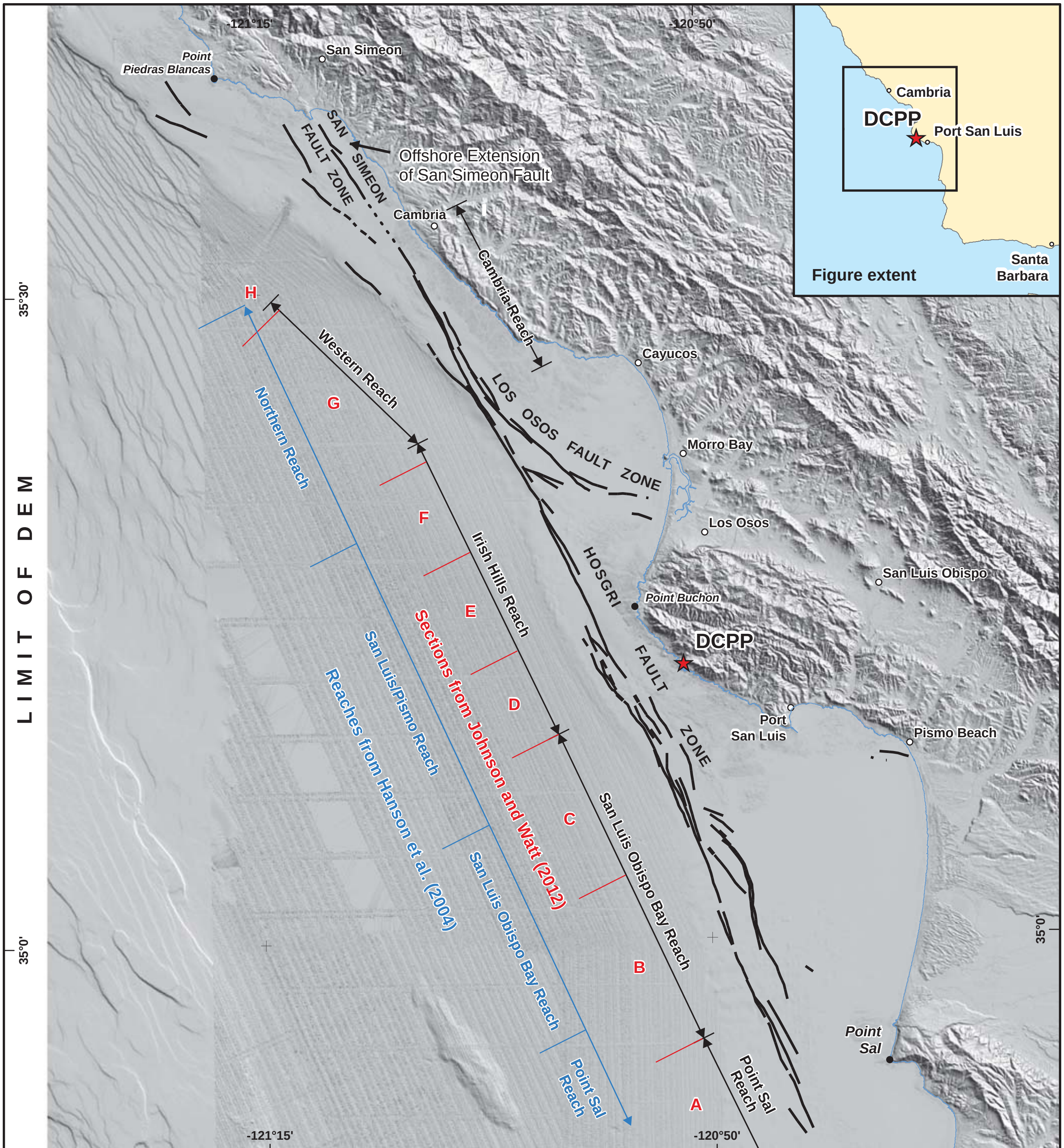

EXPLANATION

Fault interpreted from USGS seismic profiles, solid where well located, dashed where approximately located, dotted where inferred, queried where existence uncertain.

0 2 4 6 8 mi.

0 4 8 12 16 km

Map projection and scale: WGS 84 / UTM Zone 10N, 1:506,761

Sources:
- USGS seismic-reflection data (Sliter et al., 2009).
- Project DEM compilation v2013.01.
  Bathymetric contour interval is 10 m.
  Heavy contours are 50 m isobaths.

Note:
1. We divide the Hosgri fault zone into five “reaches” based on changes in fault trace complexity, amount and sense of vertical separation, relationships to adjacent crustal blocks, and relationships to intersecting faults.

Reaches of the Hosgri Fault Zone

DCPP OFFSHORE SEISMIC STRATIGRAPHY

Pacific Gas and Electric Company | Figure **7-1**

File path: S:\1005\026\GIS\Figures\Figure_7_1.mxd; Date: 05/16/2013; User: Jereme Chandler, LCI; Rev.1

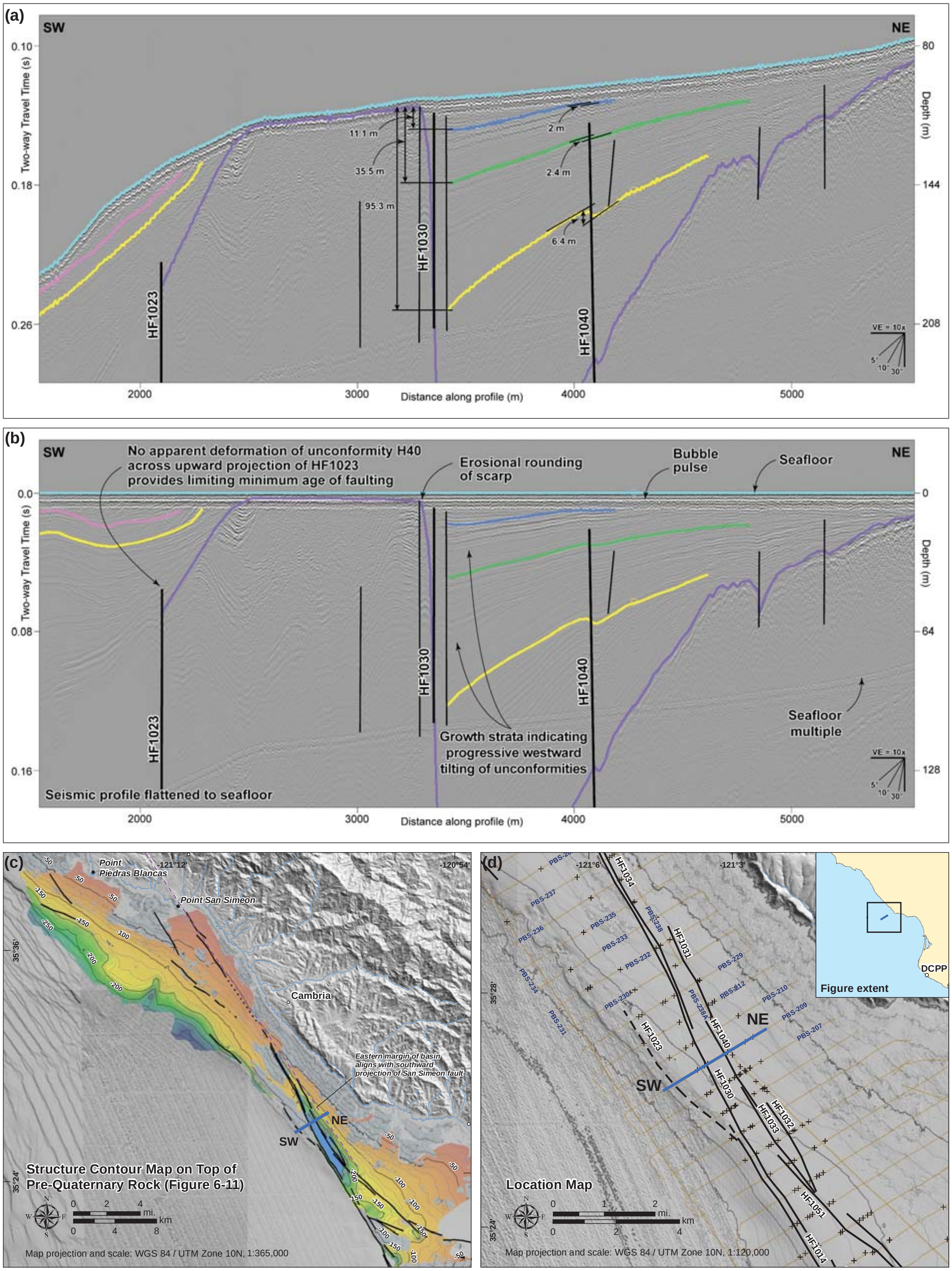

EXPLANATION

- Fault interpreted from USGS seismic profiles, solid where well located, dashed where approximately located, dotted where inferred, queried where existence uncertain.
- Location of seismic profile
- PBS-07 — USGS survey trackline, number indicated
- + Unassigned fault
- Seafloor
- Unconformity H10
- Unconformity H20
- Unconformity H30
- Unconformity H40
- Top of pre-Quaternary

Sources:
- USGS seismic-reflection data (Sliter et al., 2009).
- Project DEM compilation v2013.01. Bathymetric contour interval is 10 m. Heavy contours are 50 m isobaths.

Notes:
1. Depth values on seismic profile assume a velocity of 1,600 m/sec.
2. In profiles, thin black lines are unassigned faults, heavy black lines are named faults.
3. Panel c is an excerpt from Figure 6-11. Refer to Figure 6-11 for explanation of map symbology.

Excerpt of Profile PBS-209 Showing Half Graben Associated with Right Step in Hosgri-San Simeon Fault System

DCPP OFFSHORE SEISMIC STRATIGRAPHY

Pacific Gas and Electric Company | Figure **7-2**

File path: S:\1005\026\GIS\Figures\Figure_7_2.mxd; Date: 05/17/2013; User: Jereme Chandler, LCI; Rev.1

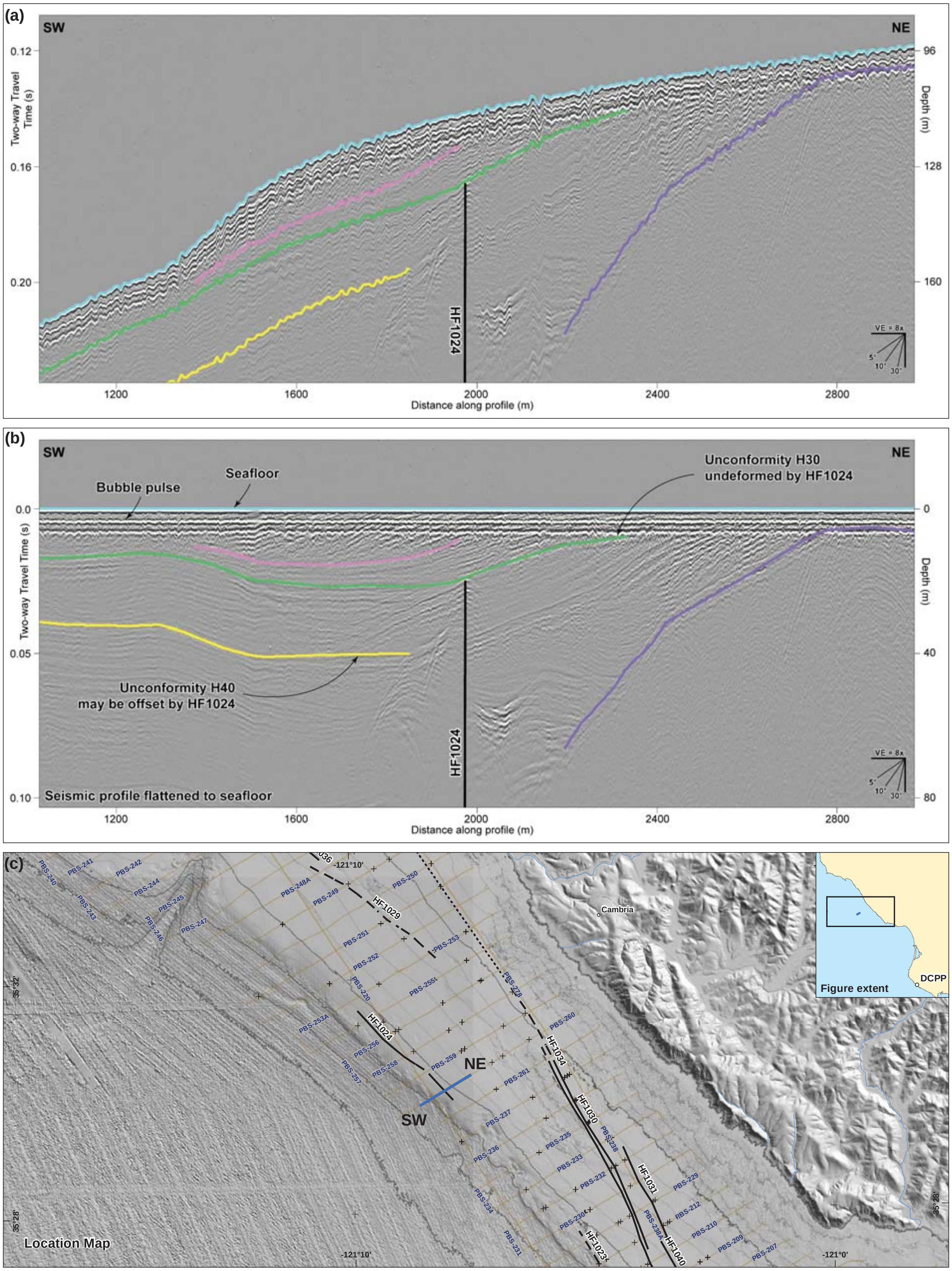

EXPLANATION

Fault interpreted from USGS seismic profiles, solid where well located, dashed where approximately located, dotted where inferred, queried where existence uncertain.

Location of seismic profile

PBS-07 USGS survey trackline, number indicated

+ Unassigned fault

Seafloor

Unconformity H20

Unconformity H30

Unconformity H40

Top of pre-Quaternary rock

0 2 4 mi.

0 4 8 km

Map projection and scale: WGS 84 / UTM Zone 10N,1:120,000

Notes:
1. Depth values on seismic profile assume a velocity of 1,600 m/s.
2. In profiles, thin black lines are unassigned faults, heavy black lines are named faults.

Sources:
- USGS seismic-reflection data (Sliter et al., 2009).
- Project DEM compilation v2013.01. Bathymetric contour interval is 10 m. Heavy contours are 50 m isobaths.

Excerpt of Profile PBS-260 Showing Continuity of Unconformity H30 Above West Branch of Hosgri Fault Zone

DCPP OFFSHORE SEISMIC STRATIGRAPHY

Pacific Gas and Electric Company | Figure **7-3**

File path: S:\1005\026\GIS\Figures\Figure_7_3.mxd; Date: 05/17/2013; User: Jereme Chandler, LCI; Rev.1

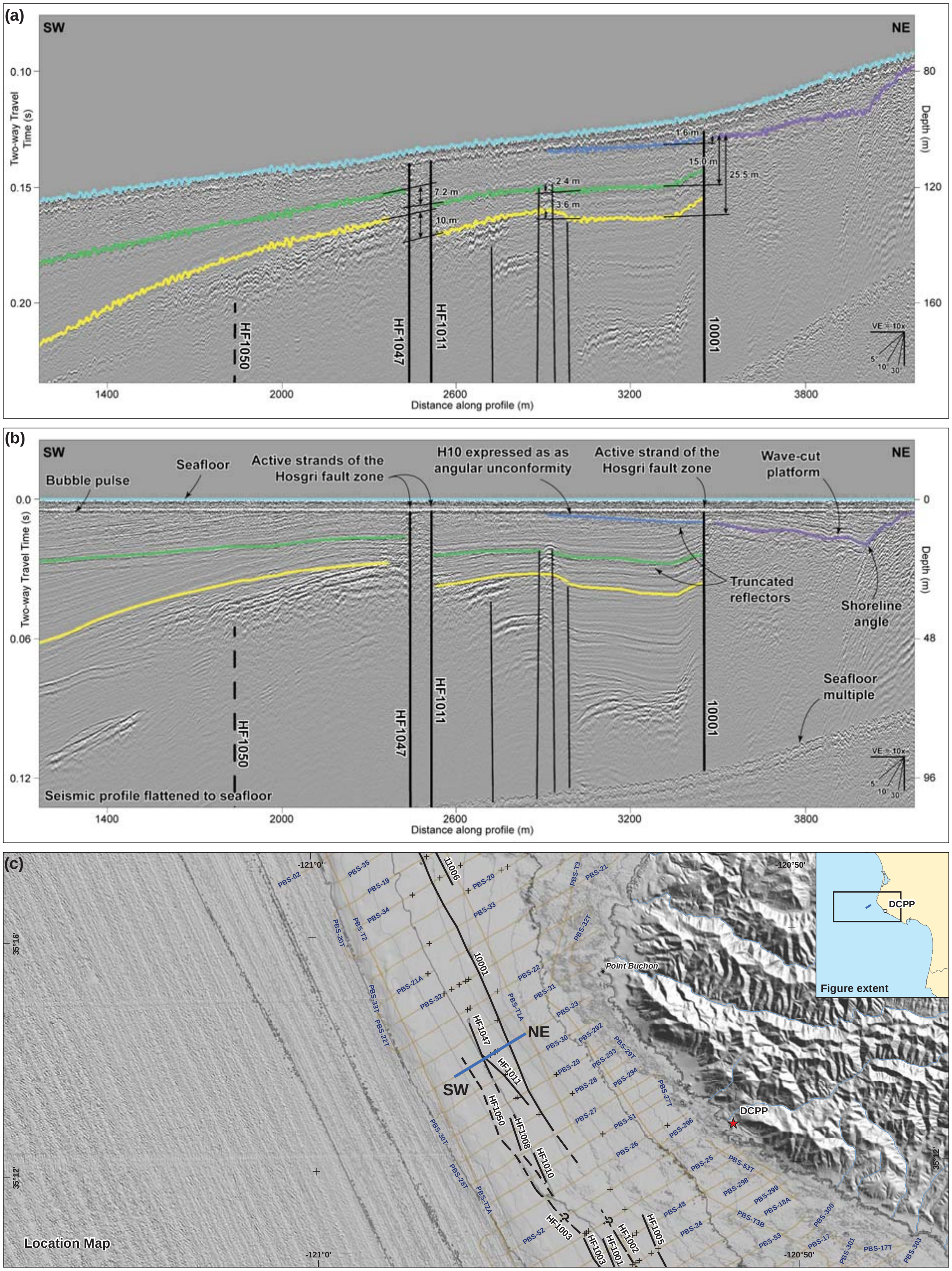

EXPLANATION

—— – ?···	Fault interpreted from USGS seismic profiles, solid where well located, dashed where approximately located, dotted where inferred, queried where existence uncertain.
——	Location of seismic profile
PBS-07	USGS survey trackline, number indicated
+	Unassigned fault
——	Seafloor
——	Unconformity H10
——	Unconformity H30
——	Unconformity H40
——	Top of pre-Quaternary rock

Sources:
- USGS seismic-reflection data (Sliter et al., 2009).
- Project DEM compilation v2013.01. Bathymetric contour interval is 10 m. Heavy contours are 50 m isobaths.

Notes:
1. Depth values on seismic profile assume a velocity of 1,600 m/s.
2. In profiles, thin black lines are unassigned faults, heavy black lines are named faults.
3. Correlation of unconformities to planated top of pre-Quaternary rock across fault 10001 implies vertical separation down to the west. However, uncertainties in amount of bedrock erosion and the potential for a fault line scarp in the pre-deformation surface of the unconformity make vertical separation measurements only approximate. Therefore, these individual measurements are not shown on Plate 2b but are included in Table 8-1.

0 2 4 mi.
0 4 8 km

Map projection and scale: WGS 84 / UTM Zone 10N,1:120,000

Excerpt of Profile PBS-23 Showing Active Traces of Hosgri Fault Zone Offshore of Point Buchon

DCPP OFFSHORE SEISMIC STRATIGRAPHY

Pacific Gas and Electric Company — Figure **7-4**

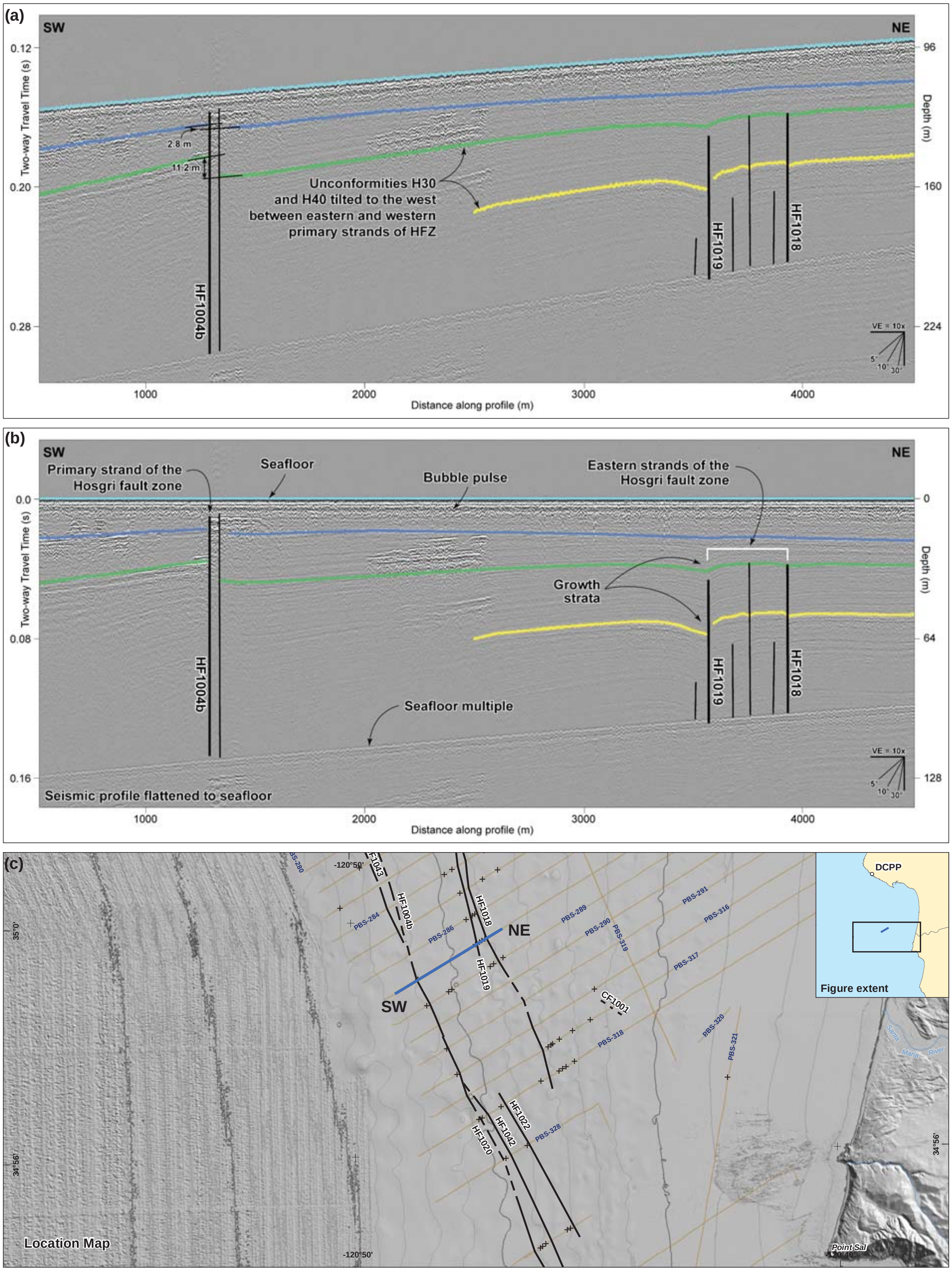

EXPLANATION

Fault interpreted from USGS seismic profiles, solid where well located, dashed where approximately located, dotted where inferred, queried where existence uncertain.

Location of seismic profile

PBS-07 USGS survey trackline, number indicated

\+ Unassigned fault

Seafloor

Unconformity H10

Unconformity H30

Unconformity H40

Sources:
- USGS seismic-reflection data (Sliter et al., 2009).
- Project DEM compilation v2013.01. Bathymetric contour interval is 10 m. Heavy contours are 50 m isobaths.

Notes:
1. Depth values on seismic profile assume a velocity of 1,600 m/s.
2. In profiles, thin black lines are unassigned faults, heavy black lines are named faults.
3. Vertical separation measurements are not shown for faults HF1019 and HF1018 due to tilting of reflectors west of the faults and large uncertainties in projections of unconformities across the faults.

0 2 4 mi.

0 4 8 km

Map projection and scale: WGS 84 / UTM Zone 10N, 1:120,000

Excerpt of Profile PBS-288 Showing Active Traces of Hosgri Fault Zone Northwest of Point Sal

DCPP OFFSHORE SEISMIC STRATIGRAPHY

Pacific Gas and Electric Company | Figure **7-5**

File path: S:\1005\026\GIS\Figures\Figure_7_5.mxd; Date: 05/15/2013; User: Jereme Chandler, LCI; Rev.1

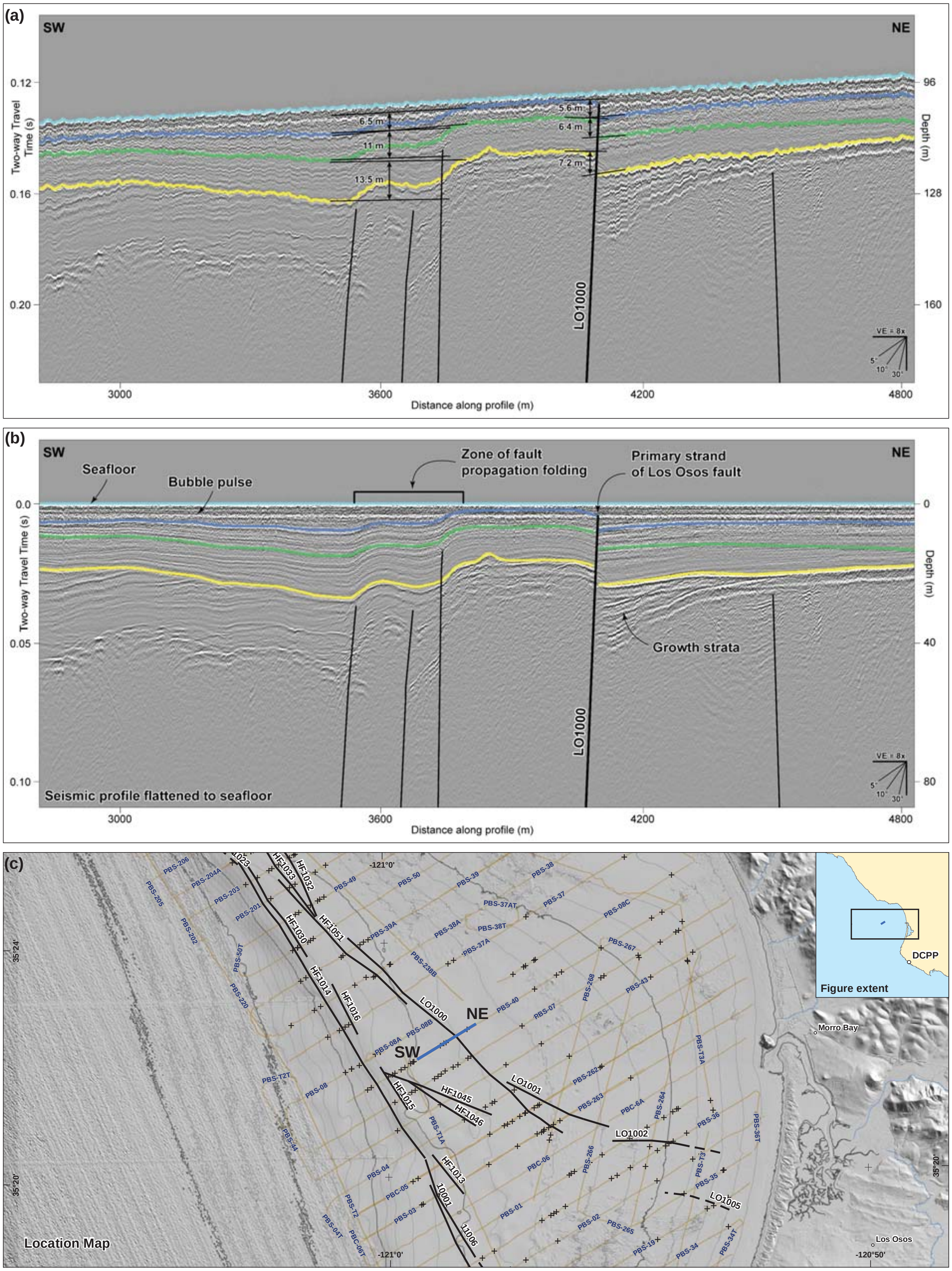

EXPLANATION

- Fault interpreted from USGS seismic profiles, solid where well located, dashed where approximately located, dotted where inferred, queried where existence uncertain.
- Location of seismic profile
- PBS-07 USGS survey trackline, number indicated
- + Unassigned fault
- Seafloor
- Unconformity H10
- Unconformity H30
- Unconformity H40

Notes:
1. Depth values on seismic profile assume a velocity of 1,600 m/s.
2. In profiles, thin black lines are unassigned faults, heavy black lines are named faults.
3. Unassigned faults west of LO1000 deform reflectors down to the west as shown. Because these faults cannot be correlated between seismic lines, it is unclear whether this deformation should be attributed to the Hosgri or Los Osos fault zone.

Sources:
- USGS seismic-reflection data (Sliter et al., 2009).
- Project DEM compilation v2013.01. Bathymetric contour interval is 10 m. Heavy contours are 50 m isobaths.

0 2 4 mi.
0 4 8 km

Map projection and scale: WGS 84 / UTM Zone 10N, 1:120,000

Excerpt of Profile PBS-40 in Estero Bay Showing Offset Quaternary Reflectors Along Offshore Projection of Los Osos Fault Zone

DCPP OFFSHORE SEISMIC STRATIGRAPHY

Pacific Gas and Electric Company | Figure **7-6**

File path: S:\1005\026\GIS\Figures\Figure_7_6.mxd; Date: 05/15/2013; User: Jereme Chandler, LCI; Rev.1

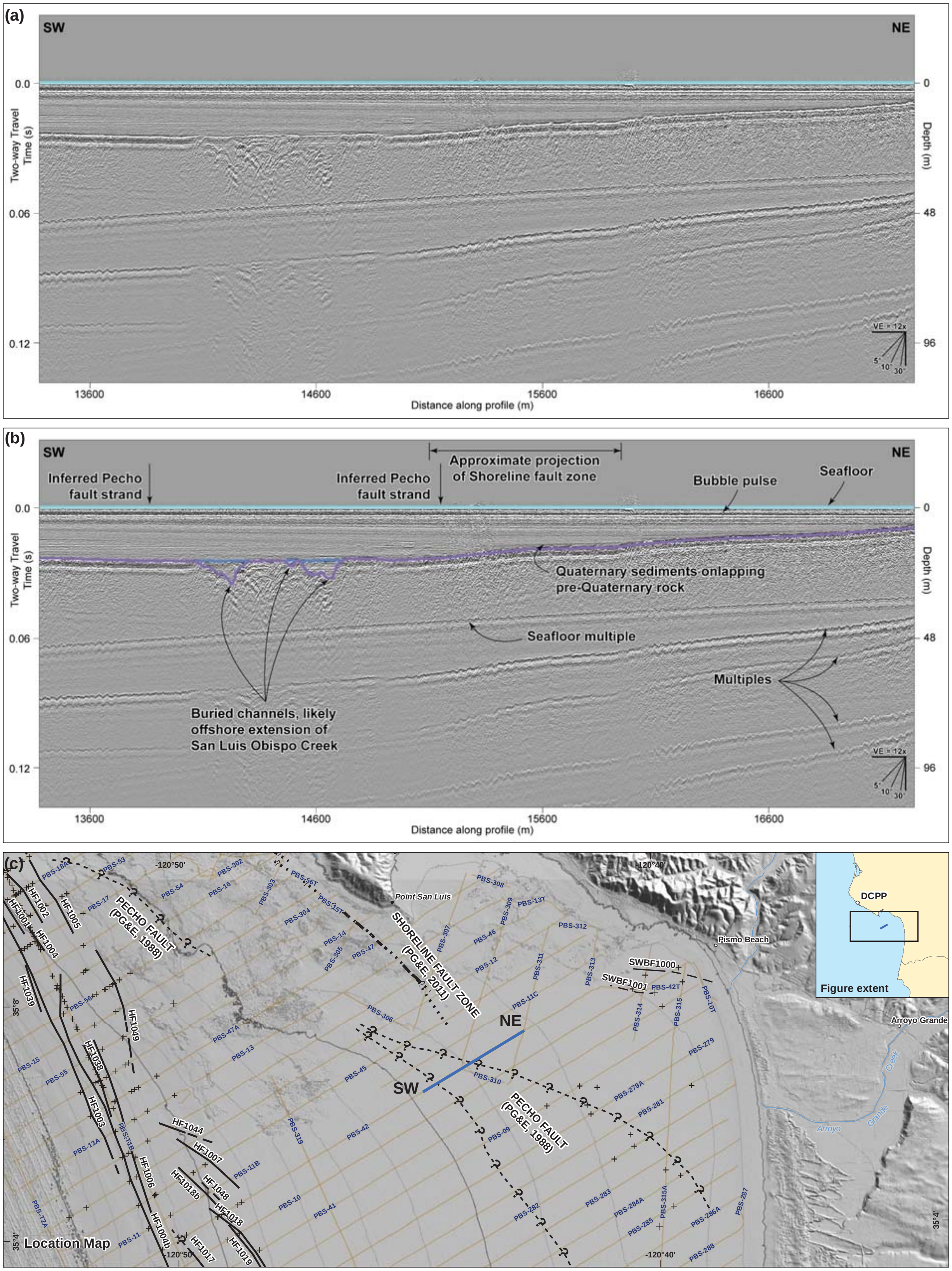

EXPLANATION

- Fault interpreted from USGS seismic profiles, solid where well located, dashed where approximately located, dotted where inferred, queried where existence uncertain.
- Location of seismic profile
- PBS-07 USGS survey trackline, number indicated
- + Unassigned fault
- Seafloor
- Top of pre-Quaternary rock

Notes:
1. Depth values on seismic profile assume a velocity of 1,600 m/s.
2. Absence of deformation of post-LGM strata suggests no post-LGM activity on inferred Pecho fault strands either through faulting or localized folding.

Sources:
- USGS seismic-reflection data (Sliter et al., 2009).
- Project DEM compilation v2013.01. Bathymetric contour interval is 10 m. Heavy contours are 50 m isobaths.
- Pecho fault from PG&E (1988).
- Shoreline fault zone from PG&E (2011).

0 2 4 mi.
0 4 8 km

Map projection and scale: WGS 84 / UTM Zone 10N,1:120,000

Excerpt of Profile PBS-42 Showing Continuous Reflectors and Absence of Step in Bedrock Surface Across Projection of Shoreline Fault Zone and Previously Mapped Traces of Pecho Fault

DCPP OFFSHORE SEISMIC STRATIGRAPHY

Pacific Gas and Electric Company | Figure **7-7**

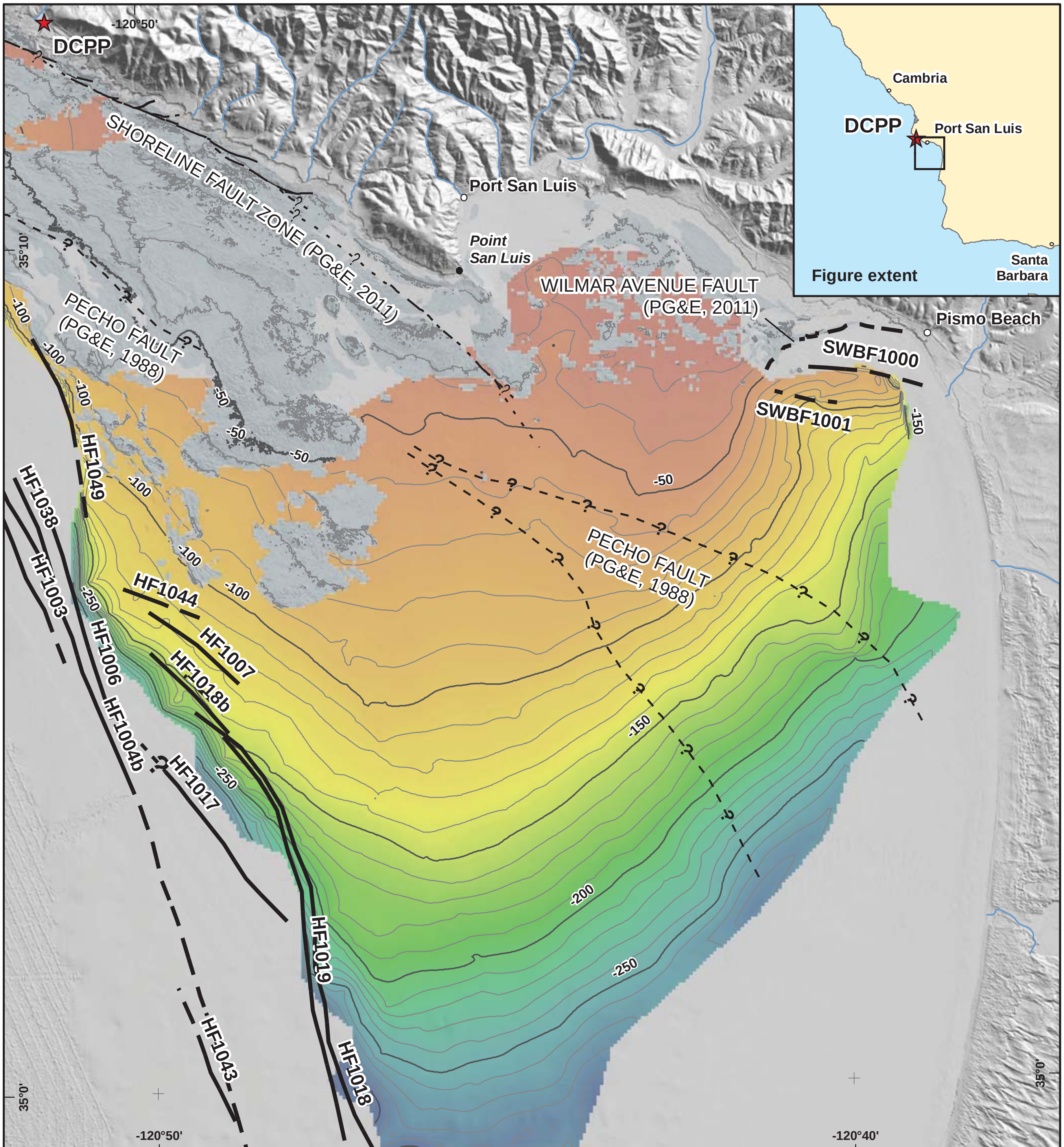

EXPLANATION

Fault interpreted from USGS seismic profiles, solid where well located, dashed where approximately located, dotted where inferred, queried where existence uncertain.

Top of Pre-Quaternary Rock Depth Below Sea Level

High : - 15 m

Low : -350 m

10 m structure contour interval, heavy contour are 50 m. Bathymetric contours are used in regions where bedrock is exposed at the seafloor.

Sources:
- Project DEM compilation v2013.01.
- Pecho fault from PG&E (1988).
- Shoreline fault zone from PG&E (2011).

Note:
1. Where they meet, bathymetric contours do not align with interpreted contours on the top of pre-Quaternary because the USGS 2D profiles are not depth-migrated, and depths of structure contours interpreted from the seismic reflection data were estimated using an assumed seismic velocity of 1,600 m/s. Therefore, the general shape of the structure contours is accurate, but the actual depths are an approximation.

0 2 4 mi.
0 4 8 km

Map projection and scale: WGS 84 / UTM Zone 10N,1:130,000

Structure Contours on Top of Pre-Quaternary Rock in San Luis Obispo Bay Showing Absence of Deformation at Location of Previously Mapped Pecho Fault and Along Projection of Shoreline Fault Zone

DCPP OFFSHORE SEISMIC STRATIGRAPHY

Pacific Gas and Electric Company | Figure **7-8**

File path: S:\1005\026\GIS\Figures\Figure_7_8.mxd; Date: 05/15/2013; User: Jereme Chandler, LCI; Rev.1

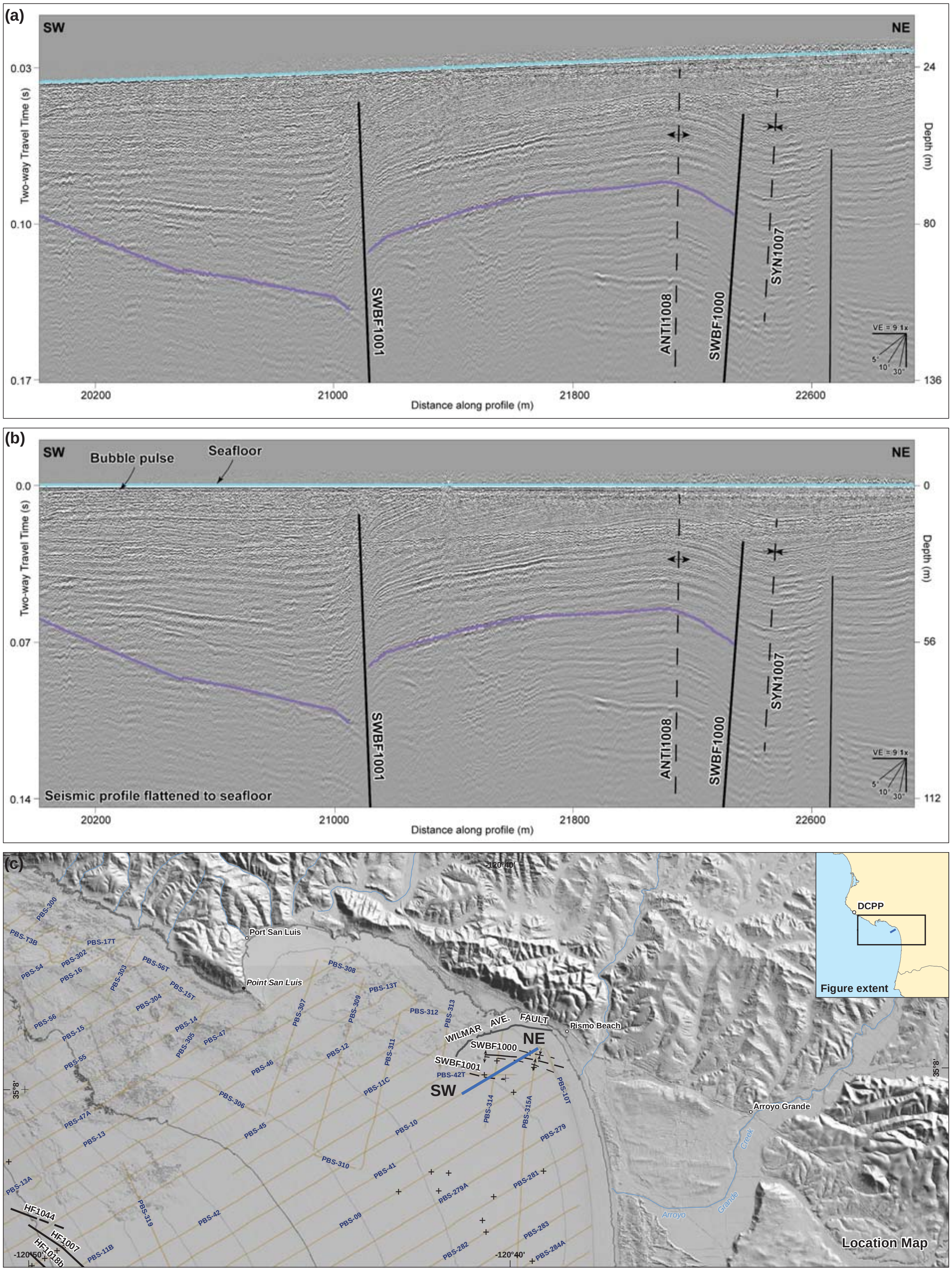

EXPLANATION

- Fault interpreted from USGS seismic profiles, solid where well located, dashed where approximately located, dotted where inferred, queried where existence uncertain.
- Location of seismic profile
- PBS-07 USGS survey trackline, number indicated
- Unassigned fault
- Syncline
- Anticline
- Seafloor
- Top of Pre-Quaternary rock

Notes:
1. Depth values on seismic profile assume a velocity of 1,600 m/s.
2. In profiles, thin black lines are unassigned faults, heavy black lines are named faults.

Sources:
- USGS seismic-reflection data (Sliter et al., 2009).
- Project DEM compilation v2013.01. Bathymetric contour interval is 10 m. Heavy contours are 50 m isobaths.
- Wilmar Avenue fault from PG&E (2011)

0 2 4 mi.
0 4 8 km

Map projection and scale: WGS 84 / UTM Zone 10N, 1:120,000

Excerpt of Profile PBS-10 Showing Quaternary Faulting and Folding Offshore and South of Wilmar Avenue Fault

DCPP OFFSHORE SEISMIC STRATIGRAPHY

Pacific Gas and Electric Company | Figure **7-9**

File path: S:\1005\026\GIS\Figures\Figure_7_9.mxd; Date: 05/15/2013; User: Jereme Chandler, LCI; Rev.1

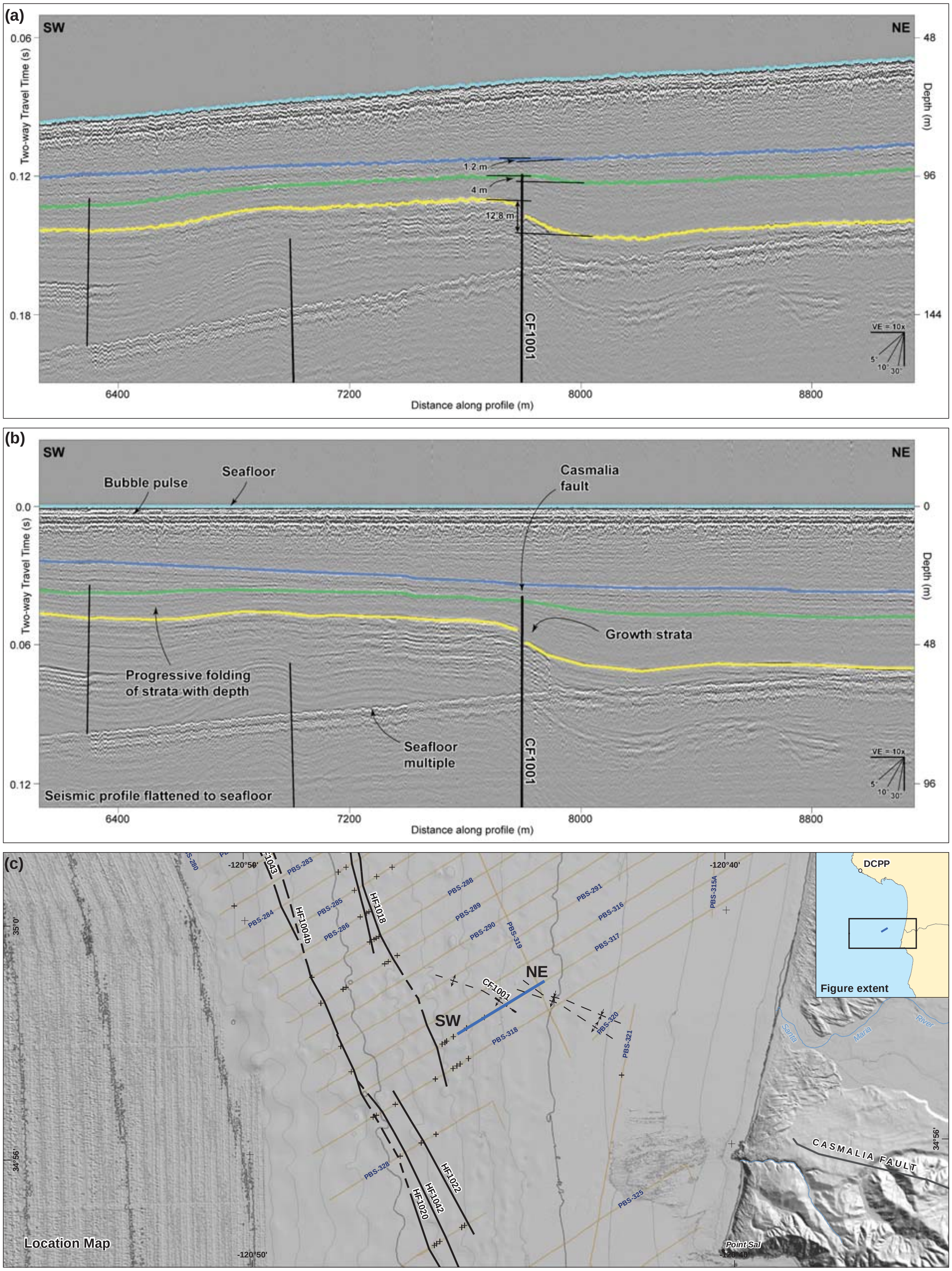

EXPLANATION

— — ? ···	Fault interpreted from USGS seismic profiles, solid where well located, dashed where approximately located, dotted where inferred, queried where existence uncertain.
———	Fault not directly studied for this project
———	Location of seismic profile
PBS-07	USGS survey trackline, number indicated
+	Unassigned fault
— ╪ —	Syncline
— ╪ —	Anticline

———	Seafloor
———	Unconformity H10
———	Unconformity H30
———	Unconformity H40

Notes:
1. Depth values on seismic profile assume a velocity of 1,600 m/s.
2. In profiles, thin black lines are unassigned faults, heavy black lines are named faults.
3. Fault CF1001 bounds the north side of a set of folds that trend southeast toward the Casmalia fault onshore.

Sources:
- USGS seismic-reflection data (Sliter et al., 2009).
- Project DEM compilation v2013.01. Bathymetric contour interval is 10 m. Heavy contours are 50 m isobaths.
- Onshore trace of Casmalia fault zone from USGS Quaternary Fault and Fold Database (2010).

0 2 4 mi.
0 4 8 km

Map projection and scale: WGS 84 / UTM Zone 10N,1:120,000

Excerpt of Profile PBS-317 Showing Quaternary Faulting and Folding related to the Casmalia Fault Offshore of Point Sal

DCPP OFFSHORE SEISMIC STRATIGRAPHY

Pacific Gas and Electric Company

Figure **7-10**

File path: S:\1005\026\GIS\Figures\Figure_7_10.mxd; Date: 05/17/2013; User: Jereme Chandler, LCI; Rev.1

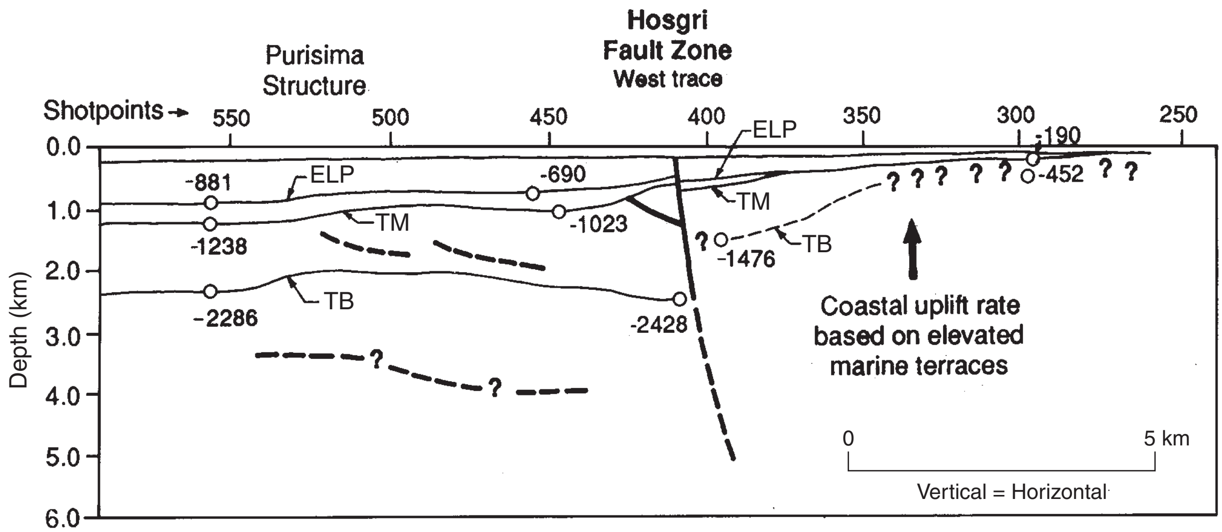

HOSGRI FAULT ZONE

	Vertical Separation (meters)	Vertical Separation Rate (mm/yr)		Coastal Uplift Rate (mm/yr)		Maximum Vertical Slip Rate (mm/yr)
ELP (2.8 Ma)	690 - 190 = 500	0.18	+	0.00	=	0.18
TM (5.1 Ma)	1,023	0.20	+	0.00	=	0.20
TB (~17 Ma)	2,428 - 452 = 1976	—		—		—

HOSGRI FAULT ZONE AND PURISIMA STRUCTURE

	Vertical Separation (meters)	Vertical Separation Rate (mm/yr)		Coastal Uplift Rate (mm/yr)		Maximum Vertical Slip Rate (mm/yr)
ELP (2.8 Ma)	[691]	[0.25]	+	0.00	=	[0.25]
TM (5.1 Ma)	[1,238]	[0.24]	+	0.00	=	[0.24]
TB (~17 Ma)	2,286 - 452 = [1,834]	—		—		—

EXPLANATION

ELP Early-late Pliocene unconformity
TM Top of Miocene unconformity
TB Top of pre-Miocene basement unconformity
o Depth in meters from sea floor to unconformity
— — ? Fault, dashed where inferred, queried where uncertain
[ ] Brackets indicate the maximum value summed across the Hosgri Fault Zone and the Purisima structure

Source:
Hanson et al. (2004), Figure 16.

Note:
Along the Point Sal and Southern reaches, as defined by Hanson et al. (2004), the Purisima structure may be considered to be the result of local strain partitioning (Lettis and Hanson, 1992) along the HFZ; therefore, the vertical structural relief of the structure was included in estimating maximum vertical separation across the HFZ.

Schematic Profile Showing Technique Used by Hanson et al. (2004) to Calculate Vertical Separations

DCPP SEISMIC STRATIGRAPHY PROJECT

Pacific Gas and Electric Company | Figure **8-1**

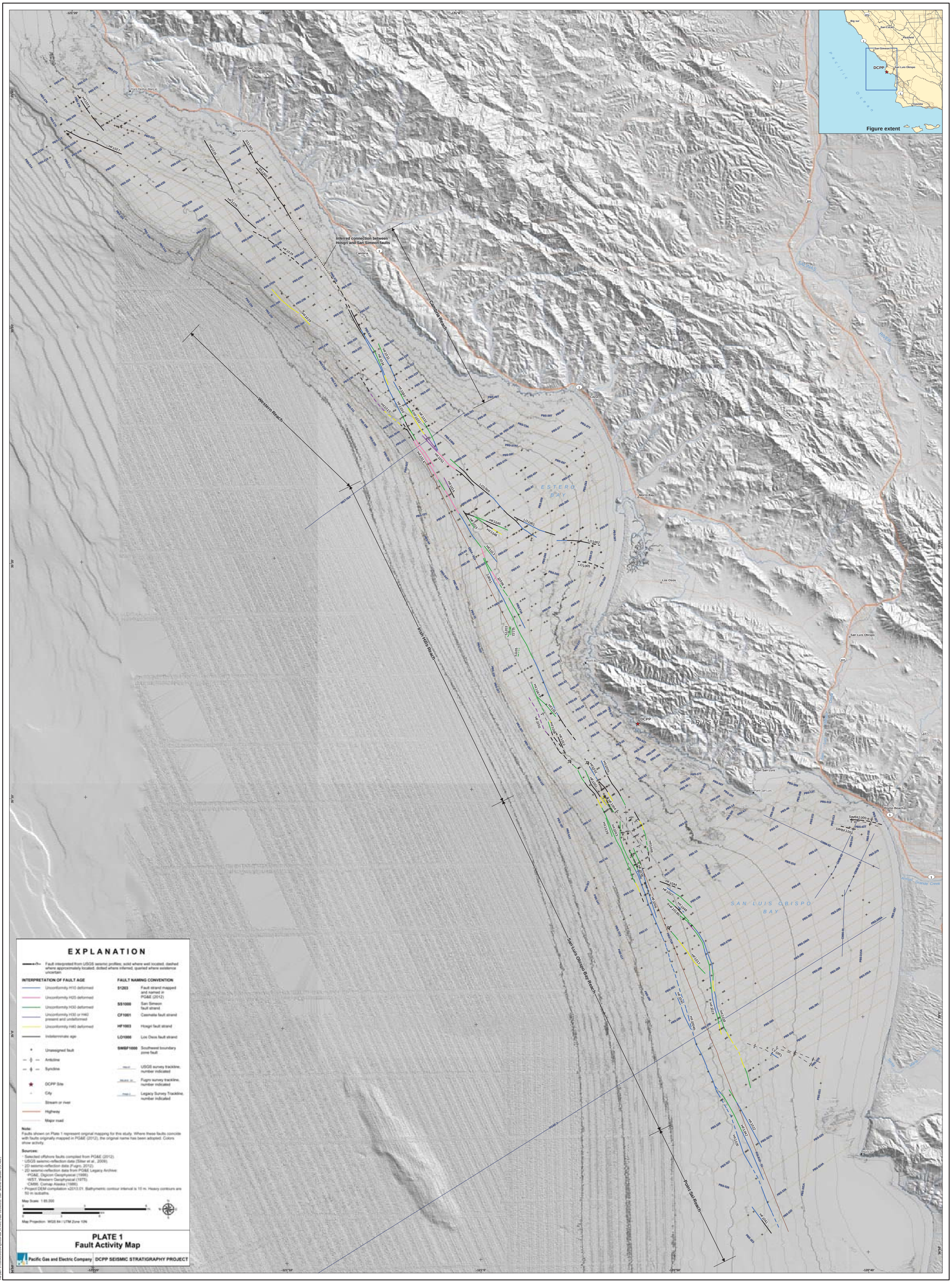

PLATE 1
Fault Activity Map

Pacific Gas and Electric Company | DCPP SEISMIC STRATIGRAPHY PROJECT

File path: S:\1005\0226\GIS\Figures\Plate_01.mxd; Date: 05/16/2013; User: Jereme Chandler, LCI; Rev.1

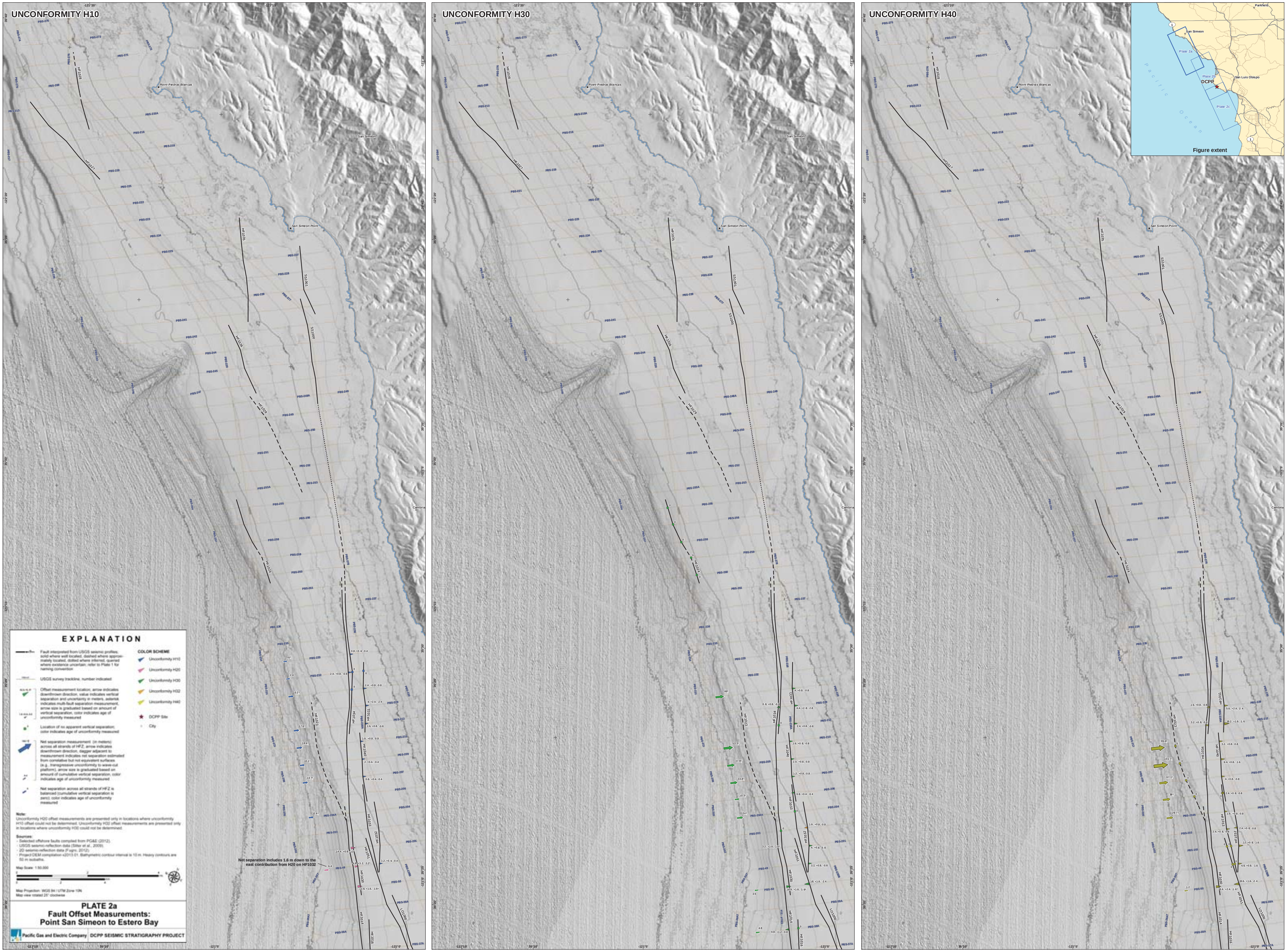

File path: S:\10005\026\GIS\Figures\Plate_02a.mxd; Date: 05/16/2013; User: Jereme Chandler, LCI; Rev.1

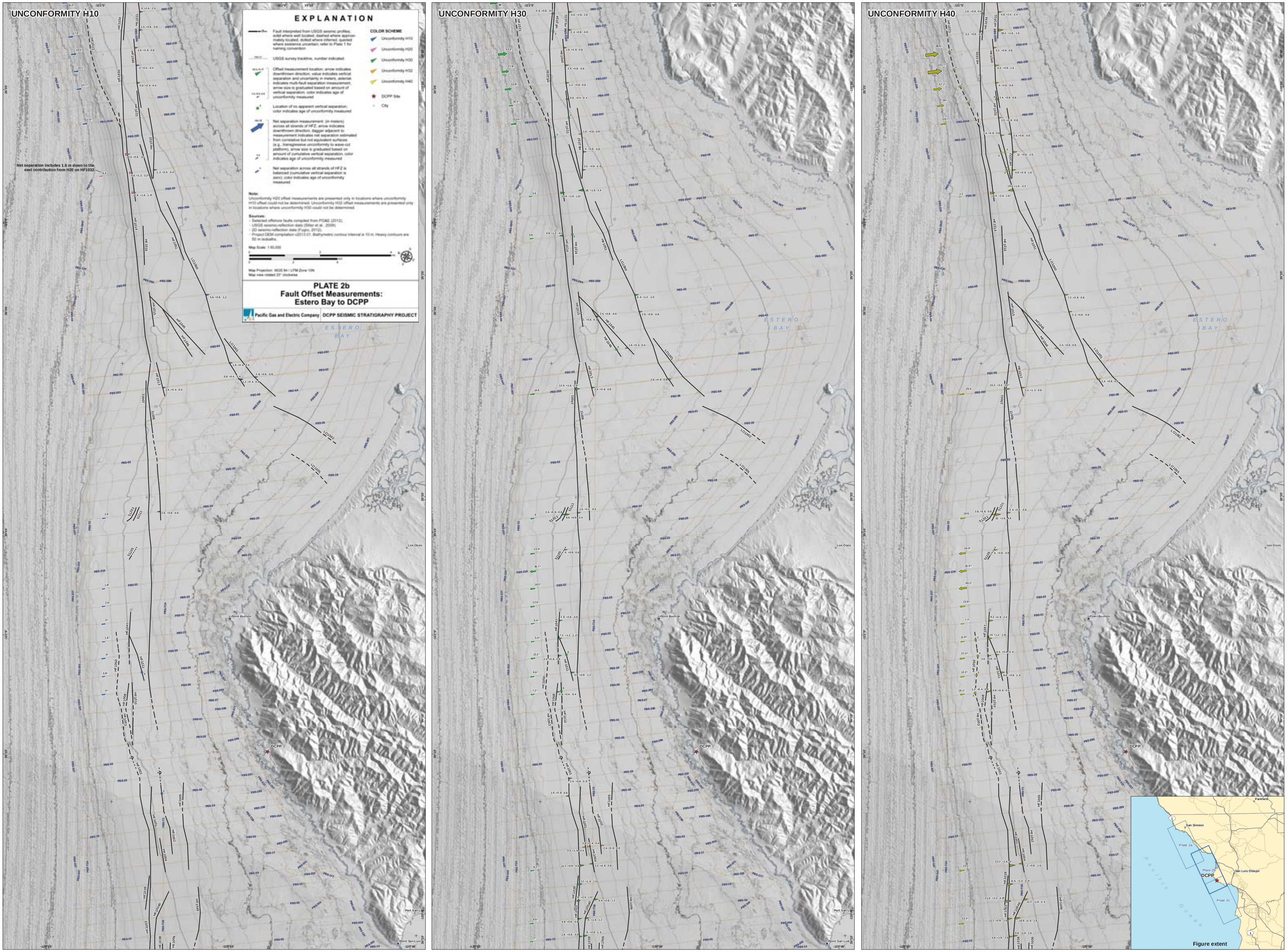

UNCONFORMITY H10
UNCONFORMITY H30
UNCONFORMITY H40
Net separation includes 1.6 m down to the east contribution from H20 on HF1032
EXPLANATION
Fault interpreted from USGS seismic profiles; solid where well located, dashed where approximately located, dotted where inferred, queried where existence uncertain; refer to Plate 1 for naming convention
USGS survey trackline, number indicated
Offset measurement location; arrow indicates downthrown direction, value indicates vertical separation and uncertainty in meters, asterisk indicates multi-fault separation measurement, arrow size is graduated based on amount of vertical separation, color indicates age of unconformity measured
Location of no apparent vertical separation; color indicates age of unconformity measured
Net separation measurement (in meters) across all strands of HFZ; arrow indicates downthrown direction, dagger adjacent to measurement indicates net separation estimated from correlative but not equivalent surfaces (e.g., transgressive unconformity to wave-cut platform), arrow size is graduated based on amount of cumulative vertical separation, color indicates age of unconformity measured
Net separation across all strands of HFZ is balanced (cumulative vertical separation is zero); color indicates age of unconformity measured
COLOR SCHEME
Unconformity H10
Unconformity H20
Unconformity H30
Unconformity H32
Unconformity H40
DCPP Site
City
Note:
Unconformity H20 offset measurements are presented only in locations where unconformity H10 offset could not be determined. Unconformity H32 offset measurements are presented only in locations where unconformity H30 could not be determined.
Sources:
- Selected offshore faults compiled from PG&E (2012).
- USGS seismic-reflection data (Sliter et al., 2009).
- 2D seismic-reflection data (Fugro, 2012).
- Project DEM compilation v2013.01. Bathymetric contour interval is 10 m. Heavy contours are 50 m isobaths.
Map Scale: 1:50,000
Map Projection: WGS 84 / UTM Zone 10N
Map view rotated 25° clockwise
PLATE 2b
Fault Offset Measurements:
Estero Bay to DCPP
Pacific Gas and Electric Company
DCPP SEISMIC STRATIGRAPHY PROJECT
ESTERO BAY
Los Osos
Point Buchon
DCPP
Port San Luis
Figure extent
Pacific Ocean
San Simeon
San Luis Obispo
Parkfield
Plate 2a
Plate 2c

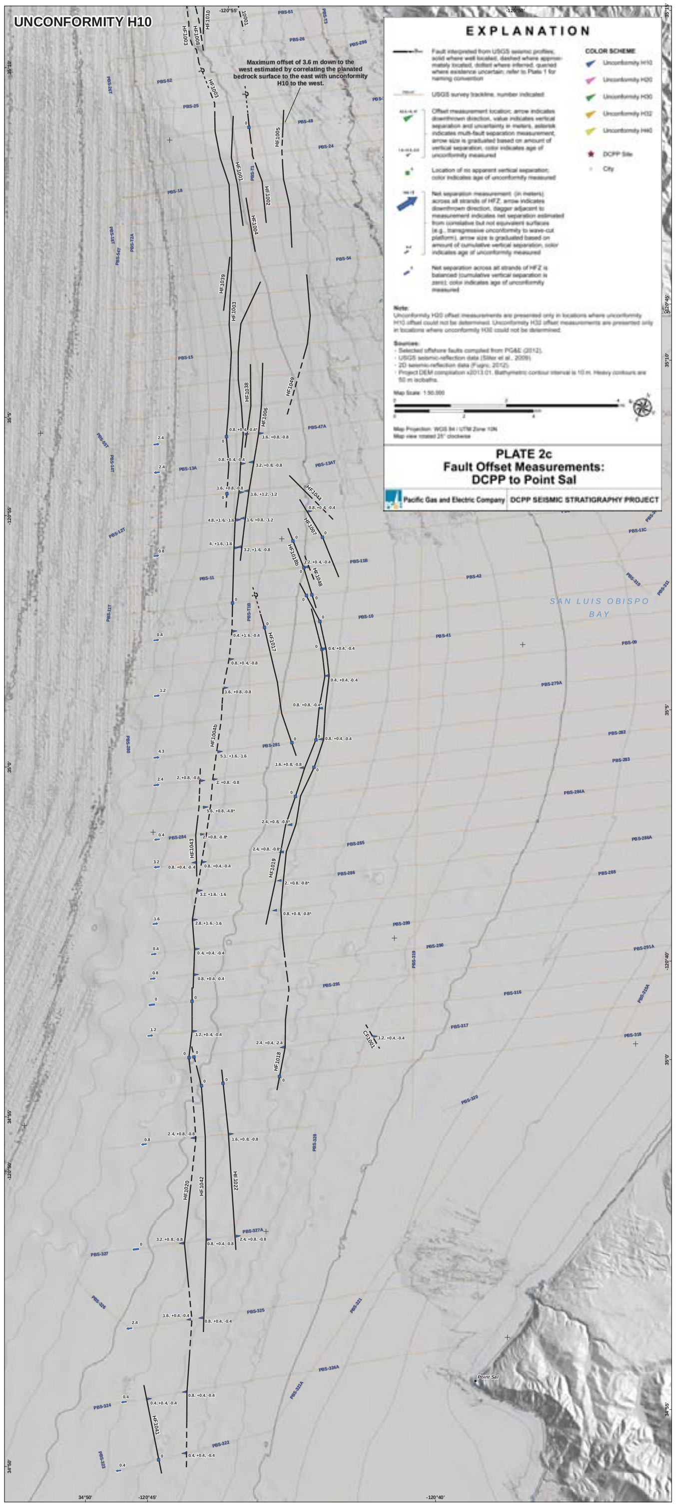

EXPLANATION

Fault interpreted from USGS seismic profiles; solid where well located, dashed where approximately located, dotted where inferred, queried where existence uncertain; refer to Plate 1 for naming convention

USGS survey trackline, number indicated

Offset measurement location; arrow indicates downthrown direction, value indicates vertical separation and uncertainty in meters, asterisk indicates multi-fault separation measurement, arrow size is graduated based on amount of vertical separation, color indicates age of unconformity measured

Location of no apparent vertical separation; color indicates age of unconformity measured

Net separation measurement (in meters) across all strands of HFZ; arrow indicates downthrown direction, dagger adjacent to measurement indicates net separation estimated from correlative but not equivalent surfaces (e.g., transgressive unconformity to wave-cut platform), arrow size is graduated based on amount of cumulative vertical separation, color indicates age of unconformity measured

Net separation across all strands of HFZ is balanced (cumulative vertical separation is zero); color indicates age of unconformity measured

COLOR SCHEME

- Unconformity H10
- Unconformity H20
- Unconformity H30
- Unconformity H32
- Unconformity H40
- DCPP Site
- City

Note:
Unconformity H20 offset measurements are presented only in locations where unconformity H10 offset could not be determined. Unconformity H32 offset measurements are presented only in locations where unconformity H30 could not be determined.

Sources:
- Selected offshore faults compiled from PG&E (2012).
- USGS seismic-reflection data (Sliter et al., 2009).
- 2D seismic-reflection data (Fugro, 2012).
- Project DEM compilation v2013.01. Bathymetric contour interval is 10 m. Heavy contours are 50 m isobaths.

Map Scale: 1:50,000

Map Projection: WGS 84 / UTM Zone 10N
Map view rotated 25° clockwise

PLATE 2c
Fault Offset Measurements: DCPP to Point Sal

Pacific Gas and Electric Company | DCPP SEISMIC STRATIGRAPHY PROJECT

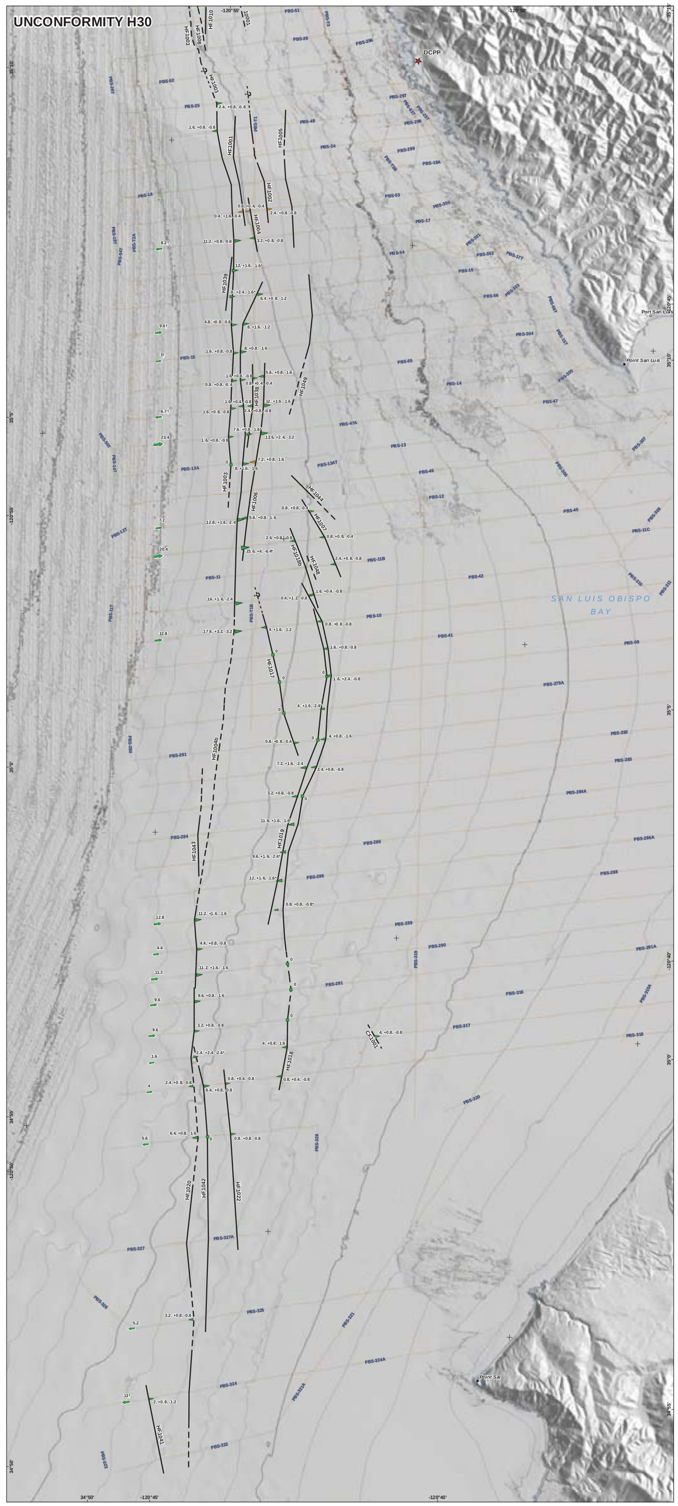

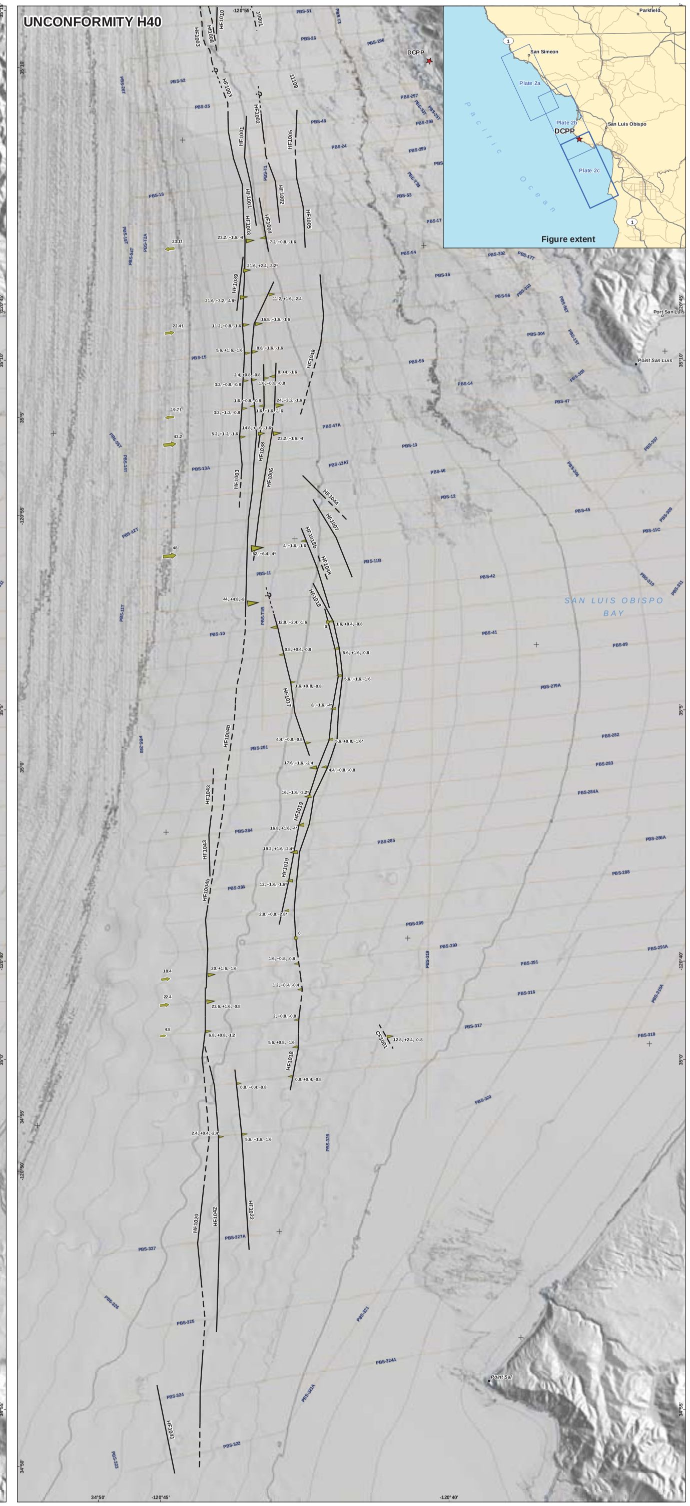

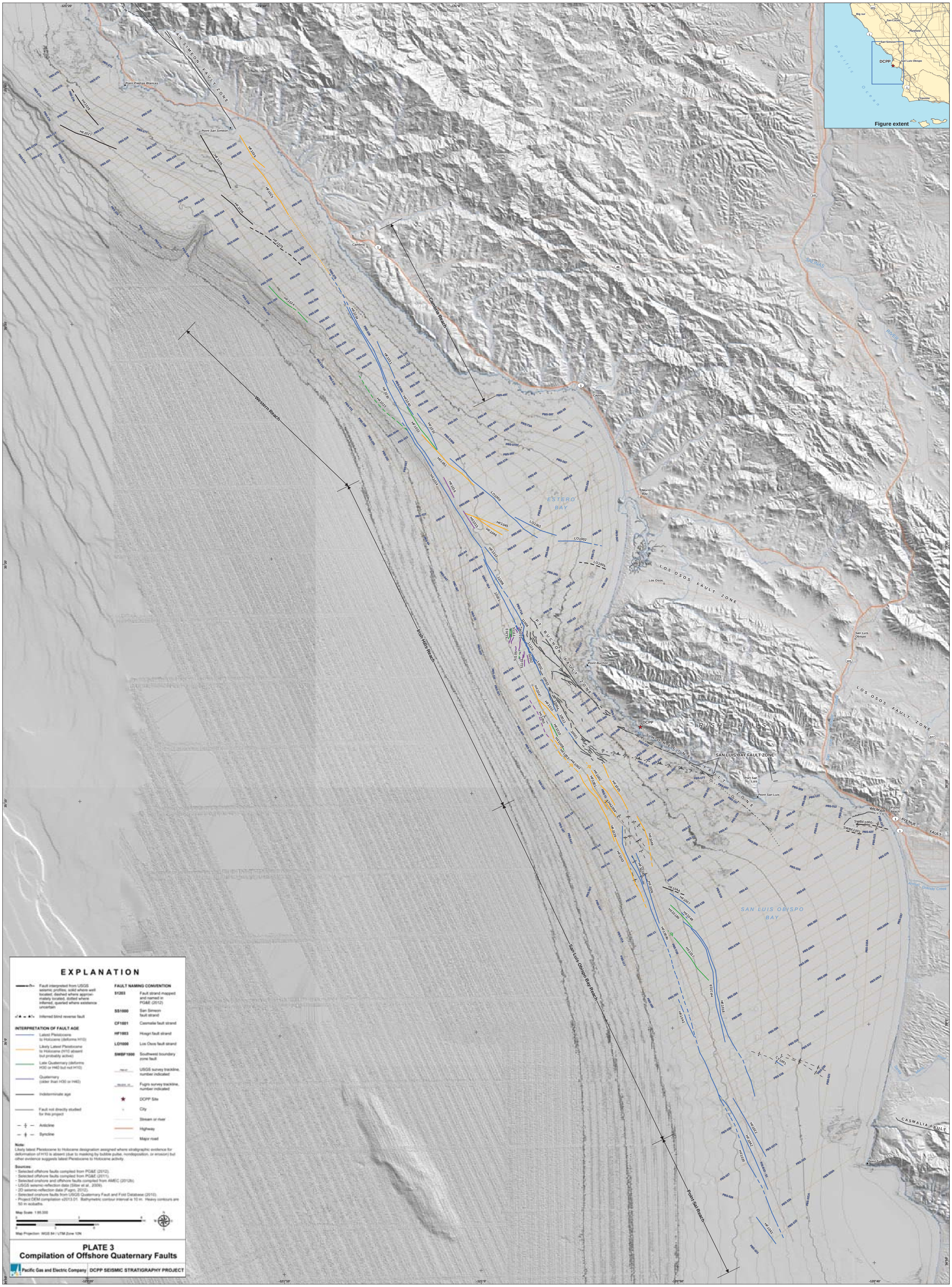

PLATE 3
Compilation of Offshore Quaternary Faults

Pacific Gas and Electric Company | DCPP SEISMIC STRATIGRAPHY PROJECT

File path: S:\10050\26\GIS\Figures\Plate_03.mxd; Date: 05/16/2013; User: Jereme Chandler, LCI; Rev.1

APPENDIX A: IDENTIFICATION AND DOCUMENTATION OF SUBMERGED PALEOSHORELINE FEATURES

Submerged remnants of erosional paleoshorelines have been identified on parts of the continental shelf offshore of the DCPP (PG&E, 2011). These features consist of relatively gently seaward-sloping wave-cut platforms that intersect relatively steeper paleosea cliffs at their landward edges. In profile view, the point of intersection between the wave-cut platform and paleosea cliff is the *shoreline angle*, which records the position of relative sea level at the time the paleoshoreline was developed. In map view, the line of intersection between a continuous paleosea cliff and its associated wave-cut platform is the *strandline*.

Potential paleoshoreline remnants were mapped where they were encountered in the seismic-reflection data examined for the Seismic Stratigraphy Project. The relatively flat wave-cut platforms were digitized manually as horizons in Kingdom software, the eastern endpoints of these horizons marking the *x* and *y* positions of their associated shoreline angles. The vertical (*z*) positions of the shoreline angles and associated uncertainties were recorded as follows:

- The depth of the shoreline angle below seafloor was measured in milliseconds twtt.
- Depths were converted to meters using an assumed seismic velocity of 1,600 m/s.
- This value was added to the depth of the seafloor directly overlying the shoreline angles indicated by the MBES bathymetric DEM.

The relative strength of the geomorphic signature of each shoreline angle offshore of the Irish Hills was evaluated, and confidence level was assigned using the criteria developed for and described in the *Shoreline Fault Zone Report* (PG&E, 2011).

The submerged strandlines and submerged shoreline angles presented on Plate A-1 are a combination of mapping from three separate efforts:

1. New mapping for this report based on interpretation of high-resolution MBES data from Estero Bay to Point Piedras Blancas and interpretation of USGS 2D data between Point Sal and Point Piedras Blancas.
2. Mapping presented in the *Shoreline Fault Zone Report* (PG&E, 2011).
3. Mapping performed by AMEC (2012) based on interpretation of the Point Buchon 3D/2D data.

Existing and updated shoreline features from previous reports and newly mapped shoreline features from this study are presented as two complete data sets (Plate A-1), as follows:

- A set of submerged shoreline angles (points) interpreted from seismic profiles.
- A set of submerged strandlines (lines) interpreted from MBES data and 3D seismic-reflection data.

In some instances, additional evaluation of flattened USGS 2D profiles performed for this project led to reinterpretations of the location or depth of submerged shoreline angles presented in the *Shoreline Fault Zone Report*. However, none of the submerged strandlines presented in that report have been modified for this appendix.

The submerged paleoshoreline features presented on Plate A-1 represent a complete data set developed with a uniform set of mapping and evaluation criteria. Preliminary analysis of this updated set of submerged paleoshoreline features was presented by Mr. Hans AbramsonWard at the DCPP SSC SSHAC Workshop 2 on November 7, 2012. It is anticipated that this set of submerged paleoshoreline features will be the subject of additional analysis by PG&E and its consultants in consideration of potential locations and rates of offshore seismic sources.

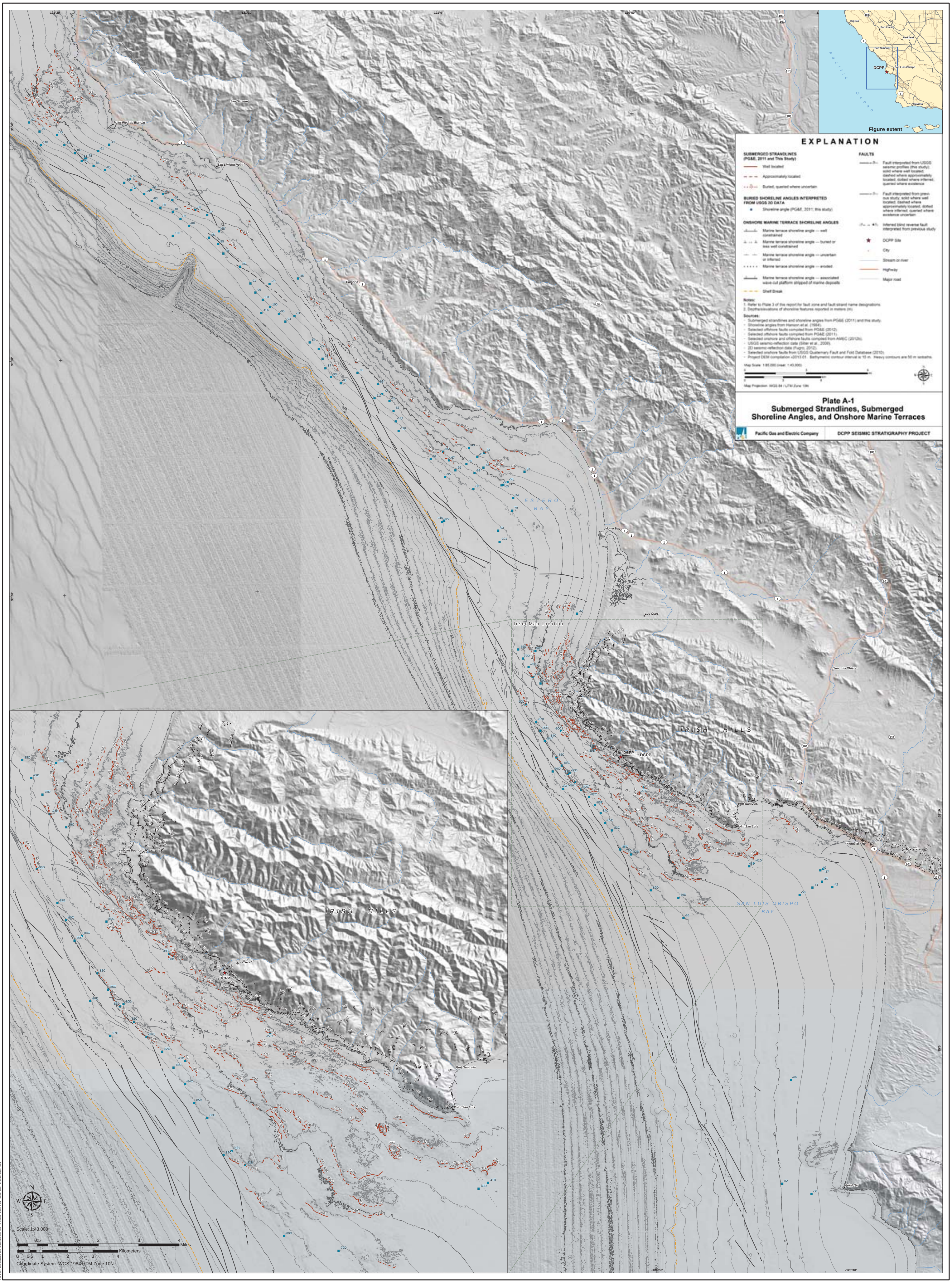
Figure extent
DCPP
San Luis Obispo
Gaviota
Pacific Ocean
EXPLANATION
SUBMERGED STRANDLINES (PG&E, 2011 and This Study)
Well located
Approximately located
Buried, queried where uncertain
BURIED SHORELINE ANGLES INTERPRETED FROM USGS 2D DATA
Shoreline angle (PG&E, 2011; this study)
ONSHORE MARINE TERRACE SHORELINE ANGLES
Marine terrace shoreline angle — well constrained
Marine terrace shoreline angle — buried or less well constrained
Marine terrace shoreline angle — uncertain or inferred
Marine terrace shoreline angle — eroded
Marine terrace shoreline angle — associated wave-cut platform stripped of marine deposits
Shelf Break
FAULTS
Fault interpreted from USGS seismic profiles (this study); solid where well located, dashed where approximately located, dotted where inferred, queried where existence uncertain
Fault interpreted from previous study; solid where well located, dashed where approximately located, dotted where inferred, queried where existence uncertain
Inferred blind reverse fault interpreted from previous study
DCPP Site
City
Stream or river
Highway
Major road
Notes:
1. Refer to Plate 3 of this report for fault zone and fault strand name designations.
2. Depths/elevations of shoreline features reported in meters (m).
Sources:
- Submerged strandlines and shoreline angles from PG&E (2011) and this study.
- Shoreline angles from Hanson et al. (1994).
- Selected offshore faults compiled from PG&E (2012).
- Selected offshore faults compiled from PG&E (2011).
- Selected onshore and offshore faults compiled from AMEC (2012b).
- USGS seismic-reflection data (Sliter et al., 2009).
- 2D seismic-reflection data (Fugro, 2012).
- Selected onshore faults from USGS Quaternary Fault and Fold Database (2010).
- Project DEM compilation v2013.01. Bathymetric contour interval is 10 m. Heavy contours are 50 m isobaths.
Map Scale: 1:85,000 (inset: 1:43,000)
Map Projection: WGS 84 / UTM Zone 10N
Plate A-1
Submerged Strandlines, Submerged Shoreline Angles, and Onshore Marine Terraces
Pacific Gas and Electric Company
DCPP SEISMIC STRATIGRAPHY PROJECT
San Simeon
Point Piedras Blancas
San Simeon Point
Cambria
Cayucos
ESTERO BAY
Morro Bay
Los Osos
Inset Map Location
San Luis Obispo
IRISH HILLS
DCPP
Port San Luis
Point San Luis
Pismo Beach
SAN LUIS OBISPO BAY
Point Sal
Point Buchon
Scale: 1:43,000
Miles
Kilometers
Coordinate System: WGS 1984 UTM Zone 10N

Appendix B: Measurements of vertical separation and uncertainties

Line	Fault	Unit§	Apparent Fault Dip	True Dip (S of seismic line)	True Dip (N of seismic line)	Dip Direction	Youngest Deformed Unconformity§	Multi-Fault Measurement? (Y/N)	Downthrown Direction (down to E or W)	Width of deformation (m) W	Width of deformation (m) E	Vertical separation (m)	Uncertainty* (+) (m)	Uncertainty* (-) (m)	Grade (A-C)**
PBS-322	HF1020	H10	67	NA	67.11	E	<H10	N	W	<20	<10	0.4	0.4	0.4	B
PBS-322	HF1041	H10	87	NA	87.01	W	>TOPQ	N	NA	-	-	-	-	-	0
PBS-324	HF1041	H10	77	77.03	NA	W	H10	N	E	120	<20	0.4	0.4	0.4	B
PBS-324	HF1041	H30	77	77.03	NA	W	H10	N	E	200	75	2	0.8	1.2	B
PBS-324	HF1020	H10	85	85.03	85.06	E	H10	N	W	<15	<30	0.8	0.4	0.4	B
PBS-325	HF1042	H10	83	NA	83.09	SW	H10	N	W	<20	<20	0.8	0.4	0.4	A
PBS-325	HF1020	H10	87	87.04	87.00	W	H10	N	W	55	<30	1.6	0.4	0.4	A
PBS-325	HF1020	H30	87	87.04	87.00	W	H10	N	W	70	40	3.2	0.8	0.8	A
PBS-327A	HF1042	H10	77	77.15	77.09	NE	H10	N	E	<10	<10	0.8	0.4	0.8	B
PBS-327A	HF1020	H10	90	90.00	90.00	NA	H10	Y	W	<10	<20	3.2	0.8	0.8	B
PBS-327A	HF1022	H10	90	NA	90.00	NA	H10	N	E	260	<10	2.4	0.8	0.8	C
PBS-328	HF1042	H30	80	80.05	80.00	NE	H40	NA	NA	-	-	-	-	-	0
PBS-328	HF1042	H40	80	80.07	80.01	NE	H40	Y	E	120	<20	2.4	0.4	2.4	C
PBS-328	HF1020	H10	88	88.04	88.00	SW	H10	N	W	<40	<100	2.4	0.8	0.8	C
PBS-328	HF1020	H30	88	88.04	88.00	SW	H10	N	W	110	<80	6.4	0.8	1.6	C
PBS-328	HF1022	H10	90	90.00	90.00	NA	H10	Y	E	120	<20	1.6	0.8	0.8	B
PBS-328	HF1022	H30	90	90.00	90.00	NA	H10	Y	E	500	<100	0.8	0.8	0.8	C
PBS-328	HF1022	H40	90	90.00	90.00	NA	H10	Y	E	500	<100	5.6	1.6	1.6	C
PBS-320	Syn_CFHing	-	-	-	-	-	-	-	-	-	-	-	-	-	Z
PBS-319	Syn_CFHing	-	-	-	-	-	-	-	-	-	-	-	-	-	Z

Line	Fault	Unit§	Apparent Fault Dip	True Dip (S of seismic line)	True Dip (N of seismic line)	Dip Direction	Youngest Deformed Unconformity§	Multi-Fault Measurement? (Y/N)	Downthrown Direction (down to E or W)	Width of deformation (m) W	Width of deformation (m) E	Vertical separation (m)	Uncertainty* (+) (m)	Uncertainty* (-) (m)	Grade (A-C)**
PBS-318	HF1042	H10	71	71.01	71.07	NE	H30	NA	NA	-	-	-	-	-	0
PBS-318	HF1042	H30	71	71.01	71.07	NE	H30	N	E	90	65	6.4	0.8	0.8	B
PBS-318	HF1018	H10	80	NA	80.48	SW	H30	NA	NA	-	-	-	-	-	0
PBS-318	HF1018	H30	81	NA	81.48	SW	H30	N	W	<20	30	0.8	0.4	0.8	B
PBS-318	HF1018	H40	81	NA	81.48	SW	H30	N	W	<20	30	0.8	0.4	0.8	B
PBS-318	HF1020	H10	90	90.00	90.00	NA	H10	?	?	?	?	?	?	?	Z
PBS-318	HF1020	H30	90	90.00	90.00	NA	H10	N	W	45	35	2.4	0.8	0.8	B
PBS-318	HF1022	H10	89	89.00	NA	NA	H30	NA	NA	-	-	-	-	-	0
PBS-318	HF1022	H30	90	90.00	NA	NA	H30	Y	E	210	<20	0.8	0.4	0.8	B
PBS-318	HF1022	H40	90	90.00	NA	NA	H30	Y	E	210	<20	0.8	0.4	0.8	B
PBS-318	Syn_CFHing	-	-	-	-	-	-	-	-	-	-	-	-	-	Z
PBS-317	HF1042	H10	81	81.03	81.01	NE	<H30	NA	NA	-	-	-	-	-	0
PBS-317	HF1042	H30	81	81.03	81.01	NE	<H30	Y	E	NA	<100	2.4	2.4	2.4	C
PBS-317	HF1018	H10	87	87.16	87.07	SW	H10	Y	W	<200	<40	2.4	0.4	2.4	A
PBS-317	HF1018	H30	87	87.16	87.07	SW	H10	Y	W	<10	200	4	0.8	1.6	A
PBS-317	HF1018	H40	87	87.16	87.07	SW	H10	Y	W	190	310	5.6	0.8	1.6	B
PBS-317	HF1020	H10	90	90.00	90.00	NA	<H30	NA	NA	-	-	-	-	-	0
PBS-317	HF1020	H30	90	90.00	90.00	NA	<H30	Y	E	100	NA	2.4	2.4	2.4	C
PBS-317	CF1001	H10	86	NA	NA	W	H10	N	E	<20	130	1.2	0.4	0.4	B
PBS-317	CF1001	H30	86	NA	NA	W	H10	N	E	<10	220	4	0.8	0.8	A

Line	Fault	Unit§	Apparent Fault Dip	True Dip (S of seismic line)	True Dip (N of seismic line)	Dip Direction	Youngest Deformed Unconformity§	Multi-Fault Measurement? (Y/N)	Downthrown Direction (down to E or W)	Width of deformation (m) W	Width of deformation (m) E	Vertical separation (m)	Uncertainty* (+) (m)	Uncertainty* (-) (m)	Grade (A-C)**
PBS-317	CF1001	H40	86	NA	NA	W	H10	N	E	80	600	12.8	2.4	0.8	B
PBS-316	HF1018	H30	81	81.19	81.26	SW	H40	NA	NA	-	-	-	-	-	0
PBS-316	HF1018	H40	81	81.19	81.26	SW	H40	N	W	40	60	2	0.8	0.8	A
PBS-316	HF1020	H10	90	90.00	90.00	NA	H10	Y	E	200	80	1.2	0.4	0.4	B
PBS-316	HF1020	H30	90	90.00	90.00	NA	H10	Y	E	250	80	3.2	0.8	0.8	B
PBS-316	HF1020	H40	90	90.00	90.00	NA	H10	Y	E	280	90	6.8	0.8	1.2	C
PBS-291	HF1020	H10	90	90.00	NA	NA	H10	NA	NA	-	-	-	-	-	0
PBS-291	HF1020	H30	90	90.00	NA	NA	H10	Y	E	60	<40	9.6	0.8	1.6	B
PBS-291	HF1020	H40	90	90.00	NA	NA	H10	Y	E	80	130	23.6	1.6	0.8	B
PBS-291	HF1018	H30	88	88.06	88.00	SW	H40	NA	NA	-	-	-	-	-	0
PBS-291	HF1018	H40	88	88.06	88.00	SW	H40	N	W	<20	<30	1.2	0.4	0.4	B
PBS-290	HF1004b	H10	90	90.00	90.00	NA	H10	N	E	<40	<30	0.8	0.4	0.4	B
PBS-290	HF1004b	H30	90	90.00	90.00	NA	H10	N	E	<50	<60	11.2	1.6	1.6	B
PBS-290	HF1004b	H40	90	90.00	90.00	NA	H10	N	E	40	210	20	1.6	1.6	B
PBS-290	HF1018	H30	68	68.00	68.00	NE	H40	NA	NA	-	-	-	-	-	0
PBS-290	HF1018	H40	68	68.00	68.00	NE	H40	N	W	20	40	1.6	0.8	0.8	B
PBS-289	HF1004b	H10	90	90.00	90.00	NA	<H10	Y	E	130	70	0.4	0.4	0.4	C
PBS-289	HF1004b	H30	90	90.00	90.00	NA	<H10	Y	E	190	150	4.4	0.8	0.8	B
PBS-289	HF1018	H30	90	90.00	90.00	NA	<H40	NA	NA	-	-	-	-	-	0
PBS-289	HF1018	H40	90	90.00	90.00	NA	<H40	NA	NA	-	-	-	-	-	0

Line	Fault	Unit§	Apparent Fault Dip	True Dip (S of seismic line)	True Dip (N of seismic line)	Dip Direction	Youngest Deformed Unconformity§	Multi-Fault Measurement? (Y/N)	Downthrown Direction (down to E or W)	Width of deformation (m) W	Width of deformation (m) E	Vertical separation (m)	Uncertainty* (+) (m)	Uncertainty* (-) (m)	Grade (A-C)**
PBS-288	HF1004b	H10	90	90.00	90.00	NA	<H10	Y	E	<300	<100	2.8	1.6	1.6	C
PBS-288	HF1004b	H30	90	90.00	90.00	NA	<H10	Y	E	<20	<130	11.2	1.6	1.6	B
PBS-288	HF1018	H10	90	90.00	90.00	NA	H10	Y	W	NA	<20	0.8	0.8	0.8	B
PBS-288	HF1018	H30	90	90.00	90.00	NA	H10	Y	W	NA	<20	0.8	0.8	0.8	A
PBS-288	HF1018	H40	90	90.00	90.00	NA	H10	Y	W	NA	20	2.8	0.8	2.8	B
PBS-288	HF1019	H10	90	NA	90.00	NA	H10	Y	W	<60	NA	0.8	0.8	0.8	B
PBS-288	HF1019	H30	90	NA	90.00	NA	H10	Y	W	70	NA	0.8	0.8	0.8	B
PBS-288	HF1019	H40	90	NA	90.00	NA	H10	Y	W	220	NA	2.8	0.8	2.8	B
PBS-286	HF1004b	H10	90	90.00	90.00	NA	H10	N	E	80	50	3.2	1.6	1.6	C
PBS-286	HF1018	H10	90	90.00	90.00	NA	H10	Y	W	NA	160	2	0.8	0.8	C
PBS-286	HF1018	H30	90	90.00	90.00	NA	H10	Y	W	NA	220	12	1.6	1.6	C
PBS-286	HF1018	H40	90	90.00	90.00	NA	H10	Y	W	NA	160	12	1.6	1.6	C
PBS-286	HF1019	H10	90	90.00	90.00	NA	H10	Y	W	<20	NA	2	0.8	0.8	C
PBS-286	HF1019	H30	90	90.00	90.00	NA	H10	Y	W	360	NA	12	1.6	1.6	C
PBS-286	HF1019	H40	90	90.00	90.00	NA	H10	Y	W	440	NA	12	1.6	1.6	C
PBS-285	HF1004b	H10	90	90.00	90.00	NA	H10	N	E	<20	<40	0.8	0.4	0.4	B
PBS-285	HF1043	H10	90	NA	90.00	NA	H10	N	W	<60	<30	0.8	0.4	0.4	B
PBS-285	HF1018	H10	87	87.10	87.26	SW	H10	Y	W	NA	70	2.4	0.8	0.8	B
PBS-285	HF1018	H30	87	87.10	87.26	SW	H10	Y	W	NA	90	9.6	1.6	2.4	B
PBS-285	HF1018	H40	87	87.10	87.26	SW	H10	Y	W	NA	150	19.2	1.6	2.4	C

Line	Fault	Unit§	Apparent Fault Dip	True Dip (S of seismic line)	True Dip (N of seismic line)	Dip Direction	Youngest Deformed Unconformity§	Multi-Fault Measurement? (Y/N)	Downthrown Direction (down to E or W)	Width of deformation (m) W	Width of deformation (m) E	Vertical separation (m)	Uncertainty* (+) (m)	Uncertainty* (-) (m)	Grade (A-C)**
PBS-285	HF1019	H10	87	87.13	87.12	SW	H10	Y	W	100	NA	2.4	0.8	0.8	B
PBS-285	HF1019	H30	90	90.00	90.00	NA	H10	Y	W	140	NA	9.6	1.6	2.4	B
PBS-285	HF1019	H40	90	90.00	90.00	NA	H10	Y	W	280	NA	19.2	1.6	2.4	C
PBS-284A	HF1004b	H10	90	90.00	90.00	NA	H10	Y	E	NA	<20	2	0.8	0.8	B
PBS-284A	HF1043	H10	90	90.00	90.00	NA	H10	Y	E	40	NA	2	0.8	0.8	B
PBS-284A	HF1018	H10	52	54.48	53.55	NA	H10	Y	W	NA	<20	2.4	0.8	0.8	B
PBS-284A	HF1018	H30	52	54.48	53.55	SW	H10	Y	W	NA	<20	11.6	1.6	1.6	B
PBS-284A	HF1018	H40	52	54.48	53.55	SW	H10	Y	W	NA	<40	16.8	1.6	4	C
PBS-284A	HF1019	H10	90	90.00	90.00	NA	H10	Y	W	<20	NA	2.4	0.8	0.8	B
PBS-284A	HF1019	H30	90	90.00	90.00	NA	H10	Y	W	<20	NA	11.6	1.6	1.6	B
PBS-284A	HF1019	H40	90	90.00	90.00	NA	H10	Y	W	240	NA	16.8	1.6	4	C
PBS-283	HF1004b	H10	90	90.00	90.00	NA	<H10?	Y	E	NA	<60	5.6	0.8	4.8	C
PBS-283	HF1043	H10	90	90.00	90.00	NA	<H10?	Y	E	<140	NA	5.6	0.8	4.8	C
PBS-283	HF1018	H30	80	80.53	81.50	SW	<H40	NA	NA	-	-	-	-	-	0
PBS-283	HF1018	H40	80	80.53	81.50	SW	<H40	Y	W	NA	60	16	1.6	3.2	C
PBS-283	HF1019	H10	86	86.40	86.37	SW	H30	NA	NA	-	-	-	-	-	0
PBS-283	HF1019	H30	86	86.40	86.37	SW	H30	N	W	210	60	3.2	0.8	0.8	B
PBS-283	HF1019	H40	86	86.40	86.37	SW	H30	Y	W	210	NA	16	1.6	3.2	C
PBS-282	HF1004b	H10	90	90.00	90.00	NA	H10	N	E	<30	<20	2	0.8	0.8	B
PBS-282	HF1043	H10	90	90.00	NA	NA	H10	N	E	<70	<80	2	0.8	0.8	B

Line	Fault	Unit§	Apparent Fault Dip	True Dip (S of seismic line)	True Dip (N of seismic line)	Dip Direction	Youngest Deformed Unconformity§	Multi-Fault Measurement? (Y/N)	Downthrown Direction (down to E or W)	Width of deformation (m) W	Width of deformation (m) E	Vertical separation (m)	Uncertainty* (+) (m)	Uncertainty* (-) (m)	Grade (A-C)**
PBS-282	HF1018	H10	67	70.20	69.12	SW	<H30	NA	NA	-	-	-	-	-	0
PBS-282	HF1018	H30	67	70.20	69.12	SW	<H30	N	W	<20	40	2.4	0.8	0.8	A
PBS-282	HF1018	H40	67	70.20	69.12	SW	<H30	N	W	<40	<30	4.4	0.8	0.8	A
PBS-282	HF1019	H10	86	86.37	86.50	SW	H10	N	W	70	60	1.6	0.8	0.8	B
PBS-282	HF1019	H30	86	86.37	86.50	SW	H10	N	W	40	70	7.2	1.6	2.4	A
PBS-282	HF1019	H40	86	86.37	86.50	SW	H10	N	W	80	<20	17.6	1.6	2.4	A
PBS-281	HF1004b	H10	?	?	?	?	H10	N	E	<200	<150	5.12	1.6	1.6	C
PBS-281	HF1017	H10	78	NA	78.18	SW	H30	NA	NA	-	-	-	-	-	0
PBS-281	HF1017	H30	78	NA	78.18	SW	H30	N	E	20	70	0.8	0.8	0.4	A
PBS-281	HF1017	H40	78	NA	78.18	SW	H30	N	E	50	35	4.4	0.8	0.8	A
PBS-281	HF1018	H10	56	58.77	56.41	SW	H10	N	W	20	<40	0.8	0.4	0.4	A
PBS-281	HF1018	H30	56	58.77	56.41	SW	H10	N	W	20	60	4	0.8	1.6	B
PBS-281	HF1018	H40	56	58.77	56.41	SW	H10	Y	W	NA	160	5.6	0.8	1.6	C
PBS-281	HF1019	H10	90	90.00	90.00	NA	H30	NA	NA	-	-	-	-	-	0
PBS-281	HF1019	H30	90	90.00	90.00	NA	H30	N	E	50	50	0	0.8	0	0
PBS-281	HF1019	H40	90	90.00	90.00	NA	H30	Y	E	<20	NA	5.6	0.8	1.6	C
PBS-279A	HF1017	H30	87	87.05	87.00	SW	<H40	N	NA	-	-	-	-	-	0
PBS-279A	HF1017	H40	87	87.05	87.00	SW	<H40	?	?	?	?	?	?	?	Z
PBS-279A	HF1018	H10	74	74.23	74.52	SW	H10	Y	W	NA	<40	0.8	0.8	0.4	B
PBS-279A	HF1018	H30	74	74.23	74.52	SW	H10	Y	W	NA	45	4	1.6	2.4	B

Line	Fault	Unit§	Apparent Fault Dip	True Dip (S of seismic line)	True Dip (N of seismic line)	Dip Direction	Youngest Deformed Unconformity§	Multi-Fault Measurement? (Y/N)	Downthrown Direction (down to E or W)	Width of deformation (m) W	Width of deformation (m) E	Vertical separation (m)	Uncertainty* (+) (m)	Uncertainty* (-) (m)	Grade (A-C)**
PBS-279A	HF1018	H40	74	74.23	74.52	SW	H10	Y	W	NA	<200	8	1.6	4	C
PBS-279A	HF1019	H10	90	90.00	90.00	NA	H10	Y	W	<20	NA	0.8	0.8	0.4	B
PBS-279A	HF1019	H30	90	90.00	90.00	NA	H10	Y	W	180	NA	4	1.6	2.4	B
PBS-279A	HF1019	H40	90	90.00	90.00	NA	H10	Y	W	300	NA	8	1.6	4	C
PBS-09	HF1004b	H10	86	86.06	86.12	E	<H10	Y	E	90	220	1.6	0.8	0.8	C
PBS-09	HF1017	H30	83	83.00	83.04	E	H40	NA	NA	-	-	-	-	-	0
PBS-09	HF1017	H40	83	83.00	83.04	E	H40	N	E	30	20	1.6	0.8	0.8	B
PBS-09	HF1018	H10	84	84.20	84.00	W	H10	N	W	70	<40	0.4	0.4	0.4	B
PBS-09	HF1018	H30	84	84.20	84.00	W	H10	N	W	80	40	1.6	2.4	0.8	B
PBS-09	HF1018	H40	84	84.20	84.00	W	H10	N	W	80	40	5.6	1.6	1.6	B
PBS-09	HF1019	H30	90	90.00	90.00	NA	<H40	NA	NA	-	-	-	-	-	0
PBS-09	HF1019	H40	90	90.00	90.00	NA	<H40	N	?	?	?	?	?	?	Z
PBS-41	HF1004b	H10	87	87.09	87.00	NE	<H10	Y	E	200	160	0.8	0.4	0.8	C
PBS-41	HF1017	H30	89	89.01	89.01	NE	H40	NA	NA	-	-	-	-	-	0
PBS-41	HF1017	H40	89	89.01	89.01	NE	H40	N	W	<60	<20	0.8	0.4	0.8	B
PBS-41	HF1018	H10	89	89.00	89.00	SW	H10	N	W	50	<20	0.4	0.4	0.4	B
PBS-41	HF1018	H30	89	89.00	89.00	SW	H10	N	W	60	20	1.6	0.8	0.8	A
PBS-41	HF1018	H40	89	89.00	89.00	SW	H10	N	W	60	<40	5.6	1.6	0.8	B
PBS-41	HF1019	H10	88	88.00	88.02	NE	<H40	NA	NA	-	-	-	-	-	0
PBS-41	HF1019	H30	88	88.00	88.02	NE	<H40	?	E	?	?	?	?	?	Z

Line	Fault	Unit§	Apparent Fault Dip	True Dip (S of seismic line)	True Dip (N of seismic line)	Dip Direction	Youngest Deformed Unconformity§	Multi-Fault Measurement? (Y/N)	Downthrown Direction (down to E or W)	Width of deformation (m) W	Width of deformation (m) E	Vertical separation (m)	Uncertainty* (+) (m)	Uncertainty* (-) (m)	Grade (A-C)**
PBS-41	HF1019	H40	88	88.00	88.02	NE	<H40	?	E	?	?	?	?	?	Z
PBS-10	HF1004b	H10	88	88.01	88.02	E	<H10?	N	E	<40	<40	0.4	1.6	0.4	C
PBS-10	HF1004b	H30	88	88.01	88.02	E	<H10?	N	E	<340	480	17.6	3.2	3.2	C
PBS-10	HF1017	H10	88	88.01	88.02	W	H30	NA	NA	-	-	-	-	-	0
PBS-10	HF1017	H30	88	88.01	88.02	W	H30	N	W	<60	130	4	1.6	1.2	B
PBS-10	HF1017	H32	88	88.01	88.02	W	H30	N	W	<60	180	12	0.8	3.2	B
PBS-10	HF1017	H40	88	88.01	88.02	W	H30	N	W	110	210	12.8	2.4	1.6	B
PBS-10	HF1018	H10	85	85.36	85.02	W	H30	NA	NA	-	-	-	-	-	0
PBS-10	HF1018	H30	85	85.36	85.02	W	H30	Y	W	130	30	0.8	0.8	0.8	C
PBS-10	HF1018	H40	85	85.36	85.02	W	H30	Y	W	140	30	1.6	0.4	0.8	C
PBS-10	HF1019	H40	90	90.00	NA	NA	>H40	NA	NA	-	-	-	-	-	0
PBS-42	HF1017	¥	?	?	?	?	?	?	?	?	?	?	?	?	Z
PBS-42	HF1004b	H10	89	89.01	89.01	W	<H10?	Y	NA	<100	<100	0	1.6	0	0
PBS-42	HF1004b	H30	89	89.01	89.01	W	<H10?	Y	E	<630	<150	16	1.6	2.4	C
PBS-42	HF1004b	H32	89	89.01	89.01	W	<H10?	Y	E	<100	<250	28.8	2.4	4	C
PBS-42	HF1004b	H40	89	89.01	89.01	W	<H10?	Y	E	<100	<250	44	4.8	8	C
PBS-42	HF1018	H10	90	90.00	NA	NA	H30	NA	NA	-	-	-	-	-	0
PBS-42	HF1018	H30	90	90.00	NA	NA	H30	Y	E	<170	80	0.4	1.2	0.8	C
PBS-42	HF1018b	H10	80	NA	80.18	W	H30	NA	NA	-	-	-	-	-	0
PBS-42	HF1018b	H30	80	NA	80.18	W	H30	N	W	<40	70	1.6	0.4	0.8	B

Line	Fault	Unit§	Apparent Fault Dip	True Dip (S of seismic line)	True Dip (N of seismic line)	Dip Direction	Youngest Deformed Unconformity§	Multi-Fault Measurement? (Y/N)	Downthrown Direction (down to E or W)	Width of deformation (m) W	Width of deformation (m) E	Vertical separation (m)	Uncertainty* (+) (m)	Uncertainty* (-) (m)	Grade (A-C)**
PBS-11B	HF1018b	H10	87	87.06	87.10	E	>H10	N	NA	-	-	-	-	-	Z
PBS-11B	HF1007	H30	90	NA	90.00	NA	H30	N	W	30	20	2.4	0.8	0.8	A
PBS-11B	HF1048	H10	90	NA	NA	NA	H10	N	W	<20	<20	1.2	0.4	0.4	B
PBS-45	HF1004b	H10	88	88.07	88.07	E	H10	Y	E	<320	<30	4	1.6	1.6	C
PBS-45	HF1004b	H30	88	88.07	88.07	E	H10	Y	E	<330	NA	23.6	4	6.4	C
PBS-45	HF1004b	H40	88	88.07	88.07	E	H10	Y	E	<330	NA	52	6.4	4	C
PBS-45	HF1006	H10	86	86.05	86.05	W	H10	Y	W	<100	60	3.2	1.6	0.8	B
PBS-45	HF1006	H30	86	86.05	86.05	W	H10	Y	W	NA	70	23.6	4	6.4	C
PBS-45	HF1006	H40	86	86.05	86.05	W	H10	Y	W	NA	<260	52	6.4	4	C
PBS-45	HF1007	H10	89	89.03	89.09	W	H30	NA	NA	-	-	-	-	-	0
PBS-45	HF1007	H30	89	89.03	89.09	W	H30	N	W	60	30	0.8	0.8	0.4	A
PBS-45	HF1018b	H10	83	83.24	NA	W	H30	NA	NA	-	-	-	-	-	0
PBS-45	HF1018b	H30	83	83.24	NA	W	H30	N	W	<20	50	2.4	0.8	0.8	B
PBS-45	HF1018b	H32	83	83.24	NA	W	H30	N	W	20	50	4	0.8	1.6	B
PBS-45	HF1018b	H40	83	83.24	NA	W	H30	N	W	40	60	4	4	1.6	B
PBS-12	HF1004b	H10	90	90.00	90.00	NA	H10	Y	E	<1140	<40	4.8	1.6	1.6	C
PBS-12	HF1004b	H30	90	90.00	90.00	NA	H10	Y	E	<220	50	12.8	1.6	2.4	C
PBS-12	HF1006	H10	81	81.11	81.26	W	H10	Y	W	100	120	1.6	0.8	1.2	C
PBS-12	HF1006	H30	81	81.11	81.26	W	H10	Y	W	130	110	5.6	0.8	1.6	C
PBS-12	HF1007	H10	89	89.09	NA	W	H10	N	E	40	20	0.8	0.4	0.4	B

Line	Fault	Unit§	Apparent Fault Dip	True Dip (S of seismic line)	True Dip (N of seismic line)	Dip Direction	Youngest Deformed Unconformity§	Multi-Fault Measurement? (Y/N)	Downthrown Direction (down to E or W)	Width of deformation (m) W	Width of deformation (m) E	Vertical separation (m)	Uncertainty* (+) (m)	Uncertainty* (-) (m)	Grade (A-C)**
PBS-12	HF1007	H30	89	89.09	NA	W	H10	N	E	50	<40	0.8	0.8	0.4	B
PBS-12	HF1044	H10	90	NA	90.00	NA	>TOPQ(H10)	?	?	?	?	?	?	?	Z
PBS-46	HF1003	H10	89	NA	89.02	E	>H10	NA	NA	-	-	-	-	-	0
PBS-46	HF1004b	H10	89	89.03	89.02	E	H10	Y	E	70	50	1.6	0.8	0.8	B
PBS-46	HF1006	H10	87	87.09	87.06	W	H10	Y	W	<40	100	1.6	1.2	1.2	B
PBS-46	HF1044	TOPQ	90	90.00	NA	NA	>TOPQ (H10)	?	?	?	?	?	?	?	Z
PBS-13A	HF1003	H30	88	88.04	88.00	E	<H40	NA	NA	-	-	-	-	-	0
PBS-13A	HF1004b	H10	90	90.00	90.00	NA	H10	Y	E	<10	90	0.8	0.4	0.4	C
PBS-13A	HF1004b	H30	90	90.00	90.00	NA	H10	Y	E	<150	<100	8	1.6	1.6	C
PBS-13A	HF1006	H10	80	80.18	80.38	W	H10	Y	W	100	50	3.2	0.8	0.8	C
PBS-13A	HF1006	H32	80	80.18	80.38	W	H10	Y	W	210	80	7.2	0.8	1.6	C
PBS-47A	HF1003	H10	78	78.00	78.21	E	H30	NA	NA	-	-	-	-	-	0
PBS-47A	HF1003	H30	79	79.01	79.23	E	H30	Y	E	20	30	1.6	0.8	0.8	B
PBS-47A	HF1003	H32	79	79.01	79.23	E	H30	Y	E	70	30	4	0.8	1.6	B
PBS-47A	HF1003	H40	79	79.01	79.23	E	H30	Y	E	70	30	5.2	1.2	1.6	B
PBS-47A	HF1004b	H10	85	85.11	85.01	E	H10	Y	E	60	NA	0.8	0.4	0.4	C
PBS-47A	HF1004b	H28	85	85.11	85.01	E	H10	Y	E	80	NA	7.2	0.8	0.8	C
PBS-47A	HF1004b	H30	85	85.11	85.01	E	H10	Y	E	100	NA	7.6	0.8	1.6	C
PBS-47A	HF1004b	H32	85	85.11	85.01	E	H10	Y	E	120	NA	12.8	1.6	2.4	C
PBS-47A	HF1004b	H40	85	85.11	85.01	E	H10	Y	E	120	NA	14.8	1.6	1.6	C

Line	Fault	Unit§	Apparent Fault Dip	True Dip (S of seismic line)	True Dip (N of seismic line)	Dip Direction	Youngest Deformed Unconformity§	Multi-Fault Measurement? (Y/N)	Downthrown Direction (down to E or W)	Width of deformation (m) W	Width of deformation (m) E	Vertical separation (m)	Uncertainty* (+) (m)	Uncertainty* (-) (m)	Grade (A-C)**
PBS-47A	HF1006	H10	80	80.38	80.25	W	H10	Y	E	220	20	1.6	0.8	0.8	B
PBS-47A	HF1006	H28	80	80.38	80.25	W	H10	Y	E	240	60	8.8	1.6	3.2	B
PBS-47A	HF1006	H30	80	80.38	80.25	W	H10	Y	E	240	80	13.6	2.4	3.2	B
PBS-47A	HF1006	H32	80	80.38	80.25	W	H10	Y	E	240	80	19.2	1.6	4	B
PBS-47A	HF1006	H40	80	80.38	80.25	W	H10	Y	E	240	100	23.2	1.6	4	B
PBS-47A	HF1038	H10	87	NA	87.09	W	H10	Y	E	NA	60	0.8	0.4	0.4	C
PBS-47A	HF1038	H28	87	NA	87.09	W	H10	Y	E	NA	70	7.2	0.8	0.8	C
PBS-47A	HF1038	H30	87	NA	87.09	W	H10	Y	E	NA	70	7.6	0.8	1.6	C
PBS-47A	HF1038	H32	87	NA	87.09	W	H10	Y	E	NA	80	12.8	1.6	2.4	C
PBS-47A	HF1038	H40	87	NA	87.09	W	H10	Y	E	NA	80	14.8	1.6	1.6	C
PBS-14	HF1003	H30	83	83.15	83.09	E	<H30	N	E	60	40	1.6	0.8	0.8	B
PBS-14	HF1003	H32	83	83.15	83.09	E	<H30	N	E	80	60	2.4	1.2	0.8	B
PBS-14	HF1003	H40	83	83.15	83.09	E	<H30	N	E	100	60	3.2	1.2	0.8	B
PBS-14	HF1004b	H30	89	89.00	89.00	W	<H30	N	W	0	40	1.6	0.4	0.8	A
PBS-14	HF1004b	H32	89	89.00	89.00	W	<H30	N	W	0	40	0.8	0.8	0.4	A
PBS-14	HF1004b	H40	89	89.00	89.00	W	<H30	N	W	0	40	1.6	0.8	0.8	A
PBS-14	HF1049	H28	84	NA	84.47	E	<H30	?	?	?	?	?	?	?	Z
PBS-14	HF1006	H28	90	90.00	90.00	NA	<H30	Y	E	200	0	5.6	0.8	0.8	B
PBS-14	HF1006	H30	90	90.00	90.00	NA	<H30	Y	E	170	60	12	1.6	1.6	B
PBS-14	HF1006	H32	90	90.00	90.00	NA	<H30	Y	E	180	70	15.2	2.4	2.4	B

Line	Fault	Unit§	Apparent Fault Dip	True Dip (S of seismic line)	True Dip (N of seismic line)	Dip Direction	Youngest Deformed Unconformity§	Multi-Fault Measurement? (Y/N)	Downthrown Direction (down to E or W)	Width of deformation (m) W	Width of deformation (m) E	Vertical separation (m)	Uncertainty* (+) (m)	Uncertainty* (-) (m)	Grade (A-C)**
PBS-14	HF1006	H40	90	90.00	90.00	NA	<H30	Y	E	220	80	24	3.2	1.6	B
PBS-14	HF1038	H28	89	89.03	89.01	W	<H30	Y	W	100	80	2.4	0.8	0.8	B
PBS-14	HF1038	H30	89	89.03	89.01	W	<H30	Y	W	100	60	2.4	0.8	0.8	B
PBS-14	HF1038	H32	89	89.03	89.01	W	<H30	Y	W	200	80	0.8	0.8	0.8	B
PBS-14	HF1038	H40	89	89.03	89.01	W	<H30	Y	W	200	100	1.6	1.6	1.6	B
PBS-55	HF1003	H28	90	90.00	90.00	NA	<H30	N	E	55	<50	0.8	0.8	0.8	B
PBS-55	HF1003	H30	90	90.00	90.00	NA	<H30	N	E	55	<50	0.8	0.8	0.4	A
PBS-55	HF1003	H32	90	90.00	90.00	NA	<H30	N	E	<35	<40	3.2	0.8	0.8	A
PBS-55	HF1003	H40	90	90.00	90.00	NA	<H30	N	E	<50	<30	3.2	0.8	0.8	A
PBS-55	HF1004b	H28	87	87.00	87.02	E	<H30	N	E	75	220	3.2	0.8	0.8	B
PBS-55	HF1004b	H30	87	87.00	87.02	E	<H30	N	E	75	220	1.6	0.8	0.8	A
PBS-55	HF1004b	H32	87	87.00	87.02	E	<H30	N	E	75	220	2.4	0.8	0.8	A
PBS-55	HF1004b	H40	87	87.00	87.02	E	<H30	N	E	75	220	2.4	0.8	0.8	A
PBS-55	HF1006	H28	72	72.16	73.47	W	<H30	N	W	150	230	4	0.8	0.8	C
PBS-55	HF1006	H30	72	72.16	73.47	W	<H30	N	W	150	230	5.6	0.8	1.6	B
PBS-55	HF1006	H32	72	72.16	73.47	W	<H30	N	W	150	230	7.2	1.6	1.6	B
PBS-55	HF1006	H40	72	72.16	73.47	W	<H30	N	W	150	300	8	4	1.6	C
PBS-55	HF1038	H28	87	87.02	NA	W	<H30	N	E	95	20	0.4	0.4	0.4	A
PBS-55	HF1038	H30	87	87.02	NA	W	<H30	N	E	95	20	0.8	0.4	0.4	A
PBS-55	HF1038	H32	87	87.02	NA	W	<H30	N	E	65	20	0.8	0.4	0.4	A

Line	Fault	Unit§	Apparent Fault Dip	True Dip (S of seismic line)	True Dip (N of seismic line)	Dip Direction	Youngest Deformed Unconformity§	Multi-Fault Measurement? (Y/N)	Downthrown Direction (down to E or W)	Width of deformation (m) W	Width of deformation (m) E	Vertical separation (m)	Uncertainty* (+) (m)	Uncertainty* (-) (m)	Grade (A-C)**
PBS-55	HF1038	H40	87	87.02	NA	W	<H30	N	E	65	20	1.6	0.8	0.8	A
PBS-55	HF1049	H28	76	77.07	77.07	W	<H30?	N	?	?	?	?	?	?	Z
PBS-15	HF1003	H28	81	81.11	81.01	W	<H30	N	E	20	20	0.4	0.4	0.4	B
PBS-15	HF1003	H30	81	81.11	81.01	W	<H30	N	E	80	0	1.6	0.8	0.8	B
PBS-15	HF1003	H32	81	81.11	81.01	W	<H30	N	E	80	0	3.2	0.8	0.8	B
PBS-15	HF1003	H40	81	81.11	81.01	W	<H30	N	E	NA	0	5.6	1.6	1.6	C
PBS-15	HF1004b	H28	76	76.07	76.29	W	<H30	N	E	90	340	7.2	0.8	1.6	B
PBS-15	HF1004b	H30	76	76.07	76.29	W	<H30	N	E	90	340	8	0.8	1.6	B
PBS-15	HF1004b	H32	76	76.07	76.29	W	<H30	N	E	90	340	9.6	1.6	1.6	B
PBS-15	HF1004b	H40	76	76.07	76.29	W	<H30	N	E	90	370	8.8	1.6	1.6	B
PBS-15	HF1049	H30	74	75.21	74.33	W	<H30	N	?	?	?	?	?	?	Z
PBS-29	10001	H10	86	86.00	86.05	E	<H10	?	?	?	?	?	?	?	Z
PBS-30	10001	H10	90	90.00	90.00	NA	<H30	?	?	?	?	?	?	?	Z
PBS-23	10001	H10	89	89.01	89.01	E	<H10	?	?	?	?	?	?	?	Z
PBS-31	10001	H10	88	88.02	88.02	E	<H10	?	?	?	?	?	?	?	Z
PBS-22	10001	H10	90	90.00	90.00	NA	<H10	?	?	?	?	?	?	?	Z
PBS-56	HF1003	H28	82	82.01	82.10	W	<H30	N	E	105	10	2.4	0.8	0.8	B
PBS-56	HF1003	H30	82	82.01	82.10	W	<H30	N	E	135	10	4.8	0.8	0.8	B
PBS-56	HF1003	H32	82	82.01	82.10	W	<H30	N	E	135	10	6.4	0.8	1.2	B
PBS-56	HF1003	H40	82	82.01	82.10	W	<H30	N	E	155	10	11.2	0.8	1.6	B

Line	Fault	Unit§	Apparent Fault Dip	True Dip (S of seismic line)	True Dip (N of seismic line)	Dip Direction	Youngest Deformed Unconformity§	Multi-Fault Measurement? (Y/N)	Downthrown Direction (down to E or W)	Width of deformation (m) W	Width of deformation (m) E	Vertical separation (m)	Uncertainty* (+) (m)	Uncertainty* (-) (m)	Grade (A-C)**
PBS-56	HF1004b	H28	90	90.00	90.00	NA	<H30	N	E	75	5	8.8	0.8	1.2	A
PBS-56	HF1004b	H30	90	90.00	90.00	NA	<H30	N	E	75	10	8	1.6	1.2	A
PBS-56	HF1004b	H32	90	90.00	90.00	NA	<H30	N	E	75	10	11.2	1.6	1.6	A
PBS-56	HF1004b	H40	90	90.00	90.00	NA	<H30	N	E	55	25	16.8	1.6	1.6	A
PBS-56	HF1049	H32	74	74.33	74.04	W	<H40	N	?	?	?	?	?	?	Z
PBS-16	HF1039	H28	90	90.00	90.00	NA	<H30	Y	E	<55	NA	8	1.2	1.2	B
PBS-16	HF1039	H30	90	90.00	90.00	NA	<H30	Y	E	<30	NA	8	2.4	1.6	B
PBS-16	HF1003	H28	87	87.04	87.04	E	<H30	Y	E	NA	200	8	1.2	1.2	A
PBS-16	HF1003	H30	87	87.04	87.04	E	<H30	Y	E	NA	200	8	2.4	1.6	A
PBS-16	HF1003	H32	87	87.04	87.04	E	<H30	Y	NA	NA	200	-	-	-	Z
PBS-16	HF1003	H40	87	87.04	87.04	E	<H30	Y	E	NA	180	21.6	3.2	4.8	C
PBS-16	HF1004b	H28	74	76.33	NA	E	<H30	N	E	130	280	4.8	0.8	0.8	A
PBS-16	HF1004b	H30	74	76.33	NA	E	<H30	N	E	170	280	6.4	0.8	1.2	A
PBS-16	HF1004b	H32	74	76.33	NA	E	<H30	N	E	220	280	9.6	0.8	1.6	A
PBS-16	HF1004b	H40	74	76.33	NA	E	<H30	N	E	220	280	11.2	1.6	2.4	B
PBS-16	HF1049	TOPQ	89	89.00	89.05	W	?	N	?	?	?	?	?	?	Z
PBS-54	HF1039	H30	90	90.00	NA	NA	<H30	Y	E	80	NA	12	1.6	1.6	A
PBS-54	HF1039	H40	90	90.00	NA	NA	<H30	Y	E	75	NA	21.6	2.4	3.2	A
PBS-54	HF1003	H30	88	88.02	88.01	W	<H30	Y	E	NA	10	12	1.6	1.6	A
PBS-54	HF1003	H40	88	88.02	88.01	W	<H30	Y	E	NA	10	21.6	2.4	3.2	A

Line	Fault	Unit§	Apparent Fault Dip	True Dip (S of seismic line)	True Dip (N of seismic line)	Dip Direction	Youngest Deformed Unconformity§	Multi-Fault Measurement? (Y/N)	Downthrown Direction (down to E or W)	Width of deformation (m) W	Width of deformation (m) E	Vertical separation (m)	Uncertainty* (+) (m)	Uncertainty* (-) (m)	Grade (A-C)**
PBS-17	HF1003	H28	86	86.03	86.01	W	<H30	N	E	10	10	10.4	0.8	2.4	C
PBS-17	HF1003	H30	86	86.03	86.01	W	<H30	N	E	10	10	11.2	0.8	0.8	A
PBS-17	HF1003	H40	86	86.03	86.01	W	<H30	N	E	10	10	23.2	1.6	4	A
PBS-17	HF1004	H28	83	NA	83.00	W	<H30	N	W	140	120	2.4	0.8	0.8	A
PBS-17	HF1004	H30	83	NA	83.00	W	<H30	N	W	190	130	3.2	0.8	0.8	A
PBS-17	HF1004	H32	83	NA	83.00	W	<H30	N	W	190	130	4.8	1.2	0.8	A
PBS-17	HF1004	H40	83	NA	83.00	W	<H30	N	W	190	130	7.2	0.8	1.6	A
PBS-17	HF1005	H30	87	87.00	87.01	W	<H30	N	?	?	?	?	?	?	Z
PBS-53	HF1003	H32	84	84.01	84.03	W	<H40	N	NA	70	<10	?	?	?	Z
PBS-53	HF1001	H32	86	NA	86.00	E	<H40	N	W	0.5	NA	0.4	1.6	0.4	A
PBS-53	HF1004	H32	89	89.00	NA	W	<H40	N	W	<10	20	0.8	0.4	0.4	A
PBS-53	HF1002	H32	75	NA	75.01	E	<H40	N	E	80	60	2.4	0.8	0.8	A
PBS-53	HF1005	H32	86	86.01	86.02	W	?	N	NA	?	?	?	?	?	Z
PBS-18A	HF1003	¥	88	88.01	88.04	W	?	?	?	?	?	?	?	?	Z
PBS-18A	HF1001	¥	88	88.00	88.00	E	?	?	?	?	?	?	?	?	Z
PBS-18A	HF1002	¥	79	79.01	79.13	E	?	?	?	?	?	?	?	?	Z
PBS-18A	HF1005	¥	88	88.01	88.00	W	?	?	?	?	?	?	?	?	Z
PBS-24	HF1003	¥	86	86.07	86.02	W	?	?	?	?	?	?	?	?	Z
PBS-24	HF1001	¥	86	86.01	86.04	E	?	?	?	?	?	?	?	?	Z
PBS-24	HF1002	¥	84	84.07	84.00	E	?	?	?	?	?	?	?	?	Z

Line	Fault	Unit§	Apparent Fault Dip	True Dip (S of seismic line)	True Dip (N of seismic line)	Dip Direction	Youngest Deformed Unconformity§	Multi-Fault Measurement? (Y/N)	Downthrown Direction (down to E or W)	Width of deformation (m) W	Width of deformation (m) E	Vertical separation (m)	Uncertainty* (+) (m)	Uncertainty* (-) (m)	Grade (A-C)**
PBS-24	HF1005	¥	90	90.00	90.00	-	?	?	?	?	?	?	?	?	Z
PBS-T1	HF1002	¥	83	89.51	89.14	E	<H10?	?	?	?	?	?	?	?	Z
PBS-48	HF1003	H30	86	86.02	86.02	W	<H30	N	W	<40	25	1.6	0.8	0.8	A
PBS-48	HF1001	¥	84	84.06	NA	E	<H30?	?	?	?	?	?	?	?	Z
PBS-48	HF1002	H10	72	72.00	72.01	E	>H10	NA	NA	-	-	-	-	-	0
PBS-48	HF1005	H10	87	87.04	NA	W	H10?	?	?	?	?	?	?	?	Z
PBS-25	HF1003	H30	90	90.00	90.00	NA	<H30	N	E	<10	<10	2.4	0.8	0.8	A
PBS-25	HF1003	H45	90	90.00	90.00	NA	<H30	N	E	40	<10	3.2	0.8	0.8	A
PBS-25	11109	¥	84	NA	84.18	W	>TOPQ	?	?	?	?	?	?	?	Z
PBS-25	HF1002	¥	85	85.00	NA	E	?	?	?	?	?	?	?	?	Z
PBS-52	11109	¥	90	90.00	90.00	NA	>TOPQ	?	?	?	?	?	?	?	Z
PBS-52	HF1003	¥	-	NA	NA	NA	?	?	?	?	?	?	?	?	Z
PBS-26	HF1003	¥	88	88.05	88.00	W	?	?	?	?	?	?	?	?	Z
PBS-26	Hf1008	¥	89	NA	89.00	E	?	?	?	?	?	?	?	?	Z
PBS-26	11109	¥	87	87.07	87.03	E	>TOPQ	?	?	?	?	?	?	?	Z
PBS-51	HF1003	¥	90	90.00	90.00	NA	?	?	?	?	?	?	?	?	Z
PBS-51	Hf1008	¥	90	90.00	90.00	NA	?	?	?	?	?	?	?	?	Z
PBS-51	HF1010	¥	90	NA	90.00	NA	?	?	?	?	?	?	?	?	Z
PBS-51	10001	¥	90	NA	90.00	NA	?	?	?	?	?	?	?	?	Z
PBS-51	11109	¥	81	81.09	81.03	E	>TOPQ	?	?	?	?	?	?	?	Z

Line	Fault	Unit§	Apparent Fault Dip	True Dip (S of seismic line)	True Dip (N of seismic line)	Dip Direction	Youngest Deformed Unconformity§	Multi-Fault Measurement? (Y/N)	Downthrown Direction (down to E or W)	Width of deformation (m) W	Width of deformation (m) E	Vertical separation (m)	Uncertainty* (+) (m)	Uncertainty* (-) (m)	Grade (A-C)**
PBS-27	HF1003	¥	90	90.00	90.00	NA	?	?	?	?	?	?	?	?	Z
PBS-27	Hf1008	¥	90	90.00	90.00	NA	?	?	?	?	?	?	?	?	Z
PBS-27	HF1010	¥	90	90.00	90.00	NA	?	?	?	?	?	?	?	?	Z
PBS-27	11109	¥	89	89.00	89.00	W	>TOPQ	?	?	?	?	?	?	?	Z
PBS-27	10001	¥	90	90.00	90.00	-	?	?	?	?	?	?	?	?	Z
PBS-28	HF1050	H40	89	89.02	89.02	W	>H40	NA	NA	-	-	-	-	-	0
PBS-28	HF1008	H30	90	90.00	NA	NA	<H30	N	E	<50	<50	0.8	0.4	0.4	B
PBS-28	HF1008	H40	90	90.00	NA	NA	<H30	N	E	<50	<50	1.2	0.4	0.4	B
PBS-28	HF1010	H30	89	89.00	NA	E	H40	NA	NA	-	-	-	-	-	0
PBS-28	HF1010	H40	89	89.00	NA	E	H40	N	W	<50	<50	0.8	0.4	0.4	C
PBS-28	10001	H10	89	89.00	89.00	W	H10?	?	?	?	?	?	?	?	Z
PBS-28	11109	¥	88	88.01	88.00	W	>TOPQ	?	?	?	?	?	?	?	Z
PBS-29	HF1050	H40	90	90.00	90.00	NA	>H40	N	NA	-	-	-	-	-	0
PBS-29	HF1011	H10	90	NA	90.00	NA	<H30	NA	NA	-	-	-	-	-	0
PBS-29	HF1011	H30	90	NA	90.00	NA	<H30	Y	E	180	<20	4.8	0.8	1.2	B
PBS-29	HF1011	H40	90	NA	90.00	NA	<H30	Y	E	180	<20	8.8	0.8	1.6	B
PBS-29	11109	¥	86	86.00	86.00	E	>TOPQ	?	?	?	?	?	?	?	Z
PBS-30	HF1050	H40	90	90.00	90.00	NA	>H40	N	NA	-	-	-	-	-	0
PBS-30	HF1011	H30	90	90.00	90.00	NA	<H30	N	NA	-	-	-	-	-	0
PBS-30	HF1011	H40	90	90.00	90.00	NA	<H30	N	E	<20	70	0.4	0.4	0.4	B

Line	Fault	Unit§	Apparent Fault Dip	True Dip (S of seismic line)	True Dip (N of seismic line)	Dip Direction	Youngest Deformed Unconformity§	Multi-Fault Measurement? (Y/N)	Downthrown Direction (down to E or W)	Width of deformation (m) W	Width of deformation (m) E	Vertical separation (m)	Uncertainty* (+) (m)	Uncertainty* (-) (m)	Grade (A-C)**
PBS-30	HF1047	H30	87	NA	87.02	E	<H30	N	E	<160	120	2.4	0.8	0.8	B
PBS-30	HF1047	H40	87	NA	87.02	E	<H30	N	E	<200	140	3.6	0.8	0.8	B
PBS-30	11109	¥	88	88.00	NA	E	>TOPQ	?	?	?	?	?	?	?	Z
PBS-23	HF1050	H40	86	86.00	NA	W	>H40	N	NA	-	-	-	-	-	0
PBS-23	HF1011	H30	90	90.00	90.00	NA	<H30	Y	E	NA	<20	7.2	1.2	1.2	B
PBS-23	HF1011	H40	90	90.00	90.00	NA	<H30	Y	E	NA	<20	10	1.2	1.6	B
PBS-23	HF1047	H30	89	89.01	89.02	E	<H30	Y	E	<40	NA	7.2	1.2	1.2	B
PBS-23	HF1047	H40	89	89.01	89.02	E	<H30	Y	E	<80	NA	10	1.2	1.6	B
PBS-31	HF1047	H30	88	88.01	NA	E	H30	N	E	50	60	2.8	0.8	0.8	A
PBS-31	HF1047	H40	88	88.01	NA	E	H30	N	E	<60	70	9.2	0.8	2.4	B
PBS-32	10001	H10	90	90.00	90.00	NA	<H10	?	?	?	?	?	?	?	Z
PBS-21	10001	¥	90	90.00	90.00	NA	<H30	?	?	?	?	?	?	?	Z
PBS-33	10001	¥	88	88.02	88.00	E	<H30	?	?	?	?	?	?	?	Z
PBS-33	51105	H30	80	NA	NA	E	<H30	N	E	80	50	4	0.8	0.8	A
PBS-33	51105	H40	80	NA	NA	E	<H30	N	E	100	50	6	0.8	0.8	A
PBS-20	10001	¥	88	88.00	88.00	E	<H30	?	?	?	?	?	?	?	Z
PBS-34	51203	H30	90	NA	NA	NA	<H30	Y	E	40	60	2.4	0.8	0.8	A
PBS-34	51203	H40	90	NA	NA	NA	<H30	Y	E	70	60	2.8	0.8	0.8	B
PBS-34	10001	H30	90	90.00	90.00	NA	<H30	N	E	50	30	1.6	0.4	0.4	A
PBS-34	10001	H40	90	90.00	90.00	NA	<H30	N	E	80	30	2.4	0.8	0.8	B

Line	Fault	Unit§	Apparent Fault Dip	True Dip (S of seismic line)	True Dip (N of seismic line)	Dip Direction	Youngest Deformed Unconformity§	Multi-Fault Measurement? (Y/N)	Downthrown Direction (down to E or W)	Width of deformation (m) W	Width of deformation (m) E	Vertical separation (m)	Uncertainty* (+) (m)	Uncertainty* (-) (m)	Grade (A-C)**
PBS-34	51111	H30	90	NA	NA	NA	<H30	N	E	50	230	9.6	0.8	2.4	A
PBS-34	51111	H40	90	NA	NA	NA	<H30	N	E	60	230	22	1.6	4.8	B
PBS-34	11006	H10	84	NA	84.03	W	<H10	N	W	<10	<20	2.8	0.8	0.8	A
PBS-19	10001	¥	88	88.03	88.00	E	<H30	?	?	?	?	?	?	?	Z
PBS-19	11006	¥	90	90.00	90.00	NA	<H30	?	?	?	?	?	?	?	Z
PBS-19	LO1005	¥	80	NA	82.31	W	?	?	?	?	?	?	?	?	Z
PBS-T3	LO1005	¥	62	67.84	71.13	W	?	?	?	?	?	?	?	?	Z
PBS-35	10001	H30	90	90.00	90.00	NA	<H30	?	?	?	?	?	?	?	Z
PBS-35	11006	¥	84	84.00	84.01	W	<H30?	?	?	?	?	?	?	?	Z
PBS-35	LO1005	¥	58	68.12	NA	W	?	?	?	?	?	?	?	?	Z
PBS-02	10001	H10	90	90.00	90.00	NA	<H10	?	?	?	?	?	?	?	Z
PBS-02	11006	¥	90	90.00	90.00	NA	<H30?	?	?	?	?	?	?	?	Z
PBS-02	LO1002	¥	36	NA	46.29	S-SW	?	?	?	?	?	?	?	?	Z
PBS-36	10001	H10	90	90.00	90.00	NA	<H10	?	?	?	?	?	?	?	Z
PBS-36	11006	¥	90	90.00	90.00	NA	<H30?	?	?	?	?	?	?	?	Z
PBS-36	LO1002	¥	45	55.21	58.96	S-SW	?	?	?	?	?	?	?	?	Z
PBS-264	LO1002	¥	54	54.34	54.94	S-SW	?	?	?	?	?	?	?	?	Z
PBS-01	10001	H10	90	90.00	90.00	NA	<H10	?	?	?	?	?	?	?	Z
PBS-01	11006	¥	90	90.00	90.00	NA	<H20?	?	?	?	?	?	?	?	Z
PBS-01	LO1002	H10	71	79.94	NA	S-SW	H10	?	?	?	?	?	?	?	Z

Appendix B: Measurements of vertical separation and uncertainties

Line	Fault	Unit§	Apparent Fault Dip	True Dip (S of seismic line)	True Dip (N of seismic line)	Dip Direction	Youngest Deformed Unconformity§	Multi-Fault Measurement? (Y/N)	Downthrown Direction (down to E or W)	Width of deformation (m) W	Width of deformation (m) E	Vertical separation (m)	Uncertainty* (+) (m)	Uncertainty* (-) (m)	Grade (A-C)**
PBC-06	?	?	-	?	?	NA	?	?	?	?	?	?	?	?	Z
PBS-266	LO1001	¥	60	NA	60.02	S-SW	?	?	?	?	?	?	?	?	Z
PBS-268	LO1000	H10	51	NA	52.25	S-SW	H10	N	E	<20	<20	1.2	0.4	0.4	C
PBS-03	10001	H30	90	90.00	NA	NA	<H30	Y	E	<40	NA	12.4	1.6	2.4	B
PBS-03	10001	H40	90	90.00	NA	NA	<H30	Y	E	?	NA	15.2	3.2	3.2	C
PBS-03	11006	H10	89	89.00	89.03	E	<H30	?	?	?	?	?	?	?	Z
PBS-03	11006	H30	89	89.00	89.03	E	<H30	Y	E	NA	<10	12.4	1.6	2.4	B
PBS-03	11006	H40	89	89.00	89.03	E	<H30	Y	E	NA	60	15.2	3.2	3.2	C
PBS-03	HF1013	H10	76	NA	76.10	W	H10	N	E	10	10	1.6	0.4	0.4	A
PBS-03	HF1013	H30	76	NA	76.10	W	H10	N	E	10	10	2.4	0.8	0.8	A
PBS-03	HF1013	H40	76	NA	76.10	W	H10	N	E	10	10	5.2	1.2	0.8	A
PBS-03	LO1000	H10	63	76.12	65.04	S-SW	H10	N	E	60	<10	0.8	0.4	0.4	B
PBS-03	LO1000	H30	63	76.12	65.04	S-SW	H10	N	E	60	<10	2.8	0.8	0.8	C
PBS-03	LO1000	H40	63	76.12	65.04	S-SW	H10	N	E	80	10	2.4	0.8	0.8	B
PBS-03	LO1001	H10	62	69.73	65.50	S-SW	H10	N	E	20	20	2.8	0.8	0.8	C
PBS-262	11006	¥	88	88.05	90	E	<H20	?	?	?	?	?	?	?	Z
PBS-262	HF1013	¥	70	70.14	90	W	<H30?	?	?	?	-	?	?	?	Z
PBS-262	LO1000	H10	75	76.25	75.26	S-SW	H10	N	E	60	<10	1.6	0.4	0.4	B
PBS-262	LO1001	H10	75	77.06	77.06	S-SW	H10	?	?	<10	<50	?	?	?	Z
PBS-04	HF1014	¥	88	90	88.00	E	<H30	?	?	?	?	?	?	?	Z

Line	Fault	Unit§	Apparent Fault Dip	True Dip (S of seismic line)	True Dip (N of seismic line)	Dip Direction	Youngest Deformed Unconformity§	Multi-Fault Measurement? (Y/N)	Downthrown Direction (down to E or W)	Width of deformation (m) W	Width of deformation (m) E	Vertical separation (m)	Uncertainty* (+) (m)	Uncertainty* (-) (m)	Grade (A-C)**
PBS-04	HF1046	H30	84	90	84.70	E	H40	NA	NA	-	-	-	-	-	0
PBS-04	HF1046	H40	85	NA	85.54	E	H40	?	?	?	?	?	?	?	Z
PBS-04	HF1045	H30	90	NA	90.00	NA	H30	N	W	10	30	1.6	0.4	0.4	A
PBS-04	HF1045	H40	90	NA	90.00	NA	H30	N	W	10	40	2.4	0.8	0.8	A
PBS-04	LO1000	¥	52	52.51	53.55	W	?	?	?	?	?	?	?	?	Z
PBS-04	LO1001	¥	61	64.59	-	W	?	?	?	?	?	?	?	?	Z
PBS-43	HF1014	¥	89	89.00	89.00	W	<H10	?	?	?	?	?	?	?	Z
PBS-43	LO1000	¥	51	52.56	51.52	W	?	?	?	?	?	?	?	?	Z
PBS-43	HF1046	¥	88	88.22	88.16	E	?	?	?	?	?	?	?	?	Z
PBS-43	HF1045	¥	89	89.19	89.18	E	?	?	?	?	?	?	?	?	Z
PBS-07	HF1014	¥	89	89.00	89.00	E	<H10	?	?	?	?	?	?	?	Z
PBS-07	HF1045	H30	90	90.00	90.00	NA	<H30	N	W	10	20	2.4	0.8	0.8	A
PBS-07	HF1046	H30	81	81.71	-	E	<H30	N	E	20	20	2	0.8	0.8	A
PBS-07	HF1015	¥	87	NA	87.00	E	>H30?	?	?	?	?	?	?	?	Z
PBS-07	LO1000	H10	78	78.21	78.01	W	H10	N	?	?	?	?	?	?	Z
PBS-07	LO1000	H30	78	78.21	78.11	W	H10	N	E	20	<10	2.8	0.8	0.8	C
PBS-07	LO1000	H40	78	78.21	78.11	W	H10	N	E	20	<10	3.2	0.8	0.8	C
PBS-40	HF1014	¥	89	89.00	89.00	E	<H10	?	?	?	?	?	?	?	Z
PBS-40	HF1045	¥	89	89.21	NA	E	?	?	?	?	?	?	?	?	Z
PBS-40	HF1015	¥	86	86.00	NA	W	?	?	?	?	?	?	?	?	Z

Line	Fault	Unit§	Apparent Fault Dip	True Dip (S of seismic line)	True Dip (N of seismic line)	Dip Direction	Youngest Deformed Unconformity§	Multi-Fault Measurement? (Y/N)	Downthrown Direction (down to E or W)	Width of deformation (m) W	Width of deformation (m) E	Vertical separation (m)	Uncertainty* (+) (m)	Uncertainty* (-) (m)	Grade (A-C)**
PBS-40	LO1000	H10	71	71.17	71.97	W	H10	N	E	70	30	5.6	0.8	1.2	A
PBS-40	LO1000	H30	71	71.17	71.97	W	H10	N	E	70	30	6.4	1.2	1.6	A
PBS-40	LO1000	H40	71	71.17	71.97	W	H10	N	E	65	30	7.2	0.8	0.8	A
PBS-08	HF1014	¥	89	89.00	89.00	E	<H20	?	?	?	?	?	?	?	Z
PBS-08B	LO1000	¥	74	74.83	74.83	W	?	?	?	?	?	?	?	?	Z
PBS-37A	HF1014	¥	89	89.00	89.00	E	<H20	?	?	?	?	?	?	?	Z
PBS-37A	HF1016	¥	89	NA	89.00	W	?	?	?	?	?	?	?	?	Z
PBS-37A	HF1051	¥	89	NA	89.03	E	?	?	?	?	?	?	?	?	Z
PBS-37A	LO1000	¥	62	63.31	62.29	W	?	?	?	?	?	?	?	?	Z
PBS-38A	HF1014	H30	87	87.00	87.00	E	<H30	N	W	245	>30	4.8	1.2	0.8	C
PBS-38A	HF1016	H30	79	79.03	NA	E	>H30	NA	NA	-	-	-	-	-	0
PBS-38A	HF1051	¥	90	90.00	90.00	NA	?	?	?	?	?	?	?	?	Z
PBS-38A	LO1000	¥	75	75.18	75.56	W	?	?	?	?	?	?	?	?	Z
PBS-39A	HF1014	¥	90	90.00	90.00	NA	<H20	?	?	?	?	?	?	?	Z
PBS-39A	HF1051	¥	89	89.09	89.02	W	<H20	?	?	?	?	?	?	?	Z
PBS-39A	LO1000	¥	68	68.78	NA	W	<H30	?	?	?	?	?	?	?	Z
PBS-50	HF1014	H20	90	90.00	90.00	NA	<H20	Y	E	20	NA	12.8	1.6	1.6	B
PBS-50	HF1014	H30	90	90.00	90.00	NA	<H20	Y	E	20	NA	14.4	1.6	1.6	B
PBS-50	HF1014	H40	90	90.00	90.00	NA	<H20	Y	E	35	NA	18.4	2.4	1.6	B
PBS-50	HF1030	H20	80	NA	80.00	W	<H20	Y	E	NA	50	12.8	1.6	1.6	B

Line	Fault	Unit§	Apparent Fault Dip	True Dip (S of seismic line)	True Dip (N of seismic line)	Dip Direction	Youngest Deformed Unconformity§	Multi-Fault Measurement? (Y/N)	Downthrown Direction (down to E or W)	Width of deformation (m) W	Width of deformation (m) E	Vertical separation (m)	Uncertainty* (+) (m)	Uncertainty* (-) (m)	Grade (A-C)**
PBS-50	HF1030	H30	80	NA	80.00	W	<H20	Y	E	NA	50	14.4	1.6	1.6	B
PBS-50	HF1030	H40	80	NA	80.00	W	<H20	Y	E	NA	125	18.4	2.4	1.6	B
PBS-50	HF1051	H30	80	80.15	80.21	W	<H20	N	W	<10	70	18	1.6	2.4	B
PBS-50	HF1051	H40	80	80.15	80.21	W	<H20	N	W	<10	70	19.6	1.6	2.4	B
PBS-49	HF1014	H20	88	88.00	88.01	E	<H20	Y	E	<50	NA	4.8	3.2	3.2	C
PBS-49	HF1014	H30	88	88.00	88.01	E	<H20	Y	?	?	?	?	?	?	Z
PBS-49	HF1014	H40	88	88.00	88.01	E	<H20	Y	?	?	?	?	?	?	Z
PBS-49	HF1030	H20	84	84.00	84.04	E	<H20	Y	E	NA	220	4.8	3.2	3.2	C
PBS-49	HF1030	H30	84	84.00	84.04	E	<H20	Y	?	?	?	?	?	?	Z
PBS-49	HF1030	H40	84	84.00	84.04	E	<H20	Y	?	?	?	?	?	?	Z
PBS-49	HF1051	H40	83	83.15	83.13	E	>H40	NA	NA	-	-	-	-	-	0
PBS-49	HF1033	H40	85	NA	85.02	E	>H40	NA	NA	-	-	-	-	-	0
PBS-49	HF1032	H10	85	NA	85.05	E	H10	Y	E	110	30	1.2	0.4	0.4	C
PBS-49	HF1032	H20	85	NA	85.05	E	H10	Y	E	110	30	1.6	0.8	0.8	C
PBS-49	HF1032	H30	85	NA	85.05	E	H10	Y	E	160	40	3.2	0.8	0.8	C
PBS-49	HF1032	H32	85	NA	85.05	E	H10	Y	E	190	50	4.8	0.8	1.6	C
PBS-49	HF1032	H40	85	NA	85.05	E	H10	Y	E	190	50	4.8	0.8	1.6	C
PBS-201	HF1014	H20	85	85.02	85.00	E	<H20	Y	E	<10	NA	14.4	0.8	12	C
PBS-201	HF1014	H30	88	88.01	88.00	E	<H20	Y	?	?	?	?	?	?	Z
PBS-201	HF1014	H40	88	88.01	88.00	E	<H20	Y	?	?	?	?	?	?	Z

Appendix B: Measurements of vertical separation and uncertainties

Line	Fault	Unit§	Apparent Fault Dip	True Dip (S of seismic line)	True Dip (N of seismic line)	Dip Direction	Youngest Deformed Unconformity§	Multi-Fault Measurement? (Y/N)	Downthrown Direction (down to E or W)	Width of deformation (m) W	Width of deformation (m) E	Vertical separation (m)	Uncertainty* (+) (m)	Uncertainty* (-) (m)	Grade (A-C)**
PBS-201	HF1030	H20	85	85.04	85.01	E	<H20	Y	E	NA	<10	14.4	0.8	12	C
PBS-201	HF1030	H30	87	87.02	87.00	E	<H20	Y	?	?	?	?	?	?	Z
PBS-201	HF1030	H40	87	87.02	87.00	E	<H20	Y	?	?	?	?	?	?	Z
PBS-201	HF1051	H40	79	79.20	NA	E	>H40	NA	NA	-	-	-	-	-	0
PBS-201	HF1033	H40	86	86.02	86.04	E	>H40	NA	NA	-	-	-	-	-	0
PBS-201	HF1032	H30	84	84.06	84.00	E	<H30	N	E	<10	<10	4	0.8	0.8	C
PBS-201	HF1032	H40	84	84.06	84.00	E	<H30	N	E	20	<10	12	0.8	1.6	C
PBS-203	HF1014	H20	90	90.00	90.00	NA	>H20	NA	NA	-	-	-	-	-	Z
PBS-203	HF1030	H30	90	90.00	90.00	NA	<H30	NA	NA	-	-	-	-	-	0
PBS-203	HF1033	H40	90	90.00	90.00	NA	H40	N	E	60	<40	2.4	0.8	0.8	B
PBS-203	HF1032	H32	88	88.00	88.00	E	<H30?	N	W	<20	<40	1.6	0.8	0.8	B
PBS-203	HF1032	H40	88	88.00	88.00	E	<H30?	N	W	<40	85	2.4	0.8	0.8	B
PBS-204A	HF1023	¥	87	NA	87.12	E	?	?	?	?	?	?	?	?	Z
PBS-204A	HF1014	¥	90	90.00	90.00	NA	?	?	?	?	?	?	?	?	Z
PBS-204A	HF1030	¥	88	88.00	88.01	E	?	?	?	?	?	?	?	?	Z
PBS-204	HF1033	H30		0.00	0.00	NA	H40	NA	NA	-	-	-	-	-	0
PBS-204	HF1033	H40	88	88.00	88.00	E	H40	N	E	<40	<20	1.6	0.8	0.8	B
PBS-204	HF1032	H40	90	90.00	90.00	NA	H40	N	E	?	?	?	?	?	Z
PBS-206	HF1023	H40	90	90.00	90.00	NA	H40	NA	NA	-	-	-	-	-	0
PBS-206	HF1030	H30	90	90.00	90.00	NA	<H30	?	?	?	?	?	?	?	Z

Line	Fault	Unit§	Apparent Fault Dip	True Dip (S of seismic line)	True Dip (N of seismic line)	Dip Direction	Youngest Deformed Unconformity§	Multi-Fault Measurement? (Y/N)	Downthrown Direction (down to E or W)	Width of deformation (m) W	Width of deformation (m) E	Vertical separation (m)	Uncertainty* (+) (m)	Uncertainty* (-) (m)	Grade (A-C)**
PBS-206	HF1033	H40	57	57.00	NA	E	>H40	NA	NA	-	-	-	-	-	0
PBS-206	HF1040	H30	87	NA	87.00	E	H30	N	W	<20	<20	0.8	0.4	0.4	A
PBS-206	HF1040	H32	87	NA	87.00	E	H30	N	W	<20	30	1.6	0.8	0.8	A
PBS-206	HF1040	H40	87	NA	87.00	E	H30	N	W	30	40	2.4	0.8	0.8	A
PBS-207	HF1023	H40	90	90.00	90.00	NA	>H40	NA	NA	-	-	-	-	-	0
PBS-207	HF1030	H10	90	90.00	90.00	NA	<H10	?	?	?	?	?	?	?	Z
PBS-207	HF1040	H10	88	88.00	88.01	E	H10	N	E	20	10	0.8	0.4	0.4	A
PBS-207	HF1040	H30	88	88.00	88.01	E	H10	N	E	20	10	1.2	0.8	0.8	A
PBS-207	HF1040	H32	88	88.00	88.01	E	H10	N	E	20	10	1.2	0.8	0.8	A
PBS-207	HF1040	H40	88	88.00	88.01	E	H10	N	E	20	10	4	0.8	0.8	A
PBS-209	HF1023	H40	90	90.00	90.00	NA	>H40	NA	NA	-	-	-	-	-	0
PBS-209	HF1030	H10	90	90.00	90.00	NA	H10	?	?	?	?	?	?	?	Z
PBS-209	HF1040	H10	79	79.04	79.01	E	H10	N	E	50	40	2	0.4	0.4	B
PBS-209	HF1040	H30	79	79.04	79.01	E	H10	N	E	30	20	2.4	0.8	0.8	A
PBS-209	HF1040	H32	79	79.04	79.01	E	H10	N	E	50	30	4.8	0.8	1.2	A
PBS-209	HF1040	H40	79	79.04	79.01	E	H10	N	E	50	30	6.4	0.8	1.6	A
PBS-210	HF1023	H40	89	89.01	89.00	E	>H40	NA	NA	-	-	-	-	-	0
PBS-210	HF1030	H10	88	88.00	88.02	E	<H10	?	?	?	?	?	?	?	Z
PBS-210	HF1040	H10	88	88.00	NA	E	<H10	N	E	30	20	1.6	0.8	0.8	A
PBS-210	HF1040	H30	88	88.00	NA	E	<H10	N	E	30	20	1.6	0.8	0.8	A

Line	Fault	Unit§	Apparent Fault Dip	True Dip (S of seismic line)	True Dip (N of seismic line)	Dip Direction	Youngest Deformed Unconformity§	Multi-Fault Measurement? (Y/N)	Downthrown Direction (down to E or W)	Width of deformation (m) W	Width of deformation (m) E	Vertical separation (m)	Uncertainty* (+) (m)	Uncertainty* (-) (m)	Grade (A-C)**
PBS-210	HF1040	H32	88	88.00	NA	E	<H10	N	E	30	20	2.4	0.8	0.8	A
PBS-210	HF1040	H40	88	88.00	NA	E	<H10	N	E	30	20	3.2	0.8	0.8	A
PBS-212	HF1023	?	-	?	?	?	?	?	?	?	?	?	?	?	Z
PBS-212	HF1030	H10	89	89.01	89.03	E	<H10	Y	?	?	?	?	?	?	Z
PBS-212	HF1034	H30	90	NA	90.00	NA	H40	NA	NA	-	-	-	-	-	0
PBS-212	HF1034	H40	90	NA	90.00	NA	H40	Y	W	20	25	3.2	0.8	0.8	B
PBS-212	HF1031	H10	64	NA	64.22	E	<H10	Y	E	<10	35	1.6	0.8	0.8	A
PBS-212	HF1031	H30	64	NA	64.22	E	<H10	Y	E	<10	40	2.4	0.8	0.8	A
PBS-212	HF1031	H32	64	NA	64.22	E	<H10	Y	E	<10	35	8	0.8	1.6	A
PBS-212	HF1031	H40	64	NA	64.22	E	<H10	Y	E	<10	15	19.2	1.6	1.6	B
PBS-229	HF1023	¥	89	89.00	NA	E	?	NA	NA	-	-	-	-	-	Z
PBS-229	HF1030	H10	75	75.37	75.08	E	<H10	Y	?	?	?	?	?	?	Z
PBS-229	HF1034	H30	90	90.00	90.00	NA	<H10	Y	W	15	20	0.8	0.8	0.8	C
PBS-229	HF1034	H40	90	90.00	90.00	NA	<H10	Y	W	<10	20	1.6	0.8	0.8	C
PBS-229	HF1031	H10	72	72.16	72.01	E	H10	Y	E	45	140	4	2.4	2.4	C
PBS-229	HF1031	H30	72	72.16	72.01	E	H10	Y	E	45	140	4.4	2.8	2.8	C
PBS-229	HF1031	H40	72	72.16	72.01	E	H10	Y	E	45	140	5.6	2.4	2.4	C
PBS-230	HF1030	H10	90	90.00	90.00	NA	<H10	Y	?	?	?	?	?	?	Z
PBS-230	HF1034	H10	90	90.00	90.00	NA	<H30	NA	NA	-	-	-	-	-	0
PBS-230	HF1034	H30	90	90.00	90.00	NA	<H30	?	?	?	?	?	?	?	Z

Line	Fault	Unit§	Apparent Fault Dip	True Dip (S of seismic line)	True Dip (N of seismic line)	Dip Direction	Youngest Deformed Unconformity§	Multi-Fault Measurement? (Y/N)	Downthrown Direction (down to E or W)	Width of deformation (m) W	Width of deformation (m) E	Vertical separation (m)	Uncertainty* (+) (m)	Uncertainty* (-) (m)	Grade (A-C)**
PBS-230	HF1031	H10	81	81.01	81.09	E	<H10	N	E	25	<10	2.4	0.8	0.8	A
PBS-230	HF1031	H30	81	81.01	81.09	E	<H10	N	E	35	<10	4	0.8	0.8	A
PBS-232	HF1030	H10	82	82.01	82.00	E	<H10	Y	E	<10	<10	2.4	0.8	0.8	A
PBS-232	HF1034	H10	79	79.10	79.00	E	<H30	NA	NA	-	-	-	-	-	0
PBS-232	HF1034	H30	79	79.10	79.00	E	<H30	?	?	?	?	?	?	?	Z
PBS-232	HF1031	H10	90	90.00	NA	NA	<H30	NA	NA	-	-	-	-	-	0
PBS-233	HF1030	H10	88	88.00	88.00	E	<H10	?	?	?	?	?	?	?	Z
PBS-233	HF1034	H10	86	86.00	86.00	E	H10	Y	E	20	<10	0.8	0.4	0.4	B
PBS-235	HF1030	¥	90	90.00	90.00	NA	?	Y	?	?	?	?	?	?	Z
PBS-235	HF1034	H10	85	85.00	85.00	E	<H10?	?	?	?	?	?	?	?	Z
PBS-236	HF1030	¥	84	84.00	84.01	E	?	?	?	?	?	?	?	?	Z
PBS-236	HF1034	¥	82	82.00	82.03	E	?	?	?	?	?	?	?	?	Z
PBS-237	HF1030	¥	75	75.03	75.08	E	?	?	?	?	?	?	?	?	Z
PBS-237	HF1034	¥	77	77.05	77.05	E	?	?	?	?	?	?	?	?	Z
PBS-261	HF1030	¥	88	88.01	NA	E	?	?	?	?	?	?	?	?	Z
PBS-261	HF1034	¥	90	90.00	90.00	NA	?	?	?	?	?	?	?	?	Z
PBS-260	HF1024	H30	90	NA	90.00	NA	<H40	NA	NA	-	-	-	-	-	0
PBS-260	HF1034	¥	79	79.03	79.01	E	?	?	?	?	?	?	?	?	Z
PBS-259	HF1024	H30	90	90.00	90.00	NA	<H40	NA	NA	-	-	-	-	-	0
PBS-259	HF1034	¥	82	82.01	82.00	E	?	?	NA	?	?	?	?	?	Z

Line	Fault	Unit§	Apparent Fault Dip	True Dip (S of seismic line)	True Dip (N of seismic line)	Dip Direction	Youngest Deformed Unconformity§	Multi-Fault Measurement? (Y/N)	Downthrown Direction (down to E or W)	Width of deformation (m) W	Width of deformation (m) E	Vertical separation (m)	Uncertainty* (+) (m)	Uncertainty* (-) (m)	Grade (A-C)**
PBS-258	HF1024	H30	90	90.00	90.00	NA	<H40	NA	NA	-	-	-	-	-	0
PBS-258	HF1034	¥	79	79.01	NA	E	?	?	NA	?	?	?	?	?	Z
PBS-256	HF1024	H30	90	90.00	90.00	NA	<H40	NA	NA	-	-	-	-	-	0
PBS-255	HF1024	H30	90	90.00	NA	NA	<H40	NA	NA	-	-	-	-	-	0
PBS-253	HF1029	TOPQ(H10)	90	NA	90.00	NA	>TOPQ(H10)	NA	NA	-	-	-	-	-	0
PBS-252	HF1029	TOPQ(H10)	90	90.00	90.00	NA	>TOPQ(H10)	NA	NA	-	-	-	-	-	0
PBS-251	HF1029	TOPQ(H10)	90	90.00	90.00	NA	>TOPQ(H10)	NA	NA	-	-	-	-	-	0
PBS-250	HF1029	TOPQ(H10)	90	90.00	90.00	NA	>TOPQ(H10)	NA	NA	-	-	-	-	-	0
PBS-249	HF1029	TOPQ(H10)	90	90.00	90.00	NA	>TOPQ(H10)	NA	NA	-	-	-	-	-	0
PBS-248A	HF1029	TOPQ(H10)	90	90.00	NA	NA	>TOPQ(H10)	NA	NA	-	-	-	-	-	0
PBS-248A	SS1000	TOPQ(H10)	90	NA	90.00	NA	TOPQ(H10)	N	W	20	<10	0.8	0.4	0.4	C
PBS-247	HF1036	TOPQ(H10)	90	NA	90.00	NA	TOPQ(H10)	NA	NA	-	-	-	-	-	0
PBS-247	SS1000	TOPQ(H10)	90	90.00	90.00	NA	TOPQ(H10)	NA	NA	-	-	-	-	-	0
PBS-245	HF1036	TOPQ(H10)	90	90.00	90.00	NA	TOPQ(H10)	NA	NA	-	-	-	-	-	0
PBS-245	SS1000	TOPQ(H10)	90	90.00	90.00	NA	>TOPQ(H10)?	NA	NA	-	-	-	-	-	0
PBS-244	HF1036	TOPQ(H10)	90	90.00	90.00	NA	>TOPQ(H10) ?	NA	NA	-	-	-	-	-	0
PBS-244	SS1000	TOPQ(H10)	90	90.00	90.00	NA	>TOPQ(H10)?	NA	NA	-	-	-	-	-	0
PBS-242	HF1036	TOPQ(H10)	90	90.00	NA	NA	TOPQ(H10)	NA	NA	-	-	-	-	-	0
PBS-242	SS1000	TOPQ(H10)	90	90.00	90.00	NA	>TOPQ(H10)	NA	NA	-	-	-	-	-	0
PBS-241	HF1035	TOPQ(H10)	90	NA	90.00	NA	>TOPQ(H10)	NA	NA	-	-	-	-	-	0

Line	Fault	Unit§	Apparent Fault Dip	True Dip (S of seismic line)	True Dip (N of seismic line)	Dip Direction	Youngest Deformed Unconformity§	Multi-Fault Measurement? (Y/N)	Downthrown Direction (down to E or W)	Width of deformation (m) W	Width of deformation (m) E	Vertical separation (m)	Uncertainty* (+) (m)	Uncertainty* (-) (m)	Grade (A-C)**
PBS-241	SS1000	TOPQ(H10)	90	90.00	NA	NA	>TOPQ(H10)	NA	NA	-	-	-	-	-	0
PBS-241	SS1001	TOPQ(H10)	90	NA	90.00	NA	>TOPQ(H10)	NA	NA	-	-	-	-	-	0
PBS-239	HF1035	TOPQ(H10)	90	90.00	90.00	NA	>TOPQ(H10)	NA	NA	-	-	-	-	-	0
PBS-239	SS1001	TOPQ(H10)	90	90.00	90.00	NA	TOPQ(H10)	NA	NA	-	-	-	-	-	0
PBS-228	HF1035	TOPQ(H10)	90	90.00	90.00	NA	TOPQ(H10)	NA	NA	-	-	-	-	-	0
PBS-228	SS1001	TOPQ(H10)	90	90.00	90.00	NA	TOPQ(H10)	NA	NA	-	-	-	-	-	0
PBS-227	HF1035	TOPQ(H10)	90	90.00	90.00	NA	TOPQ(H10)	NA	NA	-	-	-	-	-	0
PBS-227	SS1001	TOPQ(H10)	90	90.00	NA	NA	TOPQ(H10)	NA	NA	-	-	-	-	-	0
PBS-225	HF1035	TOPQ(H10)	90	90.00	90.00	NA	TOPQ(H10)	NA	NA	-	-	-	-	-	0
PBS-224	HF1035	TOPQ(H10)	90	90.00	NA	NA	TOPQ(H10)	NA	NA	-	-	-	-	-	0
PBS-219	HF1027	TOPQ	84	NA	85.14	E	>TOPQ	?	?	?	?	?	?	?	Z
PBS-218	HF1027	TOPQ	89	89.19	89.15	E	>TOPQ	?	?	?	?	?	?	?	Z
PBS-216	HF1027	TOPQ	83	84.06	84.71	E	>TOPQ	?	?	?	?	?	?	?	Z
PBS-215A	HF1027	TOPQ	85	86.22	85.67	E	>TOPQ	?	?	?	?	?	?	?	Z
PBS-215A	HF1028	TOPQ(H10)	90	NA	90.00	NA	TOPQ(H10)	NA	NA	-	-	-	-	-	0
PBS-213	HF1027	TOPQ	68	70.72	NA	E	>TOPQ	?	?	?	?	?	?	?	Z
PBS-213	HF1028	TOPQ(H10)	90	90.00	90.00	NA	>TOPQ (H10)	NA	NA	-	-	-	-	-	0
PBS-277	HF1028	TOPQ(H10)	88	88.85	88.85	E	>TOPQ (H10)	NA	NA	-	-	-	-	-	0
PBS-269	HF1028	TOPQ(H10)	84	84.01	84.00	E	>TOPQ (H10)	NA	NA	-	-	-	-	-	0
PBS-271	HF1028	TOPQ(H10)	87	87.00	NA	E	>TOPQ (H10)	NA	NA	-	-	-	-	-	0

Line	Fault	Unit§	Apparent Fault Dip	True Dip (S of seismic line)	True Dip (N of seismic line)	Dip Direction	Youngest Deformed Unconformity§	Multi-Fault Measurement? (Y/N)	Downthrown Direction (down to E or W)	Width of deformation (m) W	Width of deformation (m) E	Vertical separation (m)	Uncertainty* (+) (m)	Uncertainty* (-) (m)	Grade (A-C)**

Additional Information:
Heading for all primary inlines is 058.
Vertical separation measurements are reported to a level of precision commensurate with the interpreted resolution of the data. The majority of measurements are reported with 0.5 millisecond precision, but some are reported with higher precision.
Vertical separation measurements were converted from milliseconds to meters using an assumed velocity of 1600 m/s as a conversion factor.
NA = measurement/field not applicable
? = could not measure because of a data gap, poor data interpretability, and/or inability to correlate unconformities
 - = no measurable deformation
> = The youngest deformed unconformity is older than the unconformity listed but cannot be better constrained.
< = In the youngest deformed unconformity column, symbol indicates the youngest deformed unconformity is younger than the unconformity listed but cannot be better constrained. In the width of deformation columns, symbol indicates the width of deformation is less than is reported but cannot be better constrained.
*Uncertainty (+) and (-) values are based on the vertical amount a separation measurement can change due uncertainty in the projection of a unconformity and/or the difference in measuring from the top or bottom of a reflector (vertical separation measurements are made on unflattened unconformitys that are affected by the swell of the seafloor).
**Grade level indicates the interpretability of data (i.e. gas clouding fault offset would have a low grade "C"). A=high correlation confidence, C=low correlation confidence, 0 = unconformity is not offset by fault,
Z = offset could not be determined either because of a data gap or inability to map unconformity proximal to the fault
¥ = no unconformities mapped across fault; only fault strike and dip measured
§ = TOPQ = Top of pre-Quaternary strata, no unconformities mapped across; TOPQ(H10) = Top of pre-Quaternary strata and likely H10 unconformity, no unconformities mapped across

ATTACHMENT 1

ITR REPORT VERIFICATION SUMMARY

Kathryn L. Hanson served as an Independent Technical Reviewer (ITR) for this Technical Report and supporting documents.

Report Verification Summary

Item	Parameter	Yes	No*	N/A*
1	Purpose is clearly stated and the report satisfies the Purpose.	x		
2	Data to be interpreted and/or analyzed are included or referenced.	x		
3	Methodology is appropriate and properly applied.	x		
4	Assumptions are reasonable, adequately described, and based on sound geotechnical principles and practices.	x		
5	Software is identified and properly applied. Validation is referenced or included, and is acceptable. Input files are correct and accurate.	x		
6	Interpretation and/or Analysis is complete, accurate, and leads logically to Results and Conclusions.	x		
7	Results and Conclusions are accurate, acceptable, and reasonable compared to the Data, Interpretation and/or Analysis, and Assumptions.	x		
8	The Limitation on the use of the Results has been addressed and is accurate and complete.	x		
9	The Impact Evaluation has been included and is accurate and complete.	x		
10	References are valid for intended use.	x		
11	Appendices are complete and accurate, and support the text.	x		

* Explain "No" or "N/A" entries. (For example, Items 3 thru 7 would be N/A for a data report that simply presents the collected data.) As needed, add additional pages to support verification.

As part of the review process for this report, I participated in periodic teleconference calls, and provided review comments to earlier drafts of the report (February 5, 2013 draft; March 26, 2013 draft, April 8, 2013draft, and May 16,2013 draft). The final report addressed all my earlier comments to previous drafts.

Kathryn L. Hanson

Verifier (ITR): Kathryn L Hanson 17 May 2013

(name/signature) (date)